Electron Paramagnetic Resonance of Mn^{2+}, Cu^{2+} and Gd^{3+} Ions Doping Some dia- and para- magnetic Single Crystals

Mojtaba Kahrizi

A Thesis

in

The Department

of

Physics

Presented in Partial Fulfillment of the Requirements
for the Degree of Doctor of Philosophy at
Concordia University
Montréal, Québec, Canada

March 1985

ABSTRACT

"Electron Paramagnetic Resonance of Mn^{2+}, Cu^{2+} and Gd^{3+} Ions Doping Some dia- and para- magnetic Single Crystals

Mojtaba Kahrizi, Ph.D.
Concordia University, 1985

X-band EPR measurements on several Mn^{2+}-doped single crystals have been made at room and low temperatures. The spin-Hamiltonian parameters are evaluated from the data using a rigorous least-squares-fitting program suitable for electron-nuclear spin coupled systems. The signs of the parameters are determined from the observed relative intensities of EPR lines at liquid helium temperature. The temperature variation of zero-field splitting parameter b_2^0 as well as that of the linewidths have been studied. Using the shift of g-values in the paramagnetic Ni^{2+} lattices, from those in the corresponding isostructural diamagnetic lattices, the exchange constant between Mn^{2+}-Ni^{2+} ions in nickel salts has been estimated. For the case of hosts containing paramagnetic Co^{2+} ions the spin-lattice relaxation time was estimated at room and liquid nitrogen temperatures.

X-band EPR measurements on Cu^{2+} in copper pentakisantipyrine perchlorate were performed at room and

low temperatures. The principal values of g and A tensors and their direction cosines were evaluated using a rigorous least-squares fitting technique.

Finally, X-band EPR studies of Gd^{3+}-doped single crystals of $LiYF_4$ and $LiYbF_4$ have been made at room and low temperatures. In the case of paramagnetic host $LiYbF_4$ the EPR lines broadened very fast as the temperature was lowered from room temperature, and below 270 K no EPR lines were observed. The parameters were evaluated using a least squares fitting method. The temperature variation of the parameters was studied. Using the g-shift in $LiYbF_4$ from its value in $LiYF_4$ the exchange constant between Gd^{3+} and its paramagnetic neighbor ions Yb^{3+}, was estimated.

ACKNOWLEDGEMENTS

The author expresses his deep gratitude and sincere appreciation to Professor S.K.Misra for suggesting the research problems included in this thesis. Without his continued availability and active guidance the completion of this thesis would not have been possible.

The author is grateful to the personnel of Concordia University Computer center, Science and Engineering Library and Concordia Faculty of Arts and Sciences Workshop for appropriate assistances. He is also grateful to the Natural Sciences and Engineering Research Council of Canada for partial fianancial support (Grant No. A4485). He acknowledges gratefully the teaching assistantship received from the Physics Department.

Lastly, but not the least, the auther wishes to extend his appreciation to his parents, his wife Nahid, and his daughter Magnolia for their patient and continued encouragement in all of his endeavors.

TABLE OF CONTENTS

CHAPTER I

INTRODUCTION

The accurate knowledge of spin-Hamiltonian parameters (S.H.P.), leads to a proper understanding of the interaction of paramagnetic ions with their environment. For this reason the main motivation in the present studies was to determine accurate values of the spin Hamiltonain parameters of some transition ions doped several diamagnetic and paramagnetic single crystals.

The major part of this work is focussed on the metal ion Mn^{2+} ($3d^5$, $^6S_{5/2}$). The manganese ion is the source of a vast amount of literature on magnetism. Since it has an odd number of electrons, it is a Kramers ion, and EPR spectra may be observed under a wide variety of conditions. The manganese atom has an electron spin of S=5/2 and nuclear spin of I=5/2. The g-values are almost isotropic, at about 2.0, and zero-field splittings are ususally small at room temperature of the order of 10-1 GHz in cubic environments. Mn^{2+} electron paramagnetic resonance (EPR) measurements in some of the host lattices studied in this thesis, have been reported previously. These measurements were generally confined to room temperature. Further, the (S.H.P.) were evaluated from pertubation expressions, by using only the

resonant line positions obtained for the external magnetic field orientation along the Z- and/or X-axes. Consequently, it was not possible to determine all the S.H.P. values individually, since the line positions for any particular orientation of the external magnetic field depend only upon certain linear combinations of some S.H.P. On the other hand, it is not possible to determine the absolute sign of zero field parameters at room temperature.

The main purpose of this work is to determine more accurately the (S.H.P.) of Mn^{2+} in several crystals at room, liquid nitrogen and liquid helium temperatures. For this reason a rigorous computer technique was employed,[1] for the evaluation of S.H.P. for the electron-nuclear spin coupled system, using exact numerical diagonalization of the spin-Hamiltonain matrix (instead of perturbation theory) fitting simultaneously all line positions obtained for various orientaions of the external magnetic field. The technique gives the correct relative sign of S.H.P.. The absolute signs can be determined from the observed relative intensities of EPR lines at liquid helium temperature.

Temperature variation of S.H.P. as well as linewidths have also been investigated. The possibility of the magnetic-field dependence of EPR linewidths in paramagnetic lattices has been studied. For the crystals containing paramagnetic host Co^{2+}, the spin-lattice relaxation time of Co^{2+} was estimated.

For the host lattices containing paramagnetic Ni^{2+} ions the exchange interaction constant between the paramagnetic ions Mn^{2+} and Ni^{2+}, has been estimated, using the shift of the g-value of Mn^{2+} in the paramagnetic lattice from its value in the corresponding isostructural diamagnetic lattice. In these experiments, the samples containing paramagnetic hosts were prepared in spherical shape in order to avoid the demagnetization effect at low temperatures.

EPR measurements of (Cu^{2+}, Mn^{2+}) doped calcium hexakisantipyrine perchlorate, $M(C_{11}H_{12}ON_2)_6(ClO_4)_2$. (M stands for divalent metals), were also performed in the hope of estimating the Mn^{2+}-Cu^{2+} exchange interaction. These measurements led us to investigate the EPR spectra of Cu^{2+} in copper pentakisantipyrine perchlorate. This has also been studied from room to liquid helium temperature. Copper has an electronic spin of only 1/2 and nuclear spin of 3/2, so there are no zero-field splitting effects. The g-values are often anisotropic. The principal values of the g and A tensors, as well as the direction cosines of the principal axes of the g and A tensors were evaluated using the computer technique.

Furthermore, the EPR spectra of Gd^{3+}-doped single crystals of $LiYF_4$ and $LiYbF_4$ have been performed at room and low temperatures. Gd^{3+} has a half-filled shell of seven unpaired electrons and the ground state is ^8S, the elctron spin is S=7/2. The EPR measurements on Gd^{3+}-doped

paramagnetic lattice of $LiYbF_4$ as presented in this thesis are the first ever to be reported. The (S.H.P.) are evaluated using a rigorous computer technique, as mentioned above. The temperature variation of S.H.P. is studied and the exchange interaction constant between Gd^{3+} and neighbouring paramagnetic ions is estimated from the observed g-shift of Gd^{3+} in $LiYbF_4$ from its value in $LiYF_4$. The organization of the thesis is as follows. The spin Hamiltonian for the systems studied is introduced in chapter II. Chapter III includes the procedure for the analysis of data. The details of experimental arrangement are given in chapter IV. Chapter V deals with the details of the experimental results. The conclusions are summerized in chapter VI. Appendices are brought at the end of the thesis.

CHAPTER II

SPIN HAMILTONIAN

The EPR spectra of paramagnetic impurities in single crystals can be represented in most of cases by fitting to an appropriate spin Hamiltonian.

The formalism of the spin Hamiltonian is based on the concept of an effective spin in the model in which a magnetic dipole with an intrinsic magnetic moment M_J interacts with the crystal field, the external magnetic field, the nuclear charges, etc. Thus the spin Hamiltonian is an energy operator containing only spin variables. The dependence of the spin Hamiltonian on all other variables is included in its constants.

When the ground state is an orbital singlet as, for example, in ions of the iron group, the spin Hamiltonian is derived from the complete Hamiltonian of the system, and its form may be established from symmetry considerations. The problem of interpreting EPR spectra consists of the following: a) identification of EPR lines with the corresponding transitions, calculated with the aid of a suitable spin Hamiltonian; b) calculation of the spin Hamiltonian parameters.

Thus the complete spin Hamiltonian must contain terms describing all possible types of interctions of the magnetic electrons of the impurity ion with the crystal field, the external magnetic field, nuclear charge, etc. Therefore it is best to discuss spin Hamiltonian in a definite sequence. In the first approximation one discusses the Zeeman term and the terms responsible for the fine structure, then, in the second approximation, one considers the hyperfine structure and weaker interactions. Generally, spin Hamiltonian can be written as:

$$\mathcal{H} = \mu_B \vec{H} \cdot \tilde{g} \cdot \vec{S} + \mathcal{H}_f + \mathcal{H}_{hf} \qquad \text{(II. 1)}$$

where the first term represents the Zeeman interaction and $\mathcal{H}_f$ represents the fine structure part of spin Hamiltonian and for different symmetry groups can be expressed as:[2]

1. Cubic symmetry

$$\mathcal{H} = B_4^0 \left(O_4^0 + 5O_4^4 \right) + B_6^0 \left(O_6^0 + 21O_6^4 \right) \qquad \text{(II. 2)}$$

2. Hexagonal symmetry:

$$\mathcal{H} = B_2^0 O_2^0 + B_4^0 O_4^0 + B_6^0 O_6^0 + B_6^6 O_6^6 \qquad \text{(II. 3)}$$

3. Trigonal symmetry:

$$\mathcal{H} = B_2^0 O_2^0 + B_4^0 O_4^0 + B_4^3 O_4^3 + B_6^3 O_6^3 + B_6^6 O_6^6 \qquad \text{(II. 4)}$$

4. Tetragonal symmetry:

$$\mathcal{H} = B_2^0 O_2^0 + B_4^0 O_4^0 + B_4^4 O_4^4 + B_6^0 O_6^0 + B_6^4 O_6^4 \qquad \text{(II. 5)}$$

5. Axial symmetry:

$$\mathcal{H} = B_2^0 O_2^0 + B_4^0 O_4^0 + B_6^0 O_6^0 \qquad \text{(II. 6)}$$

6. Orthorhombic and lower symmetries:

$$\mathcal{H} = B_2^0 O_2^0 + B_4^0 O_4^0 + B_2^2 O_2^2 + B_4^2 O_4^2 + B_4^4 O_4^4 + B_6^0 O_6^0 + B_6^2 O_6^2 + B_6^4 O_6^4 + B_6^6 O_6^6 \qquad \text{(II. 7)}$$

In Eq. (II.1) $\mathcal{H}_{hf}$ is the hyperfine-structure part of spin Hamiltonian and in general can be expressed as:

$$\mathcal{H}_{hf} = \vec{S} \cdot \vec{A} \cdot \vec{I} + Q' \left[I_z^2 - \frac{1}{3} (I + 1) \right] + Q'' \left[I_x^2 - I_y^2 \right] \qquad \text{(II. 8)}$$

In the above expressions g, B_ℓ^m, A, Q' and Q" are the spin Hamiltonian parameters, O_ℓ^m are the spin operators[3] (see

Appendix A), is the Bohr magneton, H is the external magnetic field, S and I are the electron and nuclear spins respectively. X, Y and Z are the principal axes of the zero-field splitting parameter B_2^0. In what follows the following fine structure spin Hamiltonian parameters will be used: $b_2^m = 3B_2^m$, $b_4^m = 60B_4^m$ and $b_6^m = 1260B_6^m$.

EPR spectra depend on the symmetry of the crystal field around the paramagnetic ion, on the direction of the crystallographic axes relative to the magnetic field, and on the symmetry of the paramagnetic susceptibility tensor. Therefore, in order to interpret EPR spectra, one must establish the angular dependence of the spectra for a given symmetry of the crystal field.

CHAPTER III

PROCEDURE OF EVALUATION OF S.H.P.

III.1 Analysis of data

The EPR data in this thesis have been analysed using the least-squares fitting (LSF) technique,[1] in which all resonant line positions obtained for several orientations of the external magnetic field are simultaneously fitted on a computer program. In the estimation of parameters by least-squares fitting, the "chi-squared" value (χ^2) defined below is minimised by varying the vector a, the components of which are the various S.H.P. X^2 for EPR data is defined as

$$\chi^2 = \sum_i (|\Delta E_i| - h\nu_i)^2 / \sigma_i^2 \qquad \text{(III.1)}$$

where ΔE_i is the calculated energy difference between the energy levels participating in resonance, ν_i is the klystron frequency and h is Planck's constant. The index i covers all the resonant line positions (data points) used simultaneously in the fitting, σ_i is an effective weight factor.

A detailed accounts of the least-squares fitting method is given by Misra.1 The method works equally well for cases of both small and large off-diagonal elements of the spin Hamiltonian matrix, and it can be applied to electron-nuclear spin- coupled systems.

To use this method for the electron-nuclear coupled systems (like Mn^{2+}) there are two problems to consider:

(i) Minimization of computer time. The large $(2S+1)(2I+1) \times (2S+1)(2I+1)$ dimensional spin Hamiltonian matrix (for e.g. Mn^{2+}, electron spin S=5/2, and nuclear spin I=5/2, so the spin Hamiltonian matrix is 36 x 36) and the large number of EPR line positions fitted simultaneously, make the total computer time required, prohibitively long. In order to minimize the computer time one should estimate quite well the initial values of as many S.H.P. as possible.

The large terms of the hyperfine structure in spin Hamiltonian in the standard notation are:

$$H_{hf} = A S_z I_z + B(S_x I_x + S_y I_y) \qquad \text{(III. 2)}$$

where $\vec{I}$ and $\vec{S}$ are the nuclear and electronic spins respectively, and A and B are the hyperfine parameters. Using the perturbation theory, the contribution of these terms to the resonant magnetic field value (H_{hf}) for the

transition $M \leftrightarrow M \pm 1$, $m \leftrightarrow m$, (M and m are electronic and nuclear magnetic quantum numbers respectively) for the magnetic field orientation along the Z-axis ($\vec{H} \parallel Z$) is given by Bleaney and Ingram.[3]

$$H_{hf}(M,m) = -Am - \frac{B^2}{2H_0}\left[I(I+1) - m^2 + m(2M-1) \right] \qquad \text{(III. 3)}$$

where $H_0 = \frac{h\nu}{g\mu_B}$, g and μ_B are the g-factor and Bohr magneton respectively. When $\vec{H} \parallel X$, one has to replace A by B and B^2 by $(A^2 + B^2)/2$ in the above equation. Now by manipulating equation (III. 3), using the (2I + 1) resonant hyperfine transitions ($m \leftrightarrow m$) corresponding to a chosen transition $M \leftrightarrow M-1$ one can easily deduce the resonant line position $H_f(M)$ for the transition $M \leftrightarrow M-1$ had the hyperfine interaction been reduced to zero. For example, for the Mn^{2+} ion (S=I=5/2), there are six $\Delta m=0$ hyperfine lines corresponding to a $\Delta M = \pm 1$ transition. All these six hyperfine line positions $H(M,m) = H_f(M) + H_{hf}(M,m)$ can be used to deduce $H_f(M)$,

$$H_f(M) = \frac{3}{4}\left[H(M,5/2) + H(M,-5/2)\right] - \frac{1}{8}\left\{\left[H(M,3/2) + H(M,-3/2)\right] + \left[H(M,1/2) + H(M,-1/2)\right]\right\} \qquad \text{(III. 4)}$$

The 2S resonant field values $H_{f(M)}$ ($\Delta M = \pm 1$) obtained when the hyperfine interaction has been reduced to zero, can now be used in a rigorous LSF procedure to estimate the fine structure parameters.

Since the spacing of successive (2I + 1) hyperfine lines corresponding to the fine transition $M \leftrightarrow M-1$, for $\vec{H} \| Z$, is the absolute value of $\left[A + \frac{B^2}{H_0} (M-m) \right]$, so the value of A is very closely the average of separations of the hyperfine structure transition in the 2S fine-structure groups as the average of m for $m = -I, -(I-1), \ldots (I-1), I$ is zero. B can be similarly estimated for $\vec{H} \| X$.

(ii) Determination of the eigenvalues participating in resonance

Due to the splitting of electronic energy levels by hyperfine interaction, there are a number of energy level pairs which have energy differences close to $h\nu_i$, so it is very difficult for the computer to choose the unique pair of energy levels which really participate in resonance.

To determine the nergy levels participating in resonance, knowing the particular fine-structure energy levels that participate in resonance when the hyperfine interaction has been reduced to zero, makes it easy to decide which particular hyperfine energy levels participate in resonance when the hyperfine interaction is turned on.

Noting that contribution of hyperfine term in spin Hamiltonian $(\vec{S}.\tilde{A}.\vec{I})$ to the eigenvalues is Am and, depending upon the sign of the hyperfine parameters A and B, the (2I+1) hyperfine energy levels corresponding to a chosen value of M for the external magnetic field parallel to one of the principal axes of crystal field or around it, occur in order of increasing energy as follows:

$$m = -I,-(I-1),\ldots(I-1),I \qquad \text{if } MA > 0$$

whereas, they will be

$$m = I,(I-1),\ldots-(I-1),-I \qquad \text{if } MA < 0$$

For the external field perpendicular to principal axis, A is replaced by B. It is now possible to pick the two eigenvalues which participate in resonance out of the (2S+1) x (2I+1) eigenvalues, as they are outputted by the computer in order of increasing (or decreasing) value of energy for a given resonant magnetic field value.

III.2 Determination of Signs of Parameters

The LSF method gives also the correct relative signs of the fine structure, as well as those of the hyperfine structure parameters.The absolute sign of parameters can be determined by identifying the absolute sign of b_2^0, the largest fine structure parameter by comparing the observed

line intensities of $\Delta M = \pm 1$ transitions at room and at liquid helium temperatures.[3]

The intensities of lines are proportional to the population differences of the levels between which the resonance takes place, and larger the population of a level, the lower is its energy, thus, b_2^0 is positive (negative) if the observed intensity of $M = 1$ lines which occur at the higher magnetic field are greater (smaller) than the intensities of the lines which occur at lower magnetic field values.

III.3. Calculation of S.H.P. Errors in the Analysis of Data

The procedure for the determination of parameter errors in fitting of EPR data, based on standard statistical analysis[4], has been described by Misra and Subramanian.[5] According to statistical analysis the parameter errors can be expressed as:

$$\Delta a_j = \varepsilon_{jj}^{1/2} \qquad \text{(III. 5)}$$

where a_j are the spin Hamiltonian parameters and ε_{jj} is the jth diagonal element of the error matix $\vec{\varepsilon}$, which is the inverse of the A matrix whose elements A_{ij} are one-half of the second derivatives of χ^2, defined by Eq. (III.1),

$$\vec{\varepsilon} = \vec{A}^{-1} \qquad \text{(III. 6)}$$

$$A_{ij} = 1/2\left(\partial^2\chi^2/\partial a_i\,\partial a_j\right)_a \qquad \text{(III. 7)}$$

When all σ_i in Eq. (III.1) are equal, the parameter errors can be estimated from the following expression[4]

$$\Delta a_j^2 = \left[\chi^2(1)/(N-r)\right]\,\varepsilon_{jj}(1) \qquad \text{(III. 8)}$$

where $\vec{\varepsilon}(1)$ is the error matrix obtained when all $\sigma_i = 1$, N is the number of data points fitted and r is the number of parameters. Eq. (III.8) is easily understood when one notes that the estimated variance of the data points, S^2, is expressed as:[4]

$$S^2 = \chi^2(1)/(N-r) \qquad \text{(III. 9)}$$

CHAPTER IV

EXPRIMENTAL APPARATUS

All the EPR measurements were performed on a reflection cavity X-band spectrometer. A block diagram of the spectrometer is shown in Figure 1.

IV. 1 Microwave Spectrometer

A reflex klystron oscillator, Varian model V-58 operating in the range of 8.5 - 10 GHz and minimum output of 500 mW, was used as a mirowave source. A Micro - Now model 753 power supply produced the required beam votage of 50 to 500 Vdc with a ripple of less than 10mV and a beam current of 50 mA. A range of reflector voltages from -50 to -500 Vdc with respect to the beam supply available with a ripple of less than 10 mV. The filament voltage supply provides 1.3 Amps at 6.3 Vac.

Electronic control of the klystron operating frequency is acheived by a Micro-Now model 210 frequency stabilizer. The klystron frequency is stabilized by locking it to the resonant frequency of the same cavity (rather than to an external reference cavity), so that if for any reason, such as small temperature changes of the sample cavity, there is a change in its resonant frequency, the klystron frequency will follow the change. Stabilization is achieved by

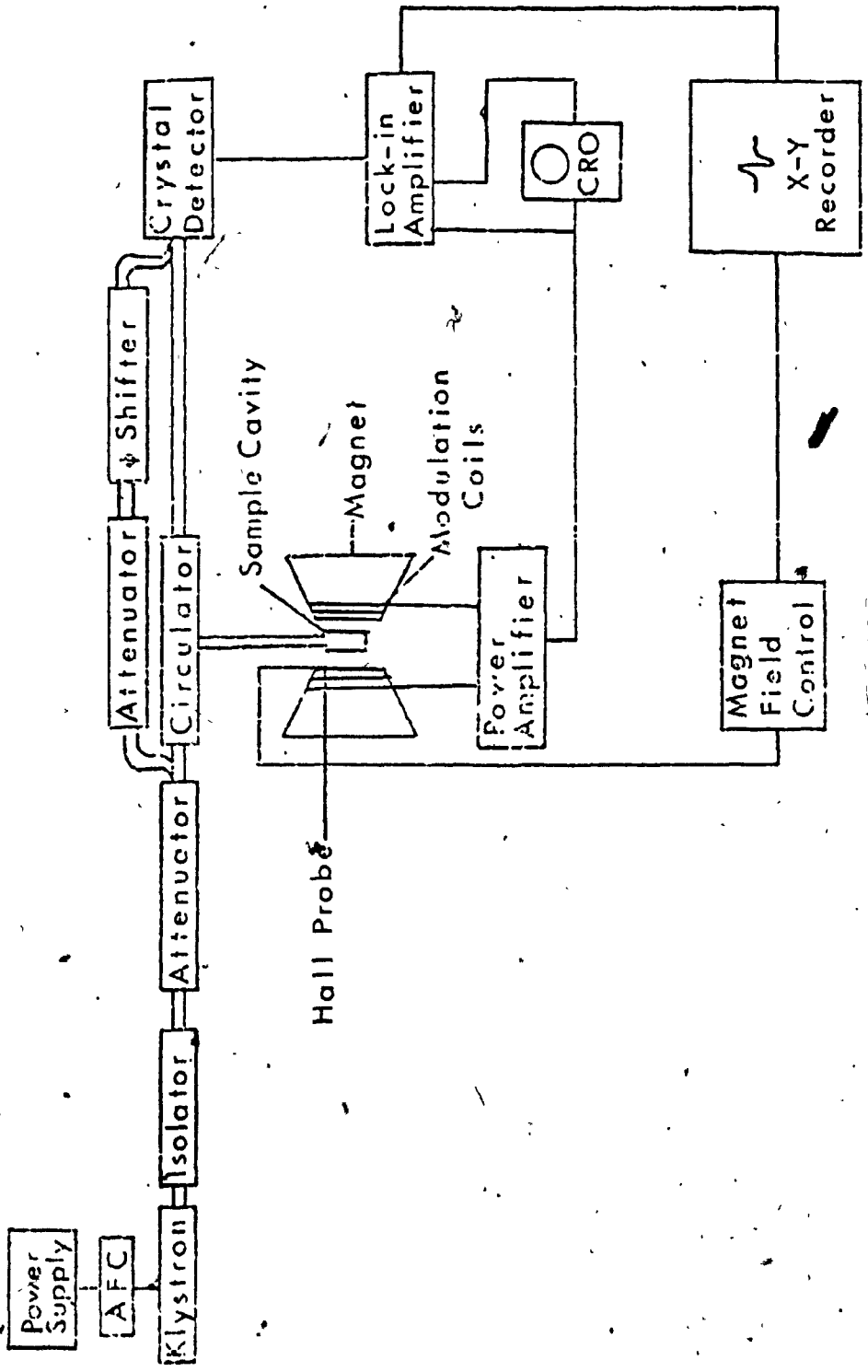

Fig. IV.1. Block diagram of the X-band spectrometer.

applying a 70 kHz sine wave modulation voltage and a dc voltage in series with the klystron reflector voltage.

A Hewlett Packard model 382 calibrated attenuator is connected between the load and the klystron to reduce the power incident upon the load. This is adjusted to give optimum signal to noise ratio.

The cavity arm of the spectrometer is a rectangular type resonating in the TE_{102} mode at a frequency of approximately 9.41 GHz at room temperature. It was designed for use inside the cryostat and the top flange is sealed off for evacuation purposes by means of a mica sheet. The cavity arm is evacuated in order to reduce condensation which otherwise disturbs the tuning of the sample cavity at low temperatures.

A Princeton Applied Research model HR-8 lock-in-amplifier was used to obtain a modulation field of 100 Hz and 100 kHz. The modulation amplitude is adjusted to give a good representation of the desired derivative of absorption curves.

The field modulation coils of 100 Hz are rigidly mounted on the magnet pole pieces. Each coil is 90 turns of number 12 insulated copper wire embedded in varnish. This is done to reduce the vibrations of the coils at large magnetic fields. The field modulation coil of 100 KHz is one turn of insulated wire around the cavity.

The crystal detector demodulates the microwave power which is transfered by coaxial cable to the lock-in-amplifier. The resulting dc output from the lock-in-amplifier is plotted on a Moseley model 7005AM X-Y recorder. The X-axis is driven by a fraction of the signal provided by the "X-axis drive" of the Varian Fieldial Mark II magnet controller, which is used to regulate and sweep the magnetic field. The Y-axis is driven by the output of the lock-in-amplifier, thus yielding a plot of the derivative of absorption versus magnetic field.

IV.2 The Magnetic Field and its Measurement

An electromagnet model Varian V-3900 with 12 inch pole pieces was used to provide a magnetic field up to 13 kG across a 3 inch gap. The magnetic field was controlled by a Fieldial Mark II power supply, with sweep ranges from 0.25 G to 40 kG and sweep times of 0.50 min to 100 min. The magnetic field was measured using an NMR oscillator model Bruker B-NM 20, with the sensitivity of 0.001 gauss. Since the position of magnet probe was slightly different from the position of samples, a calibration curve was used to obtain the actual magnetic field which the samples experinced. However, in all the EPR measurements presented in this thesis, a small amount of diphenyl picryl hydrazl (d.p.p.h.) for which $g = 2.0036 \pm .0002$, was used as a reference to check the accuracy of resonant frequency and the magnetic field values.

IV.3 Low Temperature Appuratus and Temperature Measurements.

Full description of the metallic variable temperature cryostat, is given in Ref. 6. It was constructed in the Concordia faculty of arts and science workshop, and is similar to many commercially available units.

The temperature was controlled by an Artronix model 5301 temperature controller capable of control over a range of 1.0 K to 320 K. Two temperature sensors are mounted in the brass flange above the sample cavity. A germanium resistor is calibrated from 1.5 to 37.1 K with an error of 0.95% and a platinum resistor from 30 to 300 K with an error of 0.75%. The temperature was controlled by a 100 ohm heating resistor mounted beside the cavity.

CHAPTER V

EXPERIMENTAL DETAILS

V.1 Experimental Results

In order to simplify the discussion of experimental results due to the large number of samples investigated, we classify the samples according to the similarity of their molecular and/or crystal structures. The crystal structure, the details of the EPR spectra, and spin Hamiltonian parameters for each class are given at the same time.

V.1.1 Mn2+:

a. $ZnK_2(SO_4)_2.6H_2O$ and $NiK_2(SO_4)_2.6H_2O$.

Zinc potassium sulfate hexahydrate (hereafter ZPSH), and nickel potassium sulfate hexahydrate (hereafter NPSH), belong to the monoclinic symmetry[7], with space group $P2_1/a$ (C_{2h}^4). The unit cell contains two formula units. Six water molecules form an octahedron around the divalent metal ion. The unit cell dimensions are a = 8.98 Å, b = 12.22 Å, c = 6.10 A, and β is equal to 105°.

Single crystals of Mn2+-doped ZPSH and NPSH were grown by slow evaporation at room temperature of solutions of ZPSH and NPSH, each containing 0.1 weight% $MnSO_4.H_2O$. In order

to avoid sample demagnetization effects (see Sec. V.4) at low temperatures, in the paramagnetic lattices , spheres of 1-2 mm diameter of NPSH sample were prepared by blowing the roughly cubic single crystals on emery paper.

EPR spectra of Mn^{2+}-doped single crystals of ZPSH and NPSH were recorded at room, liquid-nitrogen and liquid-helium temperatures.[8] For the ZPSH host two sets of spectra corresponding to two inequivalent Mn^{2+} ions in the unit cell were observed. For each, along their respective Z and X axes, (Z, X, Y axes as mentioned in chapter II are the principal axes of b_2^0 tensor, so the overall splitting of EPR spectra is maximum along the Z and minimum along the Y axis[9]), 30 distinguishable hyperfine lines, plus some,forbidden lines appearing mostly near the central fine transition $-1/2 \leftrightarrow 1/2$, were observed. Along the Y axis, the number of overlapped lines was increased and only 24 lines appeared. The feature of the spectra remained the same at all temperatures, however, the overall splitting increased on lowering the temperature. The angular variation of spectra for ZPSH is shown in figure (V.1).

In the case of spherical crystals of NPSH also two sets of spectra were observed corresponding to the two magnetically inequivalent sites for the Mn^{2+} ions. At room temperature, while all the 30 hyperfine lines (corresponding to an inequivalent site) were observable for magnetic field orientation along the X-axis, or within an angle of 10 from

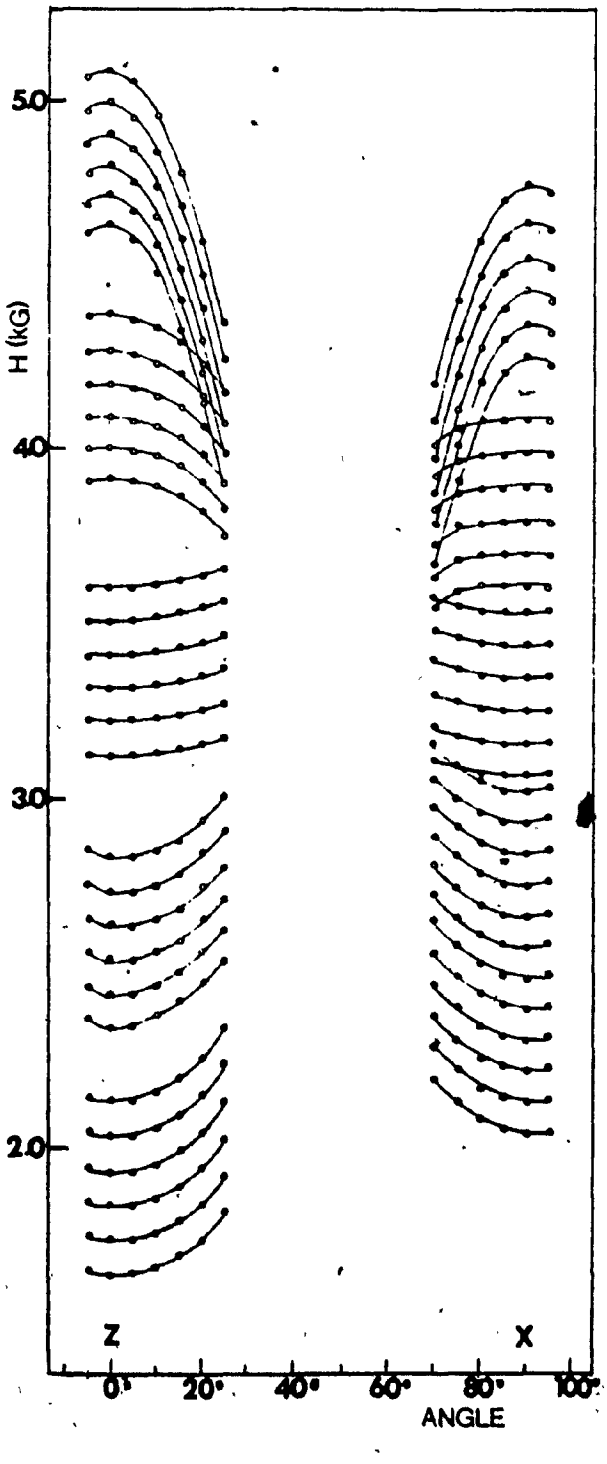

Fig. (V.1). The angular variation of EPR spectra for ZPSH

it, fewer lines were observed for the magnetic field orientation away from the X axis. For orientation of the magnetic field along or near the Z-axis, only 6 or 7 lines at lower magnetic field were observed. As the temperature was lowered from room to liquid-helium temperature, the situation remained the same insofar as the observation of the resonant lines is concerned.

The spin Hamiltonian appropriate to present samples of monoclinic symmetry is[3]

$$\mathcal{H} = \mu_B \vec{H} \cdot \tilde{g} \cdot \vec{S} + \sum_{m=0,2} \frac{1}{3} b_2^m \, O_2^m + \sum_{m=0,2,4} \frac{1}{60} b_4^m \, O_4^m + A \, S_x \, I_x + Q' \left[I_z^2 - \frac{1}{3} (I+1) \right] + Q'' (I_x^2 + I_y^2) \qquad (V.1)$$

the notations are as defined in chapter II.

EPR measurements on a Mn^{2+}-doped single crystal of ZPSH, have been previously reported by Kasthurirengan and Navalgund[10] at room temperature and those on Mn^{2+}-doped NPSH by Upreti[11] at room temperature, and by Misra and Jalochowski[12] at room and low temperatures (the shape of the host crystal used, was arbitrary, thus being susceptible to demagnetization effects at low temperatures.)

The values of the parameters obtained here for ZPSH are significantly different from those reported in Ref. 10.

The fourth-order parameters, neglected in Ref. 10 are found to have small, but significant values. The absolute sign of b_2^0 determined from relative intensities of lines at liquid helium temperature, is negative, since the intensity of the highest-field sextet decreased relative to that of the lowest-field sextet as the temperature was lowered to liquid-helium temperature. The values of the S.H.P. for NPSH and ZPSH samples evaluated in the present work, are given in tables 1 and 2 at various temperatures, and the parameters at room temperature, as reported in Ref. 10, have also been included in table 1 for comparison.

b. $MgSO_4.7H_2O$ and $NiSO_4.7H_2O$.

The isostructural crystals of magnesium sulphate heptahydrate (hereafter MSO) and nickel sulphate heptahydrate (hereafter NSO) have a unit cell of orthorhombic symmetry[13], containing four formula units related to each by the operation of the space group $P2_12_12_12_1$ Each Ni^{2+}, or Mg^{2+}, ion is surrounded by a distorted octahedron of six water molecules. The seventh water molecule is not coordinated with the Ni^{2+}, or Mg^{2+}, ion but instead fills what would otherwise be a hole in the structure. The unit cell dimensions are for MSO a = 11.91 Å, b = 12.01 Å and c = 6.87 Å, and for NSO a = 11.86 Å, b = 12.08 Å, and c = 6.81 Å. The four Mg^{2+} or Ni^{2+}, sites in the unit cell are magnetically inequivalent.

TABLE 1. Values of S.H.P. for Mn^{2+} -doped ZPSH host. n is the number of data points used in each fitting. The S.H.P. are expressed in units of GHz. A negative sign has been assumed for the value of A.

Temperature	295 K	85 K	5 K	295 K *
g_{zz}	1.996 ± .001	2.001 ± .001	2.002 ± .001	2.016
g_{xx}	1.999 ± .001	2.021 ± .001	2.013 ± .001	2.016
b_2^0	-1.068 ± .002	-1.315 ± .002	-1.359 ± .002	0.730
b_2^2	0.504 ± .005	0.528 ± .005	0.489 ± .005	0.605
b_4^0	0.018 ± .001	0.019 ± .001	0.021 ± .001	---
b_4^2	-0.014 ± .023	0.002 ± .025	-0.225 ± .025	---
b_4^4	0.011 ± .023	0.047 ± .023	-0.133 ± .026	---
Q'	-0.021 ± .006	-0.015 ± .006	0.002 ± .006	0.004
Q"	-0.058 ± .011	-0.040 ± .001	0.015 ± .011	0.025
A	-0.265 ± .004	-0.259 ± .004	-0.258 ± .004	-0.244
B	-0.269 ± .004	-0.264 ± .004	-0.260 ± .004	-0.246
n	287	297	232	--

* Ref. 10

TABLE 2. Values of spin Hamiltonian parameters of spherical sample for Mn^{2+}-doped NPSH host (0.1%). Other details and notations are the same as those given in the caption of Table 1.

Temperature	295 K	5K	1.8 K
g_{zz}	2.058 ± .002	2.017 ± .002	2.024 ± .002
g_{xx}	2.025 ± .002	1.991 ± .002	1.974 ± .002
b_2^0	-0.750 ± .026	-1.198 ± .025	-1.260 ± .023
b_2^2	0.564 ± .025	0.432 ± .022	0.395 ± .021
b_4^0	0.300 ± .068	0.125 ± .083	0.111 ± .082
b_4^2	0.910 ± .236	0.454 ± .300	0.342 ± .300
b_4^4	0.153 ± .047	0.200 ± .079	0.125 ± .076
Q'	0.009 ± .001	0.001 ± .001	-0.001 ± .001
Q''	-0.003 ± .030	0.014 ± .030	0.042 ± .030
A''	-0.275 ± .004	-0.115 ± .004	-0.169 ± .004
B	-0.232 ± .004	-0.228 ± .004	-0.228 ± .004
n	149	160	160

Single crystals of Mn^{2+}-doped MSO and NSO were grown by slow evaporation at room temperature of solutions of MSO and NSO respectively, each containing amount of 0.1 weight % of manganese sulphate.

EPR spectra of Mn^{2+} doped MSO were recorded for various orientation of external magnetic field in the ZX plane at room, liquid-nitrogen, and liquid-helium temperatures.[14] An overlap of EPR spectra corresponding to four magnetically inequivalent sites was observed. For each inequivalent Mn^{2+} ion, along its Z axis, five well-separated sets of fine structure lines ($\Delta M = \pm 1$) appeared, each set being split into six hyperfine lines ($\Delta m = 0$). The intensities of the lines around the centre of the spectrum are almost symmetric, and the linewidth remains the same throughout the spectrum. Figure (V.2) exhibits the angular variation of the spectrum corresponding to one inequivalent site at room temperature.

EPR spectra for spherical crystals of Mn^{2+}-doped NSO were also recorded at room, liquid nitrogen, and liquid-helium temperatures.[14] The feature and angular variation of the EPR spectra are the same as those for MSO. However, there are differences in the linewidths and intensities as caused by the presence of paramagnetic Ni^{2+} ion in the NSO lattice (see Sec, V.3).

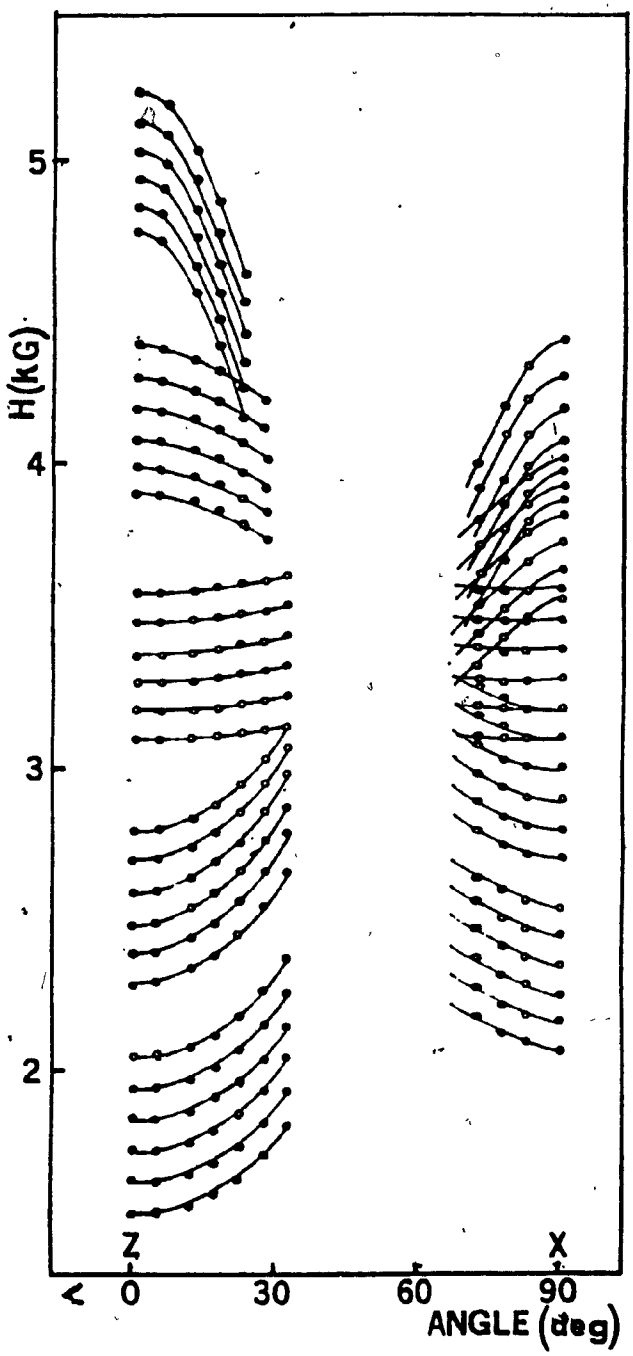

Fig. (V.2) The angular variation of EPR spectra for MSO

The spin Hamiltonian appropriate to the orthorhombic symmetry is the same as given by Eq. (V.1).[3]

The S.H.P. of Mn^{2+}-doped single crystals of MSO at room temperature have been reported by Janakiraman and Upreti[15] and Hayashi and Ono.[16] On the other hand, Bramley and Starch,[17] estimated the S.H.P. of Mn^{2+} in this crystal at room temperature from zero magnetic field resonance (ZFR). EPR measurements on Mn^{2+}-doped single crystals of NSO have been previously reported by Misra and Mikoljczak[18] at room and low temperatures for the sample with arbitrary shapes.

The S.H.P. evaluated in this work for MSO and NSO are presented in tables 3 and 4. The absolute sign of b_2^0 was found to be negative, for both the samples, since the intensity of the highest-field sextet relative to lowest-field sextet along the Z axis, was found to be 1.10, 1.08, 0.30 at 295, 85 and 3 K respectively for MSO and 0.43, 0.41, and 0.10 at 295, 85, and 2 K respectively for NSO, i.e. it decreases considerably at liquid helium temperature. The parameters as reported by the other researchers for MSO, have also been included in table 3 for comparison.

c. $Mg(CH_3COO)_2.4H_2O$ and $Ni(CH_3COO)_2.4H_2O$.

Temperature	295 K	85 K	3 K	Ref. 15	Ref. 16
g_{zz}	2.002 ±.002	1.996 ±.002	2.006 ±.002	2.003 ±.005	2.000 ±.005
g_{xx}	1.968 ±.002	1.998 ±.002	1.963 ±.002	-	-
b_2^0	-1.118 ±.002	-1.241 ±.002	-1.292 ±.002	1.154 ±.014	1.200
b_2^2	0.367 ±.005	0.254 ±.007	0.670 ±.007	0.266 ±.028	≈0.000
b_4^0	0.004 ±.001	0.006 ±.001	0.007 ±.001	-	-
b_4^2	-0.203 ±.023	-0.590 ±.038	-0.173 ±.047	-	-
b_4^4	0.243 ±.-27	0.430 ±.044	0.336 ±.049	-	-
Q'	-0.018 ±.006	-0.003 ±.039	-0.013 ±.012	-	-
Q''	-0.017 ±.012	-0.005 ±.114	-0.011 ±.032	-	-
A	-0.268 ±.004	-0.276 ±.004	-0.277 ±.004	-0.258 ±.014	0.265
B	-0.267 ±.004	-0.258 ±.004	-0.271 ±.004	-0.244 ±.028	-
n	217	155	155	--	--

TABLE 3. S.H.P. of Mn^{2+}-doped MSO host (0.1%). For details see caption of Table 1.

TABLE 4.

Values of the spin Hamiltonian parameters for the spherical sample of Mn^{2+}-doped NSO host (0.1%). Other details and notations are the same as those given in the caption of Table 1.

Temperature	295K	85K	2K
g_{zz}	1.970 ±.002	2.015 ±.002	1.995 ±.002
g_{xx}	1.979 ±.002	1.985 ±.002	1.999 ±.002
b_2^0	-1.257 ±.002	-1.535 ±.003	-1.595 ±.002
b_2^2	0.383 ±.010	0.520 ±.009	0.321 ±.007
b_4^0	-0.003 ±.002	-0.009 ±.002	-0.004 ±.002
b_4^2	0.014 ±.040	0.002 ±.041	-0.799 ±.036
b_4^4	0.012 ±.045	0.159 ±.049	-0.448 ±.033
Q'	-0.002 ±.014	-0.009 ±.010	0.014 ±.013
Q''	-0.026 ±.030	-0.027 ±.020	-0.007 ±.035
A	-0.265 ±.004	-0.272 ±.004	-0.264 ±.005
B	-0.262 ±.005	-0.254 ±.006	-0.265 ±.005
n	192	232	141

The crystal structure of nickel acetate tetrahydrate (hereafter NiATH) and magnesium acetate tetrahydrate (hereafter MgATH) were determined by Van Niekerk and Schoening[19] and Shanker et al.[20] respectively. These crystals are monoclinic with space group $P2_1/c$, having indentical unitcell dimensions. There are two formula units in the unitcell of dimension: a = 4.75 Å, b = 11.77 Å, c = 8.44 Å, and $\beta = 93^{\circ}36'$. The nickel or magnesium atoms (indicated below as M) see exactly the same site symmetry, and are surrounded octahedrally by four water molecules and by two oxygen atoms, which belong to two different acetate groups as follows:

$d_{M - O_1} = 2.12$ A, $\quad \angle(O_1 - M - H_2O(1)) = 90\ 44$

$d_{M - H_2O(2)} = 2.06$ A, $\quad \angle(O_1 - M - H_2O(2)) = 90\ 33$

$d_{M - H_2O(2)} = 2.06$ A, $\quad \angle(H_2O(1) - M - H_2O(2)) = 88\ 03$,

Single crystals of Mn^{2+}-doped NiATH and MgATH were grown by slow evaporation at room temperature of 0.1 weight % solution of $Mn(CH_3COO)_2.4H_2O$ in nickel acetate tetrahydrate and magnesium acetate tetrahydrate respectively. Spheres of 1-2 mm diameter of paramagnetic lattice NiATH were prepared by the same method as described above for NPSH.

EPR measurements on Mn^{2+}-doped single crystal of MgATH were reported presiously by Manakkil[21], at room temperature only. The measurements reported in this thesis were

performed at room, liquid-nitrogen and liquid-helium temperatures.[22] The EPR spectra for the external magnetic field orientation in ZX plane, revealed the existence of two inequivalent ions. Thirty well-resolved transition lines belonging to one inequivalent ion were observed along both the Z and X axes. The other inequivalent ion had exactly the same spectra, except for a different orientation of its X,Y,Z axes. The overall splitting of the spectra increased as the temperature was lowered.

The EPR spectra on Mn^{2+}-doped NiATH were also recorded at room, liquid nitrogen and liquid helium temperatures at ZX plane. (The EPR measurements on this sample were proviously reported by Janakiraman and Upreti[23] at room temperature, while Misra and Jalochowski[21] reported their measurements at room and low temperatures on a sample of arbitrary shape.)

In the present report, the paramagnetic NiATH sample was prepared in spherical shapes in order to avoid the demagnetization effect at low temperatures. The features of the spectra and angular variation of resonant lines at room temperature were the same as those for the MgATH host (except for the linewidths, see Sec.V.3). The spectra at 85 K and 1.8 K had the same angular variation pattern as at room temperature, with the following differences insofar as the observation of resonant line positions is concerned. While at room temperature almost all the 30 hyperfine lines

were observed at all magnetic field orientations, at 85 K all the 30 hyperfine lines were observed only for the magnetic field orientation within an angle of 30° from the Z axis in the ZX plane. For the orientation of the external field along the X-axis, or within 20° from it, only the lowest-field six hyperfine lines were observed. As the temperature was lowered to liquid-helium temperature (1.8 K), the lines were harder to observe, only the lowest-field 24 hyperfine lines were observed for magnetic field orientation along the Z-axis, or within an angle of 10° from it, while along the X-axis, and within 10° from it (in the ZX plane), only the lowest six hyperfine lines were observed.

The spin Hamiltonian appropriate to the orthorhombic symmetry[3] has the same form as that given by Eq. (V.1).

The list of the S.H.P. for MgATH and NiATH at different temperatures are given in Table 5 and 6. The values of these parameters for the MgATH host are found to be significantly different from those reported proviously.[21] The ratio of the average intensity for the highest-field sextet to that of the lowest one for the external maghetic field orientation along the Z axis for MgATH host, was 0.8, 0.8 and 2.4 at 298, 85, and 2.5 K respectively, while, for NiATH it was, 0.24, 0.56 and 1.7 at 298, 85 and 1.8 respectively. Thus the absolute sign of b_2^0 is positive for both the samples, as the intensity of the highest-field

TABLE 5.

Values of spin-Hamiltonian parameters for the Mn^{2+}-doped MATH host (0.1%). Other details and notations are the same as those given in the caption of Table 1.

Temperature	295 K	85 K	2.5 K
g_{zz}	1.996 ± .002	2.019 ± .002	1.952 ± .002
g_{xx}	1.993 ± .002	2.005 ± .002	1.981 ± .002
b_2^0	1.160 ± .002	1.257 ± .002	1.350 ± .002
b_2^2	-0.350 ± .006	-0.594 ± .006	-0.450 ± .006
b_4^0	0.017 ± .002	0.047 ± .002	0.017 ± .002
b_4^2	-0.017 ± .012	-0.332 ± .026	-0.036 ± .019
b_4^4	-0.071 ± .027	-0.318 ± .028	-0.181 ± .023
Q'	0.016 ± .006	-0.001 ± .016	0.018 ± .006
Q"	0.048 ± .011	-0.009 ± .047	0.053 ± .010
A	-0.250 ± .004	-0.263 ± .004	-0.258 ± .004
B	-0.243 ± .004	-0.259 ± 0.004	-0.255 ± .004
n	270	256	250

TABLE 6.

Values of spin-Hamiltonian parameters for the Mn^{2+}-doped NATH host (0.1%). Other details and notations are the same as those given in the caption of Table 1.

Temperature	295 K	85 K	1.8 K
g_{zz}	1.959±.002	1.960±.002	1.948±.002
g_{xx}	1.971±.002	2.007±.002	1.959±.002
b_2^0	1.272±.003	1.341±.003	1.430±.003
b_2^2	-0.356±.009	-0.298±.009	-0.283±.009
b_4^0	0.016±.002	0.023±.002	0.010±.002
b_4^2	-0.239±.030	-0.200±.046	0.050±.047
b_4^4	-0.099±.041	-0.707±.129	-0.505±.054
Q'	0.001±.008	0.030±.006	0.008±.008
Q''	0.047±.013	0.087±.010	0.026±.013
A	-0.264±.004	-0.268±.004	-0.259±.004
B	-0.250±.004	-0.273±.006	-0.269±.004
n	234	186	161

lines relative to the lowest-field lines increases at liquid helium temperature.

d. $Zn(CH_3COO)_2.2H_2O$

EPR measurements of Mn^{2+}-doped zinc acetate dihydrate (hereafter ZnADH) were reported proviously by Janaakirman and Upreti[24] at room temperature. The structure of ZnADH crystal was determined by Van Niekerk, at al[25]. The unit cell is of dimensions a = 14.50, b = 5.32, c = 11.02 Å and $\beta = 100^{\circ}\,0'$, it is monoclinic with space group C_2/c. There are four formula units in the unit cell, the zinc atoms lie on the two fold axis parallel to the b axis. (The site symmetries for all the zinc ions are exactly the same.) The six nearest neighbors of a zinc atom are four oxygen atoms (two pairs: O_1, and O_2) and two water molecules which form a distorted octahedron around the zinc atom. The ditances are, $d_{Zn} - O_1 = 2.18$ Å, $d_{Zn} - O_2 = 2.17$ Å and $d_{Zn} - H_2O = 2.14$ Å. Single crystals were grown by slow evaporation at room temperature of a solution of zinc acetate dihydrate containing 0.1% (by weight) of manganese acetate in distilled water.

EPR spectra for ZnADH reported in this thesis were measured[22] at room, liquid nitrogen and liquid helium temperatures for the magnetic field orientation in the ZX and XY planes. With $\vec{H}$ parallel to either the Z or the X

axis, clearly-resolved 30 allowed hyperfine lines ($\Delta M=\pm 1$ and $\Delta m=0$) were observed, indicating that all Mn^{2+} ions are magnetically equivalent. At liquid-nitrogen and liquid helium temperatures the spectra showed the same angular variation as at room temperature. As the temperature was lowered the overall splitting increased and at liquid helium temperature the five sextets were completely seperated. The last sextet of the spectrum was observed down to 11K, but below this temperature the intensity of these lines diminished rapidly and at 5 K these disappeared completely. The angular variation of EPR spectrum of Mn^{2+} ion in ZnADH is shown in Fig. (V.3). The evaluated (S.H.P.) fitted to the spin Hamiltonian of Eq. (V.1), which is appropriate to monoclinic symmetry[3], are tabulated in Table 7. The parameters estimated by other researchers[24] are also given for comparison. The absolute sign of b_2^0 was found to be negative, since the ratios of the intensity for the highest-field sextet to that of lowest one for the external magnetic field orientation along the Z-axis, were 3.7, 3.6 and 1.5 and 0.0 at 298, 85, 11 and 3.5 K respectively, i.e. The intensity of the highest field lines relative to that of the lowest field lines decreased at liquid helium temperature. The values of (S.H.P.) of Mn^{2+} in this sample were found to be significantly different from those reported previously,[24] pertticularly the fourth-order parameters b_4^m corresponding to cubic symmetry.

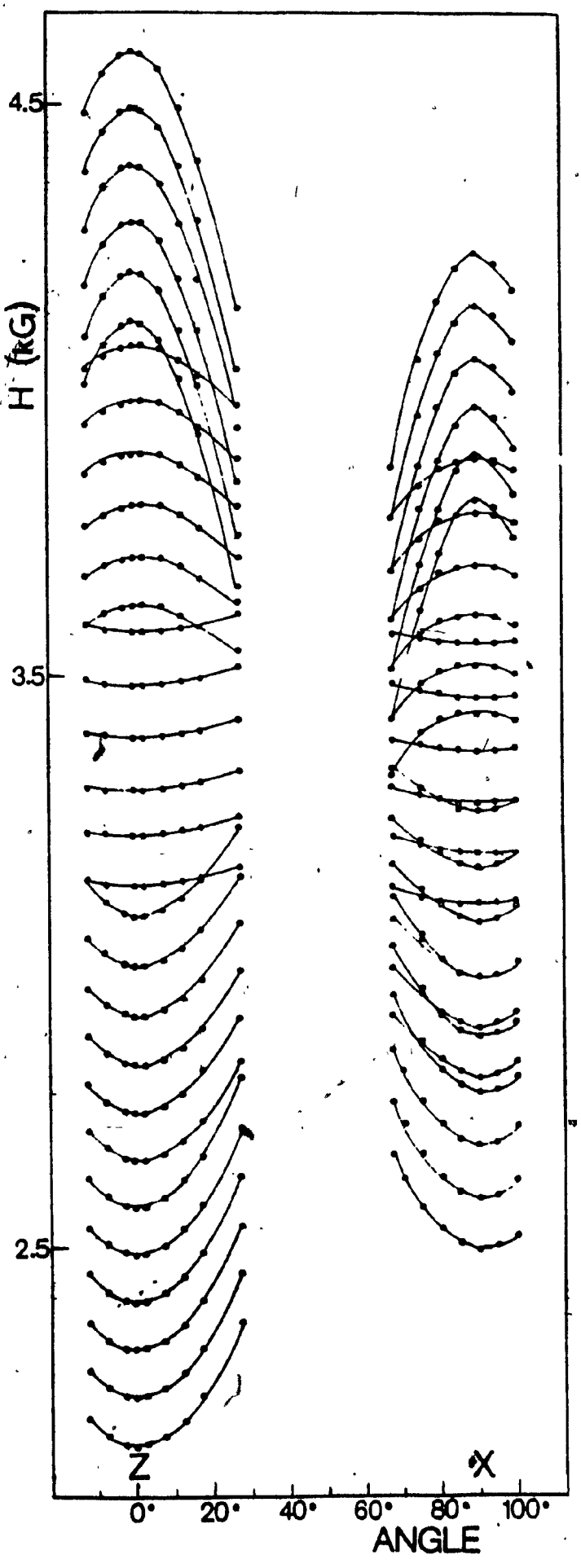

Fig. (V.3) The angular variation of EPR spectra for ZADH.

TABLE 1 (continued)

Temperature	295 K	85 K	11 K	Ref. 1 (RT)
g_{zz}	2.000 ± .001	2.027 ± .001	2.031 ±.001	2.001 ± .001
g_{xx}	2.001 ± .001	2.023 ± .001	2.013 ±.001	2.001 ± .001
b_2^0	-0.702 ± .002	-0.941 ± .002	-1.037 ±.002	0.694 ± .001
b_2^2	0.202 ± .002	0.436 ± .002	0.566 ±.002	-0.214 ± .004
b_4^0	0.000 ± .001	0.00 ± .001	0.002 ±.001	---
b_4^2	0.037 ± .013	0.013 ± .013	0.026 ±.013	---
b_4^4	0.054 ± .013	0.036 ± .015	0.134 ±.038	---
Q'	0.005 ± .002	0.002 ± .001	-0.003 ±.001	0.001
Q"	0.021 ± .009	0.30 ± .010	0.008 ±.004	0.013
A	-0.251 ± .002	-0.254 ± .002	-0.247 ±.003	-0.251 ± .001
B	-0.252 ± .002	-0.257 ± .002	-0.244 ±.004	-0.251 ± .001
n	272	262	218	

TABLE 7. Values of S.H.P. for Mn^{2+}-doped ZnADH host (0.1%).

For more details see caption of Table 1.

e. $MgSiF_6 \cdot 6H_2O$

EPR measurements on Mn^{2+}-doped single crystal of magnesium fluorosilicate hexahydrate (hereafter MFS) at room temperature have been proviously reported by Arakawa.[26] The latest crystallographic studies[27,28] indicate that below 300 K the crystal lattice of MFS is described by the space group $P2_1/c$ (monoclinic) while at temperatures higher than 300 K it is described by $R\bar{3}m$ (hexagonal). The phase transition between the two symmetries takes place at about 300 K. Thus, for all the temperatures (from room to liquid helium temperature) for which EPR measurements are described in this thesis, the crystal is in monoclinic phase, for which the crystal data are: a = 6.460±.005 Å, b = 9.524±.005 Å, c = 8.460±.005 Å, $\beta = 99^\circ 24' \pm 3'$ and Z = 2.[27]

The EPR data, as described below, are, however, apparently incompatible with the monoclinic symmetry. Upon close examination the data can, indeed, be understood to conform to the monoclinic symmetry if one takes into account the fact that the speciman used in Ref. 26, as well as in the present work, consists of three-fold twins of the low-temperature form[27] (the single crystals twin extremely easily). The explanation of the observed EPR spectra, described below, is, thus, valid provided that one understands by the trigonal axis, the pseudo-trigonal axis similar to that given for $FeSiF_6 \cdot 6H_2O$ by Hamilton.[29] In a projection along this pseudo-trigonal axis, the $\left[Mg(H_2O)_6\right]^{2+}$

ions are surrounded by SiF_6^{2-} ions with two different orientations.[27] This fact combined with the three-fold twinning of the sample used explains the appearance of six inequivalent Mn^{2+} ions as revealed by the EPR spectra (see below).

The samples were prepared by first dissolving calculated stoichiometric amounts of Mg metal in hydrofluosilicic acid ($H_2SiF_6.6H_2O$) and adding appropriate amount of $MnSiF_6.6H_2O$ solution (0.1 weight%) to the $MgSiF_6.6H_2O$ solution so obtained. The resultant solution was allowed to evaporate slowly till decent crystals were obtained.

EPR measurements of Mn^{2+}-doped MFS were recorded at room, liquid nitrogen and liquid helium temperatures for the magnetic field orientation in the ZX and XY planes.[30] The Z-axis was found to be parallel to the trigonal axis. The EPR measurements for external magnetic field orientation in ZX (parallel to trigonal axis) and XY (perpendicular to trigonal axis) planes, revealed the existence of six inequivalent Mn^{2+} ions. In particular, this was deduced from the following observations. (i) When the external magnetic field is nearly parallel to the trigonal axis in the ZX plane there is line splitting of the lowest field line. (ii) When the magnetic field orientation is in the XY plane, a plot of the lowest-field lines corresponding to the various inequivalent ions exhibits angular variation patterns of type $a - b\cos\{(2\phi + \delta_i)\}$, where

$(\delta_{i+1} - \delta_i) = 30$, $i = 1,2,3,4,5$, ϕ being the angle between the magnetic field and a fixed direction in the XY plane. Therefore, there are six sets of X and Y axes in the XY plane which have different orientations about the trigonal axis in equal interval of 30 . Figure (V.4) exhibits the angular variation of spectra (ZX plane) for an inequivalent Mn^{2+} ion at room temperature.

For any inequivalent Mn^{2+} ion, the spectra were fitted to the spin Hamiltonian in the form of Eq. (V.1). Table 8 contains the listing of the parameters at various temperatures. The g values are found to be less than or equal to the free-electron value, implying the absence of covalent bonding between the Mn^{2+} ion and the surrounding ligands.[21]

The ratio of the average intensity of the highest-field sextet to that for the lowest-field sextet, for the external field orientation along the Z axis, are observed to be 0.52, 0.63, 1.10, 1.11, 1.13 at temperatures 295, 85, 5, 3.5 and 2 K respectively. Thus the absolute sign of the parameter b_2^0 turns out to be positive, since the intensity of the highest-field line relative to the lowest-field line increases at liquid helium temperature.

f. Isomorphic Metal Hexakisantipyrine Perchlorate.

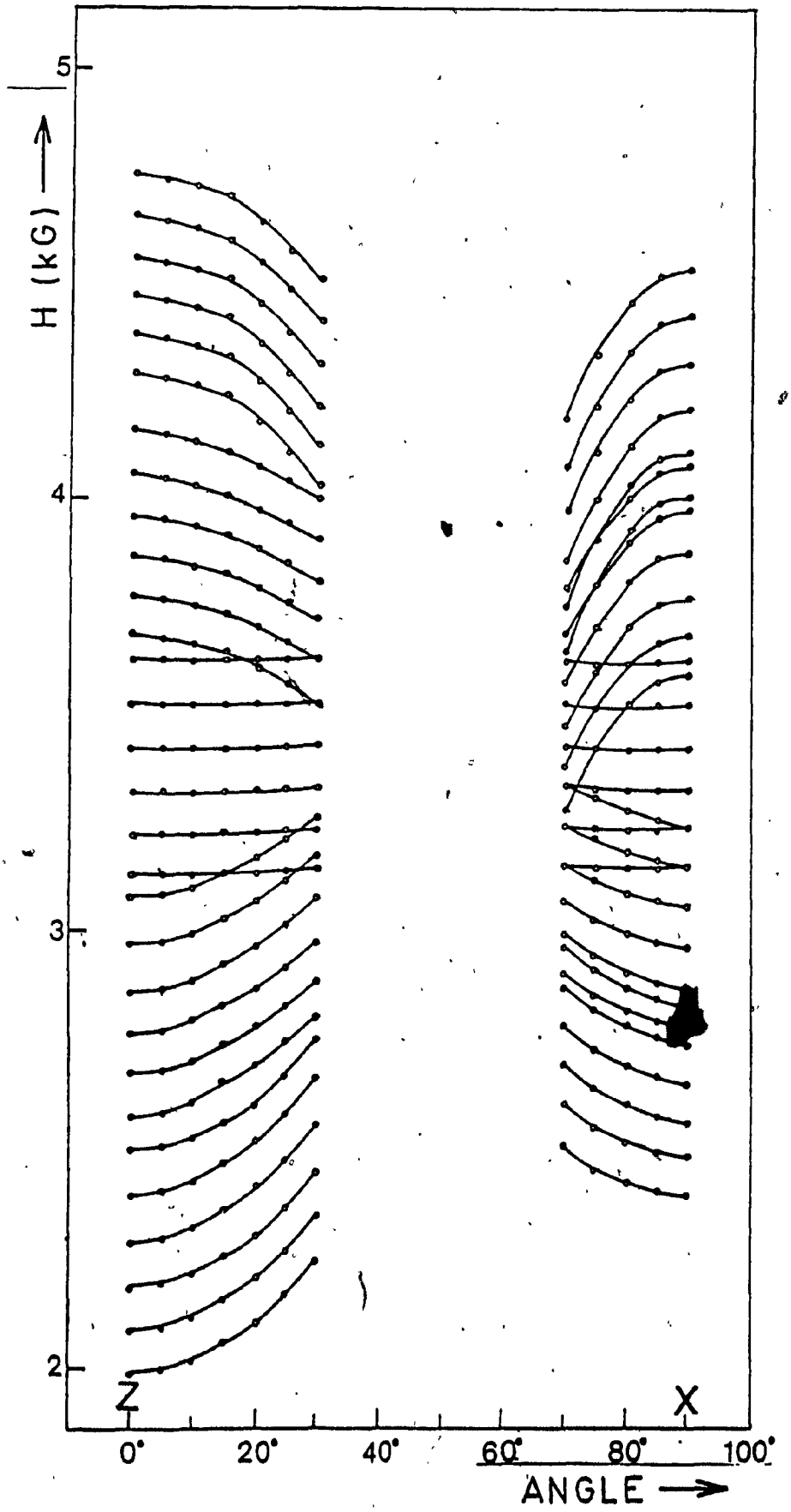

Fig. (V.4) The angular variation of EPR spectra for MFS.

Temperature	295 K	85 K	5 K
g_{zz}	1.962 ± .001	1.992 ± .001	2.000 ± .001
g_{xx}	1.959 ± .001	1.963 ± .001	1.962 ± .001
b_2^0	0.836 ± .003	0.787 ± .003	0.0788 ± .003
b_2^2	-0.235 ± .006	-0.350 ± .006	-0.401 ± .006
b_4^0	0.008 ± 0.002	0.010 ± .002	0.015 ± .002
b_4^2	-0.183 ± 0.031	-0.577 ± .028	-0.279 ± .030
b_4^4	-0.245 ± 0.032	-0.147 ± .030	-0.353 ± .030
Q'	0.021 ± .008	0.015 ± .007	0.022 ± .008
Q"	0.034 ± .013	0.044 ± .011	0.030 ± .013
A	-0.278 ± .004	-0.284 ± .004	-0.276 ± .004
B	-0.257 ± .004	-0.249 ± .004	-0.251 ± .004
n	250	267	255

TABLE 8. Values of S.H.P. for Mn^{2+}-doped MFS. For more details see caption of Table 1.

The crystal structure of (isomorphous) divalent metal hexakisantipyrine perchlorate (hereafter metal HKAP), $M(C_{11}H_{12}ON_2)_6(ClO_4)_2$ (M stands for divalent metals), has been reported by Vijayan and Viswamitra.[31] According to them, there is one formula unit per unit cell, and the crystal is characterized by the space group symmetry P3, all metal HKAP having almost identical lattice dimensions of a = 14 Å and c = 10 Å. Each divalent metal ion is surrounded by six antipyrine oxygen atoms in the form of a slightly distorted octahedron.

Mn^{2+}-doped metal HKAP crystals with well-developed hexagonal faces were obtained by adding 0.1 weight% of divalent manganese perchlorate hexahydrate, to a solution consisting of stoichiometric amounts of antipyrine (1-phenyl1-2,3-dimethyl-5-pyrazolone) and metal perchlorate and letting the solution to evaporate slowly at room temperature.

EPR studies of Mn^{2+}-doped divalent metal hexakisantipyrine perchlorate have been reported by Woltermann and Wasson.[32] These measurements were performed at room temperature, and the spin Hamiltonian parameters were evaluated using perturbation expressions.

In the present work EPR spectrum for Mn^{2+}-doped metal HKAP (metal M = Ca,Cd,Mg,Co and Pb) hosts were recorded at room temperature, for the magnetic field orientations in the

ZX and XY planes.[33] For the magnetic field orientation along the Z- and X-axes only 22 allowed hyperfine lines (instead of the expected 30 lines) appeared for all the crystals since many lines overlapped due to the rather small value of the zero-field splitting parameter b_2^0. The features of the EPR spectra are the same for all the hosts, except that the overall splitting of the spectrum for the external-field orientation along the Z-axis changes from host to host, being maximum for Mg and minimum for Pb.

For calcium HKAP and cadmium HKAP samples, the EPR spectra were also recorded at liquid-nitrogen and liquid-helium temperatures. The features of the spectra at lower temperatures are the same as those at room temperature. For the magnetic field orientation along the Z-axis measurements were also made, in temperature steps of 10 K, between room to liquid helium temperature. The overall splitting increased slowly with the decrease of the temperature, such that at liquid helium temperature, 24 hyperfine lines were clearly resolved as compared to 22 resolved lines at room temperature. For the magnetic field orientation in the XY plane the spectra remained invariant with respect to the orientation of the magnetic field at all temperatures.

For the magnetic field orientation along the Z-axis the intensities of the lines were found to be symmetric with respect to the center of the spectrum at room- and

liquid-nitrogen temperatures. However, at liquid helium temperature the lines belonging to the highest-field sextet had considerably smaller intensity relative to those belonging to the lowest-field sextet. This indicates that the sign of b_2^0 is negative. The room-temperature angular variation of EPR spectra for the magnetic field orintation in the ZX plane of calcium HKAP is displayed in Fig. V.5.

EPR measurements on Mn^{2+} and Cu^{2+}-doped calcium HKAP hosts were performed in the hope of estimating the Mn^{2+}-Cu^{2+} exchange interaction, similar to that for Mn^{2+}-Ni^{2+} (see Sec. V.4). EPR spectra of the Mn^{2+}-doped (Cu_xCa_{1-x})HKAP (x=0.05 and 0.50) were also recorded at room, liquid-nitrogen and liquid-helium temperatures in the ZX and XY planes. At room and liquid-nitrogen temperatures only one unresolved broad Cu^{2+} line was observed at lower magnetic field value, while for Mn^{2+} the spectra were found to be the same as those for the Mn^{2+}- doped calcium HKAP host, described above. However, at liquid-helium temeprature, besides the hyperfine lines of Mn^{2+} ion, four well- resolved hyperfine lines corresponding to Cu^{2+} (electron spin $S=\frac{1}{2}$, nuclear spin $I=\frac{3}{2}$) appeared. For the magnetic field orientation along the Z-axis these overlapped the Mn^{2+} lines. However, as the external magnetic field was rotated away from the Z-axis (for the Mn^{2+} ion) the Mn^{2+} and Cu^{2+} spectra moved in opposite directions, and at $\sim 45^{\circ}$ from the Z-axis the Cu^{2+} were quite distinct and at maximum

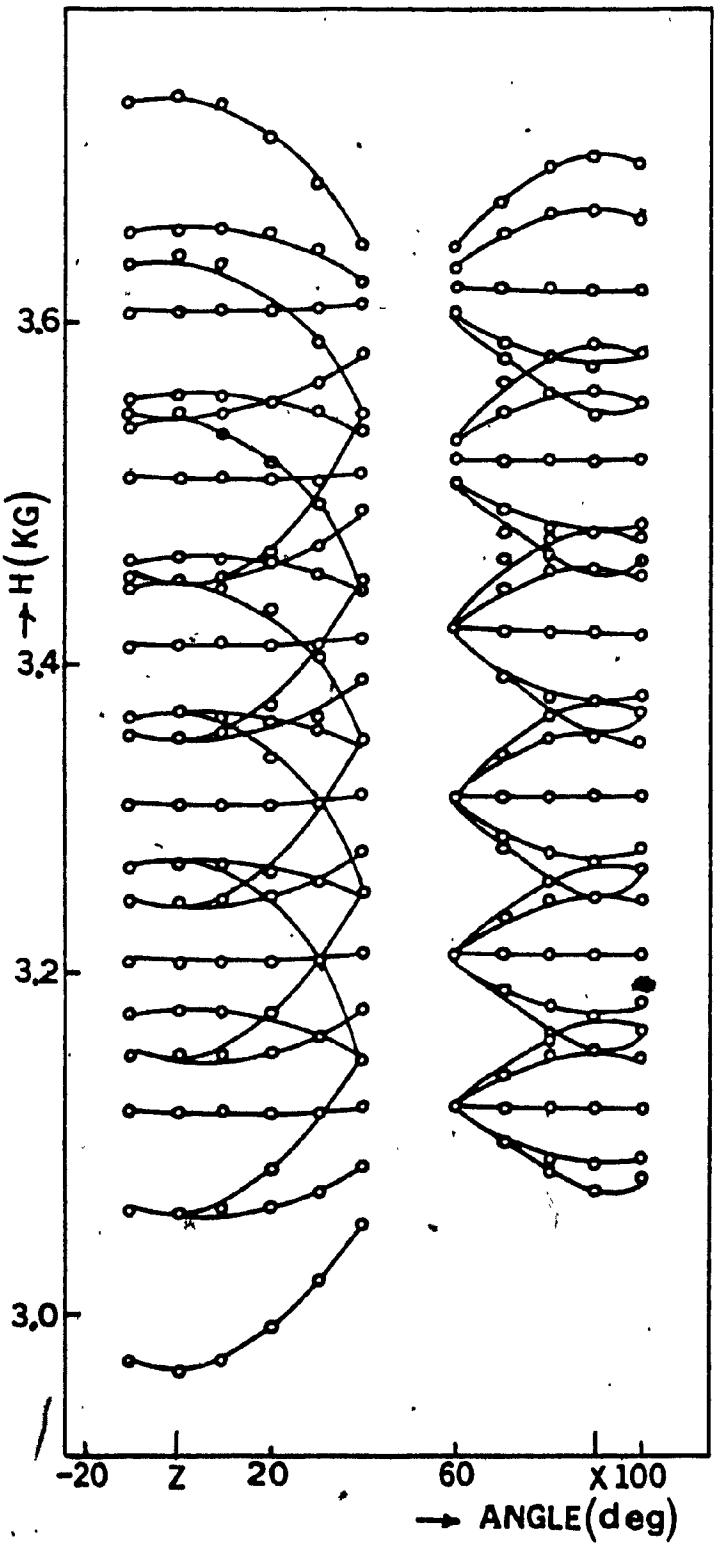

Fig.(V.5) The angular variation of EPR spectra for calcium HKAP.

distance from those for Mn^{2+}.

Attempts to observe the Mn^{2+} spectra for higher cocentration of Cu^{2+} ($\sim$0.5) in this crystal failed. As the concentration of Cu^{2+} was increased to 75%, the EPR lines of Mn^{2+} completely disappeared, and only Cu^{2+} spectra were observed.

The spin Hamiltonian appropriate to Mn^{2+} in axially symmetric site of metal HKAP host, can be expressed as:[3]

$$\mathcal{H} = \mu_B \vec{H} \cdot \tilde{g} \cdot \vec{S} + \frac{1}{3} b_2^0 O_2^0 + \frac{1}{60} (b_4^0 O_4^0 + b_4^4 O_4^4) + A S_x I_x$$

$$+ B(S_x I_x + S_y I_y) + Q' \left[I_z^2 - \frac{1}{3} I(I+1) \right] \qquad (V.2)$$

Here the Z-axis is the axis of symmetry. The absolute sign of b_2^0 was determined to be negative from the relative intensities of high and low field lines at liquid helium temperature. The resulting parameters of Mn^{2+} for the various hosts are given in Tables 9-13.

The most interesting variations of the parameters to be studied are those of b_2^0 and b_4^0 as a function of host metal-ion radius r in the isomorphous hosts metal HKAP. These variations for the room temperature values are shown in Fig. V.6. As is clearly seen, the b_2^0 and b_4^0 are approximately linear (except for cobalt HKAP host) with respect to r, b_2^0 decreases, while b_4^0 increases as the ionic radius increases. (The coblt HKAP lattice, being

Temperature	295 K	85 K	5 K
g_{zz}	2.0014 ± 0.0007	2.0051 ± 0.0007	2.0111 ± 0.0007
g_{xx}	2.0093 ± 0.0007	2.0121 ± 0.0007	2.0120 ± 0.0007
b_2^0	-0.0972 ± 0.0010	-0.1570 ± 0.0013	-0.1811 ± 0.0013
b_4^0	-0.0079 ± 0.0009	-0.0078 ± 0.0012	-0.0096 ± 0.0012
b_4^4	-0.0128 ± 0.0078	-0.0311 ± 0.0098	-0.0106 ± 0.0089
Q'	-0.0090 ± 0.0091	-0.0102 ± 0.0097	-0.0025 ± 0.0090
A	-0.2599 ± 0.0025	-0.2729 ± 0.0025	-0.2733 ± 0.0025
B	-0.2660 ± 0.0025	-0.2677 ± 0.0025	-0.2702 ± 0.0025
n	322	321	233

TABLE 9. Values of S.H.P. of Mn^{2+}-doped CaHKAP host. Other details as those given in the caption of Table 1.

Temperature	295 K	85 K	5 K
g_{zz}	2.0037 ± 0.0007	2.0044 ± 0.0007	2.0097 ± 0.0007
g_{xx}	1.9991 ± 0.0007	2.0080 ± 0.0007	1.9994 ± 0.0007
b_2^0	-0.0911 ± 0.0011	-0.1812 ± 0.0011	-0.2415 ± 0.0011
b_4^0	-0.0070 ± 0.0009	-0.0064 ± 0.0009	-0.0170 ± 0.0009
b_4^4	0.0062 ± 0.0076	0.0153 ± 0.0074	0.0436 ± 0.0057
Q'	-0.0158 ± 0.0080	-0.0035 ± 0.0106	-0.0069 ± 0.0060
A	-0.2570 ± 0.0020	-0.2547 ± 0.0020	-0.2515 ± 0.0016
B	-0.2617 ± 0.0020	-0.2514 ± 0.0020	-0.2496 ± 0.0020
n	321	318	270

TABLE 10. Values of S.H.P. for Mn^{2+}-doped Cd HKAP host. The other details are the same as those given in the caption of Table 1.

	PbHKAP	CoHKAP	MgHKAP
Temperature	295	295	295
g_{zz}	1.9981 ± 0.0007	2.0019 ± 0.0007	1.9985 ± 0.0007
g_{xx}	1.9932 ± 0.0007	1.9933 ± 0.0007	1.9980 ± 0.0007
b_2^0	-0.0216 ± 0.0010	-0.1194 ± 0.0010	-0.1385 ± 0.0010
b_4^0	-0.0096 ± 0.0010	-0.0087 ± 0.0010	-0.0058 ± 0.0010
b_4^4	-0.0122 ± 0.0075	-0.0207 ± 0.0075	-0.0269 ± 0.0075
Q'	-0.0074 ± 0.0180	-0.0025 ± 0.0180	-0.0042 ± 0.0130
A	-0.2615 ± 0.0020	-0.2638 ± 0.0020	-0.2693 ± 0.0020
B	-0.2615 ± 0.0020	-0.2623 ± 0.0020	-0.2659 ± 0.0020
n	298	330	330

TABLE 11. Values of S.H.P. for Mn^{2+}-doped metal HKAP hosts. Other details are as those given in caption of Table 1.

Temperature	295 K	85 K	5 K
g_{zz}	2.0049 ± 0.0007	2.0050 ± 0.0007	2.0130 ± 0.0007
g_{xx}	2.0021 ± 0.0007	1.9999 ± 0.0007	2.0110 ± 0.0007
b_2^0	-0.0893 ± 0.0010	-0.1900 ± 0.0013	-0.2200 ± 0.0017
b_4^0	-0.0078 ± 0.0009	-0.0094 ± 0.0012	-0.0055 ± 0.0013
b_4^4	0.0087 ± 0.0078	-0.0033 ± 0.0092	-0.0100 ± 0.0120
Q'	-0.0053 ± 0.0156	-0.0160 ± 0.0150	-0.0044 ± 0.0135
A	-0.2705 ± 0.0025	-0.2703 ± 0.0025	-0.2712 ± 0.0025
B	-0.2695 ± 0.0025	-0.2701 ± 0.0025	-0.2710 ± 0.0025
n	292	270	210

TABLE 12. Values of spin Hamiltonian Parameters of Mn^{2+}-doped $(Cu_{.05}Ca_{.95})$ HKAP host. Other details are the same as caption Table 1.

Temperature	295 K	85 K	5 K
g_{zz}	2.0018 ± 0.0007	2.0087 ± 0.0007	2.0119 ± 0.0007
g_{xx}	2.0066 ± 0.0007	2.0041 ± 0.0007	2.0023 ± 0.0007
b_2^0	-0.1016 ± 0.0010	-0.1679 ± 0.0013	-0.2428 ± 0.0017
b_4^0	-0.0062 ± 0.0009	-0.0080 ± 0.0012	-0.0064 ± 0.0012
b_4^4	-0.0099 ± 0.0081	0.0079 ± 0.0096	0.0117 ± 0.0124
Q'	-0.0056 ± 0.0128	-0.0056 ± 0.0118	0.0043 ± 0.0026
A	-0.2685 ± 0.0025	-0.2712 ± 0.0025	-0.2745 ± 0.0025
B	-0.2610 ± 0.0025	-0.2679 ± 0.0025	-0.2793 ± 0.0025
n	270	330	180

TABLE 13. Values of S.H.P. for Mn^{2+}-doped $(Cu_{.5}Ca_{.5})$HKAP host. Other details are the same as those given in the caption of Table 1.

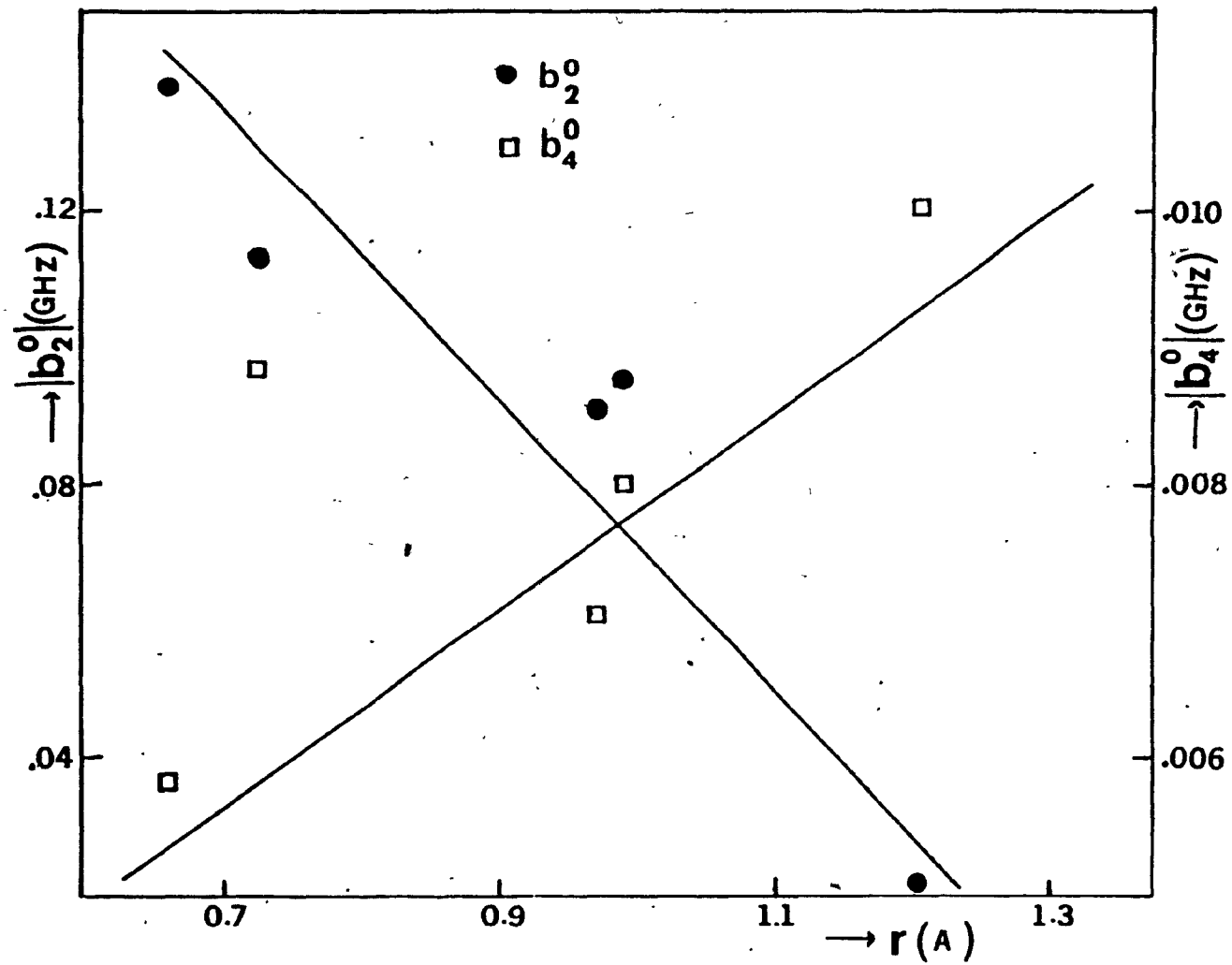

Fig. (V.6) Variation of the zero-field splitting parameters b_2^0 and b_4^0 for Mn^{2+}-doped metal HKAP lattices as a function of the host ion radius.

paramagnetic, might introduce modification in the values of b_2^0 and b_4^0 due to Mn^{2+}-Co^{2+} exchange interaction from those in corresponding diamagnetic lattices.) This linear behavier of b_2^0 can be understood on theoretical grounds. Hutchings[34] suggested that b_2^0 is proportional to $1/R^3$ where R is the metal-ligand distance. As the radius changes the distance between metal-ligand changes from R to R+d where d is the increment in the ionic radius, thus a Taylor-series expansion will give a linear dependence of b_2^0 on d. On the other hand, Watanabe[35] and Nicholson[36] have found that b_2^0 depends on the axial crystal field, as r increases the axial field potential, and consequently b_2^0 decreases.

As far as the variation of the parameter b_4^4 as a function of host metal-ion radius is concerned, no trend was found. It is to be noted that b_4^4 is very sensitive to local distortions.

g. $Co_{0.5}Zn_{0.5}SO_4.7H_2O$ and $Co_{0.5}Zn_{0.5}SiF_6.6H_2O$.

EPR in paramagnetic host is interesting because if the host paramagnetic ions do not completely widen out the probe EPR lines, one could study the host spin-lattice relaxation time via the linewidths of the probe ion. A system that satisfies this condition is offered by Mn^{2+} used as probe, while Co^{2+} constitute the paramagnetic host lattice. This is because Mn^{2+} has a very long spin-lattice relaxation

time, and Co^{2+} has a very short spin-lattice relaxation time, thus despite strong Mn^{2+}-Co^{2+} interaction one could observe reasonably sharp Mn^{2+} EPR lines.

On the other hand, one could dilute the paramagnetic lattice by substituting the paramagnetic ions by appropriate diamagnetic ions, e.g. replacing Co^{2+} by Zn^{2+}. In these dilute lattices it is possible to extend the temperature range over which well-resolved probe EPR lines can be observed.

EPR measurements on Mn^{2+} in 100% pure lattices of $CoSO_4.7H_2O$ and $CoSiF_6.6H_2O$ have been previously reported by Saraswat and Upreti[37] (at room and liquid nitrogen temperatures), and by Jayaram and Sastry[38] (at room and lower temperatures) respectively. The S.H.P. in both these reports were evaluated by the use of perturbation expressions.

The crystal structure of cobalt sulphate heptahydrate has not yet been reported. Preliminary and unpublished work of Ananathanarayanan[39] indicate that $CoSO_4.7H_2O$ belongs to monoclinic class, space group C_{2h}^6 or C_{2h}^5 having eight molecules per unit cell with a = 14.05, b = 12.85, c = 11.04 Å and $\beta = 105^\circ 24'$. However, EPR results of Bleaney et al.[40] in undiluted $CoSO_4.7H_2O$ crystals show the presence of two inequivalent Co^{2+} sites per unit cell. (This is consistent with the observed EPR spectra in the

present work.) Single crystals of $Co_{0.5}Zn_{0.5}SO_4.7H_2O$ (hereafter CoZnS), were grown at room temperature (295 K) by slow evaporation of a solution containing equimolecular amounts of $CoSO_4.7H_2O$ and $ZnSO_4.7H_2O$ containing 0.1% (by weight) of manganese sulphate. The growth habit , indeed, corresponds to those grown below 298 K (type I in Ref. 37).

$CoSiF_6.6H_2O$ and $ZnSiF_6.6H_2O$ crystals are isomorphous, possessing hexagonal symmetry[41] with a unimolecular rhombohedral unit cell of dimensions a = 6.297 Å, β = 96° 6′ for $ZnSiF_6.6H_2O$ and a = 6.260 Å, β = 96° 1′ for $CoSiF_6.6H_2O$. The space group is $R\bar{3}$ and, the corresponding trimolecular hexagonal cell would have the edges: a = 9.362, c = 9.965 Å for $ZnSiF_6.6H_2O$ and a = 9.330, c = 9.670 A for $CoSiF_6.6H_2O$. Single crystals of $Co_{0.5}Zn_{0.5}SiF_6.6H_2O$ (hereafter CoZnF) were grown at room temperature by slow evaporation of solution containing equimolecular amount of $CoSiF_6.6H_2O$ and $ZnSiF_6.6H_2O$ and 0.1 weight % of $MnSiF_6.6H_2O$.

EPR measurements on Mn^{2+} doped CoZnS and CoZnF were performed from room to liquid nitrogen temperature, in steps of 10 K.[42]

EPR spectra of CoZnS were recorded in the ZX plane. For the magnetic field $\vec{H} \parallel Z$, the features of the spectra were the same as those reported in Ref. 37 for the pure paramagnetic sample. The spectra indicate the presence of two magnetically inequivalent ions per unit cell. For $\vec{H} \parallel Z$

and $\vec{H} \parallel X$, for any inequivalent ion, the five well seperated hyperfine sextets for Mn^{2+} were observed. The Mn^{2+} spectra were further superimposed by a single broad line corresponding to Co^{2+} ions. Figure V.7 shows the angular variation of the EPR spectra corresponding to an inequivalent ion as a function of the external magnetic field.

For CoZnS, Mn^{2+} EPR spectra were recorded for $\vec{H} \parallel Z$ and $\vec{H} \parallel X$ in successive temperature intervals from room to liquid nitrogen temperature. The features of the spectra remained the same down to 200 K, in this temperature range the overall splitting increased slowly as the temperature decreased, while the hight of the lines decreased continuously. Below 200 K, the number of clearly resolved lines decreased, finally at 100 K only a few hyperfine lines were observed. Below 100 K, the hyperfine lines overlapped considerably, resulting into a few broad lines. Finally, at 77 K the hyperfine structure completely disappeared. Upon raising the temperature, the hyperfine structure was regained. Figure V.8 exhibits the temperature variation of the first and the last hyperfine line positions for $\vec{H} \parallel Z$. Comparing the present results with those reported in Ref. 37 for 100% cobalt host, it is seen that the spectra of Mn^{2+} at room temperature for the two samples are the same, however, as the temperature was lowered, the linewidths for CoZnS increased more slowly than in the host $CoSO_4.7H_2O$.[37]

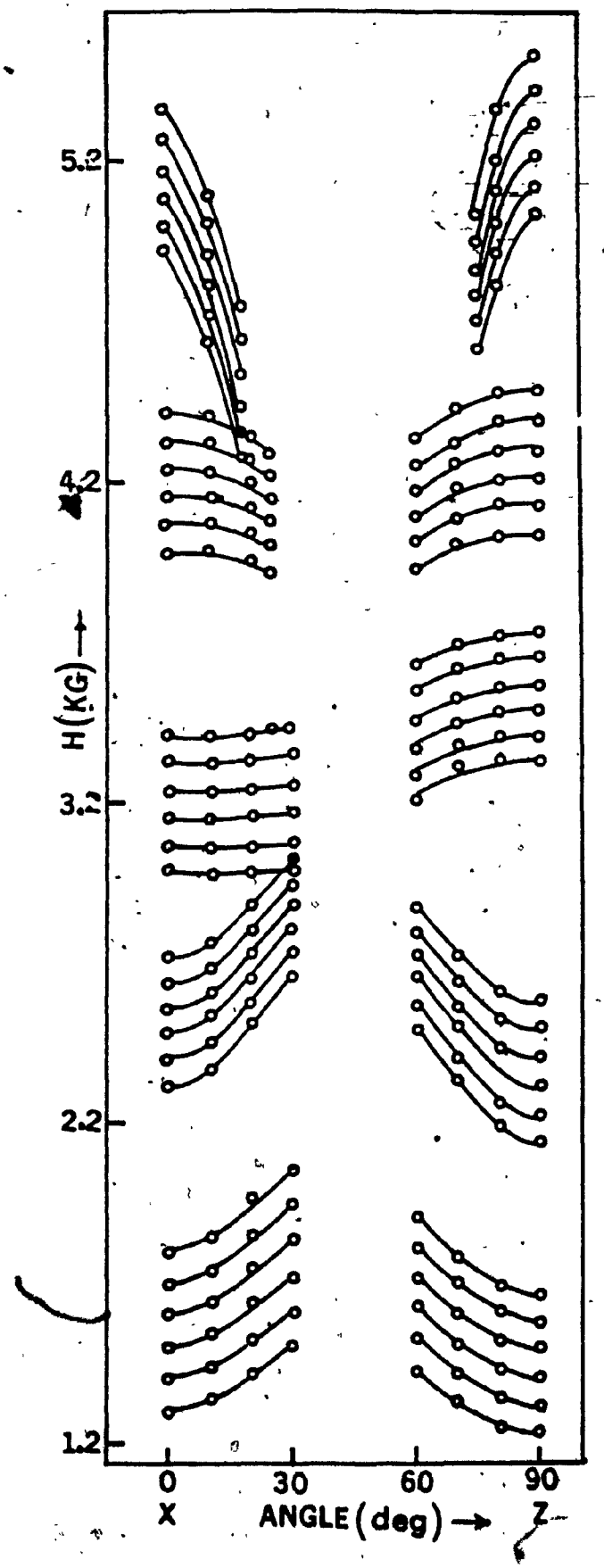

Fig. (V.7) The angular variation of EPR spectra for CoZnS

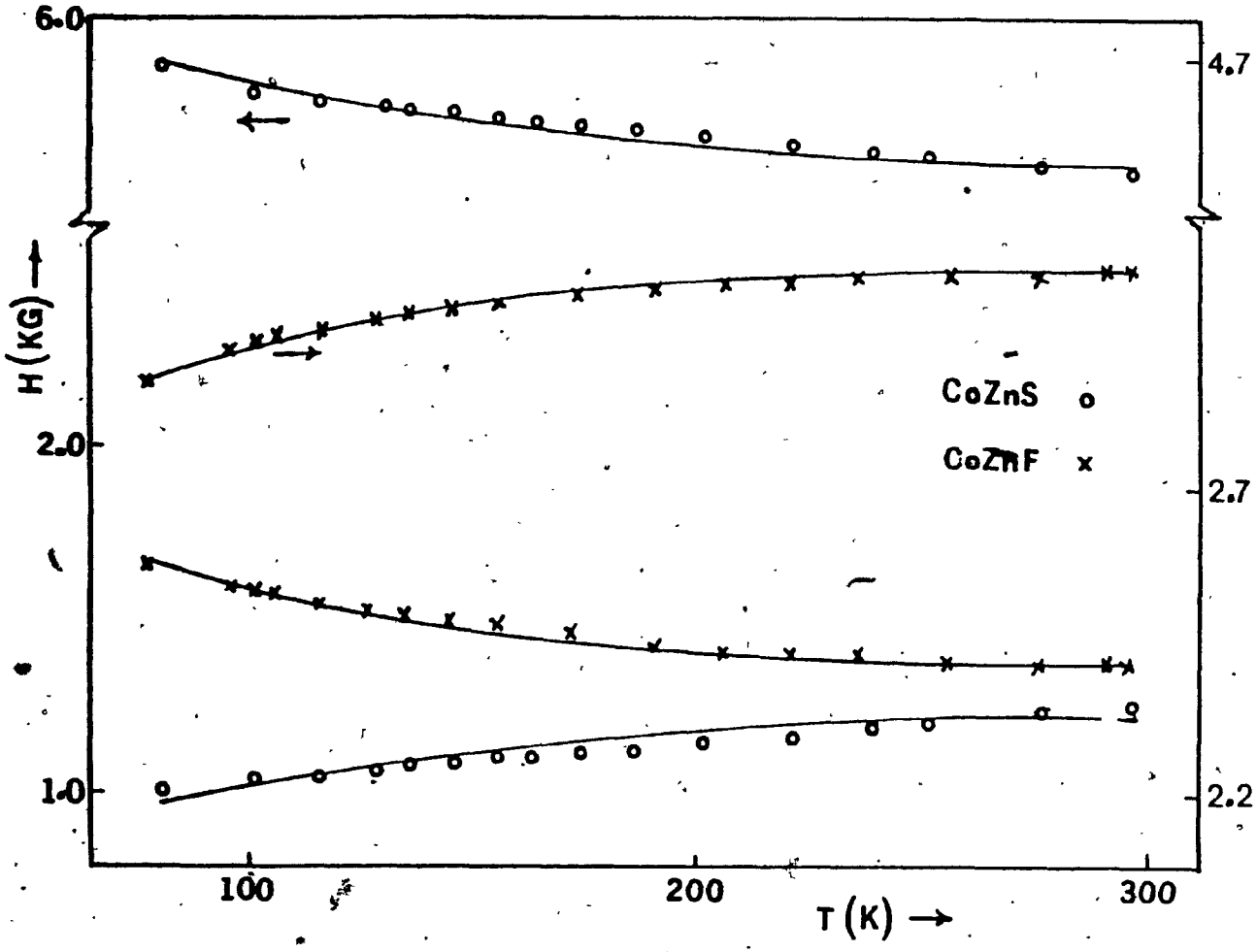

Fig. (V.8) Variation of the lowest and the highest field hyperfine line positions for Mn^{2+}-doped CoZnS and CoZnF hosts, as a function of temperature.

At 77 K, in addition to what was reported for $CoSO_4.7H_2O$ a few additional broad fine structure lines of Mn^{2+} were observed for CoZnS. This indicates that in the CoZnS sample the Co^{2+} lattice is indeed diluted by Zn^{2+} ions.

For CoZnF also the Mn^{2+} EPR spectra were recorded from room down to liquid nitrogen for $\vec{H} \| Z$ and $\vec{H} \| X$. At room temperature the spectra for various orientations of H in the ZX plane were recorded. The features of the spectra were similar to those found for Mn^{2+}-doped $ZnSiF_6.6H_2O$[43], except that the linewidths for the latter host were smaller (see Sec. V.3). Due to the rather small value of the zero field splitting parameter b_2^0 in CoZnF, the five sextets were not well-separated, however, the 30 allowed lines could be easily discerned. As the temperature was lowered from room temperature, the linewidths increased, while the overall splitting decreased continuously. Consequently, fewer lines were observed at lower temperatures. Finally, at 77 K only 18 lines about 3 times broader than those at room temperature, were observed. At this temperature, the intensity of the higher-field lines was greater than that for the lower-field lines. The temperature variation of the first and last transition lines for $\vec{H} \| Z$ in this crystal is also shown in Fig. (V.8)

A spin Hamiltonian that corresponds to the monoclinic symmetry[3] was used to fit the data for CoZnS, described by Eq. (V.1), while a spin Hamiltonian appropriate to the

trigonal symmetry was used for CoZnF[3]:

$$\mathcal{H} = \mu_B \vec{H} \cdot \tilde{g} \cdot \vec{S} + \frac{1}{3} b_2^0 O_2^0 + \sum_{m=0,3} \frac{1}{60} b_4^m O_4^m + A S_z I_z$$

$$+ B (S_x I_x + S_y I_y) + Q \left[I_z^2 - \frac{1}{3} I(I+1) \right] \qquad (V.3)$$

The evaluated S.H.P. for both the hosts are given in Table 14. hich also includes the parameters reported by other authers[37,38] for 100% pure Co^{2+} lattices for comparison. The absolute signs of parameters could not be determined due to the impossibility of observing the spectra at liquid-helium temperature. A negative sign has been assumed for b_2^0 in CoZnS and CoZnF in accordance with those determined from the liquid-helium temperature data for Mn^{2+}-doped $ZnSiF_6.6H_2O$[43] and $MgSO_4.7H_2O$.[14]

V.1.2 Cu^{2+}: Copper Pentakisantipyrine Perchlorate.

The crystal structure of copper pentakisantipyrine perchlorate, $Cu(C_{11}H_{12}ON_2)_5(ClO_4)_2$, (hereafter copper PKAP) was reported by Vijayan and Viswamitra,[31] it belongs to the monoclinic symmetry with space group $P2_1/c$, with unit cell dimensions a = 10.52 Å, b = 16.27 Å, c = 18.99 Å and β = 102° 36'. There are four formula units per unit cell.

Parameters	CoZnS	Ref. 37	CoZnF	Ref. 38
g_{zz}	2.0090 ± .0010	2.001 ± .001	1.9986 ± .0005	1.9975
g_{xx}	1.9970 ± .0010	.....	2.0060 ± .0005	.....
b_2^0	-1.3833 ± .0022	1.285 ± .005	-0.5111 ± .0009	-0.5127
b_2^2	1.1915 ± .0055	1.125 ± .011	.....	.....
b_4^0	0.0015 ± .0017	0.005 ± .005	-0.0083 ± .0008	.....
b_4^2	-0.1353 ± .0255	.....	.....	.....
b_4^3	.....	.....	0.0027 ± .0004	.....
b_4^4	0.1643 ± .0278	.....	.....	.....
Q'	0.0214 ± .0055	.....	-0.0025 ± .0038	.....
Q"	0.0757 ± .0104	.....	.....	.....
A	-0.2679 ± .0040	-0.241 ± .005	-0.2708 ± .0016	-0.2660
B	-0.2514 ± .0040	-0.247 ± .005	-0.2622 ± .0016	.....
n	217	.....	330	.....

TABLE 14. Values of S.H.P. for Mn^{2+}-doped CoZnS and CoZnF host. For more details see caption of Table 1.

Crystals of copper PKAP were prepared by slow evaporation of a solution of appropriate stoichiometric amounts of $Cu(ClO_4)_2.6H_2O$ and antipyrine at room temperature.

The S.H.P. for Cu^{2+} in copper PKAP crystal at room temperature have been previously estimated by Srinivasan and Subramanian[44] by the use of perturbation expressions. They concluded from their studies that the four formula units contained in the unit cell were magnetically equivalent.

The EPR spectra of Cu^{2+} were recorded for the magnetic field orientation in the ZX, ZY and XY planes at room, liquid nitrogen and liquid helium temperatures.[42] The existence of four formula units per unit cell in this crystal has, indeed, been affirmed by the EPR spectra. Two of these are found to be magnetically equivalent, while the remaining two are somewhat magnetically inequivalent. (This is incompatible with the finding of Ref. 44 that all the Cu^{2+} sites are magnetically equivalent.) Consequently, the spectrum for the magnetic field orientation along the Z-axis was characterized by three distinct sets of Cu^{2+} spectra. The spectra of the two equivalent ions coincide for all directions of the external magnetic field, and thus the lines corresponding to these sites have the intensity twice that for each of the other ions. Fig. (V.9) shows the EPR spectra of Cu^{2+} in copper PKAP for the magnetic field orientation along the Z-axis at room temperature. Since the

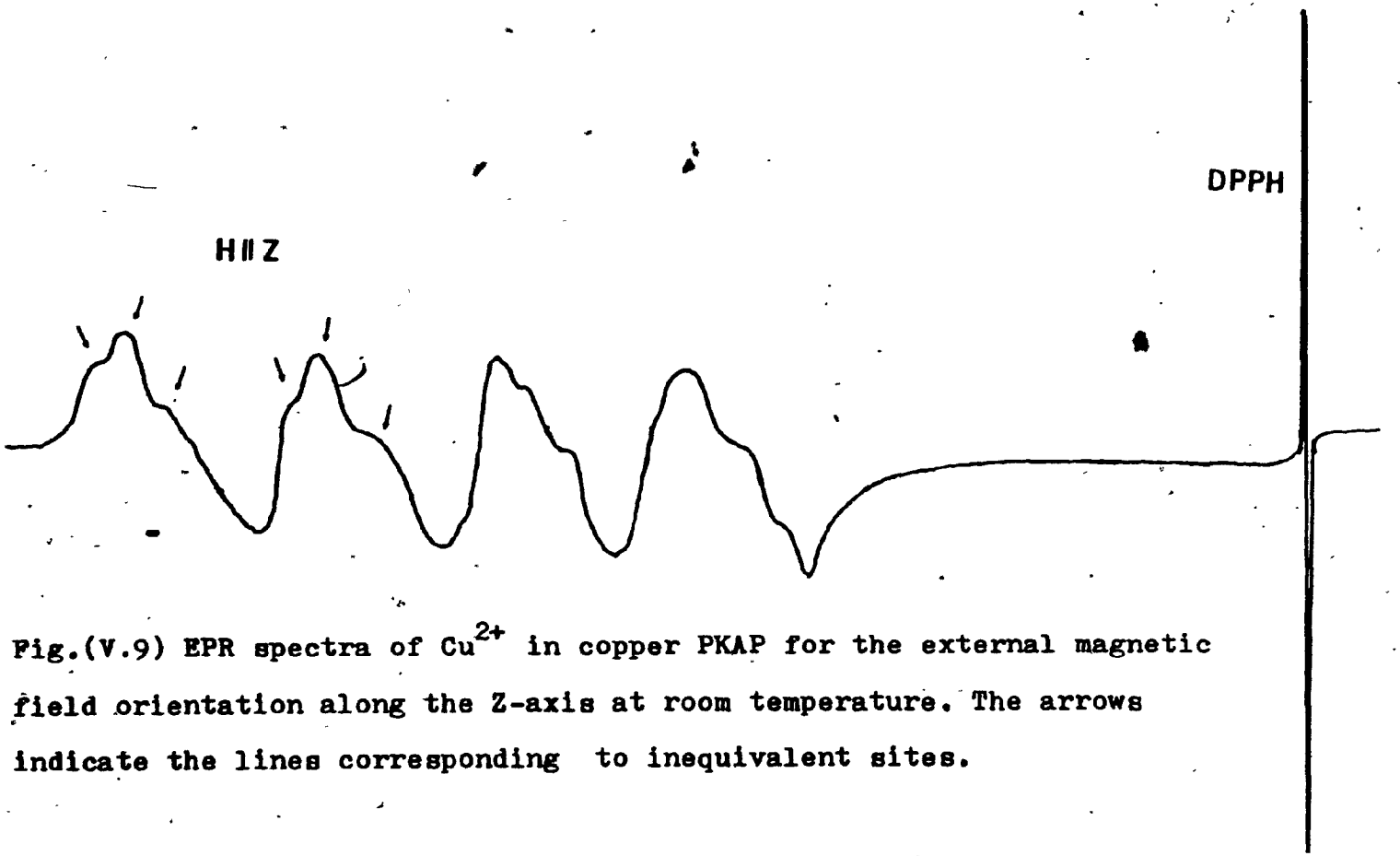

Fig.(V.9) EPR spectra of Cu^{2+} in copper PKAP for the external magnetic field orientation along the Z-axis at room temperature. The arrows indicate the lines corresponding to inequivalent sites.

Cu^{2+} sites are only slightly inequivalent magnetically, the Cu^{2+} spectra corresponding to various sites overlap considerably. It was thus difficult to determine individually the principal axes of the g- and A- tensors corresponding to these sites.

In the XY plane only one broad line was observed, whose position remained invariant with respect to the direction of the magnetic field.

Although the host lattice is 100% concentrated in Cu^{2+}, the distances between Cu^{2+} ions are sufficiently large so as to allow the appearance of four well-resolved hyperfine lines for Cu^{2+} for each inequivalent site at all temperatures. With the lowering of the temperature, the spectra remained the same, as the magnetic field direction was rotated away from the Z-axis, toward the X-axis, the overall splitting decreased while the lines moved toward higher magnetic field, finally, for $\vec{H} \parallel X$ axis only one broad line was observed. Fig. (V.10) shows angular variation of the EPR spectra of Cu^{2+} at room temperature corresponding to the two equivalent sites for Cu^{2+} (doubly-intense lines) in the ZX plane.

The observed EPR spectra of Cu^{2+} in copper PKAP ($P\bar{3}$ site symmetry) are fitted to the following spin Hamiltonain:

$$\mathcal{H} = \mu_B \vec{H} \cdot \tilde{g} \cdot \vec{S} + \vec{S} \cdot \tilde{A} \cdot \vec{I} \qquad (V.4)$$

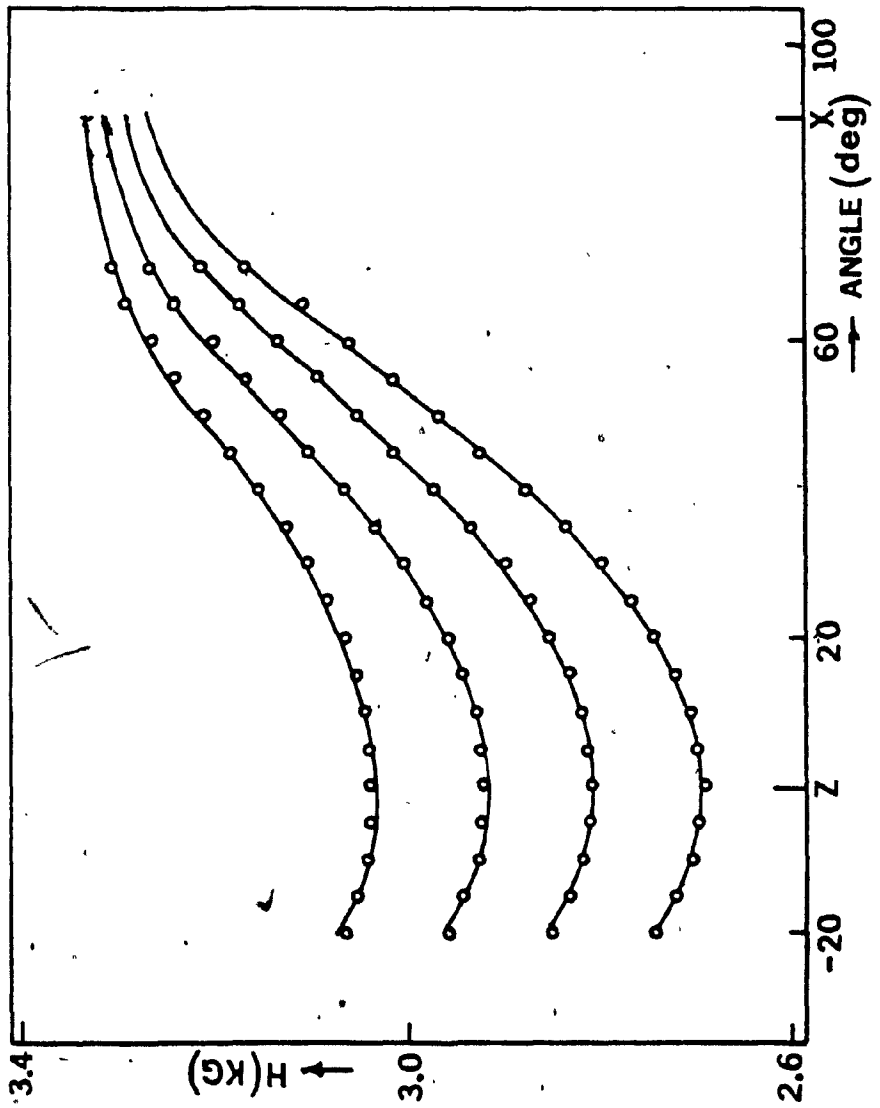

Fig. (V.10) The angular variation of EPR spectra for Cu^{2+} in copper PKAP.

where for Cu^{2+} the electronic spin S = $\frac{1}{2}$ and the nuclear spin I = $\frac{3}{2}$.

The spin Hamiltonian parameters for Cu^{2+}, i.e. the principal values of its g and A tensors and their direction cosines were evaluated using a rigorous least-squares fitting technique as described in Ref. 45. Briefly the method is as follow:

By averaging the positions of the four hyperfine lines in any direction, the positions of the resulting fine-structure lines are deduced. These line positions are then used to determine the components of the g^2-tensor. The g^2- tensor can be diagonalized to obtain the principal values of the g^2- tensor (which are squares of the principal values of the g^2- tensor) and the direction cosines of its principal axes. This procedure was carried out for the data obtained at all temperatures. Table 15 shows the g-values of Cu^{2+} corresponding to the two equivalent ions at room, liquid nitrogen and liquid helium temperatures. The direction cosines of the principal axes of g^2- tensor with respect to the X,Y and Z axes are given in Table 16 (X and Y axes are coicident with the a and b axes of the unit cell respectively, while the Z axis is prependicular to the ab plane, making an angle of 12° 36′ with the c-axis).

Using these principal g-values and their direction cosines, the components of the A^2- tensor are next obtained

TABLE 15. The principal values of the g- and A- tensors for Cu^{2+} in copper PKAP lattice. g is dimensionless, while A is expressed in units of GHz . The indicated errors are as estimated by the use of a statistical method (Ref. 5).

Temperature	295 K	85 K	5 K
$g_{z'}$	2.3416 ± .0017	2.3817 ± .0017	2.3865 ± .0017
$g_{x'}$	2.0376 ± .0017	2.0665 ± .0017	2.0865 ± .0017
$g_{y'}$	2.0360 ± .0017	2.0634 ± .0017	2.0812 ± .0017
$A_{z''}$	0.3651 ± .0020	0.4097 ± .0020	0.4168 ± .0020
$A_{x''}$	0.0870 ± .0040	0.0687 ± .0040	0.0713 ± .0040
$A_{y''}$	0.0473 ± .0040	0.0040 ± .0040	0.0673 ± .0040

TABLE 16. Direction cosines of the principal axes of the g^2- and A^2- tensor of Cu^{2+} in copper PKAP lattice. The direction cosines of the g^2-tensor are given with respect to the X,Y,Z axes (as defined in Chapter II), while those of the A^2 - tensor are expressed relative to (X', Y', Z'), the principal axes of the g^2- tensor. The direction cosines of the principal axes of the A^2- tensor at liquid nitrogen and liquid helium temperatures are exactly the same as

Direction cosines of the g - tensor			
	Z	X	Y
Z'	0.9999	0.0097	0.0097
X'	0.0000	0.7071	-0.7071
Y'	-0.0137	0.7070	0.7070

Direction cosines of the A^2-tensor			
	Z'	X'	Y'
Z"	0.9996	-0.0232	-0.0133
X"	0.0233	0.9997	0.0040
Y"	0.0132	-0.0043	0.9999

by simultaneously fitting all hyperfine lines obtained at various orientations of the external magnetic field. Thus the six independent elements of the symmetric tensor $A^2_{\alpha\beta}$ (α,β = X,Y,Z) were evaluated by fitting simultaneously all clearly resolved hyperfine lines obtained for the external magnetic field in the three planes (XY), (YZ) and (ZX). The tensor A^2 was then diagonalized, giving the squares of the principal values of the A^2-tensor, as well as its direction cosines with respect to the principal axes of the g-tensor. These principal values are also included in Table 15, while the direction cosines of the principal axes of the A^2-tensor are given in Table 16.

It is seen that the principal g and A values either remain the same within experimental error, or increases slightly, as the temperature is lowered.

V.1.3 Gd^{3+}: $LiYF_4$ and $LiYbF_4$.

The crystal structure of $LiYF_4$ and $LiYbF_4$ have been reported in Refs. 46 and 47. Both have $CaWO_4$-type structure, crystallizing in tetragonal structure with the space group symmetry $I4_1/a$. The unit cell of $LiYF_4$ has the dimensions a = 5.175 + .005 and c = 10.740 + .010 Å, while that of $LiYbF_4$ has the dimensions a = 5.132 + ,005 and c = 10.590 + .010 Å. Each rare-earth ion is surrounded by eight nearest-neighbor fluorines, four of which are at a distance R_1 = 2.246 A, while the remaining four are at a

distance R_2 = 2.293 Å.

Single crystals of $LiYF_4$ and $LiYbF_4$ doped Gd^{3+} were grown by modified Bridgman-stockberger method[48] in the Department of Experimental Physics, Marie-Curie Sklodowska University, Lublin, Poland.

EPR measurements on Gd^{3+}-doped single crystals of $LiYF_4$ have been reported by Vaills and Buzare.[49] They gave a detailed analysis of the EPR spectra of Gd^{3+} in this crystal at room temperature only.

The EPR spectra of Gd^{3+}-doped $LiYF_4$ were recorded at room, liquid nitrogen and liquid helium temperatures in ZX and XY planes.[50] At room temperature, seven well-resolved lines were observed in the range of 400 to 9600 gauss, for the magnetic field orientation along the Z-axis. Beside the allowed lines, some forbidden lines were also observed at lower magnetic field values, the number of these lines increased as the magnetic field direction moved away from the Z-axis. Fig.(V.11) exhibits the angular variation of EPR spectra of Gd^{3+}-doped $LiYF_4$ at room temperature, in the ZX plane.

As the temperature was lowered from room to liquid helium temperature, the general features of the spectrum remained the same, however, the overall splitting of the spectrum increased and the intensities of lines at lower magnetic field, increased relative to those at higher field.

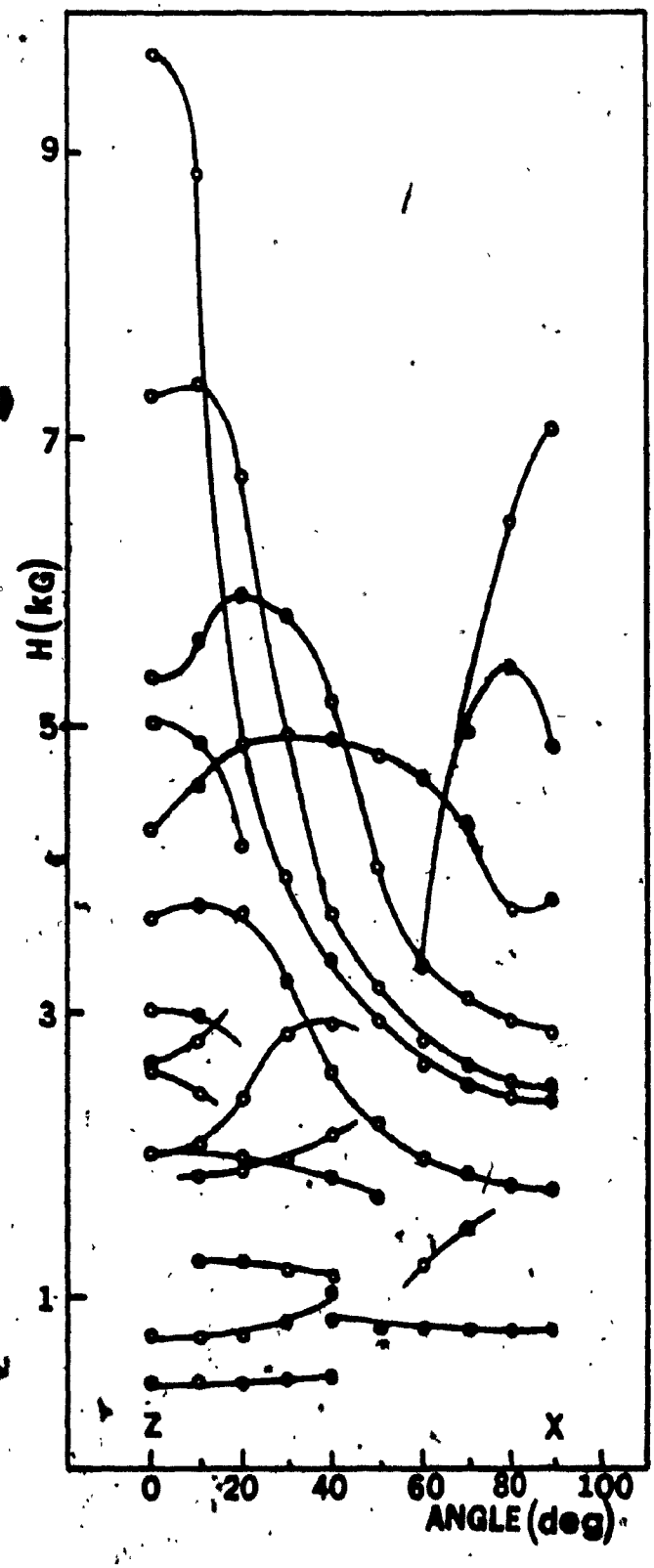

Fig. (V.11) The angular variation of EPR spectra for Gd^{3+}-doped $LiYF_4$.

The latter observation implies that the sign of the zero-field splitting parameter b_2^0 is negative.

The EPR measurements on Gd^{3+}-doped $LiYbF_4$ host are the first-ever to be reported The EPR spectra in this crystal at room temperature had the same features as those for Gd^{3+}-doped $LiYF_4$, except that the linewidths were larger, (due to the dipole-dipole interaction between Gd^{3+} and the paramagnetic host ions Yb^{3+}). As the temperature was lowered below room temperature, the lines started to broaden rapidly, below 270 K the lines completely disappeared.

The following spin Hamiltonian[3], corresponding to tetragonal symmetry, was used to fit EPR data:

$$\mathcal{H} = \mu_B \vec{H} \cdot \tilde{g} \cdot \vec{S} + \frac{1}{3} b_2^0 O_2^0 + \frac{1}{60} (b_4^0 O_4^0 + b_4^4 O_4^4)$$

$$+ \frac{1}{1260} (b_6^0 O_6^0 + b_6^4 O_6^4) \qquad (V. 5)$$

The absolute sign of b_2^0 was found to be negative for the $LiYF_4$ host, since the intensity of the highest-field line relative to that of the lowest-field line for the magnetic field orientation along the Z-axis reduced by a factor seven in going from room to liquid helium temperature. The sign of b_2^0 for Gd^{3+}-doped $LiYbF_4$ was also assumed to be negative since it could not be determined due to the

disappearence of the lines below 270 K. The S.H.P. for Gd^{3+}-doped $LiYF_4$ and $LiYbF_4$ are listed in Table 17, wherein the values reported by other authers[49] are also included for comparison.

	$LiYF_4$				$LiYbF_4$
Temperature	295K	85 K	5 K	RT(Ref.3)	295 K
g_{zz}	1.9890 ±.0010	1.9813 ±.0016	1.9804 ±.0016	1.9837 ± .0005	1.9864 ±.0076
g_{xx}	1.9871 ±.0010	1.9828 ±.0016	1.9837 ±.0016	1.9825 ± .0005	1.9870 ±.0076
b_2^0	-2.4837 ±.0015	-2.5141 ±.0017	-2.5183 ±.0017	± 2.4810 ± .0150	-2.4893 ±.0170
b_4^0	-0.0671 ±.0004	-0.0667 ±.0006	-0.0667 ±.0006	± 0.0570 ± .0030	-0.0508 ±.0017
b_4^4	0.2778 ±.0030	0.4241 ±.0040	0.4366 ±.0040	± 0.3030 ± .0150	0.4144 ±.0300
b_6^0	-0.0079 ±.0004	-0.0103 ±.0008	-0.0145 ±.0008	0.0000 ± .0060	-0.0102 ±.0020
b_6^4	0.0216 ±.0060	0.0611 ±.0100	0.0939 ±.0100	±0.0165 ± .0150	0.1788 ±.0400

TABLE 17. Values of S.H.P. of Gd^{3+}-doped $LiYF_4$ and $LiYbF_4$. For more details see caption of Table 1.

V.2. Temperature Variation oF the Zero-field splitting parameter b_2^0.

The temperature variation of the spin-Hamiltonian parameters of S-state ions in single crystals with cubic symmetry have been investigated theoretically and experimentally by several workers. Simanek and Orbach[51] calculated the temperature dependence of the hyperfine parameter A using Debye approximation which is in good accord with experimental results on Mn^{2+} in MgO. Serway[52] has investigated the temperature dependence of the spin-Hamiltonian parameters of Mn^{2+} in the trigonal site of $CaCO_3$ in terms of implicit (thermal expansion) and explicit (lattice vibration) effects. Geifman and Glinchak[53] have studied the temperature dependence of the crystal-field parameters of Fe^{3+} and Mn^{2+} in Al_2O_3. They have found the variation of the parameter b_2^0 (the most pronounced parameter in the series of our measurements) to be as follow

$$b_2^0(T) = b_2^0(0)\left[1 - 6\alpha(T - T_0)\right] \qquad (V.6)$$

In Eq. (V.6), $b_2^0(0)$ is the value of b_2^0 at T_0 (usually room temperature) and α is the coefficient of linear thermal expansion. The above expression has been drived, assuming that the thermal expansion is the dominating mechanism and, that the changes in the coordinates of the ions surrounding the Mn^{2+} ion are linear in temperature, i.e. $\Delta R = \alpha T$.

Also it has been assumed that b_2^0 is proportional to the square of the axial crystal-field potential.

Equation (V.6) shows that b_2^0 is linear in T. Fig. V.12 exhibits the temperature variation of b_2^0 for various samples. From this figure one may be tempted to that thermal expansion is the dominant mechanism determining the temperature variation of the zero-field splitting parameter for samples like MSO, NSO, CaHKAP, CdHKAP and $Cu_{.05}Ca_{.95}HKAP$ which is linear with respect to temperature, and for the remaining samples, it is seen that this parameter does not display a linear variation with temperature, and it would be interesting to look for mechanisms which predict such a non-linear variation of b_2^0 with temperature.

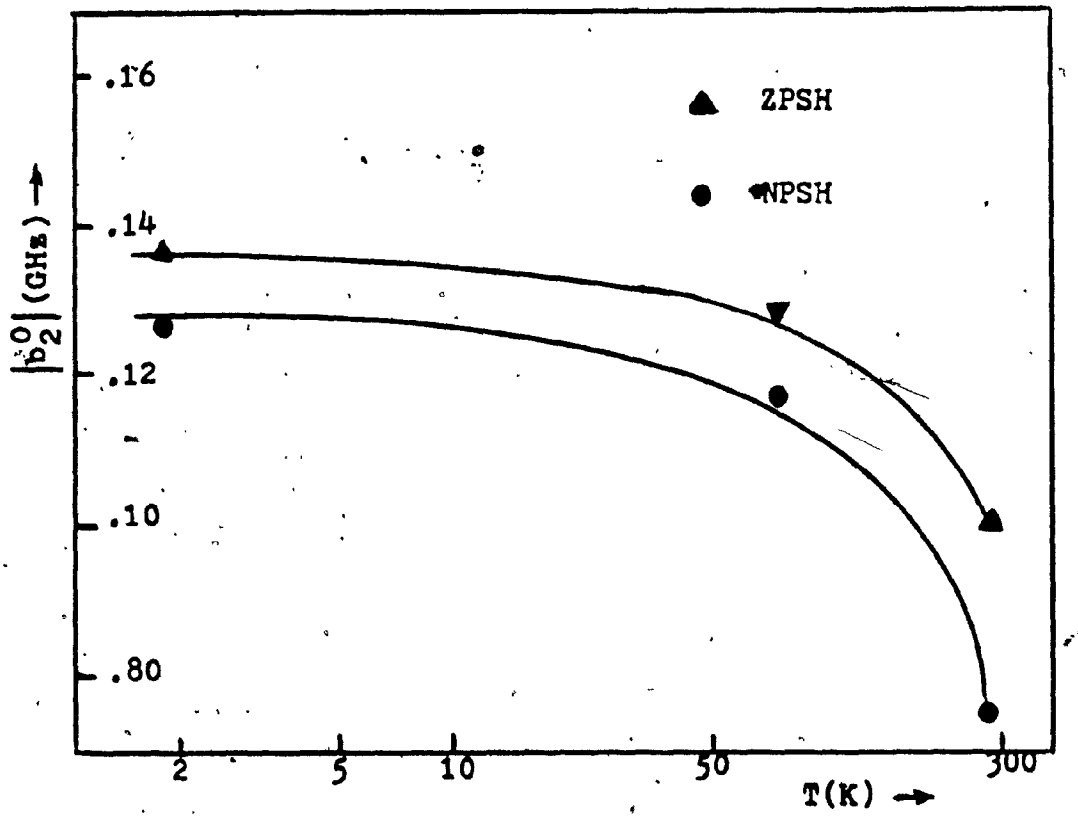

Fig. (V. 12) Variation of the zero-field splitting parameter b_2^0 for Mn^{2+} -doped ZPSH and NPSH host as a function of temperature.

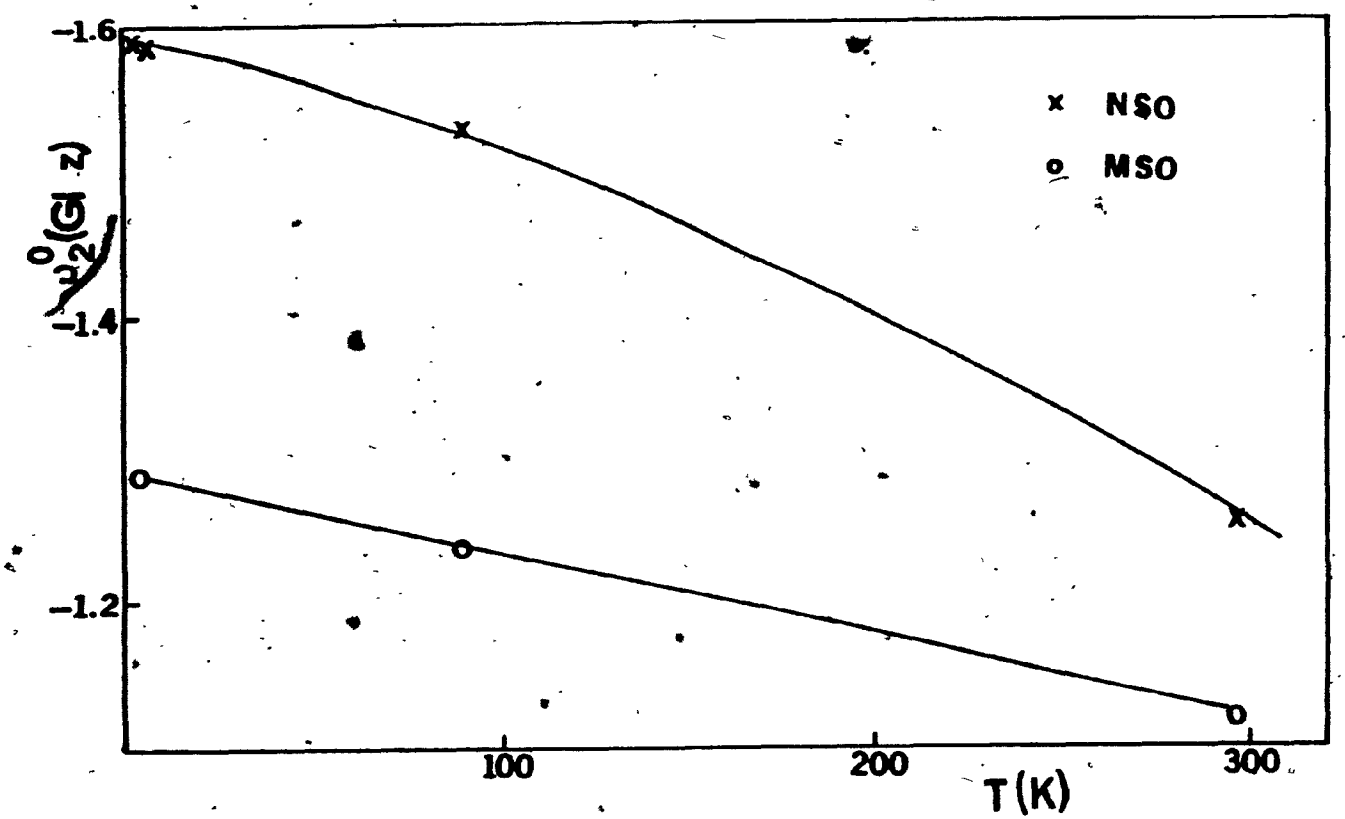

Fig. (V.13) Variation of the zero-field splitting parameter b_2^0 for Mn^{2+}- doped NSO and MSO as a function of temperature.

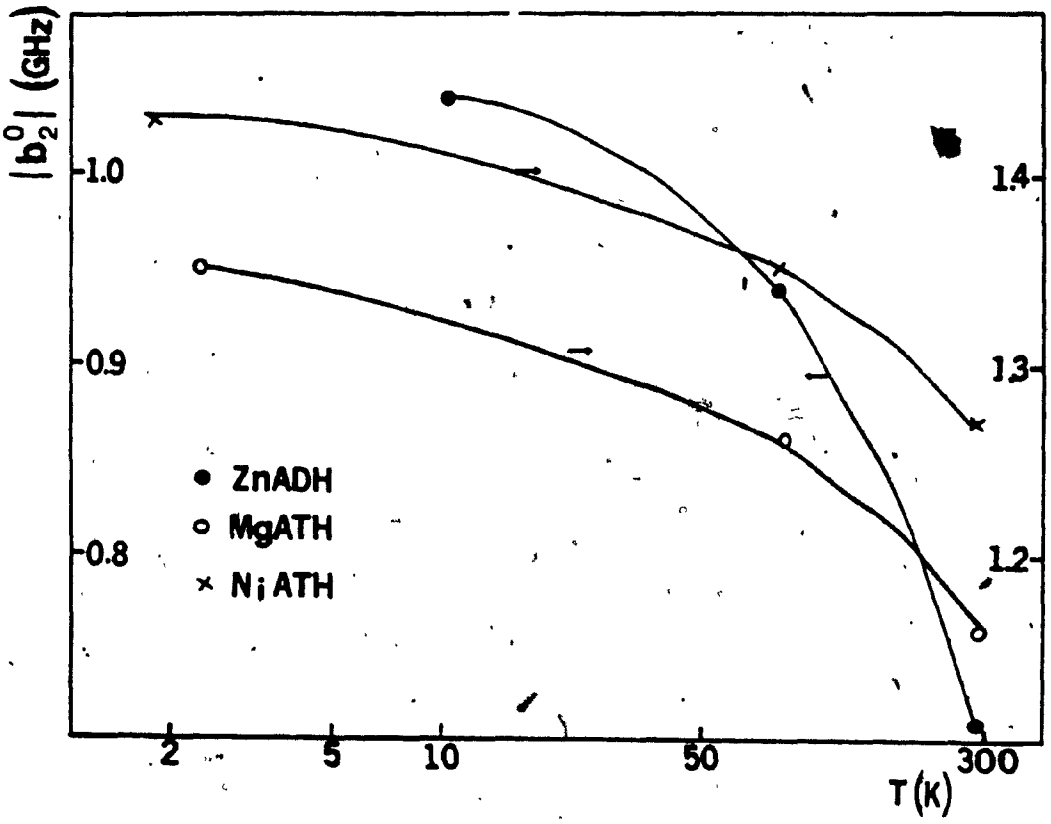

Fig. (V.14) Variation of the zero-field splitting parameter b_2^0 for Mn^{2+}-doped ZnADH, MgATH and NiATH as a function of temperature.

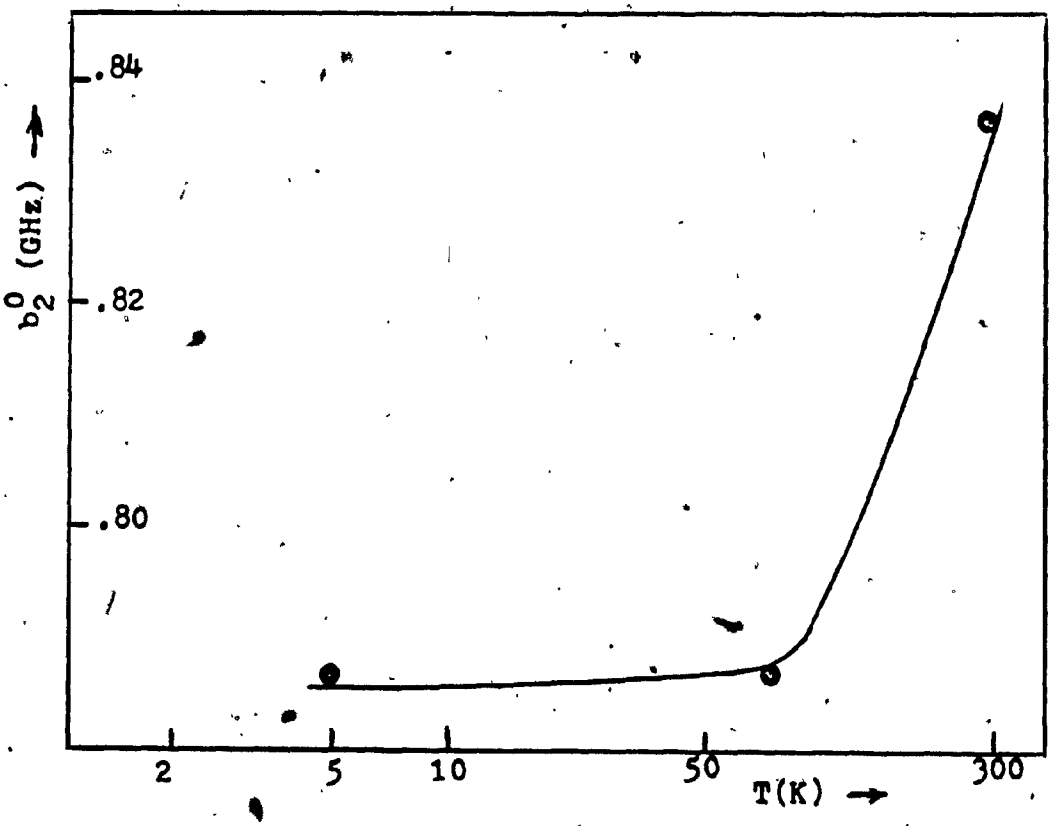

Fig.(V.15) Variation of the zero-field splitting parameter b_2^0 for Mn^{2+} -doped MFS as a function of temperature.

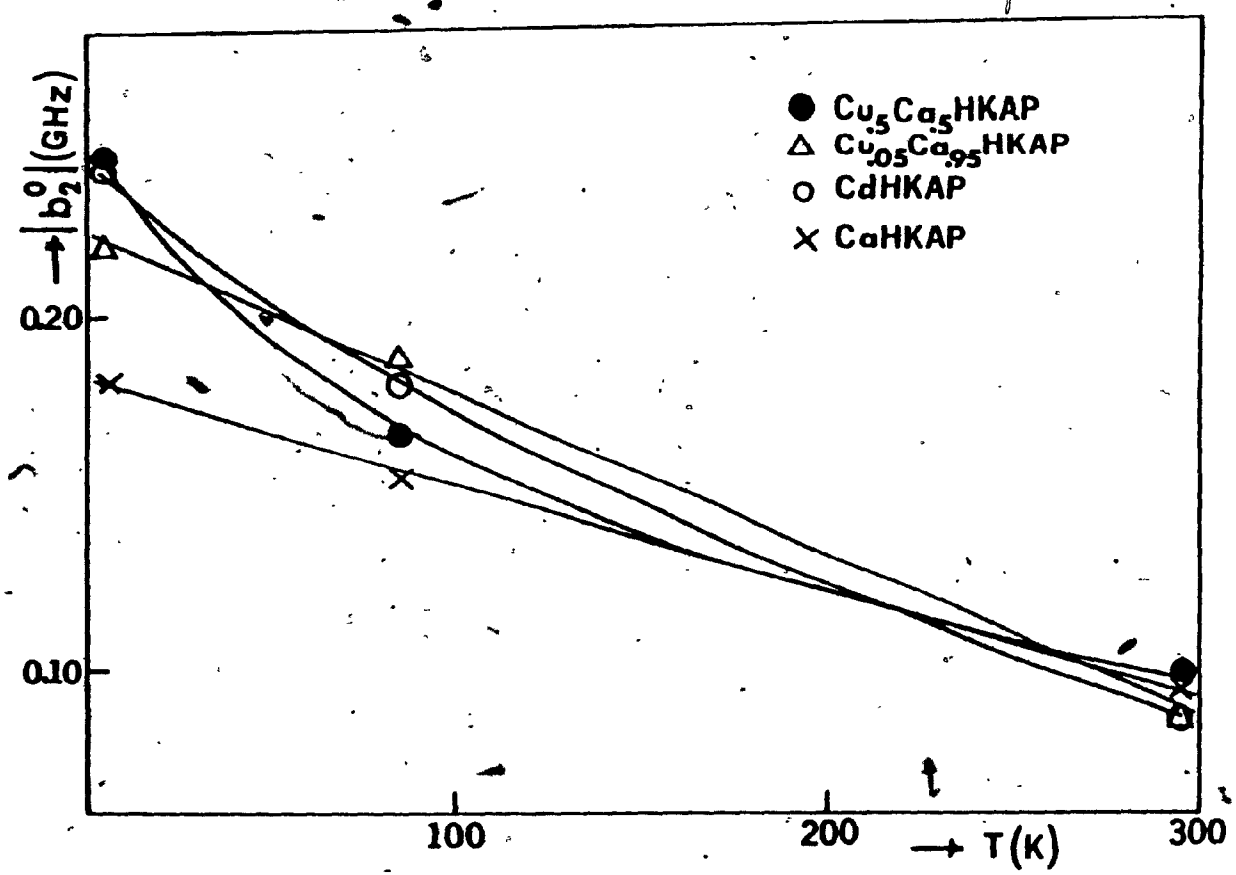

Fig. (V.16) Variation of the zero-field splitting parameter b_2^0 for Mn^{2+} doped metal HKAP as a function of temperature.

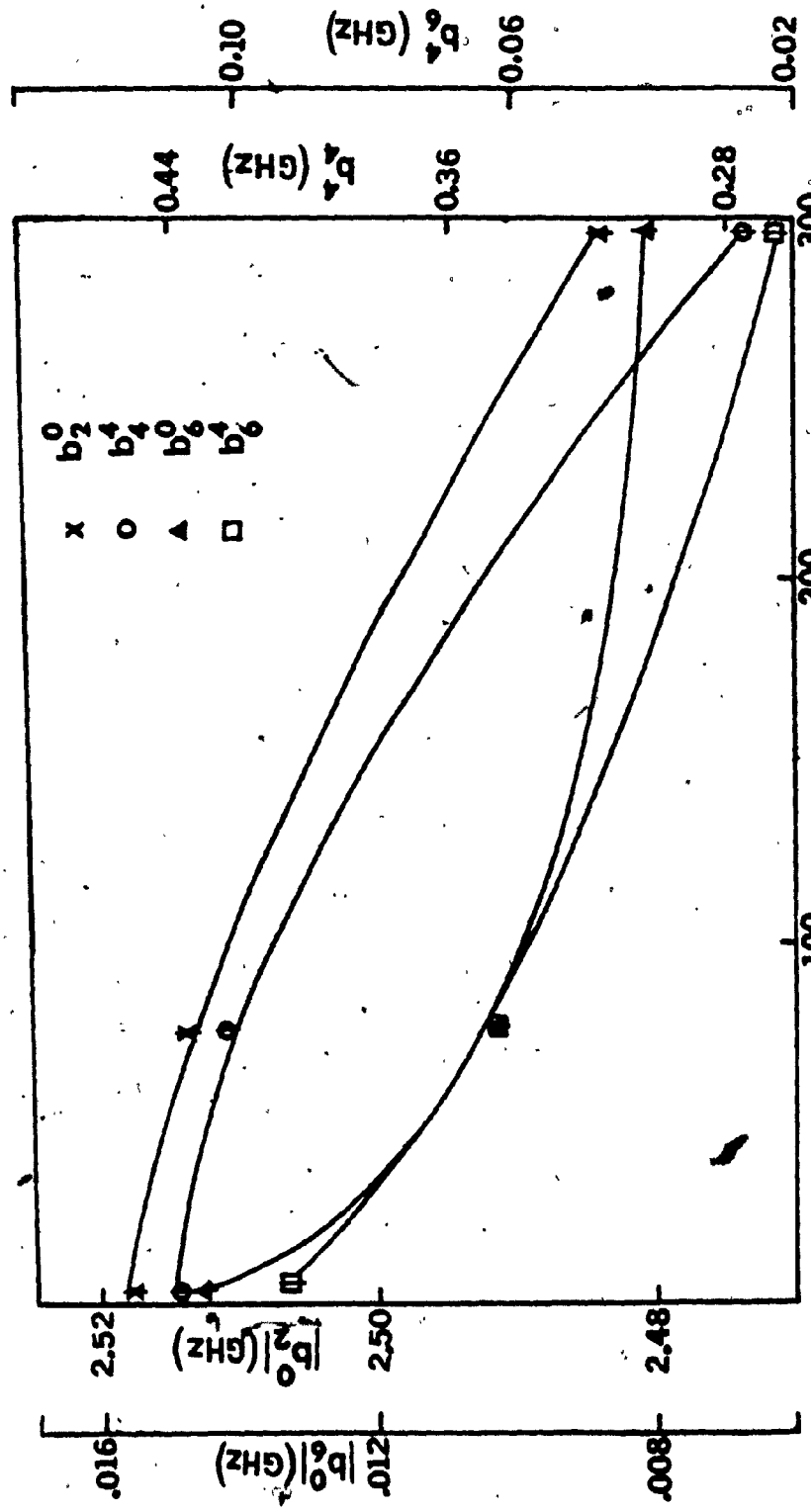

Fig. (V.17) Variation of the zero-field parameters for Gd^{3+} - $LiYF_4$ as a function of temperature.

V.3 Linewidths.

The linewidths of EPR lines of Mn^{2+} in diamagnetic hosts reported in this thesis were generally small and they showed no significant variation either for different orientations of external magnetic field or for different temperatures. Table 18 exhibits the average EPR linewidths for Mn^{2+} doped various diamagnetic hosts, studied in this thesis. EPR linewidths for Mn^{2+} doped ZnADH had a very small linewidths. The reason for such small linewidths is that four of the six ligands surrounding Mn^{2+} are oxygen, which, because of their zero nuclear spin, do not have dipolar interactions with a Mn^{2+} ion.

For isostructural paramagnetic (Ni^{2+}) salts, the linewidths were larger and they exhibited some differences from those in the diamagnetic hosts. These are (i) the anisotropy of the widths as a function of the orientation of the external magnetic field and (ii) the magnetic field dependence of linewidths (true at all temperatures). The variation of linewidhs as a function of magnetic field intensity for the various paramagnetic Ni^{2+} hosts is shown in Fig. (V.18 - 20).

In the paramagnetic hosts there will be,[11,12] in addition to the line broadening effects usually present in diamagnetic host, line broadening due to the (1) dipolar interaction between host and impurity ions, and (2) exchange

TABLE 18. The average EPR linewidth for Mn^{2+} doped various diamagnetic hosts.

Hosts	ZPSH	MFS	MgATH	ZnADH
Linewidth	20 ± 1	20 ±1	16 ± 1	8 ± 1

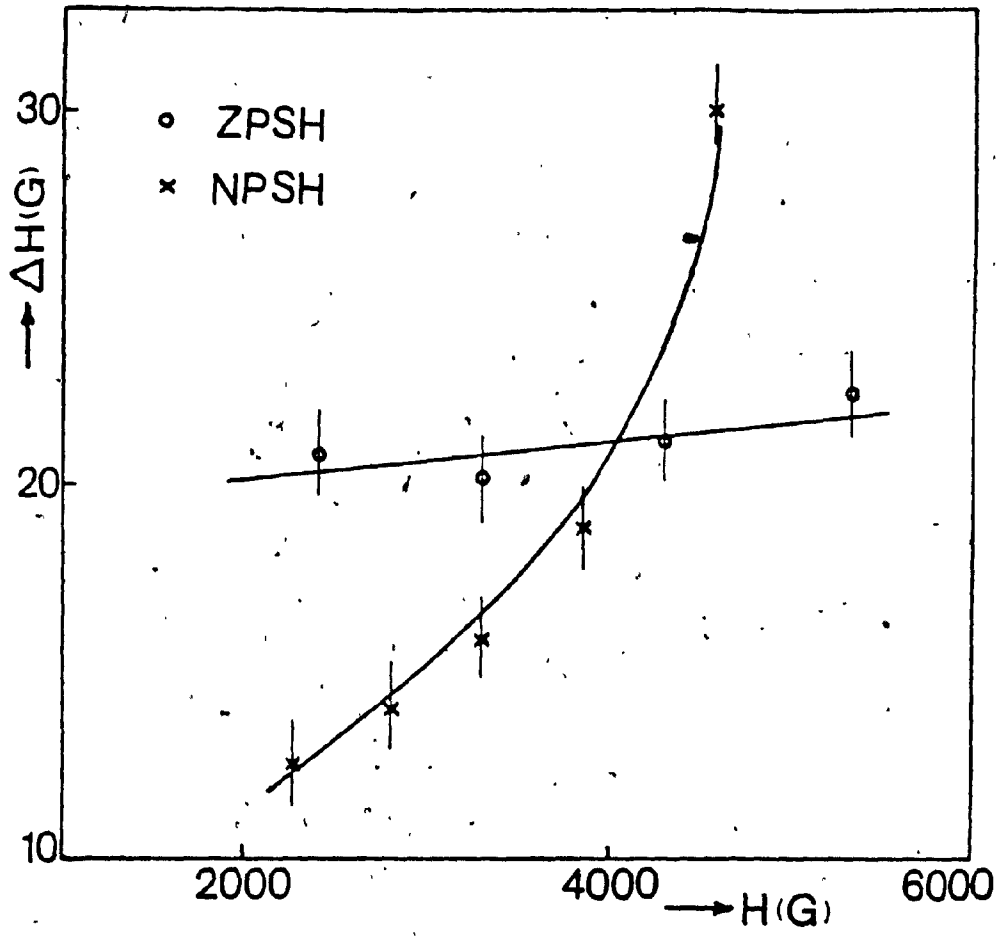

Fig. (V.18) Variation of linewidths for Mn^{2+}-doped ZPSH and NPSH as a function of external magnetic field.

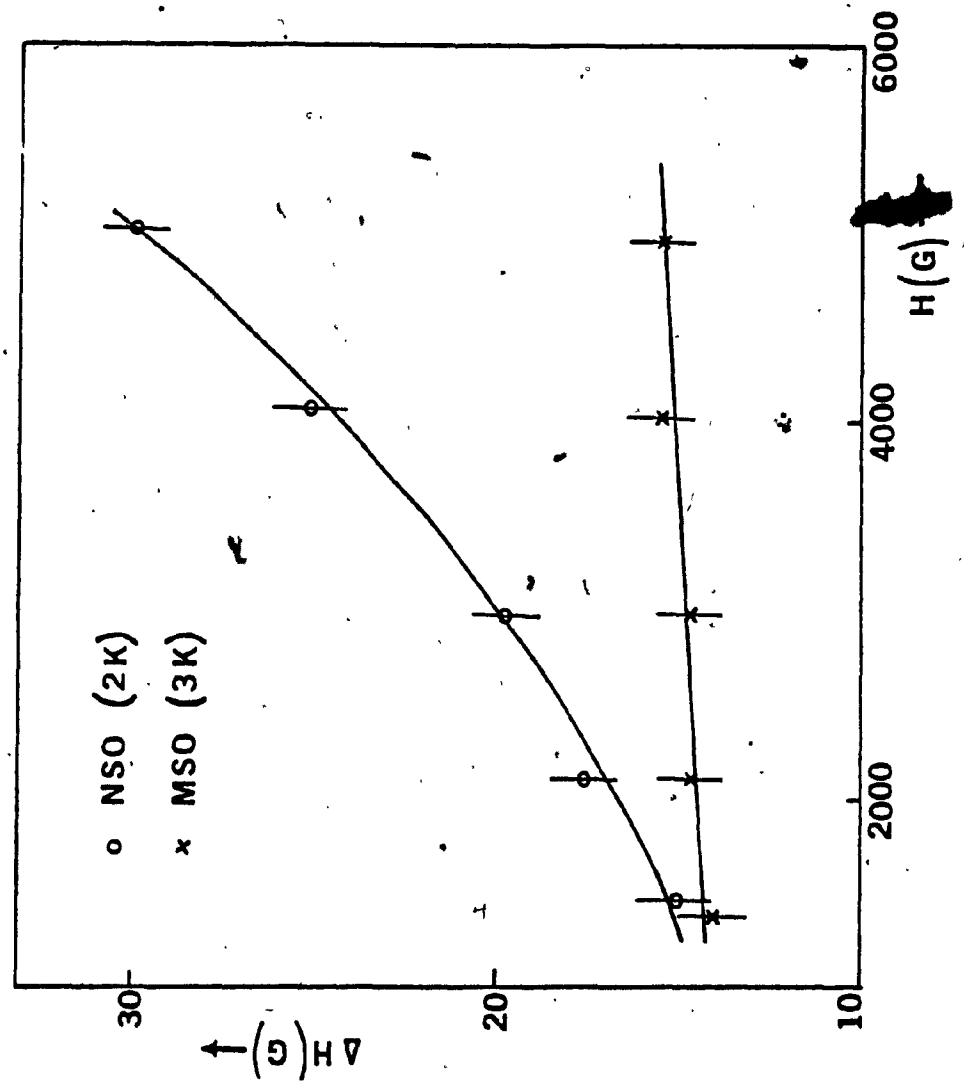

Fig. (V.19) Variation of linewidths for Mn^{2+}-doped NSO and MSO as a function of temperature.

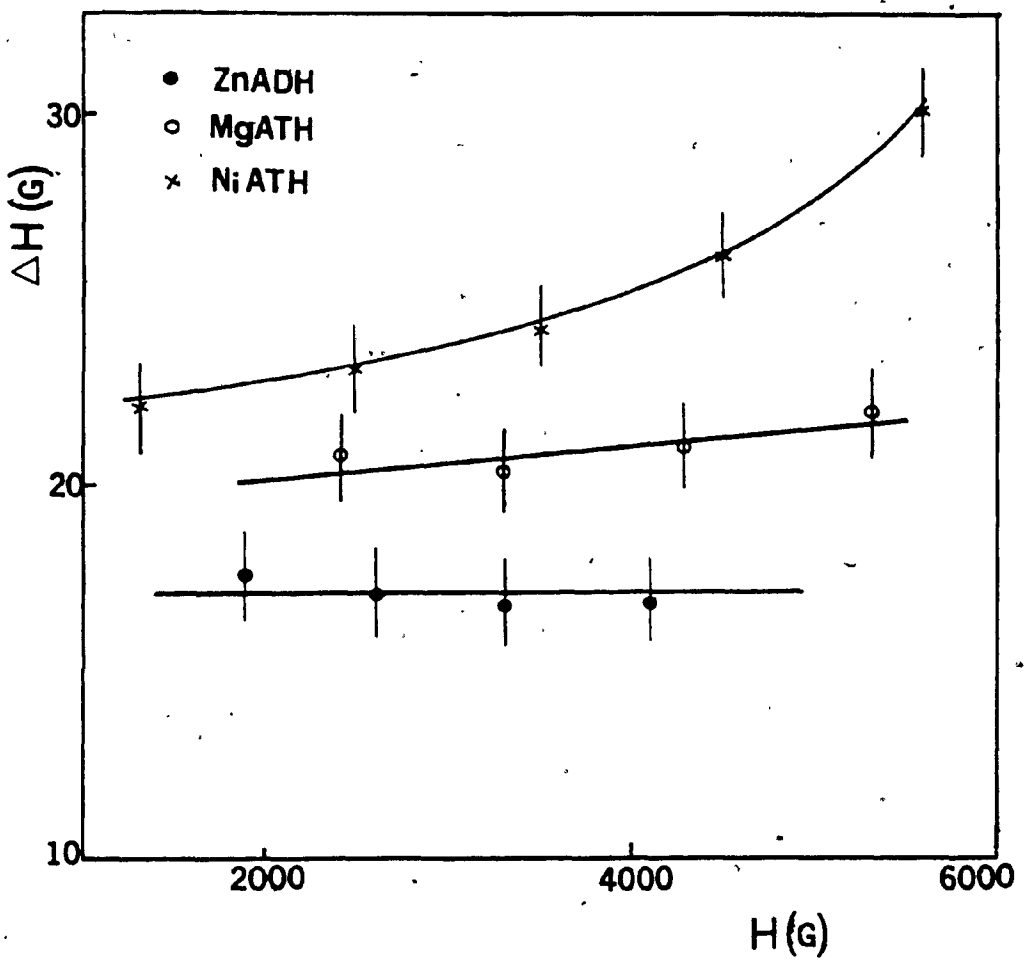

Fig. (V.20) Variation of linewidths for Mn2+ -doped ZnADH, MgATH and NiATH as a function of external magnetic field.

interaction betweeen the host and impurity ions. At room temperature the dipolar interaction contributes the most to the linewidths in most of the paramagnetic hosts. However, the effects of this interaction is reduced if a fast motion of host ions exist. This motion effectively modulates the dipolar interaction and leads to what is called "motional narrowing" of the guest resonance lines. The motional narrowing arises due to following two kinds of "motion" of host ions:

(1) Fast exchange between host ions,[54] and (2) fast spin-lattice relaxation of host ions.[55] However, in the case of Ni^{2+} salts at room temperature the exchange is not strong enough to result in motional narrowing. Further, Ni^{2+} is not a fast relaxing ion, since it is possible to observe its EPR spectrum at room temperature.

The other possibility is the apparent reduction of the magnetic moments of the host ions. This will automatically lead to a reduction in the dipolar interaction and a consequent narrowing of impurity resonance lines. This is the so-called "spin quenching" effect. Complete quenching occurs when all the spin degeneracy is removed by the crystal field and spin orbit coupling. This situation occurs when the site symmetry of the host ion is very low, i.e. rhombic or lower, and the host ions are non-Kramers ions.

From the above discussion, Ni^{2+} ions emerge ideal for spin quenching because these are commonly occuring non-Kramers ions and in many compounds such as the NPSH, NiATH and NSO, they have rhombic site symmetry.[11] Using the energy levels expressions[56] for Ni^{2+} ions in an orthorhombic crystalline field, the instantaneous magnetic moment of Ni^{2+} can be written as:

$$\mu_{ins} = -\frac{\partial W_n}{\partial H} = 0 \ , \ \pm \frac{g^2 \mu_B^2 H}{(A_{cr}^2 + g^2 \mu_B^2 H^2)^{\frac{1}{2}}}$$

$$= 0 \ , \ \pm \frac{g \mu_B}{\left\{1 + \left(\frac{A_{cr}}{g \mu_B H}\right)^2\right\}^{\frac{1}{2}}} \qquad (V, 7)$$

where W_n is the energy of state n and A_{cr} contains the crystalline field parameters of Ni^{2+}. The value of A_{cr} depends upon the orientation of the magnetic field, H. The value of A_{cr} for H along the Z, X and Y axes is

$$b_2^2/3 \ , \ \left[b_2^0 + \tfrac{1}{3} b_2^2\right]/2 \quad \text{and} \quad \left[b_2^0 - \tfrac{1}{3} b_2^2\right]/2$$

respectively.

The value of μ_{ins} will determine the mean squared dipolar fluctuation $\langle \omega^2 \rangle$. The linewidths are determined by $\langle \omega^2 \rangle$. When the zero-field term A_{cr} is much larger than $g \mu_B H$, the magnetic moment of Ni^{2+} and thus the dipolar interaction will be reduced by a sizeable factor.

One can now explain the field dependence of Mn^{2+} resonance linewidths in Ni^{2+} salts. Since μ_{ins}, which determines the linewidth, is field dependent, it is natural that the linewidth will be a function of H. The field dependences of the linewidths are found by Moriya and Obata[57] to be quadratic with narrowing and linear without narrowing. In the cases of Mn^{2+} in the above Ni^{2+} salts, the data did not fit very well to either the linear or the quadratic, it is concluded that there are effects, in addition to those considered by Moriya and Obata,[57] which contribute to the linewidths.

The anisotropy of Mn^{2+} linewidths can be explained because of the dependence of μ_{ins} on A_{cr}.[11] The magnitude of μ_{ins}, and consequently the linewidths, will depend upon the relative magnitudes of A_{cr} and $g\mu_B H$. Since A_{cr} depends upon the zero field parameters of Ni^{2+} and its value, as given above, is different for different direction of the external magnetic field. The value of $A_{cr}/g\mu_B H$ will be minimum along the Z-axis (since $b_2^2 \ll b_2^0$), and maximum along the X-axis. Thus there will be a bigger reduction in μ_{ins} along the X-axis, leading to sharper lines for H along this direction.

In the case of metal HKAP, the linewidths remained almost the same for all hosts. Further, due to the overlapping of lines it was difficult to estimate precisely all the individual linewidths.

The width of Mn^{2+} EPR lines in CoZnS and CoZnF, showed a behavior different from that in the other host crystals mentioned earlier. At room temperature the linewidths were larger than those in corresponding diamagnetic hosts. As the temperature was lowered from room temperature, the linewidths started increasing slowly. The variation of linewidths was slower for CoZnS than that for CoZnF. For CoZnS, at 77 K, only a few broad lines due to the overlapping of all hyperfine lines of Mn^{2+} were observed, which compares well with the observations of Ref. 37 for $CoSO_4.7H_2O$, for which no EPR lines could be observed at 77 K. For CoZnF, although the lines broadened faster than those for CoZnS, at 77 K one could still observe some broad lines for both $\vec{H} \parallel Z$ and $\vec{H} \parallel X$. The variation of the average linewidths as a function of temperature is displayed for both the samples in Fig. (V. 21)

The behavior of the EPR linewidths of Mn^{2+} in the lattices of Co^{2+} can be explained[37] to be due to the fast spin-lattice relaxation (described above) of the host Co^{2+} ions, which modulates the dipolar and exchange interactions between the host and probe ions, which are both paramagnetic, (host spin-lattice relaxation narrowing). The spin lattice relaxation time (T_1) in terms of the probe (Mn^{2+}) linewidth can expressed as:[58]

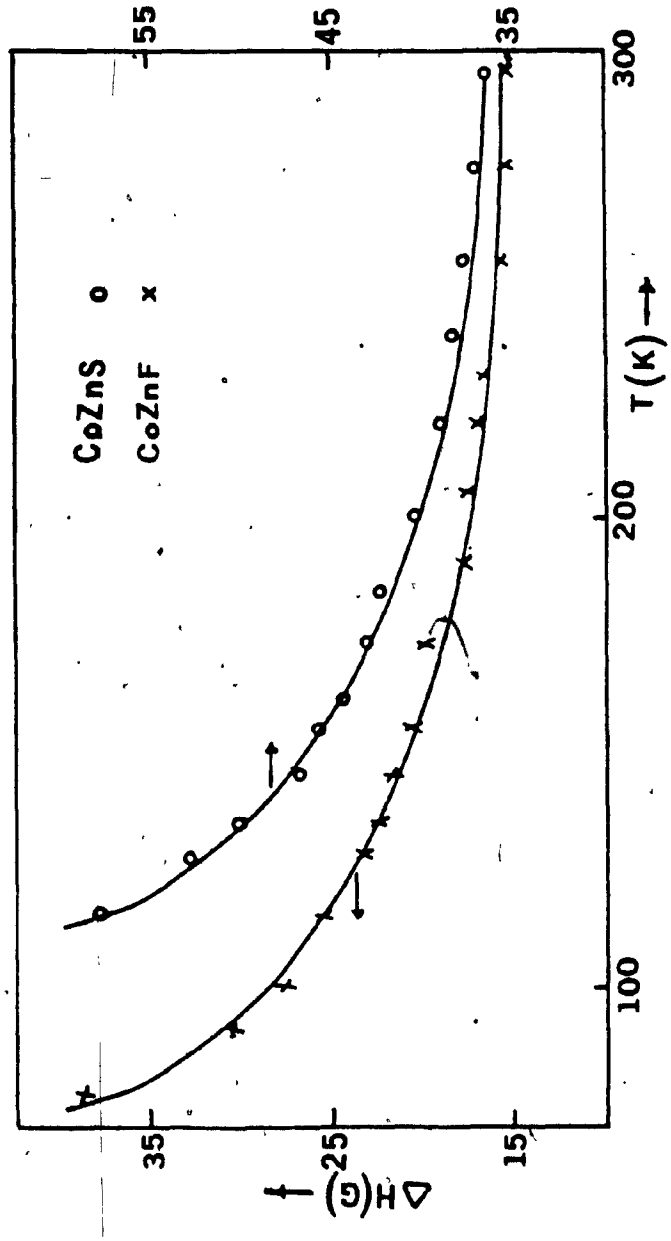

Fig. (V.21) Variation of the overall average linewidth for Mn^{2+}-doped CoZnS and CoZnF as a function of temperature.

$$T_1(\text{host}) = \frac{3\,h\,(\Delta H)}{102\,(g\mu_B)^3 n^2 \mu_0^2 S(S+1)} \qquad \text{(V. 8)}$$

Here, ΔH and g are the linewidth of the impurity and the g-factor of the host ion respectively, S is the effective spin of the host (for Co^{2+} S=1/2), n is the number of host ions per unit volume which can be calculated from the crystallographic data, μ_B is the Bohr magneton and μ_0 is the permeability constant.

Using Eq. (V.8) and the average linewidth of Mn^{2+} lines for $\vec{H} \| Z$ at room and liquid nitrogen temperatures, the following values were calculated for T_1: 3.4×10^{-11} and 5.3×10^{-11} secs at room and 100K repectively for the CoZnS host and 3.3×10^{-11} and 8.3×10^{-11} secs at room and 77 K repectively for the CoZnF host. (For CoZnS, n was calculated, using the unpublished data of Ref. 39.)

Due to the fast spin-lattice relaxation time (T_1) of Co^{2+} at room temperature the average of the host-probe dipolar interaction is zero. This enables one to observe the Mn^{2+} EPR lines at room temperature. As the temperature is lowered from room temperature, the host spin-lattice relaxation time begins to increase, eventually the guest-host dipolar interaction will not be averaged out to zero, the EPR linewidths of Mn^{2+} will thus increase . At 77K the host spin-lattice relaxation time is large enough,

so that the dipolar interactions between the Co^{2+}-Mn^{2+} ions almost broaden out completely the Mn^{2+} hyperfine lines.

As far as the EPR linewidths for Gd^{3+} are concerned, in the diamagnetic host $LiYF_4$ they were on the average about 40 G at room temperature. This average value increased to about 49 G as the temperature was lowered to liquid helium temperature. For the paramagnetic lattice $LiYbF_4$, the linewidths were much larger, about 105 G at room temperature, due to interaction between Gd^{3+} and the paramagnetic Yb^{3+} ions. As the temperature was lowered from room temperature, most of the lines disappeared, and only one line in the low magnetic field region could be observed down to 270 K, below which no lines were observed.

V.4 Exchange Interaction Between Mn^{2+}-Ni^{2+} in Nickel Salts and Gd^{3+}-Yb^{3+} in $LiYbF_4$ Paramagnetic lattices become magnetized at low temperatures, and it is shown by Kittel[59] that in these crystals, for axial symmetry the observed g-factor (g_{obs}) gets shifted from its value in the corresponding isostructural diamagnetic lattice by an amount $((4\pi/3)-N_z)1.5M/H$, where N_z is the magnetization factor along the axis of symmetry, M is the magnetization, and H is the external magnetic field intensity. (N_z is $4\pi/3$ for a spherical sample.) Thus, in order to eliminate this shift due to the demagnetization effect, one should use spherical paramagnetic host crystals.

In any ionic magnetic material in which the interactions between the neighboring magnetic ions are not negligible, the paramagnetic resonance condition for any one particular ion will explicitly depend on these interactions. In the simplest terms we may picture the neighbors polarized by the applied field producing an internal field which shifts the resonance from its "isolated" value. Unfortunately this effect is generally not observable, because in addition to setting up a time-average internal field, the interactions also produce fluctuating fields which in most cases are much larger and broaden the absorption lines. In this thesis we assume that this broadening is negligible, and that the g-shift, though small, is readily observable.

The shift of the g-value due to the presence of paramagnetic host ions is caused by the exchange interaction between the guest and the host paramagnetic ions, i.e., Mn^{2+} and Ni^{2+} in nickel salts. As a result of the polarization effect of the external field, magnetic moments are induced on the paramagnetic host ions. These magnetic moments interact with the guest Mn^{2+} ion, thus causing the presence of an internal field, resulting in the shift of resonance, equivalent to that in the g factor.[60-63]

Assuming a pairwise exchange interaction between a Mn^{2+} ion with its nearest neighbor Ni^{2+}, the total spin Hamiltonian for the pair can be expressed as

$$\mathcal{H}_T = \mathcal{H} + \mathcal{H}' + \mathcal{H}_P$$

where

$$\mathcal{H} = \mu_B \vec{S} \cdot \breve{g} \cdot \vec{H} + b_2^0 O_2^0 + b_2^2 O_2^2 + b_4^0 O_4^0 + b_4^2 O_4^2 + b_4^4 O_4^4$$

is the spin Hamiltonian of the Mn^{2+} ion (see Sec. V.1) wherein the very small contribution of hyperfine interaction is neglected.

$$\mathcal{H}' = \mu_B \vec{S}_1 \cdot \tilde{g}_1 \cdot \vec{H} + \beta_2^0 O_2^0 + \beta_2^2 O_2^2$$

is the spin Hamiltonian of the Ni^{2+} ion ($S_1=1$) and $H_p = J\vec{S}.\vec{S}_1$ represents the Ni^{2+}-Mn^{2+} exchange interaction, where J is the exchange interaction constant.

The wave function of the total system can thus be expressed as the product wave functions $\psi_1(M)\,\psi_2(M')$, where $M = \pm 5/2,\ \pm 3/2,\ \pm 1/2$ and $M' = \pm 1,\ 0$. Thus the spin Hamiltonian of the pair system is an 18 x 18 matrix If we assume now that the external magnetic field is along the Z-axis, and Mn^{2+} and Ni^{2+} ions are occupying similar sites in host lattice, the following expressions can be obtained, using perturbation expressions and neglecting smaller zero-field parameters in the spin Hamiltonian of Mn^{2+}:

$$E(\pm\tfrac{1}{2},0) = \pm\tfrac{1}{2} g\mu_B H - \tfrac{8}{3} b_2^0 - \tfrac{2}{3}\beta_2^0$$
$$+4J^2/(\mp g\mu_B H \pm g_1\mu_B H - 2b_2^0 - \beta_2^0)$$
$$+\tfrac{9}{2} J^2/(\pm g\mu_B H \mp g_1\mu_B H - \beta_2^0) \qquad (V.9)$$

From the above energy levels, using the resonance condition (for the transition $1/2 \leftrightarrow -1/2$) $h\nu = g_{obs}\mu_B H$, one obtains the following expression for the g factor as observed in a paramagnetic host lattice:[8,14,22,30]

$$g_{obs} = g + J^2 (g + g_1) / (\beta_2^0)^2 \qquad (V.10)$$

where b_2^0 has been neglected, since $b_2^0 \ll \beta_2^0$, g_{obs} and g are the g — factor for Mn^{2+} in a paramagnetic host and corresponding isostructural diamagnetic host respectively, g_1 and b_2^0 are g-factor and zero field parameter of Ni^{2+} respectively, in the paramagnetic host.

From Eq. (V.10) it is clearly seen that from the observed g factor in a paramagnetic host one can estimate the exchange constant between the host-guest paramagnetic ions if the values of the g factors for the guest (in isostructural diamagnetic lattice) and host paramagnetic ion and the zero field splitting parameter for the host ion are known.

Using the parameters given in table 1 - 6 for Mn^{2+}-doped nickel crystals and their corresponding isostructural crystals, the value of J at liquid helium temperature was estimated to be 5.88 GHz for case of NPSH (g_1 = 2.25 and b_2^0 = 99 GHz[64]), for NSO 4.293 GHz (g_1 = 2.2 and b_2^0 = 105 GHz[61]) and 3.81 GHz for NiATH (g_1 = 2.24 and b_2^0 = 123.5 as reported in Ref. 62).

An attempt was also made to estimate the exchange interaction constant between Gd^{3+} and Yb^{3+} in the paramagnetic host $LiYbF_4$. Due to the interaction between Gd^{3+} and Yb^{3+} the g-value in this sample is shifted from

that in the isostructural diamagnetic host $LiYF_4$.[63]

Assuming that the interaction of Gd^{3+} with Yb^{3+} involves both the magnetic dipole and exchange interaction, the g-shift was calculated by Birgeneau and coworkers[63] to be as follows, considering only the nearest-neighbor (nn) and next-nearest neighbor (nnn) interaction:

$$g_z = (-\frac{8}{\Delta})\left[4\,J_{nn} - 8\alpha_{nn} + 4\,J_{nnn} + 4\alpha_{nnn}(1-3\cos^2\theta)\right] \qquad (V.11)$$

$$g_x = (-\frac{8}{\Delta})\left[4\,J_{nn} + 4\alpha_{nn} + 4J_{nnn} - 2\alpha_{nnn}(1-3\cos^2\theta)\right] \qquad (V.12)$$

where Δ is the energy separation between the ground and the first excited state of the host Yb^{3+} ion, the J's are the exchange integral, the α's represent the strength of the magnetic dipole-dipole interactions and θ is the angle that the magnetic field makes with the bond between Gd^{3+} and the next-nearest neighbors. The α's are given by

$$\alpha_i = g\mu^2 / r_i^3 ,$$

where g and μ are the g-factor and the magnetic moment respectively of the host ion Yb^{3+}, and r_i is the distance between Gd^{3+} and the ith Yb^{3+}.

The isotropic part of the single-ion g-shift is independent of the magnetic dipole interaction since:

$$(\Delta g_z + 2\Delta g_x) = (g_z + 2g_x)_{para.} - (g_z + 2g_x)_{dia}$$

$$= -\left(\frac{96}{\Delta}\right)\left[J_{nn} + J_{nnn}\right] \qquad \text{(V. 13)}$$

while the anisotropic part is independent of the exchange interaction since:

$$(\Delta g_z - \Delta g_x) = (g_z - g_x)_{para} - (g_z - g_x)_{dia}$$

$$= \frac{48}{\Delta}\left[2\alpha_{nn} - \alpha_{nnn}(1 - 3\cos^2\theta)\right] \qquad \text{(V. 14)}$$

Using Eq. (V.13) and $\Delta = 29.49 \times 10^4$ GHz,[68] the total exchange interaction between Gd^{3+} and its nearest and next nearest paramagnetic neighbor Yb^{3+} in $LiYbF_4$, $(J_{nn} + J_{nnn})$ was estimated to be 8.601 GHz.

CONCLUSION

Detailed EPR studies of several single crystals doped by Mn^{2+} have been made. The (S.H.P.) have been evaluated using a rigorous least-squares technique. The variation of b_2^0, for MSO, NSO, CaHKAP, CdHKAP and $Cu_{.05}Ca_{.95}HKAP$ was found to be linear with respect to temperature, and being explained as mainly due to the thermal expansion of the lattices. Magnetic field dependence of the linewidths in the case of nickel salts was explained due to the presence of magnetic moments induced on the Ni^{2+} ions due to external magnetic field. In the case of cobalt salts the behavior of the linewidths was concluded as being due to the "host lattice relaxation narrowing". The spin lattice relaxation time was found to be 3.4×10^{-11} and 5.3×10^{-11} secs at room and 100 K respectively, for CoZnS host and 3.3×10^{-11} and 8.3×10^{-11} secs at room and 77 K respectively for the CoZnF host. The exchange constant between Mn^{2+}-Ni^{2+} was found to be 4.293 GHz in NSO, 5.880 GHz in NPSH and 3.810 GHz in NiATH.

For the case of Cu^{2+} in copper pentakisantipyrine perchlorate the principal values of g and A tensors and their direction cosines were evaluated using a rigorous least-square fitting method. The EPR spectra revealed that there are four formula units per cell, two magnetically

equivalent and the remaining two are magnetically inequivalent.

EPR measurements on Gd^{3+}-doped paramagnetic host of $LiYbF_4$ showed a different behavior from that of diamagnetic host of $LiYF_4$. The linewidths in former were broadened rapidly as the temperature was lowered from room temperature and below 270 K no EPR lines was observed. The temperature variation of (S.H.P.) indicated that there are mechanisms other than thermal expansion, which determine the variation of these parameters with respect to temperature. Using the g-shift in $LiYbF_4$ from its value in $LiYF_4$ an amount of 8.601 GHz was found for exchange constant between Gd^{3+} and its paramagnetic neighbors ($J_{nn} + J_{nnn}$).

REFERENCES

1. S.K.Misra, Physica B 121, 193 (1983).
2. L.A.Sorin and M.V.Vlasova, Electron Spin Resonance of Paramagnetic Crystals (Plenum Press, London, 1973).
3. A.Abragam and B.Bleaney, Electron Paramagnetic Resonance of Transition Ions (Oxford, Clarendon, 1970).
4. P.B.Beyington, Data Reduction and Error Analysis for the Physical Sciences (New York, McGraw-Hill 1969).
5. S.K.Misra and Subramanian, J. Phys. C 15, 7199 (1982).
6. G.R.Sharp, M.Sc. Thesis (Concordia University, 1972).
7. R.W.G Wyckoff, Crystal Structures (Interscience, New York, 1965) vol. 3, p.837
8. S.K.Misra and M.Kahrizi, Phys. Rev. B 28, 5300 (1983).
9. M.Weger and W.Low, Phys. Rev. 111, 1526 (1958).
10. S.Kasthurirengan and R.R.Navalgund, Phys. Status Solidi (b) 72, K1 (1975).
11. G.C.Upreti, J. Mag. Res. 14, 274 (1974).
12. S.K.Misra and M.Jalochowski, Physica b 112, 83 (1982).
13. R.W.G.Wyckoff, Crystal Structures (Interscience, New York 1965), Vol.3, p. 837.
14. S.K.Misra and M.Kahrizi, Phys. Rev. B 30, 5352 (1984).
15. R.Janakiraman and G.C.Upreti, Phys. Status Solidi b 47, 679 (1971).
16. I.Hyashhi and K.Ono, J. Phys. Soc. Jpn. 8, 270 (1953).

17. R.Bramley and S.J.Starch, Chem. Phys. Lett. 79, 183 (1981).

18. S.K.Misra and B.Mikolojczak, Phys. Status Solidi B 96, 807 (1979).

19. J.N.Van Niekerk and F.R.L.Schoening, Acta Crystallogr. 6, 609 (1953).

20. J.Shankar, P.G.Khubchandani and V.M. Padmanabhan, Proc. Indian Acad. Sci. Sect. A 45, 117 (1957).

21. T.J.Manakkil, Ph.D. Thesis, New Mexico State University, 1967.

22. S.K.Misra and M.Kahrizi, Phys. Rev. B 30, 2920 (1984).

23. R.S.Saraswat and G.C.Upreti, J. Mag. Res. 20, 39 (1975).

24. R.Janakiraman and G.C.Upreti, J. Phys. Chem. Solids, 31, 1419 (1969).

25. J.N. Van Niekerk, F.R.L.Schoening, and J.H.Talbot, Acta crystallogr. 6, 720 (1953).

26. T.Arakawa, J. Phys. Soc.(Japan) 9, 790 (1954).

27. S.Soyoyama and K.Osaki, Acta Cryst. B28, 2626 (1972).

28. G.Jehanno and F.Varret, Acta Cryst. A31, 857 (1975).

29. W.C.Hamilton, Acta Cryst. 15, 353 (1962).

30. S.K.Misra and Kahrizi, Solid State Commun. 45, 967 (1983).

31. M.Vijayan and M.A.Viswamitra, Z. Kristallogr. 122, 153 (1965)., and Acta Crystallogr. 23, 1000 (1967) Acta Crystalogr. B24 1067 (1968). And Acta Crystallogr. 21 522 (1966).

32. G.M.Woltermann and J.R.Wasson, J. Phys. Chem., 77 945 (1973).

33. S.K.Misra and M.Kahrizi J. Chem. Phys. (to be published).

34. M.T.Hutchings, Solid State Physics (edited by D.Turnbull and F. Seitz, Academic Press) vol. 16, p227 (1964).

35. H.Watanabe, Progr. Theort. Phys. 18, 405 (1957).

36. W.J.Nicholson and G.Burns, Phys. Rev. 129, 2490 (1983).

37. R.S.Saraswat and G.C.Upreti, J. Chem. Phys. 67 5428 (1977).

38. G.Jayaram and G.S.Sastry, Chem. Phys. Lett. 77, 314 (1981).

39. Ananthanarayanan, Ph.D. Thesis, I.I.Sc. Bangalore (India) (1961).

40. B.Bleaney and D.J.E.Ingram, Proc. R. Soc. London ser. A 208, 143 (1953).

41. R.W.G.Wyckoff, Crystal Structure, 2nd Edition, vol.3, p 797 (Wiley, New York, 1965).

42. S.K.Misra and M.Kahrizi (to be published).

43. S.K.Misra and M.Jalochowski, Physica 119B, 295 (1983).

44. R.Srinivasan and C.K.Subramanian, Ind. J. Pure and Apll. Phys. 8, 817 (1970).

45. S.K.Misra, Physica B 124 53 (1983).

46. R.E.Thoma, C.F.Weaver, H.A.Friedman, H.Insley, L.A.Harris and H.A. Yakel, J. Phys. Chem. 65, 1096 (1961).

47. C.Keller aand H. Schmutz , J. Inorg. Nucl. Chem. 27, 900 (1965).

48. H.Berman/ed./, Gmelin Handbuck der Anorganischen Chemie Seltenerdelemente, Teil. C3, No. 39, 270-295 (Springer-Verlag, Berlin-Heidelberg - New York, 1976).

49. Y.Vaills and J.Y.Buzare, Solid Stat. Commun. 45, 1093 (1983).

50. S.K.Misra and M.Kahrizi (to bepublished).

51. E.Simanek and R.Orbach, Phys. Rev. 145, 191 (1966).

52. R.A.Serway, Phys. Rev. B 3, 608 (1971).

53. I.N.Geifman and M.D.Glinchak, Fiz. Tverd. Tela (Leningrad) 13, 1050 (1971) (Sov. Phys. Solid State 13 872 (1971)).

54. P.W.Anderson and P.R.Weiss, Rev. Mol. Phys. 25, 269 (1953).

55. T.Mitsuma, J. Phys. Soc. Jap. 17, 128 (1962).

56. J.H.E.Griffiths and J.Owen, Proc. Roy. Soc. A123, 459 (1952).

57. T.Moriya and Y.Obata,, J. Phys. Soc Jap. 13, 1333 (1958).

58. S.K.Misra and P.Mikolajczak, Phys. Stat. Sol.(b) 109 59 (1982).

59. C.Kittel, Phys. Rev. 73, 155 (1948).

60. M.T.Hutchings and W.P.Wolf, Phys. Rev. Lett. 11, 187 (1963).

61. M.T.Hutchings, C.G.Windsor, and W.P.Wolf, Phys. Rev. 148, 4444 (1966).

62. M.R.St.John and R.J.Myers, Phys. Rev. B 13, 1006 (1967).

63. W.T.Batchelder, Ph.D. Thesis, University of California, Berkeley, 1970.

64. J.H.E.Griffiths and J. Owen, Proc. R. Soc. London, Ser.A 213, 459 (1952).

65. K.Ono, J. Phys. Soc. Jpn. 8, 802 (1953).

66. J.T.Schriempf and S.A.Friedberg, J. Chem. Phys. 40, 296 (1964).

67. R.J.Birgeneau, M.T.Hutchings and W.P.Wolf, Phys. Rev. 179, 275 (1969).

68. K.A.Gschneidner Jr. And L.R.Eyring, Handbook on the Physics and Chemistry of rare-earths, Vol. 2, p 478 (North-Holland, 1979).

APPENDIX A

Equivalent operators for the polynomials in Table 15. The notation $\{A, B\}_s$ *is used as a shorthand for* $(\frac{1}{2})(AB+BA)$. *Thus* $O_4^3 = \frac{1}{2}\{J_z(J_+^3+J_-^3)\}$ *denotes* $O_4^3 = \frac{1}{2}\{J_z(J_+^3+J_-^3)+(J_+^3+J_-^3)J_z\}$

$k = 2$

$$\begin{cases} O_2^0 = 3J_z^2 - J(J+1) \\ O_2^2 = \frac{1}{2}(J_+^2 + J_-^2) \end{cases}$$

$k = 4$

$$\begin{cases} O_4^0 = 35J_z^4 - 30J(J+1)J_z^2 + 25J_z^2 - 6J(J+1) + 3J^2(J+1)^2 \\ O_4^2 = \frac{1}{4}\{(7J_z^2 - J(J+1) - 5)(J_+^2 + J_-^2)\}_s \\ O_4^3 = \frac{1}{2}\{J_z(J_+^3 + J_-^3)\}_s \\ O_4^4 = \frac{1}{2}(J_+^4 + J_-^4) \end{cases}$$

$k = 6$

$$\begin{cases} O_6^0 = 231J_z^6 - 315J(J+1)J_z^4 + 735J_z^4 + 105J^2(J+1)^2J_z^2 - 525J(J+1)J_z^2 + \\ \qquad + 294J_z^2 - 5J^3(J+1)^3 + 40J^2(J+1)^2 - 60J(J+1) \\ O_6^2 = \frac{1}{4}\{(11J_z^2 - 3J(J+1)J_z - 59J_z)(J_+^2 + J_-^2)\}_s \\ O_6^4 = \frac{1}{4}\{(11J_z^2 - J(J+1) - 38)(J_+^4 + J_-^4)\}_s \\ O_6^6 = \frac{1}{2}(J_+^6 + J_-^6) \end{cases}$$

APPENDIX B

(PUBLICATIONS)

Solid State Communications, Vol. 45, No. 11, pp. 967–970, 1983.
Printed in Great Britain.

0038–1098/83/110967–04$03.00/0
Pergamon Press Ltd

EPR OF Mn^{2+}-DOPED SINGLE CRYSTAL OF $MgSiF_6 \cdot 6H_2O$

Sushil K Misra* and M. Kahrizi

Physics Department, Concordia University, S G W Campus, 1455 De Maisonneuve Boulevard West, Montreal, Canada, H3G 1M8†

(*Received* 29 *September* 1982; *in revised form* 18 *November* 1982 *by E.F. Bertaut*)

X-band EPR measurements are reported on single crystals of $MgSiF_6 \cdot 6H_2O$ doped with Mn^{2+} ions at various temperatures. The absolute signs of the spin Hamiltonian parameters are determined from liquid-helium-temperature data. The values of the parameters are evaluated rigorously using the method of least-squares fitting.

1. INTRODUCTION

EPR MEASUREMENTS ON Mn^{2+}-doped single crystal of $MgSiF_6 \cdot 6H_2O$ (referred to hereafter as MFS) have been previously reported by Arakawa [1]. The measurement was confined to room temperature only, not permitting the determination of absolute signs of parameters and perturbation expressions were used for the evaluation of parameters.

Recently [2, 3] it was found that when the host contains paramagnetic ions, such as Ni^{2+}, the EPR line-widths show certain dependence on the intensity of external magnetic field, as well as upon the temperature. Theoretical treatments have been presented on this topic; see, for example, Moriya and Obata [4]. It was first decided to undertake EPR studies of Mn^{2+}-doped $NiSiF_6 \cdot 6H_2O$. However even for very small doping (< 1%) by Mn^{2+} ions, the EPR lines were *very broad* even at room temperature, not to offer any useful data. This behaviour is found contrary to that exhibited in the nickel salts, e.g $Ni(CH_3COO)_2 \cdot 4H_2O$ and $NiK_2(SO_4)_2 \cdot 6H_2O$ hosts in which (many or all) clearly resolved EPR lines are observed at all temperatures [2, 3]. It was therefore decided to investigate the EPR spectra of Mn^{2+}-doped MFS host, which contains diamagnetic atoms (Mg) in order that one could indirectly understand what role is played by the paramagnetic nature of the host metal. It was felt that the experimental study reported in this paper would help further in understanding the interaction of the Mn^{2+} ion with its environment. The values of spin Hamiltonian parameters as presented in this paper, are evaluated using a rigorous least-squares fitting procedure in which all line positions, obtained for several orientations of the magnetic field; are simultaneously fitted and numerical diagonalization of the spin Hamiltonian matrix is utilized [5, 6]. As the data are obtained right down to liquid helium temperatures absolute signs of the fine-structure parameters can be determined from the intensities of lines.

2. SAMPLE PREPARATION AND CRYSTAL STRUCTURE

The samples were prepared by first dissolving calculated stoichiometric amounts of Mg metal in hydrofluosilicic acid ($H_2SiF_6 \cdot 6H_2O$) and adding appropriate amount of $MnSiF_6 \cdot 6H_2O$ solution to the $MgSiF_6 \cdot 6H_2O$ solution so obtained, so that there is one Mn atom for each 1000 Mg atoms in the solution. The resultant solution was allowed to evaporate slowly till decent crystals were obtained. The crystals were coated with Krylon, clear spray to prevent deliquescence.

The latest crystallographic studies [7, 8] indicate that below 300 K the crystal lattice of $MgSiF_6 \cdot 6H_2O$ is described by the space group $P2_1/c$ (monoclinic) while at temperatures higher than 300 K it is described by R3m (hexagonal). The phase transition between the two symmetries takes place at about 300 K. Thus, for all the temperatures of EPR measurements described in this paper the crystal is in the monoclinic phase, for which the crystal data are: $a = 6.460$, $b = 9.524$, $c = 8.460$ Å (all ± 0.005 Å), $\beta = 99°24' \pm 3'$, $D_0 = 1.77$, $D_c = 1.780\ g\,cm^{-3}$, $Z = 2$ [7]. The phase transition $P\bar{3}m1 \rightarrow P2_1/c$ at 300 K has also been supported by optical [9] and Mössbauer [10] studies. The EPR data, as described in Section 3 below, are, however, *apparently* incompatible with the monoclinic symmetry. Upon close examination the data can, indeed,

*On leave of absence at Laboratoire de Physique des Solides Associé au CNRS, Université Paul Sabatier, 118 Route de Narbonne, 31062 Toulouse Cédex (France) (1982–1983).

†Permanent address.

be understood to conform to the monoclinic symmetry if one takes into account the fact that the specimen used in [1] as well as in this paper, consist of three-fold twins of the low-temperature form [7] (the single crystals twin extremely easily). The explanation of Section 3 below is, thus, valid provided that one understand by the trigonal axis, the pseudotrigonal axis similar to that given for $FeSiF_6 \cdot 6H_2O$ by Hamilton [11]. The explanation of Section 3 is in terms of the planes of [1, 11]. In a projection along this pseudo-trigonal axis, the $[Mg(H_2O)_6]^{2+}$ ions are surrounded by $[SiF_6]^{2-}$ ions with two different orientations [7]. This fact combined with the threefold twinning of the sample used explains the appearance of six inequivalent Mn^{2+} ions as revealed by the EPR spectra (Section 3). It should be noted that $MnSiF_6 \cdot 6H_2O$ undergoes the same phase transition as that for $MgSiF_6 \cdot 6H_2O$ at a lower temperature (230 K). However, since the amount of Mn is only 0.1% that of Mg in the sample, the phase transition of the sample is solely that due to $MgSiF_6 \cdot 6H_2O$

3. EXPERIMENTAL DETAILS AND SPIN HAMILTONIAN

The EPR spectra were recorded on a homodyne X-band spectrometer using a 100 kHz field modulation. (For details, see [4]). The EPR measurements for external magnetic field orientation in $\{1\bar{1}0\}$ and in $\{111\}$ planes, which are parallel and perpendicular to the trigonal axis respectively, revealed the existence of six inequivalent Mn^{2+} ions. In particular, this was deduced from the following observations. (*i*) When the external magnetic field is nearly parallel to the trigonal axis in the $\{1\bar{1}0\}$ plane is line splitting of the lowest field line. (*ii*) When the magnetic field orientation is in the $\{111\}$ plane, a plot of the lowest-field lines corresponding to the various inequivalent ions exhibits angular variation patterns of type $a-b\cos\{(2\phi+\delta_i)\}$, where $(\delta_{i+1}-\delta_i)=30°$; $i=1, 2, \ldots 5$, ϕ being the angle between the magnetic field and a fixed direction in the $\{111\}$ plane. The angular variation can be ascribed to terms of rhombic symmetry [1, 11]. Therefore, there are six sets of x and y axes (for definition of axes, see the following paragraph) in the $\{111\}$ plane which have different orientations about the trigonal axis in equal intervals of 30° with deviations of 15° from the nearby directions along which the $\{1\bar{1}1\}$, $\{10\bar{1}\}$ or $\{01\bar{1}\}$ planes cut the $\{111\}$ plane. Thus for any inequivalent Mn^{2+} ion, the spectra are fitted to the following spin Hamiltonian.

$$\mathcal{H} = \beta \mathbf{H}\cdot\mathbf{g}\cdot\mathbf{S} + \sum_{m=0,2} \tfrac{1}{3} b_2^m O_2^m + \sum_{m=0,2,4} \tfrac{1}{180} b_4^m O_4^m + AS_zI_z + B(S_xI_x + S_yI_y) + Q'[I_z^2 - \tfrac{1}{3}(I+1)] + Q''[I_x^2 - I_y^2]. \quad (3.1)$$

In Equation (3.1) $S = I = 5/2$ for the Mn atom and O_i^m are spin operators as defined by Abragam and Bleaney [12]. (For further details, see [2, 3]) The x, y, z axes coincide with the principal axes of the b_2^m tensor, i e those directions of the external field for which the overall splitting of lines exhibit maxima. The z axis is the direction along which the maximum is largest, while the y axis is along the direction for which the maximum is smallest Further, the z axis is found to be parallel to the trigonal axis

It should be noted that the spin Hamiltonian represented by Equation (3 1) would also serve for the monoclinic symmetry, if one were to add to it the terms $\frac{1}{3}b_2^{-2}O_2^{-2} + \frac{1}{180}(b_4^{-2}O_4^{-2} + b_4^{-4}O_4^{-4})$. However, since the measurements are made in the zx plane only, the coefficients b_2^m with $m < 0$ cannot be determined from the data [13]. Thus (3 1) truly represents the spin Hamiltonian that describes the EPR data reported in this paper.

Figure 1 exhibits the angular variation of spectra (zx plane) for a magnetically inequivalent Mn^{2+} ion at room temperature. It is found that all the 30 hyperfine lines are clearly observable between $-30°$ and 30°, and between 70° and 110° in the zx plane at all temperatures. The spectra obtained for angles 90°–180° from the z axis in the zx plane were the mirror images of those obtained for angles 90°–0° from the z axis.

4. EVALUATION OF PARAMETERS

The parameters were evaluated by a simultaneous fitting of all clearly observed line positions using a rigorous least-squares fitting method and exact numerical diagonalization of the spin Hamiltonian matrix (for more details see [2, 6]). In particular, the initial values used were those reported by Arakawa [1]; the initial values of remaining smaller parameters were chosen to be zero. The fitting gave only the correct relative signs of the fine-structure parameters; the absolute signs were determined from the relative intensity data obtained at low temperatures. For further details, see Section 5.

Table 1 contains the listing of the parameters at various temperatures. The g values are found to be less than or equal to the free-electron value, implying the absence of covalent bonding between the Mn^{2+} ion and the surrounding ligands [15].

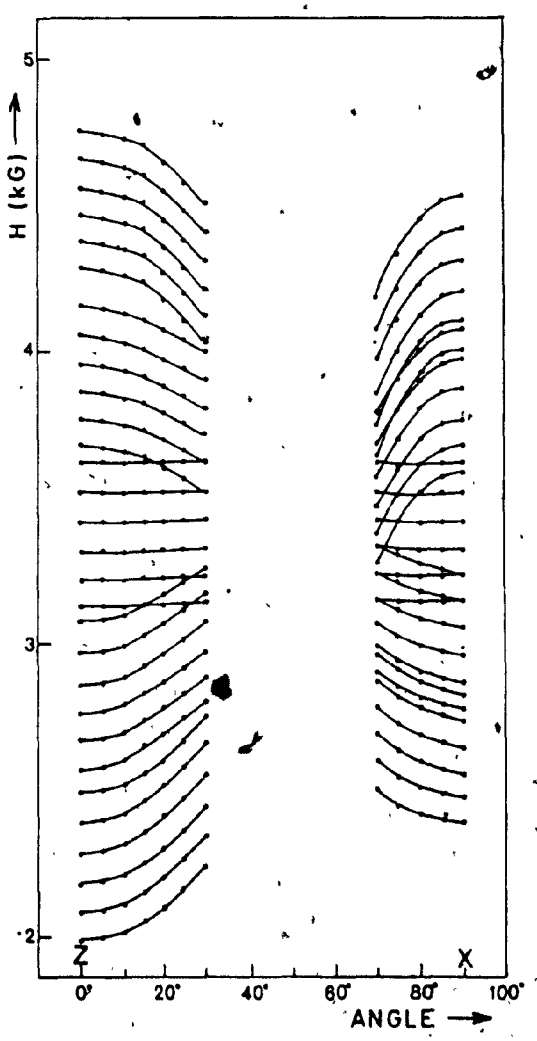

Fig. 1. Angular variation of X-band EPR spectrum in the zx plane for Mn^{2+} doping MFS host at room temperature The solid lines are smooth curves that connect data points from the same transition. Only spectra corresponding to one inequivalent Mn^{2+} ion have been exhibited.

5. INTENSITIES

The ratio of the average intensity of the highest-field sextet to that for the lowest-field sextet is, for the external field orientation along the z axis, observed to be ~ 0.522, ~ 0.626, ~ 1.102, ~ 1.117 and ~ 1.128 at temperatures 295, 85, 5, 3.5 and 2 K respectively. Thus according to the theory presented in [12] the absolute sign of the parameter b_4^3 turns out to be positive. As far as the signs of hyperfine parameters

Table 1. Values of spin Hamiltonian parameters for 0.1% Mn^{2+}*-doped MFS host. RMSL (in GHz)* = $\sqrt{\Sigma_j(|\Delta E_j| - h\nu_j)^2/n}$, *where* ΔE_j *is the calculated energy difference between levels participating in resonance for the* j^{th} *resonant magnetic field value,* $h\nu_j$ *is the energy of microwave radiation and n is the number of lines used in each fitting. The parameters* b_l^m, Q', Q", A, B *are expressed in units of* GHz. *A negative value has been assumed for the sign of* A [16]. *The indicated errors are calculated using the statistical method* [14]

Temperature	295 K	85 K	5 K
g_{zz}	1.962 ± 0 001	1.992 ± 0.001	2.000 ± 0.001
g_{xx}	1.959 ± 0 001	1.963 ± 0.001	1.962 ±,0.001
b_2^0	0 836 ± 0 003	0.787 ± 0.003	0.0788 ± 0 003
b_2^2	−0.235 ± 0.006	−0.350 ± 0.006	−0.401 ± 0.006
b_4^0	0.008 ± 0.002	0.010 ± 0.002	0.015 ± 0.002
b_4^2	−0.183 ± 0.031	−0.577 ± 0.028	−0 279 ± 0 030
b_4^4	−0.245 ± 0.032	−0.147 ± 0.030	−0 353 ± 0.030
Q'	0.021 ± 0 008	0.015 ± 0.007	0.022 ± 0 008
Q''	0 034 ± 0 013	0.044 ± 0.011	0 030 ± 0 013
A	−0.278 ± 0.004	−0.284 ± 0.004	−0.276 ± 0.004
B	−0.257 ± 0 004	−0 249 ± 0.004	−0.251 ± 0 004
n	250	267	255
RMSL	0.066	0.041	0.053

A, B are concerned, they are chosen to be negative in accordance with the hyperfine interaction data [16]. The signs of all the parameters given in Table 1 should then be considered absolute.

6. LINEWIDTHS

The average peak-to-peak linewdiths of the first-derivative lineshape for the lowest-field sextet for $H \| z$ are found to be ~ 25, ~ 22 and ~ 16 G at temperatures 295, 85 and 5 K respectively, while the corresponding values for the highest-field sextet are found to be ~ 20, ~ 18 and ~ 15 G respectively. For $H \| x$ the linewidths are found to be about the same as for $H \| z$. These represent only insignificant decrease in values as one goes to lower temperatures.

Acknowledgements – We thank the Natural Sciences and Engineering Research Council of Canada for financial support (Grant No A4485). The use of the facilities provided by the Concordia University Computer Centre is gratefully acknowledged.

REFERENCES

1. T. Arakawa, *J. Phys. Soc. (Japan)* 9, 790 (1954).
2. S.K. Misra & B. Mikolajczak, *Phys. Stat. Sol. (b)*, 96, 807 (1979)
3. S.K. Misra & M. Jalochowski, *Physica* 1f2b, 83 (1982).
4. T. Moriya & Y. Obata, *J. Phys. Soc. (Japan)* 13, 1333 (1958).
5. S.K. Misra, *J. Mag. Reson.* 23, 403 (1976)
6. S.K. Misra, *Physica b*, to be published.
7. S. Soyoyama & K. Osaki, *Acta Cryst.* B28, 2626 (1972).
8. G. Jehanno & F. Varret, *Acta Cryst.* A31, 857 (1975).
9. I. Tsujikawa & L. Coulture, *J. Phys. Rad.* 16, *430 (1955).*
10. J. Chappert, G. Jehanno & F. Varret, *Journal of Physique* 38, 412 (1977).
11. W.C. Hamilton, *Acta Cryst.* 15, 353 (1962).
12. A. Abragam & B. Bleaney, *Electron Praamagnetic Resonance of Transition Ions*, p. 140, 161, 178. Oxford (1970).
13. S.K. Misra, P. Mikolajczak & M. Jalochowski, *Phys. Stat. Sol. (b)* 111, 227 (1982)
14. S.K. Misra & S. Subramanian, *J. Phys. C.* to he published.
15. T.J. Manakkil, Ph.D., Thesis, New Mexico State University (1967).
16. A. Steudel, *Hyperfine Interactions*, p. 182, Academic Press, (1976).

PHYSICAL REVIEW B VOLUME 28, NUMBER 9 1 NOVEMBER 1983

EPR of Mn^{2+}-doped single crystals of $ZnK_2(SO_4)_2\cdot 6H_2O$ and $NiK_2(SO_4)_2\cdot 6H_2O$: Mn^{2+}-Ni^{2+} exchange constant

Sushil K Misra and Mojtaba Kahrizi
Physics Department, Concordia University, 1455 de Maisonneuve Boulevard West, Montreal, Quebec H3G 1M8, Canada
(Received 22 June 1983)

X-band EPR measurements on Mn^{2+}-doped single isostructural crystals of diamagnetic zinc potassium sulfate hexahydrate and paramagnetic nickel potassium sulfate hexahydrate have been made at room, liquid-nitrogen, and liquid-helium temperatures. To avoid the demagnetization effects, a spherical-shaped sample was used for the paramagnetic lattice. The spin-Hamiltonian parameters were evaluated using a least-squares fitting method, simultaneously fitting all resonant line positions obtained for several orientations of the external magnetic field. Using the g shift in the paramagnetic host, from that in the isostructural diamagnetic host, the Mn^{2+}-Ni^{2+} exchange constant has been estimated.

I. INTRODUCTION

EPR measurements on a Mn^{2+}-doped single crystal of zinc potassium sulfate hexahydrate, $ZnK_2(SO_4)_2\cdot 6H_2O$ (hereafter ZPSH), have been reported by Kasthurirengan and Navalgund[1] (at room temperature only), while those on Mn^{2+}-doped nickel potassium sulfate hexahydrate, $NiK_2(SO_4)_2\cdot 6H_2O$ (hereafter NPSH), have been reported by Misra and Jalochowski[2] (from room down to liquid-helium temperature). The spin-Hamiltonian parameters (ignoring the fourth-order ones) as reported in Ref. 1 were evaluated from perturbation theory by use of only the resonant line positions obtained for the external magnetic field orientation along the Z and X axes; further, these measurements were confined to room temperature only. In Ref. 2, while the parameters were rigorously evaluated by use of a least-squares fitting procedure,[3] the shape of the host crystal used was arbitrary, thus being susceptible to demagnetization effects at low temperatures.

Paramagnetic lattices become magnetized at low temperatures, and it is shown by Kittel[4] that in these crystals, for axial symmetry, the observed g factor g_{obs} gets shifted from its value g in the corresponding isostructural diamagnetic lattice by an amount $[(4\pi/3)-N_z]1.5M/H_0$, where N_z is the demagnetization factor along the axis of symmetry, M is the magnetization, and H_0 is the external magnetic field intensity. (N_z is $4\pi/3$ for a spherical sample.) Thus, in order to eliminate this shift due to the demagnetization effect, one should use spherical paramagnetic host crystals. However, there is another g shift experienced in paramagnetic lattices, i.e., that due to the exchange interaction between the host paramagnetic ions and the guest paramagnetic ion (for details see Sec. II). Thus for a Mn^{2+}-doped NPSH crystal, for a spherical sample, the g shift at low temperatures would depend only upon the Mn^{2+}-Ni^{2+} exchange interaction.

Recently, a rigorous technique using the least-squares fitting procedure, specifically applicable to the electron-nuclear spin-coupled system, e.g., that of a Mn^{2+} ion, has been proposed.[5]

It is the purpose of the present paper to report detailed *X*-band EPR measurements on Mn^{2+}-doped single crystals of ZPSH and NPSH (spherical shape) at room, liquid-nitrogen, and liquid-helium temperatures. From a comparison of the g values as found in the two hosts at liquid-helium temperature, the Mn^{2+}-Ni^{2+} exchange-interaction constant has been estimated. Section II deals with the theory of the shift of g value due to the presence of paramagnetic host ions, while the crystal structure and sample preparation are given in Sec. III. The resulting values of the spin-Hamiltonian parameters and the Mn^{2+}-Ni^{2+} exchange-interaction constant are discussed in Sec. IV. Linewidth behavior is discussed in Sec. V.

II. g SHIFT

The shift of the g value due to the presence of paramagnetic host ions is caused by the exchange interaction between the guest and host paramagnetic ions, i.e., Mn^{2+} and Ni^{2+} in the present case. As a result of the polarization effect of the external field, magnetic moments are induced on the paramagnetic host ions. These magnetic moments interact with the guest Mn^{2+} ion, thus causing the presence of an internal field, resulting in the shift of resonance, equivalent to that in the g factor.[6-9]

Assuming a pairwise exchange interaction between a Mn^{2+} ion with its nearest neighbor Ni^{2+}, the total spin Hamiltonian for the pair can be expressed as

$$H_T = H + H' + H_P \ , \tag{2.1}$$

where

$$H = g\mu_B \vec{S}\cdot\vec{H} + b_2^0 O_2^0 + b_2^1 O_2^1 + b_2^2 O_2^2 + b_2^{-1} O_2^{-1} + b_2^{-2} O_2^{-2}$$

is the spin Hamiltonian of the Mn^{2+} ion ($S=\frac{5}{2}$) (see Sec. III for further details);

$$H' = g_1\mu_B \vec{S}_1\cdot\vec{H} + \beta_2^0 O_2^0 + \beta_2^1 O_2^1$$

is the spin Hamiltonian of the Ni^{2+} ion ($S_1=1$), and $H_P = J\vec{S}\cdot\vec{S}_1$ represents the Ni^{2+}-Mn^{2+} exchange interaction, where J is the exchange-interaction constant.

The wave functions of the total system can thus be expressed as product wave functions $\psi_1(M)\psi_2(M')$, where $M = \pm\frac{1}{2}, \pm\frac{3}{2}, \pm\frac{5}{2}$, and $M' = \pm 1, 0$. Thus the spin Hamiltonian of the pair system is an 18×18 matrix. If we assume now that the external magnetic field is along the z axis, the following expressions can be obtained, using per-

turbation theory and neglecting smaller zero-order terms in the spin Hamiltonian of Mn^{2+}:

$$E(\pm\tfrac{1}{2},0) = \pm\tfrac{1}{2}g\mu_B H - \tfrac{1}{3}b_1^0 - \tfrac{2}{3}\beta_1^0 + 4J^2/(\mp g\mu_B H \pm g_1\mu_B H - 2b_1^0 - \beta_1^0) + \tfrac{9}{7}J^2/(\pm g\mu_B H \mp g_1\mu_B H - \beta_1^0) \quad . \tag{2.2}$$

From the above energy levels, using the resonance condition (for the transition $\frac{1}{2} \rightarrow -\frac{1}{2}$) $h\nu = g_{obs}\mu_B H$, one obtains the following expression for the g factor as observed in a paramagnetic host lattice

$$g_{obs} = g + J^2(g + g_1)/(\beta_1^0)^2 \quad . \tag{2.3}$$

where b_1^0 has been neglected, since $b_1^0 \ll \beta_1^0$.

From Eq. (2.3) it is clearly seen that from the observed g factor in a paramagnetic host lattice one can estimate the exchange constant between the host-guest paramagnetic ions if the values of the g factors for the guest (in isostructural diamagnetic lattice) and host paramagnetic ions and the zero-field splitting parameter for the host ions are known.

The value of $|J|$, using Eq. (2.3), as estimated in Sec. IV, turns out to be 5.88 GHz.

III. CRYSTAL STRUCTURE, SAMPLE PREPARATION, AND EXPERIMENTAL DETAILS

The ZPSH and NPSH crystals, like the other tutton salts, belong to the monoclinic symmetry, with space group $P2/a$ (C_{2h}^4). The unit cell contains two formula units. Six water molecules form an octahedron around the divalent metal ion. The unit-cell dimensions are $a = 8.98$, $b = 12.22$, and $c = 6.10$ Å, and the monoclinic angle β is about 105°. For more details see Ref. 2.

The single crystals of Mn^{2+}-doped ZPSH and NPSH were grown by slow evaporation at room temperature of solutions of ZPSH and NPSH, each containing 0.1% $MnSO_4 \cdot 6H_2O$ stoichiometrically. In order to avoid sample demagnetization effects at low temperatures, the spheres of 1–2 mm of NPSH samples were prepared by blowing the roughly cubic single crystals on emery paper.

The experimental arrangement is the same as that described in Ref. 2.

IV. SPIN HAMILTONIAN, DATA, AND EVALUATION OF PARAMETERS

The spin Hamiltonian appropriate to present samples of monoclinic symmetry is in standard notation[10]:

$$\begin{aligned} H = {} & \mu_B \vec{H} \cdot \vec{g} \cdot \vec{S} + \sum_{m=0,2} \tfrac{1}{3} b_2^m O_2^m + \sum_{m=0,2,4} \tfrac{1}{60} b_4^m O_4^m \\ & + A S_z I_z + B(S_x I_x + S_y I_y) + Q'[I_z^2 - \tfrac{1}{3} I(I+1)] \\ & + Q''(I_x^2 - I_y^2) \quad . \end{aligned} \tag{4.1}$$

Here $\vec{g}$, b_2^m, A, B, Q', and Q'' are the spin-Hamiltonian parameters, O_2^m are spin operators,[10] μ_B is the Bohr magneton, H is the external magnetic field, and S and I are the electron and nuclear spins, respectively ($S = I = \frac{1}{2}$).

The X, Y, and Z axes are chosen to coincide with the principal axes of the b_2^m tensor, so that the overall splitting of the spectra is maximum along the Z axis and minimum

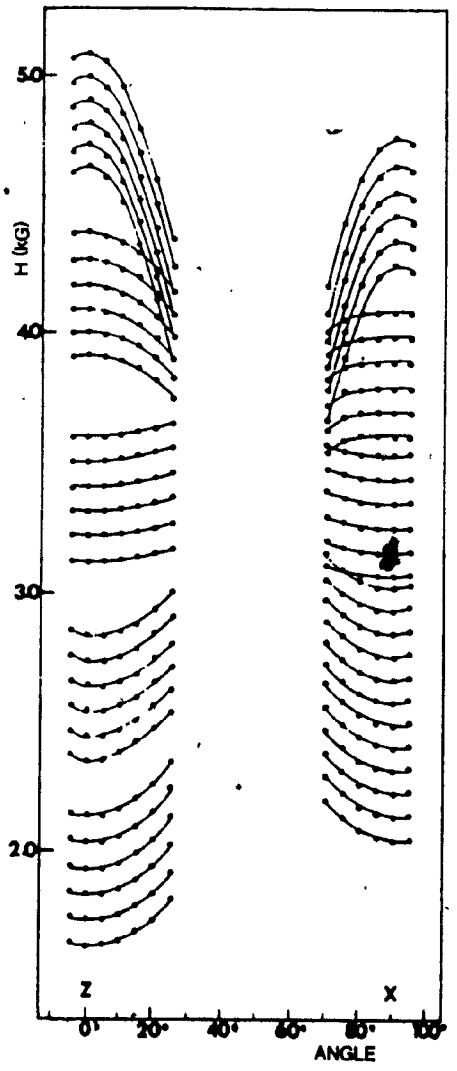

FIG. 1. Angular variation of X-band spectrum in the ZX plane for the Mn^{2+}-doped ZPSH host at room temperature. The circles represent the experimental resonant-line positions, and the solid lines are smooth curves that connect data points from the same transition. Only spectra corresponding to one inequivalent Mn^{2+} ion have been exhibited.

TABLE I Values of spin-Hamiltonian parameters for the Mn^{2+}-doped ZPSH host (0.1%). RMS linewidth (RMSL) (in GHz) is $(\sum_j(|\Delta E_j|-h\nu_j)^2/n)^{1/2}$, where ΔE_j is the calculated energy difference between levels participating in resonance for the jth resonant magnetic field value, $h\nu_j$ is the energy of microwave radiation, and n is the number of points used in each fitting. The parameters b_i^k, Q', Q'', A, and B are expressed in units of GHz. A negative sign has been assumed for the value of A. The indicated errors are calculated by use of the statistical method (Ref. 12). The parameters at room temperature, as reported in Ref. 1, have also been included for comparison.

Temperature	295 K[a]	85 K[a]	5 K[a]	295 K[b]
g_{zz}	1.996 ± 0.001	2.001 ± 0.001	2.002 ± 0.001	2.016
g_{xx}	1.999 ± 0.001	2.021 ± 0.001	2.013 ± 0.001	2.016
b_1^0	−1.068 ± 0.002	−1.315 ± 0.002	−1.359 ± 0.002	0.730
b_1^2	0.508 ± 0.005	0.528 ± 0.005	0.489 ± 0.005	0.605
b_2^0	0.018 ± 0.001	0.019 ± 0.001	0.021 ± 0.001	...
b_2^2	−0.014 ± 0.023	0.002 ± 0.025	−0.225 ± 0.025	...
b_2^4	0.011 ± 0.023	0.047 ± 0.023	−0.133 ± 0.026	
Q'	−0.021 ± 0.006	−0.015 ± 0.006	0.002 ± 0.006	0.004
Q''	−0.058 ± 0.011	−0.040 ± 0.001	0.015 ± 0.011	0.025
A	−0.265 ± 0.004	−0.259 ± 0.004	−0.258 ± 0.004	−0.244
B	−0.269 ± 0.004	−0.264 ± 0.004	−0.260 ± 0.004	−0.246
n	287	297	232	...
RMSL	0.028	0.031	0.052	

[a]This work. [b]Reference 1.

along Y.[11] The spectra for ZPSH were recorded at room, liquid-nitrogen, and liquid-helium temperatures, while that of NPSH at room and liquid-helium temperatures only. The general shape of the spectra and angular variation of resonant-line positions with respect to the external magnetic field for the NPSH host are given in Ref. 2. For the ZPSH host two sets of spectra corresponding to two inequivalent Mn^{2+} ions in the unit cell were observed. For each, along their respective Z and X axes, 30 distinguishable hyperfine lines, plus some forbidden lines appearing mostly near the central fine transition $-\frac{1}{2} \leftrightarrow \frac{1}{2}$, were observed. Along the Y axis, the number of overlapped lines increased and only 24 lines appeared. The shape of the spectra remained the same at all temperatures; however, the overall splitting increased with lowering the temperature. The angular variation of spectra for ZPSH is shown in Fig. 1.

The parameters were evaluated by use of a rigorous least-squares fitting (LSF) procedure specifically designed and adapted to the electron-nuclear spin-coupled system of Mn^{2+}.[3] First, the fine-line positions were estimated to evaluate initial values of fine-structure parameters, and LSF fitting was used in the purely electronic space,[3] fitting simultaneously all estimated fine-line positions. This saved com-

TABLE II Values of spin-Hamiltonian parameters of spherical sample for the Mn^{2+}-doped NPSH host (0.1%). Other details and notations are the same as those given in the caption of Table I.

Temperature	295 K	5 K	18 K
g_{zz}	2.058 ± 0.002	2.017 ± 0.002	2.024 ± 0.002
g_{xx}	2.025 ± 0.002	1.991 ± 0.002	1.974 ± 0.002
b_1^0	−0.750 ± 0.026	−1.198 ± 0.025	−1.260 ± 0.023
b_1^2	0.564 ± 0.025	0.432 ± 0.022	0.395 ± 0.021
b_2^0	0.300 ± 0.068	0.125 ± 0.083	0.111 ± 0.082
b_2^2	0.910 ± 0.236	0.454 ± 0.300	0.342 ± 0.300
b_2^4	0.153 ± 0.047	0.200 ± 0.079	0.125 ± 0.076
Q'	0.009 ± 0.001	0.001 ± 0.001	−0.001 ± 0.001
Q''	−0.001 ± 0.030	0.014 ± 0.030	0.042 ± 0.030
A	−0.275 ± 0.004	−0.115 ± 0.004	−0.169 ± 0.004
B	−0.232 ± 0.004	−0.228 ± 0.004	−0.228 ± 0.004
n	149	160	160
RMSL	0.052	0.036	0.043

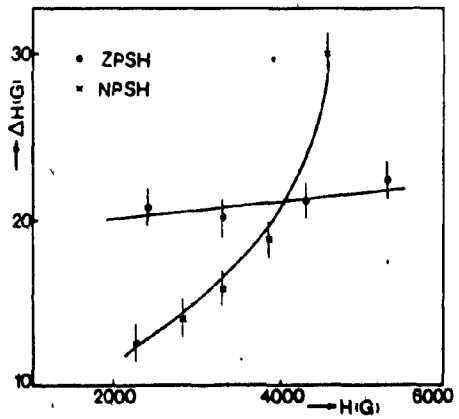

FIG. 2. Variation of linewidths as a function of magnetic field intensity at liquid-helium temperature for the orientation of the external magnetic field along the Z axis for the NPSH and ZPSH hosts.

puter time on the final fitting of all the hyperfine line positions on the LSF procedure, using the fine-structure parameter values, already obtained, as initial values

The values of the parameters so obtained for ZPSH are significantly different from those reported in Ref 1 The fourth-order parameters, neglected in Ref. 1, are found to have small, but significant values The absolute sign of b_4^0, determined from relative intensities of lines at liquid-helium temperatures, is negative, since the intensity of the highest-field sextet *decreased* relative to that of the lowest-field sextet as the temperature was lowered to liquid-helium temperatures.[10] The values of parameters for the NPSH and ZPSH samples are given in Tables I and II at various temperatures. The errors were determined by use of a statistical method [12]

From the observed g values of the spherical NPSH host at liquid-helium temperature and the g values for the ZPSH host, as given in Tables I and II, the value of J was found to be, using Eq. (2.3), $|J| = 5.88$ GHz. The values for the Ni^{2+} ion used were $g_1 = 2.25$ and $\beta_4^0 = 99$ GHz as found by Griffiths and Owen.[13]

V. LINEWIDTHS

The EPR linewidths for the ZPSH lattice were of the order of 20 G for all lines at all temperatures On the other hand, for the NPSH host, the linewidths showed anisotropy with respect to the direction of the external field. Moreover, they depend upon the intensity of the external field also These behaviors can be explained to be due to the presence of Ni^{2+} ions (see below). In particular, for the NPSH host, for the orientation of the external field along the Z axis, only a few lines at low magnetic fields were observed, the widths of the lines increased with increasing magnetic field intensity, and for sufficiently high magnetic field intensity all lines completely broadened out and disappeared. For the magnetic field along the X axis, the line *broadening is not much, and all lines are observable.*

As discussed in Ref. 2 the paramagnetic Ni^{2+} ions in the NPSH lattice are responsible for the different behaviors of linewidths in the NPSH and ZPSH lattices. This is due to the magnetic moment induced on the Ni^{2+} ions because of the presence of the external magnetic field, the moment depending upon the spin-Hamiltonian parameters g_1, β_4^0, and β_4^3 of Ni^{2+} in the NPSH lattice (for further details see Ref. 2)

The linewidth variation is shown in Fig. 2 as a function of field intensity.

ACKNOWLEDGMENTS

We are grateful to the Natural Sciences and Engineering Research Council of Canada for financial support (No A4485) and to the Concordia University Computer Centre for computing facilities.

[1] S Kasthurirengan and R. R Navalgund, Phys Status Solidi (b) 72, K1 (1975)
[2] S K Misra and M Jalochowski, Physica B 112, 83 (1982)
[3] S K Misra, J Magn. Reson. 23, 403 (1976).
[4] C Kittel, Phys Rev 73, 155 (1948)
[5] S K Misra, Physica B 121, 193 (1983)
[6] M T Hutchings and W P Wolf, Phys Rev Lett 11, 187 (1963)
[7] M T Hutchings, C G Windsor, and W P Wolf, Phys. Rev 148, 444 (1966)
[8] M. R. St. John and R. J. Myers, Phys. Rev. B 13, 1006 (1976).
[9] W T Batchelder, Ph.D thesis (University of California, Berkeley, 1970) (unpublished)
[10] A Abragam and B. Bleaney, *Electron Paramagnetic Resonance of Transition Ions* (Clarendon, Oxford, 1970).
[11] M Weger and W. Low, Phys. Rev. 111, 1526 (1958).
[12] S K. Misra and S. Subramanian, J. Phys. C 15, 7199 (1982)
[13] J H E. Griffiths and J. Owen, Proc. R. Soc. London, Ser A 213, 459 (1952).

PHYSICAL REVIEW B VOLUME 30, NUMBER 5 1 SEPTEMBER 1984

EPR of Mn^{2+}-doped $Zn(CH_3COO)_2 \cdot 2H_2O$, $Mg(CH_3COO)_2 \cdot 4H_2O$, and $Ni(CH_3COO)_2 \cdot 4H_2O$: Mn^{2+}–Ni^{2+} exchange constant

Sushil K. Misra and Mojtaba Kahrizi
Physics Department, Concordia University, 1455 de Maisonneuve boulevard West, Montreal, Quebec, Canada H3G 1M8
(Received 27 December 1983)

X-band EPR measurements on Mn^{2+}-doped single crystals of $Zn(CH_3COO)_2 \cdot 2H_2O$, $Mg(CH_3COO)_2 \cdot 4H_2O$, and $Ni(CH_3COO)_2 \cdot 4H_2O$ have been performed at room, liquid-nitrogen, and liquid-helium temperatures. The spin-Hamiltonian parameters are estimated by the use of a rigorous least-squares-fitting technique especially adapted to electron-nuclear spin-coupled systems, on a digital computer. The Mn^{2+}-Ni^{2+} exchange constant, using the shift of g value in the paramagnetic nickel salt from that in the isostructural magnesium salt at liquid-helium temperature, has been determined to be 3.81 GHz.

I. INTRODUCTION

The present paper reports *X*-band EPR measurements on three acetates doped with Mn^{2+} at room, liquid-nitrogen, and liquid-helium temperatures. These are zinc acetate dihydrate [$Zn(CH_3COO)_2 \cdot 2H_2O$, hereafter ZnADH], magnesium acetate tetrahydrate [$Mg(CH_3COO)_2 \cdot 4H_2O$, hereafter MgATH], and nickel acetate tetrahydrate [$Ni(CH_3COO)_2 \cdot 4H_2O$, hereafter NiATH]

An Mn^{2+}-doped ZnADH crystal was investigated previously by the EPR technique by Janakiraman and Upreti.[1] However, their measurements were confined to room temperature only. Moreover, perturbation expressions were used for the estimation of parameters. Thus, values of only a few spin-Hamiltonian parameters could be determined. The absolute signs of the parameters could not be determined as no data were available at liquid-helium temperature. The same comments apply to the unpublished results on an Mn^{2+}-doped MgATH crystal by Manakkil.[2]

As for an Mn^{2+}-doped NiATH crystal, measurements at room, liquid-nitrogen, and liquid-helium temperatures have been reported by Misra and Jalachowski;[3] the spin-Hamiltonian parameters there were rigorously evaluated from the data. However, the sample used was of arbitrary shape, not enabling the determination of the demagnetization factor,[4] which should be taken into account in a paramagnetic lattice, if one were to estimate the guest-host exchange constant.

Recently, a rigorous technique, simultaneously fitting all EPR line positions obtained in a least-squares-fitting procedure, especially suitable for electron-nuclear spin-coupled systems, has been proposed[5] for the evaluation of spin-Hamiltonian parameters. For a crystal sample of a known shape, the demagnetization factor effective at low temperatures can be calculated. Then the shift in the g value at liquid-helium temperature in the paramagnetic lattice due to the guest-host (Mn^{2+}-Ni^{2+}) exchange interaction from that in an isostructural diamagnetic lattice can be definitively ascertained. This will enable the determination of an Mn^{2+}-Ni^{2+} exchange interaction constant, especially since the required value of the zero-field splitting parameter for Ni^{2+} in NiATH has already been estimated.[6]

It is the purpose of the present paper to report more accurate spin-Hamiltonian parameters as evaluated from EPR data for Mn^{2+}-doped single crystals of ZnADH, MgATH, and NiATH at room, liquid-nitrogen, and liquid-helium temperatures. Further, the Mn^{2+}-Ni^{2+} exchange constant has been estimated in the NiATH host. A similar study has been reported on an Mn^{2+}-doped nickel potassium sulfate hexahydrate crystal.[7]

II. DEMAGNETIZATION EFFECT AND g SHIFT DUE TO GUEST-HOST EXCHANGE INTERACTION

According to Ref. 4 the demagnetization factor for a sample of spherical shape is zero. Thus, for the measurements presented here a NiATH sample of spherical shape was chosen. Further, the value of the exchange-interaction constant J between Mn^{2+} and Ni^{2+} ions in NiATH can be expressed as[7-11]

$$|J| = \left| \frac{g_{obs} - g}{g + g_1} \right|^{1/2} \beta_2^0 . \tag{2.1}$$

In Eq. (2.1) g_{obs}, g, and g_1 are the g values as observed for Mn^{2+} in the paramagnetic host (NiATH), for Mn^{2+} in the isostructural diamagnetic host lattice (MgATH), and for Ni^{2+} in NiATH, respectively, while β_2^0 is the zero-field splitting parameter for Ni^{2+} in NiATH.

III. CRYSTAL STRUCTURES AND SAMPLE PREPARATIONS

The structure of a ZnADH crystal was determined by Van Niekerk, Schoening, and Talbot.[12] The unit cell is of dimensions $a = 14.50$, $b = 5.32$, $c = 11.02$ Å and $\beta = 100°0'$; it is monoclinic with space group C_2/c. There are four formula units in the unit cell; the zinc atoms lie on the twofold axis parallel to the b axis. (The site symmetries for all the zinc ions are exactly the same.) The six nearest neighbors of a zinc atom are four oxygen atoms (two pairs: O_1 and O_2) and two water molecules which form a distorted octahedron around the zinc atom. The distances are $d_{Zn-O_1} = 2.18$ Å, $d_{Zn-O_2} = 2.17$ Å, and $d_{Zn-H_2O} = 2.14$ Å. Single crystals were grown by slow evaporation at room temperature of a solution of $Zn(CH_3COO)_2 \cdot 2H_2O$ containing 0.1% (by weight) of $Mn(CH_3COO)_2 \cdot 4H_2O$ in distilled water.

The crystal structures of isostructural crystals NiATH and MgATH were determined by Van Niekerk and Schoening[13]

and Shankar, Khubchandani, and Padmanabhan,[14] respectively. These crystals are monoclinic with space group $P2_1/c$, having identical unit-cell dimensions. There are two formula units in the unit cell of dimension: $a = 4.75$, $b = 11.77$, $c = 8.44$ Å, and $\beta = 93°36'$. The nickel or magnesium atoms (indicated below as M) see exactly the same site symmetry, and are surrounded octahedrally by four water molecules and by two oxygen atoms, which belong to two different acetate groups as follows:

$$d_{M-O_1} = 2.12 \text{ Å}, \quad < (O_1-M-H_2O(1)) = 90°44',$$

$$d_{M-H_2O(1)} = 2.11 \text{ Å}, \quad < (O_1-M-H_2O(2)) = 90°33',$$

$$d_{M-H_2O(2)} = 2.06 \text{ Å}, \quad < (H_2O(1)-M-H_2O(2)) = 88°03'.$$

Single crystals of Mn^{2+}-doped NiATH and MgATH were grown by slow evaporation at room temperature of 0.1% solution by weight of $Mn(CH_3COO)_2 \cdot 4H_2O$ in $Ni(CH_3COO)_2 \cdot 4H_2O$ and $Mg(CH_3COO)_2 \cdot 4H_2O$, respectively.

Spheres of 1–2 mm diameter of paramagnetic lattice NiATH were prepared by blowing the roughly cubic single crystals on emery paper.

IV. EXPERIMENTAL DETAILS, SPIN HAMILTONIAN, AND EVALUATION OF PARAMETERS

The experimental details are the same as those described in Ref. 3. EPR spectra for ZnADH were measured at room, liquid-nitrogen, and liquid-helium temperatures for the magnetic field (H) orientation in the z-x plane. [The axes are defined after Eq. (4.1) below.] With H parallel to either the z or the x axis clearly resolved 30 allowed hyperfine lines ($\Delta M = \pm 1$ and $\Delta m = 0$) were observed (M and m are the electron- and nuclear-spin quantum numbers, respectively). (All Mn^{2+} ions are magnetically equivalent.) At liquid-nitrogen and liquid-helium temperatures the spectra have the same angular variation as at room temperature. As the temperature was lowered the size of overall splitting

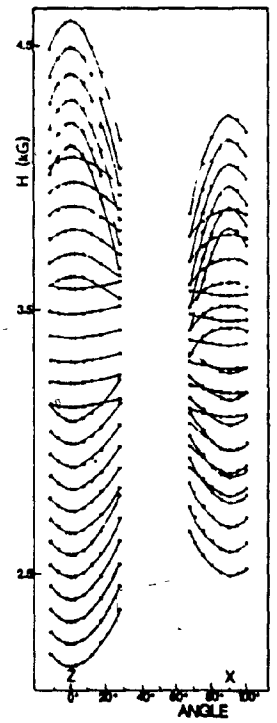

FIG. 1. Angular variation of X-band spectra in the z-x plane for the Mn^{2+}-doped ZnADH host at room temperature. The circles represent the experimental resonant-line positions, and the solid lines are smooth curves that connect data points for the same transition.

TABLE I. Values of spin-Hamiltonian parameters for the Mn^{2+}-doped ZnADH host (0.1 wt.%). n is the number of points used in each fitting. The parameters b_l^m, Q', Q'', A, and B are expressed in units of GHz. A negative sign has been assumed for the value of A. The indicated errors are calculated by use of a statistical method (Ref. 16). The parameters at room temperature (RT), as reported in Ref. 1, have also been included for comparison.

Temperature	295 K	85 K	11 K	Ref. 1 (RT)
g_z	2.000 ± 0.001	2.027 ± 0.001	2.031 ± 0.001	2.001 ± 0.001
g_x	2.001 ± 0.001	2.023 ± 0.001	2.013 ± 0.001	2.001 ± 0.001
b_2^0	−0.702 ± 0.002	−0.941 ± 0.002	−1.037 ± 0.002	0.694 ± 0.001
b_2^2	0.202 ± 0.002	0.436 ± 0.002	0.566 ± 0.002	−0.214 ± 0.004
b_4^0	0.000 ± 0.001	0.002 ± 0.001	0.002 ± 0.001	
b_4^2	0.037 ± 0.013	0.013 ± 0.013	0.026 ± 0.013	
b_4^4	0.054 ± 0.013	0.036 ± 0.015	0.134 ± 0.038	
Q'	0.005 ± 0.002	0.002 ± 0.001	−0.003 ± 0.001	0.001
Q''	0.021 ± 0.009	0.030 ± 0.010	0.008 ± 0.004	0.013
A	−0.251 ± 0.002	−0.254 ± 0.002	−0.247 ± 0.003	−0.251 ± 0.001
B	−0.252 ± 0.002	−0.257 ± 0.002	−0.244 ± 0.004	−0.251 ± 0.001
n	272	162	218	

TABLE II. Values of spin-Hamiltonian parameters for the Mn^{2+}-doped MgATH and NiATH hosts (each 0.1 wt %). Other details and notations are the same as those given in the caption of Table I

	MgATH			NiATH		
Temperature	295 K	85 K	2.5 K	295 K	85 K	1.8 K
g_z	1.996 ± 0.002	2.019 ± 0.002	1.952 ± 0.002	1.959 ± 0.002	1.960 ± 0.002	1.948 ± 0.002
g_x	1.993 ± 0.002	1.005 ± 0.002	1.981 ± 0.002	1.971 ± 0.002	2.007 ± 0.002	1.959 ± 0.002
b_2^0	1.160 ± 0.002	1.257 ± 0.002	1.350 ± 0.002	1.272 ± 0.003	1.341 ± 0.003	1.430 ± 0.003
b_2^2	−0.350 ± 0.006	−0.594 ± 0.006	−0.450 ± 0.006	−0.356 ± 0.009	−0.298 ± 0.009	−0.283 ± 0.009
b_4^0	0.017 ± 0.002	0.047 ± 0.002	0.017 ± 0.002	0.016 ± 0.002	0.023 ± 0.002	0.010 ± 0.002
b_4^2	−0.017 ± 0.012	−0.332 ± 0.026	−0.036 ± 0.019	−0.239 ± 0.030	−0.200 ± 0.046	0.050 ± 0.047
b_4^4	−0.071 ± 0.027	−0.318 ± 0.028	−0.181 ± 0.023	−0.099 ± 0.041	−0.707 ± 0.129	−0.505 ± 0.054
Q'	0.016 ± 0.006	−0.001 ± 0.016	0.018 ± 0.006	0.001 ± 0.008	0.030 ± 0.006	0.008 ± 0.008
Q''	0.048 ± 0.011	−0.009 ± 0.047	0.053 ± 0.010	0.047 ± 0.013	0.087 ± 0.010	0.026 ± 0.013
A	−0.250 ± 0.004	−0.263 ± 0.004	−0.258 ± 0.004	−0.264 ± 0.004	−0.268 ± 0.004	−0.259 ± 0.004
B	−0.243 ± 0.004	−0.259 ± 0.004	−0.255 ± 0.004	−0.250 ± 0.004	−0.273 ± 0.006	−0.269 ± 0.004
n	270	256	250	234	186	161

increased and at liquid-helium temperature the five sextets of the hyperfine lines were completely separated. The last sextet of the spectrum was observed down to 11 K, but below this temperature the intensity of these lines diminished rapidly and at 5 K they completely disappeared. The angular variation of EPR spectrum for a Mn^{2+} ion in ZnADH is shown in Fig. 1.

EPR measurements on a Mn^{2+}-doped single crystal of $Mg(CH_3COO)_2 \cdot 4H_2O$ were made at room, liquid-nitrogen, and liquid-helium temperatures in the z-x plane. Thirty well-resolved transition lines were observed along both the z and x axes (All Mn^{2+} ions are magnetically equivalent.) The overall splitting of the lines increased for this sample also as the temperature was lowered. The angular variation of the spectrum for this sample is similar to that for NiATH (as given in Ref. 3).

The EPR spectra of Mn^{2+}-doped NiATH were recorded at room, liquid-nitrogen, and liquid-helium temperatures. The shape of the spectra, the absolute sign of b_2^0, and the relative sign of parameters and angular variation of resonant lines with respect to the external magnetic field were the same as those reported in Ref. 3 (all Mn^{2+} ions are magnetically equivalent.)

The spin Hamiltonian that corresponds to the monoclinic symmetry[13] is

$$\mathcal{H} = \mu_B \vec{H} \cdot \vec{g} \cdot \vec{S} + \sum_{m=-0,2} \tfrac{1}{3} b_2^m O_2^m + \sum_{m=-0,2,4} \tfrac{1}{60} b_4^m O_4^m + A S_z I_z + B(S_x I_x + S_y I_y) + Q'[I_z^2 - \tfrac{1}{3} I(I+1)] + Q''(I_x^2 - I_y^2) \quad . \tag{4.1}$$

Here g, b_l^m, A, B, Q', and Q'' are the spin-Hamiltonian parameters, O_l^m are the spin operators as defined by Abragam and Bleaney,[15] μ_B the Bohr magneton, H the external magnetic field, and S and I the electron and nuclear spins, respectively, corresponding to the Mn atom ($S = I = \frac{5}{2}$).

The x, y, and z axes are so chosen that they coincide with the principal axes of the b_2^m tensor; the overall splitting of the spectra is maximum along the z axis and minimum along the y axis.[3]

The parameters were evaluated by the use of a rigorous least-squares-fitting procedure designed and adapted to the electron-nuclear spin-coupled system of Mn^{2+} by Misra[3] (see also Ref. 7). The spin-Hamiltonian parameters were determined by simultaneously fitting all clearly resolved resonant field positions for at least ten different orientations of the external magnetic field around the principal axes (z and x axes). The fitting gave the correct relative signs of the parameters; the absolute signs were determined from the intensities of lines at liquid-helium temperature.[15] The list of the parameters for ZnADH, MgATH, and NiATH at different temperatures are given in Tables I and II.

The values of these parameters for ZnADH and MgATH are significantly different from those reported previously.[1,2] The fourth-order parameters b_4^m corresponding to cubic-field symmetry, which were neglected by the previous workers,[1,2] are here found to have small but significant values. The absolute sign of b_2^0 was determined from the intensity ratios of the average intensity for the highest-field sextet to that of the lowest one for the external magnetic field orientation along the z axis. These ratios for ZnADH are ~3.7, ~3.6, ~1.5, and ~0.0 at 298, 85, 11, and 3.5 K, respectively, while for MgATH these are 0.8, 0.8, and 2.4 at 298, 85, and 2.5 K, respectively. Thus the absolute sign of b_2^0 is negative for ZnADH while it is positive for MgATH.[15] The errors of parameters were calculated by use of a statistical method.[14] The variation of the largest parameter b_2^0 which predominantly determines the zero-field splitting is shown as a function of temperature in Fig. 2.

The linewidths of Mn^{2+} in ZnADH lattice were of the order of 8 ± 1 G at room temperature for all the lines of the spectra, and showed no magnetic field dependence. As the temperature was decreased to liquid-helium temperature the linewidths increased to about 16 ± 1 G. The reason for such small linewidths is that four of the six ligands surrounding Mn^{2+} are oxygens, which, because of their zero nuclear spin, do not contribute to the dipolar interactions with a Mn^{2+} ion.

For the case of MgATH also, the linewidths were more or less isotropic for all spectra, and are about 20 ± 1 G at room temperature and 18 ± 1 G at liquid-helium temperature.

The linewidths of Mn^{2+} in the paramagnetic lattice of NiATH exhibited some differences from those in the diamag-

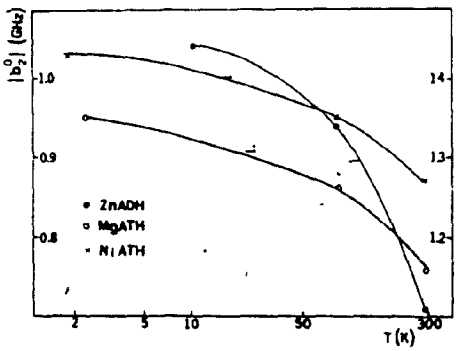

FIG 2. Variation of zero-field splitting parameter b_2^0 for Mn^{2+}-doped ZnADH, MgATH, and NiATH hosts as a function of temperature

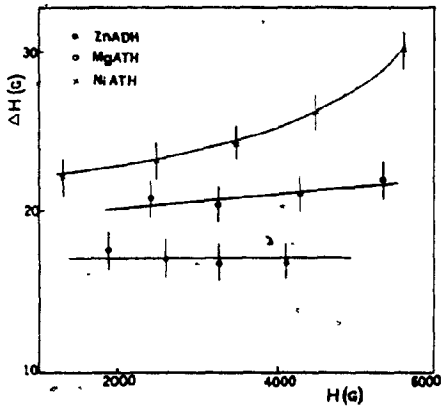

FIG 3 Variation of linewidths as a function of magnetic field intensity at room temperature for the orientation of the external magnetic field along the z axis for ZnADH, MgATH, and NiATH hosts.

netic lattices. These are (i) the anisotropy of the widths as a function of orientation of H and (ii) the magnetic field dependence of linewidths (true at all temperatures); for more details see Refs. 3 and 7. The variation of linewidths as a function of magnetic field intensity for the various host lattices is shown in Fig. 3.

V. g SHIFT AND Mn^{2+}-Ni^{2+} EXCHANGE CONSTANT

The shift of the g value in the paramagnetic lattice from its value in the isostructural diamagnetic crystal can be explained to be due to the exchange interaction between the Mn^{2+} ion and paramagnetic neighbor ions Ni^{2+}.[8,9] Due to the polarization effect of the Zeeman field, magnetic moments are induced on paramagnetic ions like Ni^{2+} (which have partly filled electron shells, and thus a nonmagnetic ground state). As a result of the interaction of this magnetic moment with the impurity ion (Mn^{2+}) an additional internal field manifests itself at the site of the Mn^{2+} ion, causing a shift of resonance and thus the shift of the the g value from its isolated value.

Using Eq. (2.1) and the g values in NiATH and MgATH hosts for Mn^{2+} at liquid-helium temperature, the value of 3.81 GHz for $|J|$ was found for the Mn^{2+}-Ni^{2+} exchange-interaction constant in NiATH at 1.8 K. The required values of $g_\parallel$ and β_2^0 for Ni^{2+} are 2.24 and 123.15 GHz, respectively, as reported by Schriempf and Friedberg.[6]

ACKNOWLEDGMENTS

We are grateful to the Natural Sciences and Engineering Research Council of Canada for financial support (Grant No. A4485) and to the Concordia University Computer Centre for providing computing facilities.

[1]R. Janakiraman and G. C. Upreti, J. Phys. Chem. Solids 31, 1419 (1969).
[2]T. J. Menakkil, Ph.D. thesis, New Mexico State University, 1967.
[3]S. K. Misra and M. Jalochowski, Physica B 112, 83 (1982).
[4]C. Kittel, Phys. Rev. 73, 155 (1948).
[5]S. K. Misra, Physica B 121, 193 (1983).
[6]J. T. Schriempf and S. A. Friedberg, J. Chem. Phys. 40, 296 (1964).
[7]S. K. Misra and M. Kahrizi, Phys. Rev. B 28, 5300 (1983).
[8]M. T. Hutchings and W. P. Wolf, Phys. Rev. Lett. 11, 187 (1963).
[9]M. T. Hutchings, C. G. Windsor, and W. P. Wolf, Phys. Rev. 148, 444 (1966).
[10]M. R. St. John and R. J. Myers, Phys. Rev. B 13, 1006 (1967).
[11]W. T. Batchelder, Ph.D. thesis, University of California, Berkeley, 1970.
[12]J. N. Van Niekerk, F. R. L. Schoening, and J. H. Talbot, Acta Crystallogr. 6, 720 (1953).
[13]J. N. Van Niekerk and F. R. L. Schoening, Acta Crystallogr. 6, 609 (1953).
[14]J. Shankar, P. G. Khubchandani, and V. M. Padmanabhan, Proc. Indian Acad. Sci. Sect. A 45, 117 (1957).
[15]A. Abragam and B. Bleaney, *Electron Paramagnetic Resonance of Transition Ions* (Clarendon, Oxford, 1970).
[16]S. K. Misra and S. Subramanian, J. Phys. C 15, 7199 (1982).

PHYSICAL REVIEW B VOLUME 30, NUMBER 9 1 NOVEMBER 1984

EPR of Mn^{2+}-doped $NiSO_4 \cdot 7H_2O$ and $MgSO_4 \cdot 7H_2O$: Mn^{2+}-Ni^{2+} exchange constant

Sushil K Misra and Mojtaba Kahrizi
Physics Department, Concordia University, 1455 de Maisonneuve Boulevard West, Montreal, Quebec, Canada H3G 1M8

(Received 19 March 1984)

X-band EPR measurements on Mn^{2+}-doped isostructural single crystals of paramagnetic $NiSO_4 \cdot 7H_2O$ and diamagnetic $MgSO_4 \cdot 7H_2O$ have been made at room, liquid-nitrogen, and liquid-helium temperatures. The spin-Hamiltonian parameters are evaluated from the data using a rigorous least-squares-fitting program suitable for electron-nuclear spin-coupled systems. Using the g shift in the paramagnetic lattice from that in the diamagnetic lattice a value of 4.293 GHz for the Mn^{2+}-Ni^{2+} exchange constant in $NiSO_4 \cdot 7H_2O$ is estimated. For $NiSO_4 \cdot 7H_2O$ host the linewidths exhibit temperature and magnetic field dependence. The temperature dependence of the zero-field splitting parameter b_2^0 for both hosts is found to be linear, thus being explained as mainly due to the thermal expansion of the lattice.

EPR studies of Mn^{2+}-doped single crystals of $MgSO_4 \cdot 7H_2O$ (hereafter MSO) have been reported by Janakiraman and Upreti[1] and Hayashi and Ono.[2] These measurements were, however, confined to room temperature only, and the spin-Hamiltonian parameters were estimated, using perturbation expressions, from resonant line positions obtained for the external magnetic field orientation being along the Z and/or X axis only. On the other hand, Bramley and Starch,[3] estimated the spin-Hamiltonian parameters of Mn^{2+} in the MSO lattice at room temperature from zero magnetic field resonance (ZFR), using a powder sample. In Refs. 1–3, the individual values of all the spin-Hamiltonian parameters could not be evaluated, due to the use of perturbation expressions for eigenvalues. Further, Bramley and Starch[3] cast doubt on the accuracy of the spin-Hamiltonian parameters obtained from EPR data, due to the uncertainty in measuring the frequency and the magnetic field intensity, misalignment of the crystalline sample, and the use of perturbation expressions in the evaluation of parameters. One of the motivations, in this continuing series of measurements, is to minimize these errors. In the present work the magnetic field intensity has been measured precisely by the use of a digital NMR gaussmeter (model B-NM-20 Bruker). (A calibration curve related the measured magnetic field intensity at the position of the probe to that at the actual position of the sample. Measurements of the magnetic field intensity and frequency were further verified using DPPH line position.) Moreover, a rigorous computer technique for the evaluation of spin-Hamiltonian parameters using exact numerical diagonalization of the spin-Hamiltonian matrix (instead of perturbation theory), fitting simultaneously all line positions obtained for various orientations of the external magnetic field to evaluate the spin-Hamiltonian parameters for electron-nuclear spin-coupled systems has recently been published.[4] All these considerations make it worthwhile to reinvestigate the Mn^{2+}-doped MSO sample by EPR.

EPR measurements on Mn^{2+}-doped single crystals of $NiSO_4 \cdot 7H_2O$ (hereafter NSO) have been previously reported by Misra and Mikolajczak.[5] These were, however, performed on a sample of *arbitrary* shape, although the spin-Hamiltonian parameters were evaluated from the data using a rigorous least-squares-fitting computer technique.[4] On the other hand, at liquid-helium temperature a paramagnetic sample becomes magnetized and the demagnetization factor cannot be estimated for a sample of arbitrary shape, making it impossible to estimate the Mn^{2+}-Ni^{2+} exchange constant from the shift of the g value in the paramagnetic lattice from that in the isostructural diamagnetic lattice. (For more details, see Refs. 6 and 7.) Further, the determination of the exchange constant requires the values of the zero-field splitting parameter β_2^0 and the g factor for Ni^{2+} in NSO (see further on in this paper). Fortunately, these values have been reported by Ono.[6]

The purpose of this paper is twofold: (i) to determine more accurately the spin-Hamiltonian parameters for Mn^{2+} in MSO at room, liquid-nitrogen, and liquid-helium temperatures; and (ii) to estimate the exchange-interaction constant between Mn^{2+}-Ni^{2+} in the paramagnetic lattice of NSO, by measuring, at liquid-helium temperature, the shift of g value in the NSO lattice of a spherical sample (so that the demagnetization factor is zero[4,7]) from that in the isostructural diamagnetic lattice of MSO. Similar investigations have already been reported for $NiK_2(SO_4)_2 \cdot 6H_2O$ (Ref. 6) and $Ni(CH_3COO)_2 \cdot 4H_2O$ (Ref. 7).

The (isostructural) crystals of MSO and NSO have a unit cell of orthorhombic symmetry,[9] containing four formula units related to each other by the operation of the space group $P2_12_12_1$. Each Ni^{2+}, or Mg^{2+}, ion is surrounded by a distorted octahedron of six water molecules. The seventh water molecule is not coordinated with the Ni^{2+}, or Mg^{2+}, ion but instead fills what would otherwise be a hole in the structure. The unit-cell dimensions are[9] for MSO $a = 11.91$, $b = 12.01$, and $c = 6.87$ Å, and for NSO $a = 11.86$, $b = 12.08$, and $c = 6.81$ Å. The four Mg^{2+}, or Ni^{2+}, sites in the unit cell are magnetically inequivalent. This is also reflected in the EPR spectra.

Single crystals of Mn^{2+}-doped MSO and NSO were grown by slow evaporation at room temperature of solutions of MSO and NSO, respectively, each containing stoichiometric amount of 0.1% of $MnSO_4$.

The spin-Hamiltonian appropriate to orthorhombic symmetry is[10]

$$\mathcal{H} = \mu_B \vec{H} \cdot \vec{g} \cdot \vec{S} + \sum_{n=0,2} \tfrac{1}{3} b_n^0 O_n^0 + \sum_{n=-2,2,4} \tfrac{1}{60} b_n^0 O_n^0 + A S_z I_z + B(S_x I_x + S_y I_y) + Q'[I_z^2 - \tfrac{1}{3} I(I+1)] + Q''(I_x^2 - I_y^2) \quad . \tag{1}$$

Here, g, b_l^m, A, B, Q', and Q'' are the spin-Hamiltonian parameters, O_l^m are the spin operators (Ref. 10), μ_B is the Bohr magneton, H is the external magnetic field, S $(=\frac{5}{2})$ and I $(=\frac{5}{2})$ are the electron and nuclear spins, respectively, for the Mn^{2+} ion. The X, Y, and Z axes are coincident with the principal axes of the zero-field splitting parameter b_2^0, so that the overall splitting of the spectra is maximum along the Z axis, while it is minimum along the Y axis.

The experimental arrangement has been described in Ref 5. EPR spectra were recorded for the external magnetic field orientation in the ZX plane at 5° intervals both from the Z and X axes for the MSO sample at room, liquid-nitrogen, and liquid-helium temperatures. As mentioned previously, there is observed an overlap of EPR spectra corresponding to four magnetically inequivalent sites. For any one inequivalent Mn^{2+} ion, along its Z axis, five well-separated sets of fine structure lines ($\Delta M = \pm 1$; M is the electronic quantum number) appeared, each set being split into six hyperfine lines ($\Delta m = 0$; m is the nuclear quantum number). The intensities of lines around the center of the spectrum are almost symmetric, and the linewidth remains the same throughout the spectrum (see below for more details). Some other lines with smaller intensities (about half), mostly corresponding to the transition $M = \pm\frac{5}{2} \rightarrow M = \pm\frac{3}{2}$ and $M = +\frac{3}{2} \rightarrow -\frac{3}{2}$, belonging to the other sites, were also observed. The angular variation of the spectrum corresponding to one inequivalent site at room temperature is shown in Fig. 1. As the temperature of measurement was lowered, the overall splitting of the spectrum increased, indicating an increase of the zero-field parameter b_2^0 (see below for more details).

EPR spectra for spherical crystal of Mn^{2+}-doped NSO were recorded at room, liquid-nitrogen, and liquid-helium temperatures in the ZX plane. The spherical samples were prepared by blowing the soft cubic-shaped samples on emery paper. The shape and angular variation of the spectra are the same as those reported by Misra and Mikolajczak.[5] The linewidths and intensities of the lines (see below) vary considerably with the intensity of the external magnetic field. The similarity of the EPR spectra of the two samples (except for the differences in the linewidths and intensities caused by the presence of the paramagnetic Ni^{2+} ion in the NSO lattice) confirms that the MSO and NSO crystals are indeed isostructural).

The Mn^{2+} spin-Hamiltonian parameters for both the samples were evaluated by fitting simultaneously all resonant line positions observed in the ZX plane up to 30° around each axis.[4] The fitting gives the correct relative signs of the parameters. The absolute signs were determined by measuring the intensity of the highest-field sextet relative to the lowest-field sextet along the Z axis, as the temperature is lowered from room down to the liquid-helium temperature. These values were found to be 1.10, 1.08, and 0.30 at 295, 85, and 3 K, respectively, for MSO, and 0.43, 0.41, and 0.10 at 295, 85, and 2 K, respectively, for NSO. They indicate that the sign of b_2^0 is negative for both the samples.[10] A negative sign has been chosen for A and B in conformity with the hyperfine data,[11] and errors are calculated by the use of a statistical method.[12] Table I lists the parameter values for the MSO and NSO hosts. The parameters, as reported by the other researchers[1-3] for MSO, have also been included in Table I for comparison. The sign of b_2^0 for MSO, as given in Refs. 1-3 is, of course, incorrect, since the room-temperature data cannot yield the absolute sign of parameters. On the other hand, the magnitude of the room-temperature values of b_2^0 for MSO, determined in the present work, agree with those reported in Refs. 1-3 within 8%.

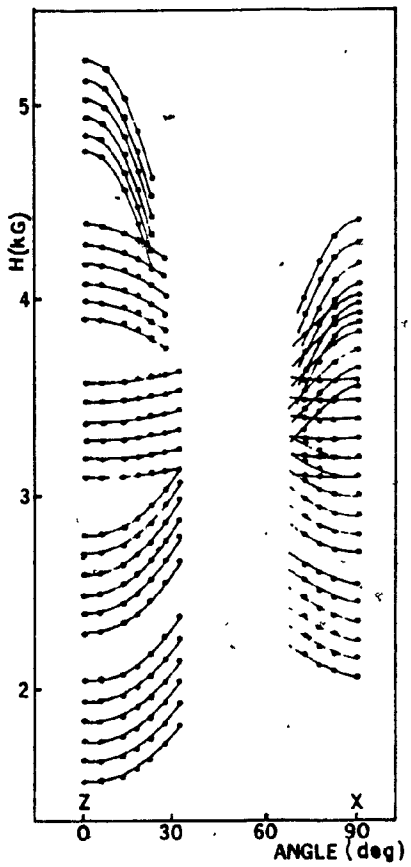

FIG. 1. Angular variation of X-band spectra in the ZX plane for the Mn^{2+}-doped MSO host at room temperature. The circles represent the experimental resonant-line positions, and the solid lines are smooth curves that connect data points for the same transition. Only spectra corresponding to one inequivalent Mn^{2+} ion have been exhibited.

The observed EPR linewidths for the MSO sample did not exhibit significant variation, either for different orientations, or for different intensities of the external magnetic field, or at different temperatures. They are generally of the order of 12 G. In the case of NSO, as has been observed in other Ni^{2+} salts,[4,7,13] the linewidths are magnetic-field-intensity dependent. The reason for this is the nonzero magnetic moment of the host Ni^{2+} ions; this is described well in Ref 13. The EPR linewidths, as a function of the magnetic field intensity for both the samples at liquid-helium temperature

TABLE I. Values of the spin-Hamiltonian parameters for Mn^{2+}-doped MSO and NSO hosts (each 0.1% by weight). n is the number of points used in each fitting. The parameters b_4^4, Q', Q'', A, and B are expressed in units of GHz. A negative sign has been assumed for the values of A and B (Ref. 11). The indicated errors are calculated by the use of a statistical method (Ref. 12). The room-temperature values of the parameters for MSO, as reported in Refs. 1, 2, and 3, have also been included for comparison.

Temperature	MSO 295 K	MSO 85 K	MSO 3 K	MSO Ref. 1	Ref. 2	Ref. 3	NSO 295 K	NSO 85 K	NSO 2 K
g_{xx}	2.002 ± 0.002	1.996 ± 0.002	2.006 ± 0.002	2.003 ± 0.005	2.000 ± 0.005		1.970 ± 0.002	2.015 ± 0.002	1.995 ± 0.002
g_{zz}	1.968 ± 0.002	1.958 ± 0.002	1.963 ± 0.002				1.979 ± 0.002	1.985 ± 0.002	1.999 ± 0.002
b_2^2	−1.118 ± 0.002	−1.241 ± 0.002	−1.292 ± 0.002	−1.154 ± 0.014	1.200	1.181 ± 0.002	−1.257 ± 0.002	−1.535 ± 0.003	−1.595 ± 0.002
b_2^0	0.367 ± 0.005	0.254 ± 0.007	0.670 ± 0.007	0.266 ± 0.028	≈ 0.000	0.183 ± 0.002	0.383 ± 0.010	0.520 ± 0.009	0.321 ± 0.007
b_4^4	0.004 ± 0.001	0.006 ± 0.001	0.007 ± 0.001			≈ 0.0003	−0.003 ± 0.002	−0.009 ± 0.002	−0.004 ± 0.002
b_4^2	−0.203 ± 0.023	−0.590 ± 0.038	−0.173 ± 0.047				0.014 ± 0.040	0.002 ± 0.041	−0.799 ± 0.036
b_4^0	0.243 ± 0.027	0.430 ± 0.044	0.336 ± 0.049				0.012 ± 0.045	0.159 ± 0.049	−0.448 ± 0.033
Q'	−0.018 ± 0.006	−0.003 ± 0.039	−0.013 ± 0.012				−0.002 ± 0.014	−0.009 ± 0.010	0.014 ± 0.013
Q''	−0.017 ± 0.012	−0.005 ± 0.114	−0.011 ± 0.032				−0.026 ± 0.030	−0.027 ± 0.020	−0.007 ± 0.035
A	−0.268 ± 0.004	−0.276 ± 0.004	−0.277 ± 0.004	−0.258 ± 0.014	0.265	−0.269 ± 0.002	−0.265 ± 0.004	−0.272 ± 0.004	−0.264 ± 0.005
B	−0.267 ± 0.004	−0.258 ± 0.004	−0.271 ± 0.004	−0.244 ± 0.028		−0.266 ± 0.002	−0.262 ± 0.005	−0.254 ± 0.006	−0.265 ± 0.005
n	217	155	155				192	232	141

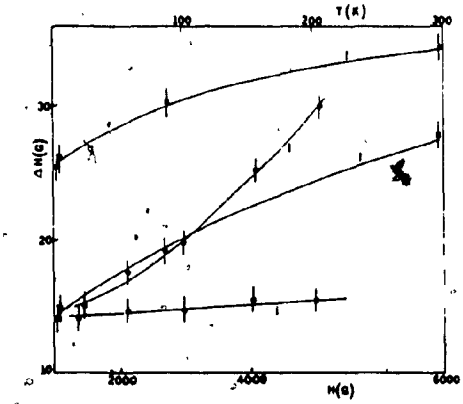

FIG. 2. Variation of the average linewidth. (i) of various sextets as a function of magnetic field intensity at liquid-helium temperature for the orientation of the external magnetic field along the Z axis for the MSO and NSO hosts (the open circles represent the NSO host, while the solid circles represent the MSO host; the abscissa scale is shown at the bottom), and (ii) of the highest- and lowest-field sextets for the NSO host as a function of temperature (the solid squares represent the highest-field sextet while the open squares represent the lowest-field sextet; the abscissa scale is shown on the top).

are exhibited in Fig. 2. The temperature variation of the average width of the lines corresponding to the lowest- and highest-field sextets for NSO is also shown in Fig. 2. These average linewidths decrease as the temperature is lowered.

Shift of the g value in a paramagnetic lattice from its value in an isostructural diamagnetic lattice has been observed previously by several researchers.[14–17] This phenomenon has been explained by Hutchings and Wolf[14] and Hutchings, Windsor, and Wolf.[15] Using this shift, they estimated the exchange interaction between Eu^{2+}, Fe^{2+}, and Gd^{2+} in europium gallium garnet crystals. Further, St. John and Myers[16] have estimated the exchange integral between Ni^{2+} and several other paramagnetic ions, e.g., Co^{2+} and Cu^{2+}, in $NiSO_4 \cdot 6H_2O$ using the same procedure.

Recently, Misra, and Kahrizi[6,7] estimated the Mn^{2+}-Ni^{2+} exchange interaction in $NiK_2(SO_4)_2 \cdot 6H_2O$[6] and $Ni(CH_3COO)_2 \cdot 4H_2O$[7] (for more details see Refs. 6 and 7). The following expression relates the g factors as observed in the paramagnetic and isostructural diamagnetic host lattices:

$$g_{obs} = g + J^1(g + g_1)/(\beta\nu)^2 \qquad (2)$$

In (2) g_{obs} and g are, respectively, the spectroscopic splitting factors of the Mn^{2+} ion in the paramagnetic lattice of NSO and its isostructural diamagnetic lattice of MSO, while $g_1 (= 2.2)$ and $\beta\nu (= 105$ GHz) are, respectively, the g value and the zero-field splitting parameter of Ni^{2+} in NSO lattice (as measured by Ono[3]). Using the above relation and the values in Table I, the exchange interaction constant between Mn^{2+} and Ni^{2+} ions in NSO is estimated to be 4.293 GHz.

The temperature variation of the spin-Hamiltonian parameters of S-state ions for simple cubic systems have been in-

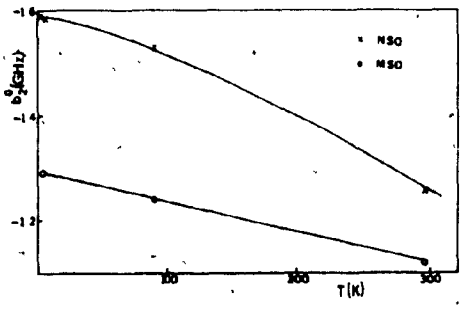

FIG. 3. Variation of the zero-field splitting parameter b_2^0 as a function of temperature for the MSO and NSO hosts.

vestigated theoretically and experimentally by several workers.[16–22] Simanek and Orbach[20] calculated the temperature dependence of the hyperfine parameters A and B using Debye approximation which is in good accord with their experimental results on Mn^{2+} in MgO. Serway[21] has investigated the temperature dependence of the spin-Hamiltonian parameters of Mn^{2+} in the trigonal site of $CaCO_3$ in terms of implicit (thermal expansion) and explicit (lattice vibration) effects. Geifman and Glinchak[22] have studied the temperature dependence of the crystal-field parameters of Fe^{3+} and Mn^{2+} in Al_2O_3.

The temperature variation of b_2^0 of Mn^{2+}-doped MSO and NSO lattices is plotted in Fig. 3 from room temperature down to liquid-helium temperature. The magnitude of b_2^0 increases linearly as the temperature is lowered, indicating the contraction of the lattice in both these hosts. Geifman and Glinchak[22] have found the temperature variation of the parameter b_2^0 as a function of temperature as follows.

$$b_2^0(T) = b_2^0(0)[1 - 6\alpha(T - T_0)] \ . \qquad (3)$$

In (3) $b_2^0(0)$ is the value of b_2^0 at T_0 (usually room temperature) and α is the coefficient of linear thermal expansion. The above expression has been derived, assuming that the thermal expansion is the dominating mechanism and, that the coordinates of the ions surrounding the Mn^{2+} ion are linear in temperature, i.e., $\Delta R = \alpha T$. Also it has been assumed that b_2^0 is proportional to the square of the axial crystal-field potential.

Equation (3) shows that b_2^0 is linear in T. This is certainly borne out by the present values for both the hosts, as can be seen from Fig. 3. From this, one may be tempted to speculate that the thermal expansion is the dominant mechanism to determine the temperature variation of the zero-field-splitting parameter, and that b_2^0 depends predominantly upon the coordinates of the surrounding ions.

We are grateful to the Natural Sciences and Engineering Research Council of Canada for financial support (Grant No. A4485), and to the Concordia University Computer Center for providing computing facilities.

[1] R. Janakiraman and G. C. Upreti, Phys. Status Solidi B 47, 679 (1971).
[2] I. Hayashi and K. Ono, J. Phys. Soc. Jpn. 8, 270 (1953).
[3] R. Bramley and S. J. Strach, Chem. Phys. Lett. 79, 183 (1981).
[4] S. K. Misra, Physica B 121, 193 (1983).
[5] S. K. Misra and B. Mikolojczak, Phys. Status Solidi B 96, 807 (1979).
[6] S. K. Misra and M. Kahrizi, Phys. Rev. B 28, 5300 (1983).
[7] S. K. Misra and M. Kahrizi, Phys. Rev. B 30, 2920 (1984).
[8] K. Ono, J. Phys. Soc. Jpn. 8, 802 (1953).
[9] R. W. G. Wyckoff, *Crystal Structures* (Wiley, New York, 1965), Vol. III, p. 837.
[10] A. Abragam and B. Bleaney, *Electron Paramagnetic Resonance of Transition Ions* (Clarendon, Oxford, 1970).
[11] A. Steudel, *Hyperfine Interactions* (Academic, New York, 1976), p. 182.
[12] S. K. Misra and S. Subramanian, J. Phys. C 15, 7199 (1982).
[13] S. K. Misra and M. Jalochowski, Physica B 112, 83 (1982).
[14] M. T. Hutchings and W. P. Wolf, Phys. Rev. Lett. 11, 187 (1963).
[15] M. T. Hutchings, C. G. Windsor, and W. P. Wolf, Phys. Rev. 148, 444 (1966).
[16] M. R. St. John and R. J. Meyers, Phys. Rev. B 13, 1006 (1976).
[17] W. T. Batchelder, Ph.D. thesis, University of California, Berkeley, 1970.
[18] W. M. Walsh, Jr., J. Jeener, and N. Bloembergen, Phys. Rev. A 139, 1338 (1965).
[19] J. Rosenthal, L. Yarmus, and R. H. Bartram, Phys. Rev. 153, 407 (1967).
[20] E. Simanek and R. Orbach, Phys. Rev. 145, 191 (1966).
[21] R. A. Serway, Phys. Rev. B 3, 608 (1971).
[22] I. N. Geifman and M. D. Glinchak, Fiz. Tverd. Tela (Leningrad) 13, 1050 (1971) [Sov. Phys. Solid State 13, 872 (1971)].

APPENDIX C

(Computer Programs)

```
      PROGRAM MATH (INPUT,OUTPUT,TAPE5=INPUT,TAPE6=OUTPUT)
C     THIS PROGRAM ALALYSIS THE EPR DATA FOR MONOCLINIC SYSTEMS
C
C     NO =THE NO. OF FIRST MAG FIELD IN DATA INCLUDED IN FITTING
C     M  =NO. OF PARAMETERS
C     L4 =NO. OF ITERATIONS ALLOWED
C     Q1 =MIN. VALUE OF SUM OF SQUARES FOR FITS( CHI-SQUARE TOLERANCE)
C     Z(I)=MAGNETIC FIELD VALUES FOR FITS
C     B  =PARAMETER MATRIX
C     N  =NO. OF  DATA POINTS USED IN LEAST-SQARES FITTING
C     Q1 =N/10
C     Q2 =TOLERANCE ON GRAD(CHI**2) =APPROX .01
C     FM(I) = MEASURED VALUES
C     FC(I) = CALCULATED VALUES
C     ERR(I)= STANDARD DEVIATION ON FM(I) = SQRT(FM(I))
C
C      DIMENSIONS OF A,B IN EXAM AND MATINV SUBROUTINES SHOULD BE THE
C     SAME AS THOSE OF B2,B1 RESPECTIVELY IN THE MAIN PROOGRAM AND IN
C     CURFIT
C
C     ENTER THETA IN DEGREES
C     DIMENSIONS OF Q,V IN JACOBI1 SHOULD BE THE SAME AS THOSE OF
C     B3,B2 RESPECTIVELY IN CURFIT
C
C     NUMBER=INDEX THAT CHANGES WITH EACH NEW CASE
C     NCASES=NO. OF CASES CONSIDERED. ITS VALUE SHOULD BE ENTERED.
C
C     IBB(II,1) AND IBB(II,2) INDICATE THE EIGENVALUES INVOLVED IN
C     RESONANCE FOR THE NO. II MAG FIELD VALUE
C
C      B=G=GPARALEL,GPERPENDICULAR,B20,B22,B40,B42,B44,QPRIME,
C     Q",A,B
C
      DIMENSION Z(350),FM(350),FC(350),DF(350),ERR(350),B(12),
     1B1(12),B2(12,12),DC(5000),ABC(2),Y(4),ZZ(350,4),G(12,20),
     2THETA(350),GG(12,4),IBB(350,2),DELER(350,4),DELB(350)
      DIMENSION TEETA(350,4),FREQ(20),FACTOR(20),NN(20),HN(20)
     1,Z1(350,4),ADD(20),Z2(350),IAB(30,2),ICC(30,2),DDF(350,4)
     1 ,SMDD(4),JJII(10,2),IA1(350,4),IA2(350,4),SS(350)
      COMMON/DATA1/ABC,Y
      COMMON/DATA2/DC
      COMMON/DATA3/DELB
      EQUIVALENCE (Z,DC),(FM,DC(501)),(FC,DC(1001)),(DF,DC(1501)),
     1(ERR,DC(2001)),(B,DC(2989)),(B1,DC(3013)),(B2,DC(3025)),
     2(N,DC(3169)),(L4,DC(3170)),(Q1,DC(3171)),(Q2,DC(3172)),
     3(M,DC(3173)),(SSMD,DC(3178)),(IBB,DC(4000)),(THETA,DC(3500))
     4 ,(I,DC(3174)),(L,DC(3175)),(BO,DC(3176)),(MD,DC(3177))
     5 ,(HN,DC(3179)),(NUMBER,DC(4999))
      DATA(ABC=2HNO,3HYES),(Y=1H ,1HC,1H*,1HM)
C     CASE1= (ROOM TEMP.)
C     CASE2= (85 K)
C      CASE3= (5 K)
      DATA(G(J,1),J=1,11)/
      DATA(G(J,2),J=1,11)/
```

```
      DATA(G(J,3),J=1,11)/
C     HERE ONE DEFINES THE QUANTUM NUMBERS FOR VARIOUS L  ES
      DATA(IAB(J,1),J=1,30)/
     130,29,28,27,26,25,24,23,22,21,20,19,18,14,15,16,17,18,
     27,8,9,10,11,12,1,2,3,4,5,6/
      DATA(IAB(J,2),J=1,30)/
     136,35,34,33,32,31,30,29,28,27,26,25,24,23,22,21,20,19,
     213,14,15,16,17,18,7,8,9,10,11,12/
      DATA(ICC(J,1),J=1,30)/
     1 1,2,3,4,5,6,7,8,9,10,11,12,13,14,15,16,17,18,
     2 24,23,22,21,20,19,30,29,28,27,26,25/
      DATA(ICC(J,2),J=1,30)/
     1 7,8,9,10,11,12,13,14,15,16,17,18,24,23,22,21,20,19,
     2 30,29,28,27,26,25,36,35,34,33,32,31/
C      JJII(,1),(,2) TELL GROUPS OF 30 LINES WHICH ARE BETWEEN
C      0 AND 25 DEG. AND BETWEEN 75 AND 90 DEG. RESPECTTIVELY.
      DATA(JJII(J,1),J=1,3)//
      DATA(JJII(J,2),J=1,3)//
      DATA(FREQ(J),J=1,3)//
      DATA(FACTOR(J),J=1,3)//
      DATA(ADD(J),J=1,3)//
      DATA(NN(J),J=1,3)/
      DO 331 JJ=1,3
      NNJJ=NN(JJ)
      DO 331 J=1,NNJJ
      DELHH(J,JJ)=FACTOR(JJ)*2
  331 CONTINUE
      NZERO=1
      NUMBER=NZERO
      NCASES=3
C        IF (NUMBER.EQ.3) NUMBER=1
    1 CONTINUE
C      IF (NUMBER.EQ.2) NUMBER=3
C      IF(NUMBER.EQ.2) NUMBER=4
C*****DEFINE HERE QUANTUM NOS. FOR VARIOUS LINES
C     FACTOR CONVERTS MMS ON GRAPH TO GAUSS
  188 FORMAT(1H1)
    8 FORMAT(1X,4HQ1 = ,E13.5,5X,4HQ2 = ,E13.5)
  137 FORMAT (3X,I2,5X,E16.6/)
  136 FORMAT(10X,19H INITIAL PARAMETERS//3X,1HJ,10X,4HB(J)//)
  135 FORMAT(1X,11H PARAMETERS//3X,1HJ,10X,4HB(J),27X,6HERRORS//)
    9 FORMAT(2X,4H HH= ,F9.4)
  140 FORMAT(3X,I2,5X,E16.6,15X,E16.6/)
  138 FORMAT(5X,14H CASE NUMBER =,I2//)
  141 FORMAT(10X,6H SMD =,E13.5//)
  235 FORMAT (15X,5(E13.5,8X)/)
  144 FORMAT(2X,*LINE NUMBER*,2X,*LINE POSITION*,2X,*ANGLE*,
     1 2X,*LINE NUMBER*,2X,*LINE POSITION*,2X,*ANGLE*,/)
  145 FORMAT(3X,I3,6X,F10.1,6X,F8.2,3X,I3,6X,F10.1,6X,F8.2)
      M=11
      MM=M
      L4=1
      Q1=1.E-8
      Q2=1.E-40
```

```
C       BO CONVERTS GAUSS TO GHZ
        BO=92.732/(6.6252*10000.)
        IG=1
  958 CONTINUE
        WRITE (6,188)
        N=NN(NUMBER)
        NN(NUMBER)=FREQ(NUMBER)
        N1=N
C       THE FOLLOWING FOR MEASURING MAGNETIC FIELD FROM THE GRAPH
C       WITH A LINEAR FACTOR
        DO 16 IJK=1,N1
        THETA(IJK)=TEETA(IJK,NUMBER)
        Z1(IJK,NUMBER)=(ZZ(IJK,NUMBER)+ADD(NUMBER))*
       1FACTOR(NUMBER)
C.      FOLLOWING PUTS SELECTED LINES EQUAL TO 0
        THI=THETA(IJK)
        IF (THI.LT.(0.)) Z1(IJK,NUMBER)=0.
        IF (THI.GT.(90.)) Z1(IJK,NUMBER)=0.
   16 CONTINUE
        DO 806 IJK=1,N1
        IF (THETA(IJK).GT.(25.)) GO TO807
        JYJ=JJII(NUMBER,1)
        DO 340 II=1,30
        DO 340 JJ=1,JYJ
        JJ1=(JJ-1)
        IIJJ=II+JJ1*30
        IBB(IIJJ,1)=IAB(II,1)
        IA1(IIJJ,NUMBER)=IBB(IIJJ,1)
        IBB(IIJJ,2)=IAB(II,2)
        IA2(IIJJ,NUMBER)=IBB(IIJJ,2)
  340 CONTINUE
        GO TO 342
  807 CONTINUE
        JXJ=JJII(NUMBER,2)
        DO343 II=1,30
        DO 343 JJ=1,JXJ
        JJ1=(JJ-1)
        IIJJ=II+JJ1*30+JJII(NUMBER,1)*30
        IBB(IIJJ,1)=ICC(II,1)
        IA1(IIJJ,NUMBER)=IBB(IIJJ,1)
        IBB(IIJJ,2)=ICC(II,2)
        IA2(IIJJ,NUMBER)=IBB(IIJJ,2)
  343 CONTINUE
  342 CONTINUE
  806 CONTINUE
        DO 210 LL=1,MM
  210 B(LL)=G(LL,NUMBER)
        WRITE (6,138) NUMBER
        WRITE (6,136)
        WRITE (6,137) (J,B(J),J=1,M)
        DO 3 IJK = 1,N1
        DELH(IJK)=DELHH(IJK,NUMBER)
    3 Z(IJK) = Z1(IJK,NUMBER)
C       IF (NUMBER.NE.I) GO TO 20
```

```
C    20 CONTINUE
C       IF(NUMBER.NE.2) GO TO 21
C    21 CONTINUE
C       IF(NUMBER.NE.3) GO TO 22
C    22 CONTINUE
       WRITE(6,144)
       DO 146 IJK=1,N1
  146  IF(Z(IJK).NE.(0.)) WRITE (6,145) IJK,Z(IJK),THETA(IJK)
       WRITE(6,8)Q1,Q2
       WRITE(6,9) HN(NUMBER)
       DO 201 II=1,N1
  201  FN(II)=HN(NUMBER)
       CALL CURFIT
       DO 202 II=1,N1
  202  DDF(II,NUMBER)=DF(II)
       SMDD(NUMBER) = SSMD
       WRITE(6,188)
       WRITE(6,135)
       DO 220 LL=1,N
  220  GG(LL,NUMBER) = B(LL)
       WRITE(6,140)(J,B(J),B1(J),J=1,N)
       WRITE(6,188)
       NUMBER = NUMBER + 1
       IF ( NUMBER - NCASE ) 1,1,2
     2 CONTINUE
       DO 230 LL=NZERO,NCASES
       N=NN(LL)
       IF (LL.GT.NZERO) WRITE(6,188)
       WRITE (6,138) LL
       WRITE (6,141) SMDD(LL)
       WRITE(6,302)
  302  FORMAT(5X,* IDENTIFICATION OF LINES*)
       DO 300 II=1,N
       IF(Z1(II,LL))563,562,563
  563  CONTINUE
  562  CONTINUE
  300  CONTINUE
       WRITE(6,301)((II,IA1(II,LL),IA2(II,LL)),II=1,N)
       WRITE (6,658)
  658  FORMAT(//)
C       SSS1 IS SMD(1),THAT IS WHEN ALL(LINES)SIGMA=1
       SSS1=0.
       NEFF=0
       DO 555 ID=1,N
       IF(ZZ(ID,LL))561,560,561
  561  CONTINUE
       NEFF=NEFF+1
       SSS(ID)=DDF(ID,LL)**2
       SSS1=SSS(ID)+SSS1
  560  CONTINUE
  555  CONTINUE
       WRITE(6,656)((ID,SSS(ID)),ID=1,N)
       ANEFF=FLOAT(NEFF)
        SSAV5= SS1*5./ANEFF
```

```
      WRITE(6,658)
      WRITE (6,657) S 1, SSAV5
  657 FORMAT (10X,*SMD(1)=*,                    , 13.5,//)
  656 FORMAT(2X,*LINE NO.=*,I3,3X,*SMD=*,E13.5,2X,*LINE NO.=*,
     1 ,I3,3X,*SMD=*,E13.5)
  301 FORMAT(2X,*FIELD NO.=*,I3,3X,*E-VAL1=*,I3,3X,*E-VAL2=*,I3,
     1 2X,*FIELD NO.=*,I3,3X,*E-VAL1=*,I3,3X,*E-VAL2=*,I3)
  230 WRITE (6,235) (GG(LM,LL),LM=1,11)
  708 CONTINUE
      STOP
      END
      SUBROUTINE CURFIT
C
C     EXAM  HANDLES ALL MATRICES OF DIMENSIONS UPTO THE DIMS.MM OF
C A,B,C THAT IS M IS LESS THAN OR EQUAL TO MM (SAME IS TRUE OF MATINV
C AND JACOBI)
C
C       IN EQUIVALENCEGRAD SHOULD BE PLACED IMMEDIATELY AFTER
C        B SINCE IN FUNC B(12,2)=BB(12),GRAD(12) IN CURFIT
C
C
C     DIMENSION OF B3 SHOULD BE M*(M+1)/2
C          F O R T R A N  4
      DIMENSION Z(350),FM(350),FC(350),DF(350),ERR(350),B(12),B1(12),
     1 B2(12,12),B4(12,12),HN(10)
     1,DC(5000),ABC(2),Y(4),X(350),GRAD(12),D1(12),D2(12,12),B3(66)
      DIMENSION IBB(350,2),THETA(350)
      COMMON/DATA1/ABC,Y
      COMMON/DATA2/DC
      EQUIVALENCE (Z,DC),(FM,DC(501)),(FC,DC(1001)),
     1(DF,DC(1501)),(ERR,DC(2001)),(B,DC(2989)),(GRAD,DC(3001)),
     2(B1,DC(3013)),(B2,DC(3025)),(N,DC(3169)),(L4,DC(3170)),
     3(Q1,DC(3171)),(Q2,DC(3172)),(M,DC(3173)),(I,DC(3174)),
     4(L,DC(3175)),(D1,DC(2501)),(D2,DC(2513)),(BO,DC(3176)),
     5(SMD,DC(3177)),(SSMD,DC(3178)),(IBB,DC(4000)),(THETA,DC(3500))
     6 ,(HN,DC(3179))
     7,( ,DC(2901)),( A,DC(2902)),(BMOD,DC(2903)),(PROD,DC(2904))
     8,(GMOD,DC(2905)),(LE,DC(2906)),(LLX,DC(4908))
      DATA(ABC=2HNO,3HYES),(Y=1H ,1HC,1H*,1.
      MM=M
      N N
      J T =  
      A  -50.0
C      SA1 I  A WITH SIGMA (ALL LINES)=1.
      SA1=0.
      DO 1000 J=1,MM
      B1(J)=0.0
      DO 1000 K=1,MM
 1000 B2(J,K)=0.0
      WRITE(6,901)
C      LLX=0 ALLOWS WRITING E.VALUES IN FUNC
      LLX=0
      DO 100 II = 1, MM
```

```
      I=II
      L=1
      CALL FUNC(2)
      X(II)=ERR(II)**2
  901 FORMAT(5X,10H FUNC2,210  )
      DF(II) =FM(II) - FC(II)
      DO 101 J=1,MM
      B1(J)=B1(J)-(2.0*DF(II)*D1(J))/X(II)
      DO 101 K=1,MM
  101 B2(J,K)=B2(J,K)-(2.0*(DF(II)*D2(J,K)-D1(J)*D1(K)))/X(II)
      SA1=SA1+DF(II)**2
  100 SA = SA + DF(II)**2/X(II)
C      LLX=1 OMITS WRITING E.VALUES IN FUNC
      LLX=1
C      EQZERO TELLS IF ELEMENTS OF B2,B1 ARE ZERO
      CALL EQZERO(B2,B1,M,IC1,IC2,IC3)
      WRITE(6,901)
      LL=1
      CALL SECO( CPU)
      WRITE(6,5)CPU,LL
    5 FORMAT(5X,*CPU=*,F8.2,*LL=*,I2)
      GMOD=0.0
      DO 102 J=1,M
  102 GMOD=GMOD+B1(J)**2                                    OF GR
      WRITE(6,243) A,GMOD
  243 FORMAT (1X,26H*INITIAL VALUE SUM OF SQ.=E13.5,20X,17H* Q MOD
     1AD =E13.5)
      WRITE(6,244) SA1
  244 FORMAT(5X,*INITIAL VALUE SUM OF SQ.(ALL SIGMA
     1=1)=*,E13.5,//)
 1751 FORMAT(14H0
      WRITE(6,240)(B1(J),J=1,M)
  240 FORMAT (15X,5(E13.5,8X)/)
      LLJJ=0
C***** FOLLOWING FOR CALCULATING INITIAL VALUES ONLY
C      LLJJ=1
      IF(LLJJ.NE.0) GOTO 559
      IF (SA - Q1) 110, 110, 200
  110 LL = 1
      GO TO 600
  200 S = 0.0
      GMOD = 0.0
      BMOD = 0.0
      PROD = 0.0
      A2=ABC(1)
      DO 210 J = 1, MM
      B1(J) = 0.0
      DO 210 K = 1, MM
  210 B2(J,K) = 0.0
      WRITE(6,902)
      DO 220 II = 1, NN
      I=II
      L=1
```

```
      CALL FUNC(2)
      X(II)=ERR(II)**2
  902 FORMAT(5X,10H FUNC2,210  )
      DF(II) = FM(II) - FC(II)
      DO 220 J = 1, MM
      B1(J) = B1(J) - (2.0*DF(II)*D1(J))/X(II)
      DO 220 K = 1, MM
  220 B2(J,K) = B2(J,K) - (2.0*(DF(II)*D2(J,K) -D1(J)*D1(K)))/X(II)
      CALL EQZERO(B2,B1,M,IC1,IC2,IC3)
      WRITE(6,902)
      LL=2
      CALL SECOND(CPU)
      WRITE(6,5)CPU,LL
       DO 230 J = 1, MM
  230 GRAD(J) = B1(J)
      L1 = L1 + 1
      WRITE(6,903)
      CALL EXAM (B2,B1,M,LF)
      WRITE(6,903)
  903 FORMAT(5X,9H EXAM,230  )
      IF (LF)  250, 250, 305
  250 DO 231 II=1,M
      DO 231 JJ=1,II
      KK=II*(II-1)/2+JJ
  231 B3(KK)=B2(II,JJ)
      WRITE(6,904)
      CALL EIGRS(B3,M,1,B1,B2,M,B4,NR)
      IF(NR.EQ.0) GO TO 387
      WRITE(6,386)NR
  386 FORMAT(5X,*NR=*,2X,I5)
  387 CONTINUE
      WRITE(6,904)
  904 FORMAT(5X,12H EIGRS,231  )
      WRITE(6,240)B1
      DO 389 I5=1,MM
      AB1=ABS(B1(I5))
      IF((AB1).GT.(1.E-10)) GO TO 388
      B1(I5)=0.
  388 CONTINUE
  389 CONTINUE
      I4=5
      IF (I4.EQ.1) GO TO 912
      A2=ABC(2)
      DO 260 J = 1, MM
  260 D1(J) = 0.0
      DO 270 J = 1, MM
      DO 270 K = 1, MM
  270 D1(K) = D1(K) + B2(J,K) *GRAD(J)
      DO 275 J = 1, MM
      IF (B1(J))  280, 290, 285
  280 B1(J) = - B1(J)
  285 D1(J) = D1(J)/B1(J)
      GO TO 275
  290 D1(J) = 0.0
```

```
 275 CONTINUE
     DO 295 J = 1, MM
 295 B1(J) = 0.0
     DO 300 J = 1, MM
     DO 300 K = 1, MM
 300 B1(J) = B1(J) + B2(J,K)*D1(K)
 305 DO 310 J=1,MM
     GMOD = GMOD + GRAD(J)**2
     BMOD = BMOD + B1(J)**2
 310 PROD = PROD + GRAD(J)*B1(J)
     IF (GMOD - Q2)  315, 315, 320
 315 LE = 2
     WRITE(6,1761) GMOD
1761 FORMAT(5X,7H GMOD =,E13.5//)
     GO TO 600
 320 C=PROD/ SQRT(BMOD*GMOD)
     IF (C) 335, 335, 400
 335 LE = 4
     GO TO 600
 400 LD = 0
     L3 = 0
     DO 410 J = 1, MM
 410 GRAD(J) = B(J) - B1(J)
     WRITE(6,905)
 450 DO 420 II = 1, NN
     I=II
     L=2
     CALL FUNC(1)
     X(II)=ERR(II)**2
 905 FORMAT(5X,10H FUNC1,450  )
     DF(II) = FM(II) - FC(II)
 420 S = S + DF(II)**2/X(II)
     LM=3
     CALL SECOND(CPU)
     WRITE(6,5)CPU,LM
     WRITE(6,905)
     IF (SA - S) 435, 500, 500
 435 LD = LD + 1
     WRITE(6,906)
 430 DO440 J = 1, MM
     B1(J) = B1(J)/2.0
 906 FORMAT(5X,16H BINARY CHOP,430  )
 440 GRAD(J) = B(J) - B1(J)
     WRITE(6,906)
     S = 0.0
     L3 = L3 + 1
     IF(L3-3)450,460,460
 460 LE = 5
     GO TO 600
 500 IF (LD) 505, 505, 506
 506 LD = 0
     GO TO 430
 505 DO 510 J = 1, MM
 510 B(J) = GRAD(J)
```

```
      SA = S
      IF (A - Q1) 507, 507, 530
  507 LE = 1
      GO TO 600
  530 IF (L4) 200, 200, 900
  900 WRITE(6,920)L1,A2,L3,  ,GMOD,(B(J),J=1,M)
  920 FORMAT(//,15H ITERATION NO.=I5,10X,43H   TRANSFORMATION MADE
 TOPR 1INCIPAL AXES = A4,10X,   18H BINARY CHOP USED=I3,6H TIMES/1X,
 2HW 2EIGHTED SUM OF SQUARES = E14.7,25X,32H  SQUARE MODULUS OF GR
 DIEN 3T = E14.7/20H   PARAMETERS B(J) -/(6E17.8)/)
      IF (L1 - L4) 200, 910, 910
  910 LE = 6
      GO TO 600
  600 DO 710 J=1,MM
      B1(J) = 0.0
      DO 710 K=1,MM
  710 B2(J,K) = 0.0
      L=1
  907 FORMAT(5X,*FUNC(2) AT 720*,/)
C*****FOLLOWING FOR INITIAL VALUES ONLY
  559 CONTINUE
      WRITE(6,907)
      DO 720 II = 1, NN
      I=II
      CALL FUNC(2)
      X(II)=ERR(II)**2
      DF(II) = FM(II) - FC(II)
      DO 720 J = 1, MM
      B1(J) = B1(J) - (2.0*DF(II)*D1(J))/X(II)
      DO 720 K = 1, MM
  720 B2(J,K) = B2(J,K) - ((DF(II)*D2(J,K) -D1(J)*D1(K)))/X(II)
      CALL EQZERO(B2,B1,M,IC1,IC2,IC3)
      LM=4
      CALL SECOND(CPU)
      WRITE(6,5)CPU,LM
      WRITE (6,3029)
 3029 FORMAT(* I AM LOST IN MANTINV*)
 3030 FORMAT(*    I AM OUT OF MATINV*)
      CALL MATINV(B2,M,B1,1,DETERM)
      WRITE (6,3030)
      DO 730 J=1,MM
      IF (B2(J,J)) 2001,2002,2002
 2001 B1(J) = -SQRT(-B2(J,J))
      GO TO 730
 2002 B1(J)= SQRT(B2(J,J))
  730 CONTINUE
      DO 740 J=1,MM
      DO 740 K=1,MM
  740 B2(J,K)=B2(J,K)/(B1(J)*B1(K))
      WRITE(6,551)LE,SA
  551 FORMAT(//,13H EXIT NUMBER=I3,20X,25H WEIGHTED SUM OF SQUARES=
E15.8 1//)
      SMD = SA
  912 CONTINUE
```

```
      RETURN
      END

      SUBROUTINE FUNC(LX)
C     SUBROUTINE FUNC
      DIMENSION SZ(6,6), X(6,6), Z0(6,6), Y40(6,6), Y42(6,6), U(6,6),
     1AK(6,6), Y(6,6),S22(6,6),SPX(6),Y44(6,6),HN(10)
      DIMENSION DC(5000),B(12,2),D1(12),D2(12,12),FC(350),Z(350),
     1SIGN(350),SP(8,12),IBB(350,2),THETA(350)
     2 ,W(36),ZK(36,36),R(36,36),CI(36,36),CC(36,36),A(666)
     3 ,ERR(350),DELH(350)
      COMMON/DATA2/DC
      COMMON/DATA3/DELH
      EQUIVALENCE (Z,DC),(B,DC(2989)),(D1,DC(2501)),(D2,DC(2513)),
     1(M,DC(3173)),(L,DC(3175)),(I,DC(3174)),(BO,DC(3176)),
     2(HN,DC(3179)),(IBB,DC(4000)),(THETA,DC(3500)),(FC,DC(1001))
     3 ,(LLX,DC(4998)),(NUMBER,DC(4999)),(ERR,DC(2001))
C      B(I,L) ARE THE LITTLE B(I,L) AS IN THE SPIN HAMILTONIAN
C      FOR RELATION TO CAP.B(I,L) SEE ABRAGAM AND BLEANEY
      DATA(SP(J,1),J=1,6)/2.5,1.5,.5,-.5,-1.5,-2.5/
      DATA(SPX(J),J=1,6)/10.,-2.,-8.,-8.,-2.,10./
      DATA(SP(J,5),J=1,6)/1.,-3.,2.,2.,-3.,1./
C    ****TO BE REMOVED LATER
      DO 91 JIJ=1,6
   91 SP(JIJ,3)=SPX(JIJ)/3.
      R2=SQRT(2.0)
      R3=SQRT(3.0)
      R5=SQRT(5.0)
      R7=SQRT(7.0)
      R10=SQRT(10.0)
      SP(1,4)=R10/3.
      SP(2,4)=R2
      SP(3,4)=R2
      SP(4,4)=R10/3.
      SP(1,6)=3.*R10/20.
      SP(2,6)=-5.*R2/20.
      SP(3,6)=-5.*R2/20.
      SP(4,6)=3.*R10/20.
      SP(1,7)=1./R5
      SP(2,7)=1./R5
      SP(1,2)=R5/2.
      SP(2,2)=R2
      SP(3,2)=1.5
      SP(4,2)=R2
      SP(5,2)=R5/2.
      IF (Z(I)) 18,21,18
   18 CONTINUE
C
C      PBBZ, PBBX, PBBY ARE COEFFS. MULTIPLYING S(Z), S(X), S(Y)
C      SPIN COMPONENTS
C

      DO 500 IX=1,6
      DO 500 JX=1,6
      SZ(IX,JX) = 0.
```

```
      SX(IX,JX) = 0.
      SY(IX,JX) = 0.
       20(IX,JX) = 0.
      .22(IX,JX) = 0.
      S40(IX,JX) = 0.
      S42(IX,JX)=0.
      S44(IX,JX) = 0.
      AR(IX,JX) = 0.
      SU(IX,JX) = 0.
  500 CONTINUE
      DO 605 IX=1,36
      R(IX) = 0.
      DO 605 JX=1,36
      SR(IX,JX)=0.
      ZR(IX,JX)=0.
      .I(IX,JX)=0.
  605 CC(IX,JX)=0.
      DO 505 IX=1,6
      SZ(IX,IX) = SP(IX,1)
      S20(IX,IX) = SP(IX,3)
      S40(IX,IX) = SP(IX,5)
      SU(IX,IX) = 1.
  505 CONTINUE
      DO 510 IX=1,4
      IX2 = IX + 2
      S22(IX,IX2) = SP(IX,4)
      .22(IX2,IX) = SP(IX,4)
  510 CONTINUE
      DO 515 IX=1,5
      IX1=IX+1
      SX(IX,IX1) = SP(IX,2)
      SX(IX1,IX) = SP(IX,2)
  515 CONTINUE
      S42(1,3)=9.*R10/60.
      S42(2,4)=-15.*R2/60.
      S42(3,5)=.42(2,4)
      .42(4,6)=.42(1,3)
      S42(3,1)= 42(1,3)
      .42(4,2)= 42(2,4)
      S42(5,3)= 42(3,5)
      .42(6,4)=.42(4,6)
      S44(1,5)=12.*R5/60.
      S44(2,6)=.44(1,5)
      S44(5,1)=S44(1,5)
      .44(6,2)=.44(2,6)
      TH = THETA(I)*3.14159264/180.
      CSTH =(COS(TH))
       NTH =(SIN(TH))
      PBBZ = B(1,L)*BO*Z(I)*CSTH
C***  NEXT TWO LINES CHANGE FROM GXX INDEPENDENT TO GXX=GZZ
      PBB      (Z,L)*BO*Z(I)*SNTH
C      PBBX=B(1,L)*BO*Z(I)*SNTH
      PBBY = 1.
      AR(1,1)=2.5*PBBZ+10.*B(3,L)/3.+B(5,L)
```

```
      AR(2,2)=1.5*PBBZ-2.*B(3,L)/3.-3.*B(5,L)
      AR(3,3)=.5*PBBZ-8.*B(3,L)/3.+2.*B(5,L)
      AR(4,4)=AR(3,3)-PBBZ
      AR(5,5)=AR(2,2)-3.*PBBZ
      AR(6,6)=AR(1,1)-5.*PBBZ
      AR(1,3)=B(4,L)*R10/3.+B(6,L)*9.*R10/60.
      AR(2,4)=B(4,L)*3.*R2/3.-B(6,L)*15.*R2/60.
      AR(3,5)=AR(2,4)
      AR(4,6)=AR(1,3)
      AR(3,1)=AR(1,3)
      AR(4,2)=AR(2,4)
      AR(5,3)=AR(3,5)
      AR(6,4)=AR(4,6)
      AR(1,5)=B(7,L)*R5*12./60.
      AR(2,6)=AR(1,5)
      AR(5,1)=AR(1,5)
      AR(6,2)=AR(2,6)
      AR(1,2)=R5*PBBX/2.
      AR(2,1)=AR(1,2)
      AR(2,3)=R2*PBBX
      AR(3,2)=AR(2,3)
      AR(3,4)=1.5*PBBX
      AR(4,3)=AR(3,4)
      AR(4,5)=R2*PBBX
      AR(5,4)=AR(4,5)
      AR(5,6)=R5*PBBX/2.
      AR(6,5)=AR(5,6)
      SY(1,2)=-R5*PBBY/2.
      SY(2,1)=-SY(1,2)
      SY(2,3)=-R2*PBBY
      SY(3,2)=-SY(2,3)
      SY(3,4)=-1.5*PBBY
      SY(4,3)=-SY(3,4)
      SY(4,5)=-R2*PBBY
      SY(5,4)=-SY(4,5)
      SY(5,6)=-R5*PBBY/2.
      SY(6,5)=-SY(5,6)
      DO 520 IY=1,6
      DO 520 JY =1,6
      DO 520 IZ=1,6
      DO 520 JZ=1,6
      IX=(IY-1)*6+IZ
      JX=(JY-1)*6+JZ
      SR(IX,JX)=AR(IY,JY)*SU(IZ,JZ)+
     1 SU(IY,JY)*(S20(IZ,JZ)*B(8,L)+S22(IZ,JZ)*B(9,L))+
     2B(10,L)*SZ(IY,JY)*SZ(IZ,JZ)+B(11,L)*(SX(IY,JY)*SX(IZ,JZ)
     3 -SY(IY,JY)*SY(IZ,JZ))
  520 CONTINUE
      DO 999 II=1,36
      DO 999 JJ=1,II
      KK=II*(II-1)/2 + JJ
  999 A(KK)=SR(II,JJ)
      CALL EIGRS(A,36,1,W,ZR,36,WI,IER)
      IF(IER)997,996,997
```

```
  997 CONTINUE
      WRITE (6,998) IER
  996 CONTINUE
  998 FORMAT(5X,*IER=*,I3)
C     ** TO BE REMOVED LATER(LLX IS DEFINED IN FUNC)
      IF(LLX)992,993,992
  993 CONTINUE
      WRITE(6,995)I
  995 FORMAT(5X,*I=*,I3)
      WRITE(6,994)W
  994 FORMAT(2X,6E12.4)
  992 CONTINUE
C  *****DEFINE HERE THE LINES WHOSE QUANTUM NOS. NOT DEFINED ABOVE
      I6=I
      IF(NUMBER.NE.1) GO TO 1814
      I1=IBB(I6,1) $ I2=IBB(I6,2)
      GO TO 803
 1814 CONTINUE
      IF(NUMBER.NE.2) GO TO 815
      I1=IBB(I6,1) $ I2=IBB(I6,2)
      GO TO 803
  815 CONTINUE
      IF(NUMBER.NE.3) GO TO 816
      I1=IBB(I6,1) $ I2=IBB(I6,2)
      GO TO 803
  816 CONTINUE
      IF (NUMBER.NE.4) GO TO 817
      I1=IBB(I6,1) $ I2=IBB(I6,2)
      GO TO 803
  817 CONTINUE
C*****DEFINE ABOVE THE LINES WHOSE QUANTUM NO . NOT DEFINED ABOVE
  802 CONTINUE
      I1=1
      I2=2
      DELMIN=ABS(ABS(W(1)-W(2))-HN(NUMBER))
      DO 85 IX=1,35
      IX1=IX+1
      DO 81 JX=IX1,36
      DELI=ABS(ABS(W(IX)-W(JX))-HN(NUMBER))
      IF(DELI-DELMIN)84,84,86
   84 DELMIN=DELI
      I1=IX
      I2=JX
      IBB(I,1)=I1
      IBB(I,2)=I2
   86 CONTINUE
   81 CONTINUE
   85 CONTINUE
  803 CONTINUE
      FC(I)=ABS(W(I1)-W(I2))
      SIGN(I)=(W(I1)-W(I2))/FC(I)
      DO 301 IY=1,6
      DO 301 JY=1,6
      DO 301 IZ=1,6
```

```
      DO 301 JZ=1,6
      IX=(IY-1)*6+IZ
      JX=(JY-1)*6+JZ
      CC(IX,JX)=BO*DELR(I)*(B(1,L)*CSTH*SZ(IY,JY)*SU(IZ,JZ)+
     1 B(2,L)*SNTH*SX(IY,JY)*SU(IZ,JZ))
  301 CONTINUE
      ERR(I)=0.
      DO 814 IX=1,36
      DO 814JX=1,36
      ERR(I)=ERR(I)+CC(IX,JX)*(ZR(JX,I1)*ZR(IX,I1)
     1 -ZR(JX,I2)*ZR(IX,I2))
  814 CONTINUE
      GO TO 17
   21 CONTINUE
      FC(I)=RN(NUMBER)
      ERR(I)=1.
      SIGN(I) =1.
   17 CONTINUE
      IF(LX-1)110,110,120
  120 CONTINUE
      DO 235 IZ=1,12
      D1(IZ) = 0.0
      DO 235 JZ=1,12
  235 D2(IZ,JZ) =0.0
      IF (Z(I)) 418,217,418
  418 CONTINUE
      DO 237 KX=1,11
      DO 236 IY=1,6
      DO 236 JY=1,6
      DO 236 IZ=1,6
      DO 236 JZ=1,6
      IX=(IY-1)*6 + IZ
      JX=(JY-1)*6 + JZ
      GO TO (705,706,707,708,709,710,711,712,713,714,715),KX
  705 CC(IX,JX)=SZ(IY,JY)*SU(IZ,JZ)
      ALPHA=BO*Z(I)*COTH
      GO TO 720
  706 CC(IX,JX)=SX(IY,JY)*SU(IZ,JZ)
      ALPHA=BO*Z(I)*SNTH
      GO TO 720
  707 CC(IX,JX)=S20(IY,JY)*SU(IZ,JZ)
      ALPHA=1.
      GO TO 720
  709 CC(IX,JX)=S40(IY,JY)*SU(IZ,JZ)
      ALPHA=1.
      GO TO 720
  714 CC(IX,JX)=SZ(IY,JY)*SZ(IZ,JZ)
      ALPHA=1.
      GO TO 720
  712 CC(IX,JX)=SU(IY,JY)*S20(IZ,JZ)
      ALPHA=1.
      GO TO 720
  710 CC(IX,JX)=S42(IY,JY)*SU(IZ,JZ)
      ALPHA=1.
```

```
      GO TO 720
  711 CC(IX,JX)=S44(IY,JY)*SU(IZ,JZ)
      ALPHA=1.
      GO TO 720
  708 CC(IX,JX)=S22(IY,JY)*SU(IZ,JZ)
      ALPHA=1.
      GO TO 720
  713 CC(IX,JX)=SU(IY,JY)*S22(IZ,JZ)
      ALPHA=1.
      GO TO 720
  715 CC(IX,JX)= X(IY,JY)*SX(IZ,JZ)
     2 -SY(IY,JY)*SY(IZ,JZ)
      ALPHA=1.
  720 CONTINUE
      SR(JX,IX)=(ZR(JX,I1)*ZR(IX,I1)-ZR(JX,I2)*ZR(IX,I2))*
     1 SIGN(I)
C FOLLOWING TWO LINES CHANGE FROM GXX INDEPENDENT TO GXX=GZZ
      KX1=KX
C      IF(KX.EQ.2) KX1=1
  236 D1(KX1)=D1(KX1)+CC(IX,JX)*SR(JX,IX)*ALPHA
C      FOLLOWING LINE CHANGES GXX INDEP. TO GXX=GZZ
C      D1(2)=0.
  237 CONTINUE
  217 CONTINUE
  110 CONTINUE
      RETURN
      END
      SUBROUTINE EXAM(A,B,M,LF)
C     SUBROUTINE EXAM
C       F O R T R A N  4
      DIMENSION A(12,12),B(12),C(12)
      DO 80 J=1,M
   80 C(J)=A(J,J)
      IF(A(1,1)) 60,200,70
   60 A(1,1) =- SQRT(-A(1,1))
      GO TO 300
   70 A(1,1) =SQRT(A(1,1))
      GO TO 100
  100 IF(M-1)400,400,110
  110 DO 115 K=2,M
  115 A(1,K)=A(1,K)/(A(1,1)          )
      DO 120 J=2,M
      J1=J-1
      S=A(J,J)
      DO 125 L=1,J1
  125 S=S-A(L,J)**2
      IF (S) 50,200,40
   50 A(J,J) =-SQRT(-S)
      GO TO 300
   40 A(J,J) =SQRT(S)
      GO TO 130
  130 IF(J-M)135,400,400
  135 J2=J+1
      DO 120 K=J2,M
```

```
      S=A(J,K)
      DO 145 L=1,J1
  145 S=S-A(L,J)*A(L,K)
  120 A(J,K)=S/A(J,J)
  400 B(1)=B(1)/A(1,1)
      IF(M-1)420,420,405
  405 DO 410 J=2,M
      S=B(J)
      J1=J-1
      DO 415 L=1,J1
  415 S=S-A(L,J)*B(L)
  410 B(J)=S/A(J,J)
  420 B(M)=B(M)/A(M,M)
      J=M-1
  435 IF(J)450,450,425
  425 S=B(J)
      J2=J+1
      DO 430 L=J2,M
  430 S=S-A(J,L)*B(L)
      B(J)= /A(J,J)
      J=J-1
      GO TO 435
  450 LF=1
      GO TO 460
  200 LF=0
      GO TO 460
  300 LF=-1
  460 DO 465 J=1,M
      A(J,J)=C(J)
      IF(J-M)470,475,475
  470 J2=J+1
      DO 465 K=J2,M
  465 A(J,K)=A(K,J)
  475 RETURN
      END

      SUBROUTINE MATINV(A,N,B,M,DETERM)
C     SUBROUTINE MATINV
C       F O R T R A N  4
C     MATRIX INVERSION WITH ACCOMPANYING SOLUTION OF LINEAR EQUATION
      DIMENSION IPIVOT(12),A(12,12),B(12,1),INDEX(12,2),PIVOT(12)
      EQUIVALENCE (IROW,JROW),(ICOLUM,JCOLUM),(AMAX,T,SWAP)
      DETERM=1.0
      DO 20 J=1,N
   20 IPIVOT(J)=0
      DO 550 I=1,N
      AMAX=0.0
      DO 105 J=1,N
      IF(IPIVOT(J)-1)60,105,60
   60 DO 100 K=1,N
      IF(IPIVOT(K)-1)80,100,740
   80 IF(ABS(AMAX)-ABS(A(J,K)))85,100,100
   85 IROW=J
      ICOLUM=K
```

```
      AMAX=A(J,K)
  100 CONTINUE
  105 CONTINUE
      IPIVOT(ICOLUM)=IPIVOT(ICOLUM)+1
      IF (IROW-ICOLUM)140,260,140
  140 DETERM=-DETERM
      DO 200 L=1,N
      SWAP=A(IROW,L)
      A(IROW,L)=A(ICOLUM,L)
  200 A(ICOLUM,L)=SWAP
      IF(M)260,260,210
  210 DO 250 L=1,M
      SWAP=B(IROW,L)
      B(IROW,L)=B(ICOLUM,L)
  250 B(ICOLUM,L)=SWAP
  260 INDEX(I,1)=IROW
      INDEX(I,2)=ICOLUM
      PIVOT(I)=A(ICOLUM,ICOLUM)
      DETERM=DETERM*PIVOT(I)
      A(ICOLUM,ICOLUM)=1.0
      DO 350 L=1,N
  350 A(ICOLUM,L)=A(ICOLUM,L)/PIVOT(I)
      IF(M)380,380,360
  360 DO 370 L=1,M
  370 B(ICOLUM,L)=B(ICOLUM,L)/PIVOT(I)
  380 DO 550 L1=1,N
      IF (L1-ICOLUM)400,550,400
  400 T=A(L1,ICOLUM)
      A(L1,ICOLUM)=0.0
      DO 450 L=1,N
  450 A(L1,L)=A(L1,L)-A(ICOLUM,L)*T
      IF(M)550,550,460
  460 DO 500 L=1,M
  500 B(L1,L)=B(L1,L)-B(ICOLUM,L)*T
  550 CONTINUE
      DO 710 I=1,N
      L=N+1-I
      IF(INDEX(L,1)-INDEX(L,2))630,710,630
  630 JROW=INDEX(L,1)
      JCOLUM=INDEX(L,2)
      DO 705 K=1,N
      SWAP=A(K,JROW)
      A(K,JROW)=A(K,JCOLUM)
      A(K,JCOLUM)=SWAP
  705 CONTINUE
  710 CONTINUE
  740 RETURN
      END

      SUBROUTINE EQZERO(A,B,N,IC1,IC2,IC3)
      DIMENSION A(12,12),B(12)
      IC1=0
      IC2=0
```

```
      IC3=0
      DO 5 J3=1,M
      IF((ABS(B(J3))).GT.(1.E-20)) GO TO 10
      B(J3)=0.
      IC1=J3
      WRITE(6,100) IC1
   10 CONTINUE
      DO 5 J4=1,M
      IF((ABS(A(J3,J4))).GT.(1.E-10)) GO TO 15
      A(J3,J4)=0.
      IC2=J3
      IC3=J4
      WRITE(6,101) IC2,IC3
   15 CONTINUE
    5 CONTINUE
  100 FORMAT(5X, I3)
  101 FORMAT(5X,2I3)
      RETURN
      END
```

```
      PROGRAM CACAF (INPUT,OUTPUT,TAPE5=INPUT,TAPE6=OUTPUT)
C
C     THIS PROGRAM FITS FINE STRUCTURE DATA FOR MN2+/(CA(CLO4)2)ANP
C
C     NO =THE NO. OF FIRST MAG FIELD IN DATA INCLUDED IN FITTING
C     M  =NO. OF PARAMETERS
C     L4 =NO. OF ITERATIONS ALLOWED
C     Q1 =MIN. VALUE OF SUM OF SQUARES FOR FITS( CHI-SQUARE TOLERANCE)
C     Z(I)=MAGNETIC FIELD VALUES FOR FITS
C     B  =PARAMETER MATRIX
C     N  =NO. OF  DATA POINTS USED IN LEAST-SQARES FITTING
C     Q1 =N/10
C     Q2 =TOLERANCE ON GRAD(CHI**2) =APPROX .01
C     FM(I) = MEASURED VALUES
C     FC(I) = CALCULATED VALUES
C     ERR(I)= STANDARD DEVIATION ON FM(I) = SQRT(FM(I))
C
C      DIMENSIONS OF A,B IN EXAM AND MATINV SUBROUTINES SHOULD BE THE
C     SAME AS THOSE OF B2,B1 RESPECTIVELY IN THE MAIN PROGRAM AND IN
C     CURFIT
C
C     ENTER THETA IN DEGREES
C     DIMENSIONS OF Q,V IN JACOBI SHOULD BE THE SAME AS THOSE OF
C     B3,B2 RESPECTIVELY IN CURFIT
C
C     NUMBER=INDEX THAT CHANGES WITH EACH NEW CASE
C     NCASES=NO. OF CASES CONSIDERED. ITS VALUE SHOULD BE ENTERED.
C
C     IBB(II,1) AND IBB(II,2) INDICATE THE EIGENVALUES INVOLVED IN
C     RESONANCE FOR THE NO. II MAG FIELD VALUE
C
C      B=G=GPARRALEL,GPERPENDICULAR,B20,B22,B40,B42,B44,QPRIME,
C      QDOUBLEPRIME,A,B.
C
C      CASE1=MN2+/CACAF(ZX PLANE RT)
C      CASE2=MN2+/CACAF(ZX PLANE LHT,90K)
C      CASE3=MN2+/CACAF(ZX PLANE LHT,6K)
      DIMENSION Z(350),FM(350),FC(350),DF(350),ERR(350),B(12),
     1B1(12),B2(12,12),DC(5000),ABC(2),Y(4),ZZ(350,20),G(12,20),
     2THETA(350),GG(12,10),IBB(350,2),DELHH(350,4),DELH(350)
      DIMENSION TEETA(350,20),FREQ(20),FACTOR(20),NN(20),HN(20)
     1,Z1(350,6),ADD(20),DDF(350,6),IBB1(350,6),IBB2(350,6),SMDD(20)
      COMMON/DATA1/ABC,Y
      COMMON/DATA2/DC
      COMMON/DATA3/DELH
      EQUIVALENCE (Z,DC),(FM,DC(501)),(FC,DC(1001)),(DF,DC(1501)),
     1(ERR,DC(2001)),(B,DC(2989)),(B1,DC(3013)),(B2,DC(3025)),
     2(N,DC(3169)),(L4,DC(3170)),(Q1,DC(3171)),(Q2,DC(3172)),
     3(M,DC(3173)),(SSMD,DC(3178)),(IBB,DC(4000)),(THETA,DC(3500))
     4 ,(I,DC(3174)),(L,DC(3175)),(NO,DC(3176)),(MD,DC(3177))
     5 ,(HN,DC(3179)),(NUMBER,DC(4999))
      DATA(ABC=2HNO,3HYES),(Y=1H ,1HC,1H*,1HM)
C      DATA(ZZ(J,1),J=1,70)/
C      DATA(TEETA(J,1),J=1,70)/
```

```
      DATA(ZZ(J,2),J=1,65)/
      DATA(TEETA(J,2),J=1,65)/
      DATA(ZZ(J,3),J=1,50)/
      DATA(TEETA(J,3),J=1,50)/
C     FREQUENCY OF KLYSTRON IN GHZ
      DATA(FREQ(J),J=1,3)//
      DATA(FACTOR(J),J=1,3)//
      DATA(ADD(J),J=1,3)//
      DATA(NN(J),J=1,3)/
     1 /
      DATA(G(J,1),J=1,7)/
      DATA(G(J,2),J=1,7)/
      DATA(G(J,3),J=1,7)/
       DO 331 JJ=1,3
      NNJJ=NN(JJ)
       DO 331 J=1,NNJJ
       DELHH(J,1)=FACTOR(1)*6
       DELHH(J,2)=FACTOR(2)*2
      DELHH(J,3)=FACTOR(3)*6
  331 CONTINUE
      NZERO=1
      NUMBER=NZERO
      NCASES=1
  188 FORMAT(1H1)
    8 FORMAT(1X,4HQ1 = ,E13.5,5X,4HQ2 = ,E13.5)
  137 FORMAT (3X,I2,5X,E16.6/)
  136 FORMAT(10X,19H INITIAL PARAMETERS//3X,1HJ,10X,4HB(J)//)
  135 FORMAT(1X,11H PARAMETER//3X,1HJ,10X,4HB(J),27X,6HERRORS//)
    9 FORMAT(2X,4H HN= ,F9.4)
  140 FORMAT(3X,I2,5X,E16.6,15X,E16.6/)
  138 FORMAT(5X,14H CASE NUMBER =,I2//)
  141 FORMAT(10X,6H SMD =,E13.5//)
  235 FORMAT (15X,5(E13.5,8X)/)
  144 FORMAT(5X,*LINE NUMBER*,5X,*LINE POSITION*,7X,*ANGLE*,/)
  145 FORMAT(6X,I3,9X,F10.1,11X,F8.2)
      M=5
      MM=M
      L4=10
      Q1=1.E-8
      Q2=1.E+40
      BO=92.732/(6.6252*10000.)
      IG=1
  958 CONTINUE
    1 CONTINUE
      WRITE (6,188)
      N=NN(NUMBER)
      HN(NUMBER)=FREQ(NUMBER)
      N1=N
C     THE FOLLOWING FOR MEASURING MAGNETIC FIELD FROM THE GRAPH
C     WITH A LINEAR FACTOR
C     FACTOR CONVERTS MM. TO GAUSS
      DO 16 IJK=1,N1
      THETA(IJK)=0.
      THETA(IJK)=TEETA(IJK,NUMBER)
```

```
      Z1(IJK,NUMBER)=(ZZ(IJK,NUMBER)+ADD(NUMBER))*
     1FACTOR(NUMBER)
C       IF(THETA(IJK).GT.(30.)) Z1(IJK,NUMBER)=0.
   16 CONTINUE
      DO 211 LL=1,12
  211 B(LL)=0.
      DO 210 LL=1,MM
  210 B(LL)=G(LL,NUMBER)
      WRITE (6,138) NUMBER
      WRITE (6,136)
      WRITE (6,137) (J,B(J),J=1,M)
      DO 3 IJK = 1,N1
      DELH(IJK)=DELHH(IJK,NUMBER)
    3 Z(IJK) = Z1(IJK,NUMBER)
C       IF (NUMBER. NE.1) GO TO 100
C      Z(5)=Z(9)=Z(31)=Z(66)=Z(10)=Z(15)=Z(20)=0.
C  100 CONTINUE
      IF (NUMBER.NE.2) GO TO 105
      Z(59)=Z(64)=Z(35)=Z(49)=Z(54)=Z(40)=Z(51)=Z(56)=0.
  105 CONTINUE
      IF(NUMBER.NE.3) GO TO 110
      Z(37)=Z(42)=Z(19)=Z(24)=Z(30)=Z(35)=Z(41)=Z(46)=0.
  110 CONTINUE
C      DO 4IJK=1,N1
C    4 IF(THETA(IJK).GT.(20.))Z(IJK)=0.
      WRITE(6,144)
      DO 146 IJK=1,N1
  146 WRITE (6,145) IJK,Z(IJK),THETA(IJK)
      WRITE(6,8)Q1,Q2
      WRITE(6,9) HN(NUMBER)
      DO 201 II=1,N1
  201 FM(II)=HN(NUMBER)
      CALL CURFIT
      DO 202 II=1,N1
      IBB1(II,NUMBER)=IBB(II,1)
      IBB2(II,NUMBER)=IBB(II,2)
  202 DDF(II,NUMBER)=DF(II)
      SMDD(NUMBER) = SSMD
      WRITE(6,188)
      WRITE(6,135)
      DO 220 LL=1,M
  220 GG(LL,NUMBER) = B(LL)
      WRITE(6,140)(J,B(J),B1(J),J=1,M)
      WRITE(6,188)
      NUMBER = NUMBER + 1
      IF ( NUMBER - NCASE ) 1,1,2
    2 CONTINUE
      DO 230 LL=NZERO,NCASES
      M=MM(LL)
      IF(LL.GT.NZERO) WRITE(6,188)
      WRITE (6,138) LL
      WRITE (6,141) SMDD(LL)
      WRITE(6,302)
  302 FORMAT(5X,* IDENTIFICATION OF LINES*)
```

```
      DO 300 II=1,N
      IF(ZZ(II,LL))563,562,563
  563 CONTINUE
      WRITE(6,301) II,IBB1(II,LL),IBB2(II,LL)
  562 CONTINUE
  300 CONTINUE
      WRITE(6,658)
C     SSS1 IS SMD(1),THAT IS WHEN ALL (LINES) SIGMA=1
      SS.1=0.
      NEFF=0.
      DO 555 ID=1,N
      IF(ZZ(ID,LL))561,560,561
  561 CONTINUE
      NEFF=NEFF+1
      SSS=DDF(ID,LL)**2
      SSS1=SS.1+SSS
      WRITE(6,656) ID,SSS
  560 CONTINUE
  555 CONTINUE
      ANEFF=FLOAT(NEFF)
      SSSAV5=SS.1*5./ANEFF
      WRITE(6,658)
      WRITE(6,657) SS1,SSSAV5
  657 FORMAT (10X,*SMD(1)=*,E13.5,5X,*SSSAV5=*,E13.5,//)
  658 FORMAT (//)
  656 FORMAT(10X,*LINE NUMBER = *,I3,5X,*SMD = *,E13.5)
  301 FORMAT(10X,*MAG. FIELD NO. =*,I3,5X,*EIGENVALUE1 =*,I3,5X,
     1* EIGENVALUE2 =*,I3)
  230 WRITE (6,235) (GG(LM,LL),LM=1,11)
  708 CONTINUE
      STOP
      END
      SUBROUTINE CURFIT
C
C     EXAMINABLE ALL MATRICES OF DIMENSIONS UPTO THE DIMS.NN OF
C A,B,C THAT IS M IS LESS THAN OR EQUAL TO NN (SAME IS TRUE OF MATINV
C AND JACOBI)
C
C      IN EQUIVALENCEGRAD SHOULD BE PLACED IMMEDIATELY AFTER
C       B SINCE IN FUNC B(12,2)=BB(12),GRAD(12)  IN CURFIT
C
C
C     DIMENSION OF B3 SHOULD BE M*(M+1)/2
C          F O R T R A N  4
      DIMENSION Z(350),FM(350),FC(350),DF(350),ERR(350),B(12),B1(12),
     1 B2(12,12),B4(12,12),HN(20)
     1,DC(5000),ABC(2),Y(4),X(350),GRAD(12),D1(12),D2(12,12),B3(66)
      DIMENSION IBB(350,2),THETA(350)
      COMMON/DATA1/ABC,Y
      COMMON/DATA2/DC
      EQUIVALENCE (Z,DC),(FM,DC(501)),(FC,DC(1001)),
     1(DF,DC(1501)),(ERR,DC(2001)),(B,DC(2989)),(GRAD,DC(3001)),
     2(B1,DC(3013)),(B2,DC(3025)),(N,DC(3169)),(L4,DC(3170)),
     3(Q1,DC(3171)),(Q2,DC(3172)),(M,DC(3173)),(I,DC(3174)),
```

```
     4(L,DC(3175)),(D1,DC(2501)),(D2,DC(2513)),(BO,DC(3176)),
     5(SMD,DC(3177)),(SSMD,DC(3178)),(IBB,DC(4000)),(THETA,DC(3500))
     6 ,(NN,DC(3179))
     7,( ,DC(2901)),( A,DC(2902)),(BMOD,DC(2903)),(PROD,DC(2904))
     8,(GMOD,DC(2905)),(LE,DC(2906)),(LLX,DC(4998))
      DATA(ABC=2HNO,3HYES),(Y=1H ,1HC,1H*,1HM)
      MM=M
      NN=N
      L1 = 0
       A = 0.0
C      SA1 IS SA WITH SIGMA(ALL LINES)=1.
      SA1=0.
      DO 1000 J=1,MM
      B1(J)=0.0
      DO 1000 K=1,MM
 1000 B2(J,K)=0.0
      WRITE(6,901)
C      LLX=0 ALLOWS WRITING E.VALUES IN FUNC
      LLX=0
      DO 100 II = 1, NN
      I=II
      L=1
      CALL FUNC(2)
      X(II)=ERR(II)**2
    9 FORMAT(5X,10H FUNC2,210  )
      DF(II) =FM(II) - FC(II)
      DO 101 J=1,MM
    3 B1(J)=B1(J)-(2.0*DF(II)*D1(J))/X(II)
      DO 101 K=1,MM
  101 B2(J,K)=B2(J,K)-(2.0*(DF(II)*D2(J,K)-D1(J)*D1(K)))/X(II)
      SA1=SA1+DF(II)**2
  100 SA = SA + DF(II)**2/X(II)
C      LLX=1 OMITS WRITING E.VALUES IN FUNC
      LLX=1
      CALL EQZERO(B2,B1,M,IC1,IC2,IC3)
      WRITE(6,901)
      LM=1
      CALL SECOND(CPU)
      WRITE(6,5)CPU,LM
    5 FORMAT(5X,*CPU=*,F8.2,*LM=*,I2)
      GMOD=0.0
      DO 102 J=1,M
  102 GMOD=GMOD+B1(J)**2
      WRITE(6,243)SA,GMOD
  243 FORMAT (1X,26H*INITIAL\VALUE SUM OF SQ.=E13.5,20X,17H* Q MOD
     GF LAD =E13.5)
      WRITE(6,244) SA1
  244 FORMAT(5X,*INITIAL SUM OF SQ. (ALL SIGMA=1)=*,E13.5,//)
      WRITE(6,1751)
 1751 FORMAT(14H0 DERIVATIVE -)
      WRITE(6,240)(B1(J),J=1,M)
  240 FORMAT (15X,5(E13.5,8X)/)
      IF (SA - Q1) 110, 110, 200
  110 LE = 1
```

```
      GO TO 600
  200 S = 0.0
      GMOD = 0.0
      DMOD = 0.0
      PROD = 0.0
      A2=ABC(1)
      DO 210 J = 1, MM
      B1(J) = 0.0
      DO 210 K = 1, MM
  210 B2(J,K) = 0.0
      WRITE(6,902)
      DO 220 II = 1, NN
      I=II
      L=1
      CALL FUNC(2)
      ERR(II)=ERR(II)**2
  902 FORMAT(5X,10H FUNC2,210  )
      DF(II) = FM(II) - FC(II)
      DO 220 J = 1, MM
      B1(J) = B1(J) - (2.0*DF(II)*D1(J))/X(II)
      DO 220 K = 1, MM
  220 B2(J,K) = B2(J,K) - (2.0*(DF(II)*D2(J,K) -D1(J)*D1(K)))/X(II)
      CALL EQZERO(B2,B1,M,IC1,IC2,IC3)
      WRITE(6,902)
      LM=2
      CALL SECOND(CPU)
      WRITE(6,5)CPU,LM
      DO 230 J = 1, MM
  230 GRAD(J) = B1(J)
      L1 = L1 + 1
      WRITE(6,903)
      CALL EXAM (B2,B1,M,LF)
      WRITE(6,903)
  903 FORMAT(5X,9H EXAM,230  )
      IF (LF)  250, 250, 305
  250 DO 231 II=1,M
      DO 231 JJ=1,II
      KK=II*(II-1)/2+JJ
  231 B3(KK)=B2(II,JJ)
      WRITE(6,904)
      CALL EIGRS(B3,M,1,B1,B2,M,B4,NR)
      IF(NR.EQ.0) GO TO 387
      WRITE(6,386)NR
  386 FORMAT(5X,*NR=*,2X,I5)
  387 CONTINUE
      WRITE(6,904)
  904 FORMAT(5X,12H EIGRS,231  )
      WRITE(6,240)B1
      DO 389 I5=1,MM
      AB1=ABS(B1(I5))
      IF((AB1).GT.(1.E-10)) GO TO 388
      B1(I5)=0.
  388 CONTINUE
  389 CONTINUE
```

```
      I4=5
      IF (I4.EQ.1) GO TO 912
      A2=ABC(2)
      DO 260 J = 1, MM
  260 D1(J) = 0.0
      DO 270 J = 1, MM
      DO 270 K = 1, MM
  270 D1(K) = D1(K) + B2(J,K) *GRAD(J)
      DO 275 J = 1, MM
      IF (B1(J))  280, 290, 285
  280 B1(J) = - B1(J)
  285 D1(J) = D1(J)/B1(J)
      GO TO 275
  290 D1(J) = 0.0
  275 CONTINUE
      DO 295 J = 1, MM
  295 B1(J) = 0.0
      DO 300 J = 1, MM
      DO 300 K = 1, MM
  300 B1(J) = B1(J) + B2(J,K)*D1(K)
  305 DO 310 J=1,MM
      GMOD = GMOD + GRAD(J)**2
      BMOD = BMOD + B1(J)**2
  310 PROD = PROD + GRAD(J)*B1(J)
      IF (GMOD - Q2)  315, 315, 320
  315 LE = 2
      WRITE(6,1761) GMOD
 1761 FORMAT(5X,7H GMOD =,E13.5//)
      GO TO 600
  320 C=PROD/SQRT(BMOD*GMOD)
      IF (C) 335, 335, 400
  335 LE = 4
      GO TO 600
  400 LD = 0
      L3 = 0
      DO 410 J = 1, MM
  410 GRAD(J) = B(J) - B1(J)
      WRITE(6,905)
  450 DO 420 II = 1, MM
      I=II
      L=2
      CALL FUNC(1)
      X(II)=ERR(II)**2
  905 FORMAT(5X,10H FUNC1,450  )
      DF(II) = FM(II) - FC(II)
  420 S = S + DF(II)**2/X(II)
      LM=3
      CALL SECOND(CPU)
      WRITE(6,5)CPU,LM
      WRITE(6,905)
      IF (LA - S) 435, 500, 500
  435 LD = LD + 1
      WRITE(6,906)
  430 DO440 J = 1, MM
```

```
      B1(J) = B1(J)/2.0
  906 FORMAT(5X,16H BINARY CHOP,430 )
  440 GRAD(J) = B(J) - B1(J)
      WRITE(6,906)
      = 0.0
      L3 = L3 + 1
C      NB TELLS MAX.NO. OF BINARY CHOPS
      NB=30
      IF(L3-NB)450,460,460
  460 LE = 5
      GO TO 600
  500 IF (LD) 505, 505, 506
  506 LD = 0
      GO TO 430
  505 DO 510 J = 1, MM
  510 B(J) = GRAD(J)
      SA = S
      IF (SA - Q1) 507, 507, 530
  507 LE = 1
      GO TO 600
  530 IF (L4) 200, 200, 900
  900 WRITE(6,920)L1,A2,L3,,GMOD,(B(J),J=1,M)
  920 FORMAT(//,15H ITERATION NO.=I5,10X,43H   TRANSFORMATION MADE
 TO PR1INCIPAL AXES = A4,10X,   18H BINARY CHOP USED=I3,6H TIME /1X,
 27H W2EIGHTED SUM OF SQUARES = E14.7,25X,32H   SQUARE MODULUS OF GR
 ADIEN 3T = E14.7/20H   PARAMETERS B(J) -/(6E17.8)/)
      IF (L1 - L4) 200, 910, 910
  910 LE = 6
      GO TO 600
  600 DO 710 J=1,MM
      B1(J) = 0.0
      DO 710 K=1,MM
  710 B2(J,K) = 0.0
      L=1
  907 FORMAT(5X,*FUNC(2) AT 720*,/)
      WRITE(6,907)
      DO 720 II = 1, MM
      I=II
      CALL FUNC(2)
      X(II)=ERR(II)**2
      DF(II) = FM(II) - FC(II)
      DO 720 J = 1, MM
      B1(J) = B1(J) - (2.0*DF(II)*D1(J))/X(II)
      DO 720 K = 1, MM
  720 B2(J,K) = B2(J,K) - ((DF(II)*D2(J,K) -D1(J)*D1(K)))/X(II)
      CALL EQZERO(B2,B1,M,IC1,IC2,IC3)
      LM=4
      CALL SECOND(CPU)
      WRITE(6,5)CPU,LM
      WRITE (6,3029)
 3029 FORMAT(* I AM LOST IN MANTINV*)
 3030 FORMAT(*   I AM OUT OF MATINV*)
      CALL MATINV(B2,M,B1,1,DETERM)
      WRITE (6,3030)
```

```
      DO 730 J=1,MM
      IF (B2(J,J)) 2001,2002,2002
2001  B1(J) = -SQRT(-B2(J,J))
      GO TO 730
2002  B1(J)= SQRT(B2(J,J))
 730  CONTINUE
      DO 740 J=1,MM
      DO 740 K=1,MM
 740  B2(J,K)=B2(J,K)/(B1(J)*B1(K))
      WRITE(6,551)LE,SA
 551  FORMAT(//,13H EXIT NUMBER=I3,20X,25H WEIGHTED SUM OF SQUARES=
     E15.8//)
      SSMD = SA
 912  CONTINUE
      RETURN
      END

      SUBROUTINE FUNC(LX)
C     SUBROUTINE FUNC
      DIMENSION SZ(6,6),SX(6,6),S20(6,6),S40(6,6),S42(6,6),SU(6,6),
     1AR(6,6),SY(6,6),S22(6,6),SPX(6),S44(6,6),HH(20)
      DIMENSION DC(5000),B(12,2),D1(12),D2(12,12),FC(350),Z(350),
     1SIGN(350),SP(8,12),IBB(350,2),THETA(350)
     2 ,W(6),ZR(6,6), R(6,6),S1(6,6),CC(6,6),A(21)
     3 ,ERR(350),DELE(350)
      DIMENSION DOLD(7)
      COMMON/DATA2/DC
      COMMON/DATA3/DELE
      EQUIVALENCE (Z,DC),(B,DC(2989)),(D1,DC(2501)),(D2,DC(2513)),
     1(M,DC(3173)),(L,DC(3175)),(I,DC(3174)),(BO,DC(3176)),
     2(HA,DC(3179)),(IBB,DC(4000)),(THETA,DC(3500)),(FC,DC(1001))
     3 ,(LLX,DC(4998)),(NUMBER,DC(4999)),(ERR,DC(2001))
C     B(I,L) ARE THE LITTLE B(I,L) AS IN THE SPIN HAMILTONIAN
C      FOR RELATION TO CAP.B(I,L) SEE ABRAGAM AND BLEANEY
      DATA(SZ(J,1),J=1,6)/2.5,1.5,.5,-.5,-1.5,-2.5/
      DATA(SPX(J),J=1,6)/10.,-2.,-8.,-8.,-2.,10./
      DATA(SP(J,5),J=1,6)/1.,-3.,2.,2.,-3.,1./
C    ****TO BE REMOVED LATER
      DO 91 JIJ=1,6
   91 SP(JIJ,3)=SPX(JIJ)/3.
      R2=SQRT(2.0)
      R3=SQRT(3.0)
      R5=SQRT(5.0)
      R7=SQRT(7.0)
      R10=SQRT(10.0)
      SP(1,4)=R10/3.
      SP(2,4)=R2
      SP(3,4)=R2
      SP(4,4)=R10/3.
      SP(1,6)=3.*R10/20.
      SP(2,6)=-5.*R2/20.
      SP(3,6)=-5.*R2/20.
      SP(4,6)=3.*R10/20.
      SP(1,7)=1./R5
```

```
      SP(2,7)=1./R5
      SP(5,2)=R5/2.
      SP(2,2)=R2
      SP(3,2)=1.5
      SP(4,2)=R2
      SP(5,2)=R5/2.
      IF (Z(1)) 18,21,18
   18 CONTINUE
C
C      PBBZ, PBBX, PBBY ARE COEFFS. MULTIPLYING S(Z), S(X), S(Y)
C      SPIN COMPONENTS
C
      DO 500 IX=1,6
      DO 500 JX=1,6
      SZ(IX,JX) = 0.
      SX(IX,JX) = 0.
      SY(IX,JX) = 0.
      S20(IX,JX) = 0.
      S22(IX,JX) = 0.
      S40(IX,JX) = 0.
      S42(IX,JX)=0.
      S44(IX,JX) = 0.
      AR(IX,JX) = 0.
      SU(IX,JX) = 0.
  500 CONTINUE
      DO 605 IX=1,6
      W(IX) = 0.
      DO 605 JX=1,6
      SR(IX,JX)=0.
      ZR(IX,JX)=0.
      CI(IX,JX)=0.
  605 CC(IX,JX)=0.
      DO 505 IX=1,6
      SZ(IX,IX) = SP(IX,1)
      S20(IX,IX) = SP(IX,3)
      S40(IX,IX) = SP(IX,5)
      SU(IX,IX) = 1.
  505 CONTINUE
      DO 510 IX=1,4
      IX2 = IX + 2
      S22(IX,IX2) = SP(IX,4)
      S22(IX2,IX) = SP(IX,4)
  510 CONTINUE
      DO 515 IX=1,5
      IX1=IX+1
      SX(IX,IX1) = SP(IX,2)
      SX(IX1,IX) = SP(IX,2)
  515 CONTINUE
      S42(1,3)=9.*R10/60.
      S42(2,4)=-15.*R2/60.
      S42(3,5)=S42(2,4)
      S42(4,6)=S42(1,3)
      S42(3,1)=S42(1,3)
      S42(4,2)=S42(2,4)
```

```
      S42(5,3)=S42(3,5)
      S42(6,4)=S42(4,6)
      S44(1,5)=12.*R5/60.
      S44(2,6)=S44(1,5)
      S44(5,1)=S44(1,5)
      S44(6,2)=S44(2,6)
      TH = THETA(I)*3.14159264/180.
      CSTH =(COS(TH))
      SNTH =(SIN(TH))
      PBBZ = B(1,L)*BO*Z(I)*CSTH
      PBBX = B(2,L)*BO*Z(I)*SNTH
C     NEXT LINE CHANGES TO GXX=GZZ (ISOTROPIC G)
C      PBBX=B(1,L)*BO*Z(I)*SNTH
      PBBY = 1.
      AR(1,1)=2.5*PBBZ+10.*B(3,L)/3.+B(4,L)
      AR(2,2)=1.5*PBBZ-2.*B(3,L)/3.-3.*B(4,L)
      AR(3,3)=.5*PBBZ-8.*B(3,L)/3.+2.*B(4,L)
      AR(4,4)=AR(3,3)-PBBZ
      AR(5,5)=AR(2,2)-3.*PBBZ
      AR(6,6)=AR(1,1)-5.*PBBZ
      AR(1,3)=B(6,L)*R10/3.+B(7,L)*9.*R10/60.
      AR(2,4)=B(6,L)*3.*R2/3.-B(7,L)*15.*R2/60.
      AR(3,5)=AR(2,4)
      AR(4,6)=AR(1,3)
      AR(3,1)=AR(1,3)
      AR(4,2)=AR(2,4)
      AR(5,3)=AR(3,5)
      AR(6,4)=AR(4,6)
      AR(1,5)=B(5,L)*R5*12./60.
      AR(2,6)=AR(1,5)
      AR(5,1)=AR(1,5)
      AR(6,2)=AR(2,6)
      AR(1,2)=R5*PBBX/2.
      AR(2,1)=AR(1,2)
      AR(2,3)=R2*PBBX
      AR(3,2)=AR(2,3)
      AR(3,4)=1.5*PBBX
      AR(4,3)=AR(3,4)
      AR(4,5)=R2*PBBX
      AR(5,4)=AR(4,5)
      AR(5,6)=R5*PBBX/2.
      AR(6,5)=AR(5,6)
      SY(1,2)=-R5*PBBY/2.
      SY(2,1)=-SY(1,2)
      SY(2,3)=-R2*PBBY
      SY(3,2)=-SY(2,3)
      SY(3,4)=-1.5*PBBY
      SY(4,3)=-SY(3,4)
      SY(4,5)=-R2*PBBY
      SY(5,4)=-SY(4,5)
      SY(5,6)=-R5*PBBY/2.
      SY(6,5)=-SY(5,6)
      DO 520 IX=1,6
      DO 520 JX =1,6
```

```
      SR(IX,JX)=AR(IX,JX)
  520 CONTINUE
      DO 999 II=1,6
      DO 999 JJ=1,11
      KK=II*(II-1)/2 + JJ
  999 A(KK)=SR(II,JJ)
      CALL EIGRS(A,6,1,W,ZR,6,.I,IER)
      IF(IER)997,996,997
  997 CONTINUE
      WRITE (6,998) IER
  996 CONTINUE
  998 FORMAT(5X,*IER=*,I3)
C     ** TO BE REMOVED LATER
      IF(LLX)992,993,992
  993 CONTINUE
      WRITE(6,995)I
  995 FORMAT(5X,*I=*,I3)
      WRITE(6,994)W
  994 FORMAT(2X,6E12.4)
  992 CONTINUE
  802 CONTINUE
      I1=1
      I2=2
      DELMIN=ABS(ABS(W(1)-W(2))-HN(NUMBER))
      DO 85 IX=1,5
      IX1=IX+1
      DO 81 JX=IX1,6
      DELI=ABS(ABS(W(IX)-W(JX))-HN(NUMBER))
      IF(DELI-DELMIN)84,84,86
   84 DELMIN=DELI
      I1=IX
      I2=JX
   86 CONTINUE
   81 CONTINUE
   85 CONTINUE
      IBB(I,1)=I1
      IBB(I,2)=I2
  803 CONTINUE
      FC(I)=ABS(W(I1)-W(I2))
      SIGN(I)=(W(I1)-W(I2))/FC(I)
      ERR(I)=0.
      DO 814 IX=1,6
      DO 814 JX=1,6
      ERR(I)=ERR(I)+BO*DELH(I)*(B(1,L)*CSTH*SZ(IX,JX)+B(2,L)
     1 *SNTH*SX(IX,JX))*(ZR(JX,I1)*ZR(IX,I1)-ZR(JX,I2)*ZR(IX,I2))
  814 CONTINUE
      IF (ERR(I).EQ.(0.)) WRITE(6,895) ERR(I)
  895 FORMAT(5X,F12.4)
      GO TO 17
   21 CONTINUE
      FC(I)=HN(NUMBER)
      SIGN(I)=1.
      ERR(I) =1.
   17 CONTINUE
```

```
      IF(LX-1)110,110,120
  120 CONTINUE
      DO 235 IZ=1,12
      D1(IZ) = 0.0
      DO 235 JZ=1,12
  235 D2(IZ,JZ) =0.0
      IF (Z(I)) 418,217,418
  418 CONTINUE
      DO 237 KX=1,7
      DO 236 IY=1,6
      DO 236 JY=1,6
      IX=IY
      JX=JY
      GO TO (705,706,707,714,708,709,715),KX
  705 CC(IX,JX)=SZ(IY,JY)
      ALPHA=BO*Z(I)*CSTH
      GO TO 720
  706 CC(IX,JX)=[illegible](IY,JY)
      ALPHA=BO*Z(I)*SNTH
      GO TO 720
  707 CC(IX,JX)=S20(IY,JY)
      ALPHA=1.
      GO TO 720
  708 CC(IX,JX)=S40(IY,JY)
      ALPHA=1.
      GO TO 720
  709 CC(IX,JX)=S42(IY,JY)
      ALPHA=1.
      GO TO 720
  714 CC(IX,JX)=S22(IX,JX)
      ALPHA=1.
      GO TO 720
  715 CC(IX,JX)=S44(IX,JX)
      ALPHA=1.
  720 CONTINUE
      SR(JX,IX)=(ZR(JX,I1)*ZR(IX,I1)-ZR(JX,I2)*ZR(IX,I2))*
     1 SIGN(I)
      KX1=KX
C     FOLLOWING LINE CHANGES TO GXX=GZZ (ISOTROPIC G)
C      IF(KX.EQ.2) KX1=1
  236 DOLD(KX1)=DOLD(KX1)+CC(IX,JX)*SR(JX,IX)*ALPHA
C      FOLLOWING LINE CHANGES GXX INDEP. TO GXX=GZZ
C      DOLD(2)=0.
  237 CONTINUE
C      REDEFINE DOLD OF MGSIF6 FOR ANTIPYRENE PROBLEM.
      D1(1)=DOLD(1)
      D1(2)=DOLD(2)
      D1(3)=DOLD(3)
      D1(4)=DOLD(6)
      D1(5)=DOLD(4)
      D1(6)=DOLD(7)
      D1(7)=DOLD(5)
  217 CONTINUE
  110 CONTINUE
```

```
      RETURN
      END
      SUBROUTINE EXAM(A,B,M,LF)
C     SUBROUTINE EXAM
C       F O R T R A N  4
      DIMENSION A(12,12),B(12),C(12)
      DO 80 J=1,M
   80 C(J)=A(J,J)
      IF(A(1,1)) 60,200,70
   60 A(1,1) =-SQRT(-A(1,1))
      GO TO 300
   70 A(1,1) =SQRT(A(1,1))
      GO TO 100
  100 IF(M-1)400,400,110
  110 DO 115 K=2,M
  115 A(1,K)=A(1,K)/(A(1,1)          )
      DO 120 J=2,M
      J1=J-1
      S=A(J,J)
      DO 125 L=1,J1
  125 S=S-A(L,J)**2
      IF (  ) 50,200,40
   50 A(J,J) =-SQRT(-  )
      GO TO 300
   40 A(J,J) =SQRT(  )
      GO TO 130
  130 IF(J-M)135,400,400
  135 J2=J+1
      DO 120 K=J2,M
      S=A(J,K)
      DO 145 L=1,J1
  145 S=S-A(L,J)*A(L,K)
  120 A(J,K)=S/A(J,J)
  400 B(1)=B(1)/A(1,1)
      IF(M-1)420,420,405
  405 DO 410 J=2,M
      S=B(J)
      J1=J-1
      DO 415 L=1,J1
  415 S=S-A(L,J)*B(L)
  410 B(J)=S/A(J,J)
  420 B(M)=B(M)/A(M,M)
      J=M-1
  435 IF(J)450,450,425
  425 S=B(J)
      J2=J+1
      DO 430 L=J2,M
  430 S=  -A(J,L)*B(L)
      B(J)=S/A(J,J)
      J=J-1
      GO TO 435
  450 LF=1
      GO TO 460
  200 LF=0
```

```
      GO TO 460
  300 LF=-1
  460 DO 465 J=1,M
      A(J,J)=C(J)
      IF(J-M)470,475,475
  470 J2=J+1
      DO 465 K=J2,M
  465 A(J,K)=A(K,J)
  475 RETURN
      END

      SUBROUTINE MATINV(A,N,B,M,DETERM)
C     SUBROUTINE MATINV
C       F O R T R A N  4
C     MATRIX INVERSION WITH ACCOMPANYING SOLUTION OF LINEAR EQUATIONS
      DIMENSION IPIVOT(12),A(12,12),B(12,1),INDEX(12,2),PIVOT(12)
      EQUIVALENCE (IROW,JROW),(ICOLUM,JCOLUM),(AMAX,T,SWAP)
      DETERM=1.0
      DO 20 J=1,N
   20 IPIVOT(J)=0
      DO 550 I=1,N
      AMAX=0.0
      DO 105 J=1,N
      IF(IPIVOT(J)-1)60,105,60
   60 DO 100 K=1,N
      IF(IPIVOT(K)-1)80,100,740
   80 IF(ABS(AMAX)-ABS(A(J,K)))85,100,100
   85 IROW=J
      ICOLUM=K
      AMAX=A(J,K)
  100 CONTINUE
  105 CONTINUE
      IPIVOT(ICOLUM)=IPIVOT(ICOLUM)+1
      IF (IROW-ICOLUM)140,260,140
  140 DETERM=-DETERM
      DO 200 L=1,N
      SWAP=A(IROW,L)
      A(IROW,L)=A(ICOLUM,L)
  200 A(ICOLUM,L)=SWAP
      IF(M)260,260,210
  210 DO 250 L=1,M
      SWAP=B(IROW,L)
      B(IROW,L)=B(ICOLUM,L)
  250 B(ICOLUM,L)=SWAP
  260 INDEX(I,1)=IROW
      INDEX(I,2)=ICOLUM
      PIVOT(I)=A(ICOLUM,ICOLUM)
      DETERM=DETERM*PIVOT(I)
      A(ICOLUM,ICOLUM)=1.0
      DO 350 L=1,N
  350 A(ICOLUM,L)=A(ICOLUM,L)/PIVOT(I)
      IF(M)380,380,3
  360 DO 370 L=1,M
  370 B(ICOLUM,L)=B(ICOLUM,L)/PIVOT(I)
```

```
380 DO 550 L1=1,N
    IF (L1-ICOLUM) 400,550,400
400 T=A(L1,ICOLUM)
    A(L1,ICOLUM)=0.0
    DO 450 L=1,N
450 A(L1,L)=A(L1,L)-A(ICOLUM,L)*T
    IF(M)550,550,460
460 DO 500 L=1,N
500 B(L1,L)=B(L1,L)-B(ICOLUM,L)*T
550 CONTINUE
    DO 710 I=1,N
    L=N+1-I
    IF(INDEX(L,1)-INDEX(L,2))630,710,630
630 JROW=INDEX(L,1)
    JCOLUM=INDEX(L,2)
    DO 705 K=1,N
    SWAP=A(K,JROW)
    A(K,JROW)=A(K,JCOLUM)
    A(K,JCOLUM)=SWAP
705 CONTINUE
710 CONTINUE
740 RETURN
    END

    SUBROUTINE EQZERO(A,B,N,IC1,IC2,IC3)
    DIMENSION A(12,12),B(12)
    IC1=0
    IC2=0
    IC3=0
    DO 5 J3=1,N
    IF((ABS(B(J3))).GT.(1.E-20)) GO TO 10
    B(J3)=0.
    IC1=J3
    WRITE(6,100) IC1
 10 CONTINUE
    DO 5 J4=1,N
    IF((ABS(A(J3,J4))).GT.(1.E-10)) GO TO 15
    A(J3,J4)=0.
    IC2=J3
    IC3=J4
    WRITE(6,101) IC2,IC3
 15 CONTINUE
  5 CONTINUE
100 FORMAT(5X, I3)
101 FORMAT(5X,2I3)
    RETURN
    END
```

```
      PROGRAM TETFLOD(INPUT,OUTPUT=121B,TAPE5=INPUT,TAPE6=OUTPUT)
C
C     THIS PROGRAM ANALYSES GD3+  EPR DATA IN RARE-EARTH YTIRIUM TET
C     RAFLOUR
C     THIS PROGRAM FITS DATA TO AN ANISOTROPIC G VALUE AND ONLY
C     TO B2M,B4M AND B6M PARAMETERS
C     B=GPARALLEL,GPERP,B20,B40,B,B06,B64 (7 PARAMETERS)
C
C     NO =THE NO. OF FIRST MAG FIELD IN DATA INCLUDED IN FITTING
C     M  =NO. OF PARAMETERS
C     L4 =NO. OF ITERATIONS ALLOWED
C     Q1 =MIN. VALUE OF SUM OF SQUARES FOR FITS( CHI-SQUARE TOLERANCE)
C     Z(I)=MAGNETIC FIELD VALUES FOR FITS
C     B  =PARAMETER MATRIX
C     N  =NO. OF  DATA POINTS USED IN LEAST-SQARES FITTING
C     Q1 =N/10
C     Q2 =TOLERANCE ON GRAD(CHI**2) =APPROX .01
C     FM(I) = MEASURED VALUES
C     FC(I) = CALCULATED VALUES
C     ERR(I)= STANDARD DEVIATION ON FM(I) = SQRT(FM(I))
C
C      DIMENSIONS OF A,B IN EXAM AND MATINV SUBROUTINES SHOULD BE THE
C     SAME AS THOSE OF B2,B1 RESPECTIVELY IN THE MAIN PROOGRAM AND IN
C     CURFIT
C
C     DIMENSIONS OF Q,V IN JACOBI1 SHOULD BE THE SAME AS THOSE OF
C     B3,B2 RESPECTIVELY IN CURFIT
C
C     NUMBER=INDEX THAT CHANGES WITH EACH NEW CASE
C     NCASES=NO. OF CASES CONSIDERED. ITS VALUE SHOULD BE ENTERED.
C
C     NN(J)=NO. OF LINES IN ZX PLANE FOR JTH CASE
C     NM(J)=NO. OF LINES IN XY PLANE FOR JTH CASE
C
C
C     CASE 1 = GD3+/LIYF4 (R.T.,ZX-XY)
C     CASE 2 = GD3+/LIYF4 (LNT,ZX-XY)
C     CASE 3 = GD3+/LIYF4 (LHT,ZX-XY)
C     CASE 4 = GD3+/LIYBF4 (RT.,ZX-XY)
C
      DIMENSION Z(400),FM(400),FC(400),DF(400),ERR(400),B(17),B1(17),
     1B2(17,17),DC(4500),ABC(2),Y(4),THETA(400),HN(400),ZZ(400,10),
     2HHDPPH(400,10),NN(25),      GG(17,10),SMD(10),IBB(400,2),
     3SSMD(400),TEETA(400,10),G(17,10),DELHH(2,10),DELH(2)
      DIMENSION ADD(2,10),FREQ(2,10),FACTR(400,6),NM(25)
      COMMON/DATA1/ABC,Y
      COMMON/DATA2/DC
      COMMON/DATA3/NN,NM,MM9,DELH
      EQUIVALENCE(Z,DC),(FM,DC(801)),(DF,DC(401)),(FC,DC(1201)),
     1(ERR,DC(1601)),(THETA,DC(2001)),(HN,DC(2401)),(B,DC(4040)),
     2(B2,DC(4100)),(N,DC(3675)),(L4,DC(3676)),(Q1,DC(3677)),
     3(Q2,DC(3678)),(M,DC(3679)),(I,DC(3680)),(L,DC(3681)),
     4 (B1,DC(4074)),(IBB,DC(2801)),(SMD,DC(3683)),
     5(NUMBER,DC(3682))
```

```
      DATA(ADC=2HNO,3HYES),(Y=1H ,1HC,1H*,1HA)
C     FOLLOWING ARE INITIAL PARAMETERS FOR 7 PARAMETER HAMILTONIAN
      DATA(G(J,1),J=1,7)/
C     1 2*1.0,6.0,4*0./
     1 2*1.983,2.48,.066,-.14,.007,-.033/
C     1 1.93,1.96,2.44,.064,-.01,.014,-.11/
      DATA(G(J,2),J=1,7)/
C     1 2*2.,.69,-.08,0.,.02,.07,.12,.05,0.,0.,.04,-.01,-.01,
C     2 -.1,.01,-.01/
     1 2*1.983,2.5,.066,-.14,.007,-.033/
      DATA(G(J,3),J=1,7)/
C     1 2*1.98,.71,0.,0.,.02,.06,.12,.02,-.01,0.,.03,-.02,.02,
C     2 -.09,-.01,.02/
     1 2*1.983,2.5,.066,-.14,.007,-.033/
      DATA(G(J,4),J=1,7)/
     1 2*1.983,2.5,.066,-.14,.007,-.033/
C     BELOW FOR GD3+ IN LIYF4 AT R.T. IN Z - X PLANE
      DATA(ZZ(J,1),J=1,135)/
     1 19.5,55.5,78.,85.5,107.,132.5,160.,219.5,305.,
     2 19.5,55.5,79.,86.5,108.,164.,224.,295.5,
     3 19.5,58.,79.,88.5,110.5,166.5,225.,285.,
     4 20.,62.,87.5,86.5,113.,143.,173.5,223.,224.5,
     5 20.5,66.,83.,111.,157.,158.,179.,216.,20.,73.,109.,148.,
     6 179.,192.5,138.5,21.5,82.,102.5,148.5,
     7 176.5,162.5,123.5,24.,85.,89.,150.,140.,111.,
     8 27.,86.5,78.5,148.,115.,102.5,85.5,71.,147.,147.,
     9 104.,96.5,66.5,145.,131.,97.,89.,
     1 63.5,144.,113.5,91.5,84.5,58.5,142.,100.,85.5,
     2 79.5,55.,139.,95.,80.,75.5,54.,133.,93.,78.,73.5,
     3 38.,53.,72.5,76.5,91.5,126.,157.5,155.,
     4 27.,52.,71.5,75.,89.,113.,164.,
     5 17.5,50.5,70.,73.5,85.5,111.,162.5,
     6 14.,50.5,69.5,73.5,84.5,114.5,153.,
     7 12.5,50.,69.5,73.,84.,114.,148./
      DATA(TEETA(J,1),J=1,135)/
     1 9*0.,8*5.,8*7.5,9*12.5,8*17.5,7*22.5,7*27.5,6*32.5,
     2 6*37.5,6*42.5,5*47.5,5*52.5,5*57.5,5*62.5,5*67.5,
     3 8*72.5,7*77.5,7*82.5,7*87.5,7*90./
C     BELOW FOR GD3+  IN LIYF4 AT R.T. IN X - Y PLANE
      DATA(ZZ(J,1),J=136,248)/
     1 4.5,16.5,53.5,60.5,73.5,89.5,115.,143.5,203.,
     2 5.,17.,53.5,60.5,73.5,89.5,115.,144.,202.,
     3 5.,20.5,53.5,61.5,74.,89.5,113.5,156.,
     4 6.5,27.,53.5,63.,74.5,90.5,112.5,160.,
     5 9.,54.,65.5,75.5,92.5,106.5,118.,
     6 11.5,55.,68.5,78.,94.5,101.,131.,
     7 16.,57.,72.,81.5,97.5,139.,27.,58.5,75.5,85.,
     8 100.,141.,62.,81.,90.,140.5,65.5,87.,96.,127.5,
     9 70.5,94.,103.,121.5,139.,24.5,57.5,85.,149.,
     1 23.,56.,84.,149.,22.5,56.,81.,147.,
     2 20.5,56.,77.5,142.5,19.5,56.,
     3 72.5,110.5,138.,19.,56.,69.,110.5,
     4 134.,142.,19.,56.,67.5,110.5,132.,
     5 141.5,19.,56.,68.,78.,110.5,132.5,142./
```

```
      DATA(TEETA(J,1),J=136,248)/
     1 9*-360.,9*-2.5,8*-7.5,8*-12.5,7*-17.5,7*-22.5,
     2 6*-27.5,6*-32.5,4*-37.5,4*-42.5,5*-47.5,4*-57.5,4*-62.5,
     3 4*-67.5,4*-72.5,5*-77.5,6*-82.5,6*-87.5,7*-90./
      DATA(ZZ(J,2),J=1,61)/
     1 430.91,1779.45,2632.97,3324.5,4965.98,6731.73,9343.46,
     2 430.91,1759.51,2545.22,3385.46,5118.25,6868.19,8979.51,
     3 430.91,1749.15,2343.44,3461.52,5361.85,6868.93,
     4 430.91,1749.15,2305.34,3461.52,5544.55,6640.7,
     5 430.91,1749.1,2300.0,3400.62,5559.77,
     6 482.6,1667.0,2342.68,2959.01,4869.77,
     7 482.6,1636.98,2296.96,2867.66,3503.30,5143.82,
     8 482.6,1621.58,2281.35,2791.53,3533.76,5235.32,
     9 482.6,1604.5,2265.85,2665.8,3585.71,4946.51,
     1 482.6,1596.12,2250.51,2652.5,3616.74,4489.34,6764.57/
C     1 7.,54.5,89.,107.5,162.,223.5,301.,7.,54.5,79.,
C     2 109.,166.,228.5,291.,7.,54.,74.5,112.,174.,228.,
C     3 7.,54.,73.5,112.,180.,219.5,8.,54.5,72.5,110.,180.5,
C     4 9.,50.5,70.5,90.5,108.,153.,9.5,49.,68.5,87.5,108.,
C     5 162.,9.5,48.5,68.5,85.,109.,165.,9.5,48.,67.5,82.,
C     6 111.,156.,9.,48.,67.,81.5,112.5,142.5,215.5/
      DATA(TEETA(J,2),J=1,61)/
     1 7*0.,7*5.,6*10.,6*15.,5*20.,5*70.,6*75.,6*80.,
C     1 7*0.,7*90./
     2 6*85.,7*90./
      DATA(ZZ(J,3),J=1,14)/
C     1 0.,54.5,80.,108.5,163.,228.,304.5,0.,54.5,77.,
C     2 110.5,167.,232.,296.5,0.,53.5,74.,113.5,179.,
C     3 230.,0.,53.5,73.5,112.5,182.5,221.,0.,53.5,
C     4 75.5,110.,182.5,0.,53.,78.,177.,0.,52.5,81.,
C     5 14.,49.5,70.,89.5,107.5,11.5,47.5,68.,86.5,108.,
C     6 164.5,11.,47.5,67.5,84.5,109.,166.5,9.,47.,67.,
C     7 82.5,112.5,160.,8.,46.5,66.,81.,113.5,141.5,220./
     1 425.7,1775.2,2626.1,3318.9,4970.5,6738.7,9348.6,
     2 479.1,1591.8,2230.5,2685.7,3630.3,4481.4,6781.3/
      DATA(TEETA(J,3),J=1,14)/
C     1 7*0.,7*5.,6*10.,6*15.,5*20.,4*25.,3*30.,5*70.,
C     2 6*75.,6*80.,6*85.,7*90./
     1 7*0.,7*90./
      DATA(ZZ(J,4),J=1,11)/
     1 1763.5,2663.7,3318.8,4998.0,6662.7,8986.5,
     2 1569.7,2302.6,3459.8,4541.3,6606.9/
C     1 29.,56.,71.5,81.,111.,152.5,171.,234.,290.,30.,56.,
C     1 54.5,82.,111.,171.,234.,289.,55.,83.,111.,175.,232.5,279.5,
C     2 55.5,83.5,110.5,180.,224.5,55.5,110.,182.5,207.5,55.5,
C     3 109.,181.5,55.5,107.5,171.5,55.5,104.5,151.5,
C     2 69.,83.5,111.,148.,175.,232.5,270.5,30.,58.5,67.,
C     3 83.5,111.,137.,180.,225.,30.,67.,110.,183.,207.,30.,
C     4 72.,109.,182.,30.,78.5,108.,171.5,30.,81.,104.5,152.,
C     4 48.5,70.,159.5,47.,68.,106.,165.,45.,65.5,107.5,161.5,
C     5 45.,65.5,109.5,155.,213.,45.,65.5,111.,149.,218./
      DATA(TEETA(J,4),J=1,11)/
C     1 6*0.,6*5.,5*10.,4*15.,3*20.,3*25.,3*30.,
C     1 9*0.,9*5.,8*10.,5*15.,4*20.,4*25.,4*30.,
```

```
C      2 3*70.,4*75.,4*80.,5*85.,5*90./
      1 6*0.,5*90./
       DATA(ADD(I,1),I=1,2)/5.203,7.7092/
       DATA(ADD(I,2),I=1,2)/2*0./
       DATA(ADD(I,3),I=1,2)/2*0./
       DATA(ADD(I,4),I=1,2)/2*3.0/
       DATA(FREQ(I,1),I=1,2)/9.377,9.353/
       DATA(FREQ(I,2),I=1,2)/2*9.397/
       DATA(FREQ(I,3),I=1,2)/2*9.
       DATA(FRE
C       DATA(FACTR(I,1),I=1,2)/30.106,30.0513/
       DATA(FACTR(J,1),J=1,135)/
      1 2*29.6,3*29.7,4*29.75,2*29.6,3*29.7,3*29.75,
      2 2*29.6,3*29.7,3*29.75,2*29.6,3*29.7,4*29.75,
      3 2*29.6,2*29.7,4*29.75,29.6,2*29.7,4*29.75,29.6,
      4 2*29.7,4*29.75,29.6,2*29.7,2*29.75,29.7,29.6,2*29.7,
      5 29.75,2*29.7,29.7,29.6,2*29.75,2*29.7,29.6,2*29.7,
      6 2*29.6,29.6,29.75,3*29.7,29.6,29.75,3*29.7,29.6,29.75,
      7 3*29.1,29.1,29.15,3*29.1,3*29.1,2*29.1,3*29.15,3*29.1,
      8 3*29.1,29.15,3*29.1,3*29.1,29.15,3*29.1,2*29.1,29.15,
      9 4*29.1,2*29.1,29.15/
       DATA(FACTR(J,2),J=1,61)/
C      1 3*29.4,29.445,3*29.586,3*29.56132,
C      2 29.505,3*29.562,3*29.56132,29.505,2*29.562,3*29.56132,
C      3 29.505,2*29.562,3*29.56132,29.505,29.562,4*29.56132,
C      4 29.805,29.762,4*29.76132,29.805,29.762,4*29.76132,
C      5 29.805,29.8052,4*29.805132,29.805,29.8052,4*29.805132,
C      6 29.805,2*29.8052/
      1 61*1.0/
       DATA(FACTR(J,3),J=1,14)/14*1.0/
       DATA(FACTR(J,4),J=1,11)/11*1.0/
C       IF(ZZ(IJK,NUMBER).GT.(70.).AND.LT.(120.))
C      1(FACTR(I,1),I=1,2)/29.7,30.05/
C       IF(ZZ(IJK,NUMBER).GT.(120.))(FACTR(I,1),I=1,2)/29.75/,30.05
       DATA(NN(J),J=1,4)/
      1135,61,14,11/
       DATA(NM(J),J=1,4)/
      10,0,0,0/
       DATA(DELHH(I,1),I=1,2)/35.0,40.0/
       DATA(DELHH(I,2),I=1,2)/40.0,40.0/
       DATA(DELHH(I,3),I=1,2)/40.0,40.0/
       DATA(DELHH(I,4),I=1,2)/40.0,40.0/
  188 FORMAT(1H1)
    8 FORMAT(1X,4HQ1 = ,E13.5,5X,4HQ2 = ,E13.5)
  137 FORMAT (3X,I2,5X,E16.6/)
  136 FORMAT(10X,19H INITIAL PARAMETERS//3X,1HJ,10X,4HB(J)//)
  135 FORMAT(1X,11H PARAMETERS//3X,1HJ,10X,4HB(J),27X,6HERRORS//)
    9 FORMAT(2X,*HH=*,10(F9.4,4X))
  140 FORMAT(3X,I2,5X,E16.6,15X,E16.6/)
  138 FORMAT(5X,14H CASE NUMBER =,I2//)
  141 FORMAT(10X,6H SMD =,E13.5//)
  235 FORMAT (15X,5(E13.5,8X)/)
       NUMBER=4
       NCASES=4
```

```
      NUMBII=NUMBER
      MM9=7
      M=MM9
      MM=M
      L4=5
      Q1 =1.E-8
      Q2 =1.E-40
      WRITE (6,188)
    1 CONTINUE
      N=NN(NUMBER) + MM(NUMBER)
      DO 210 LL=1,7
  210 B(LL)=0.
      DO 211 LL=1,MM9
  211 B(LL)=G(LL,NUMBER)
      WRITE (6,138) NUMBER
      WRITE (6,136)
      WRITE (6,137) (J,B(J),J=1,M)
      N1=N
      DO 3 IJK = 1,N1
      IND=1
      IF(IJK.GT.NN(NUMBER))IND=2
      HN(IJK) = FREQ(IND,NUMBER)
      THETA(IJK) = TEETA(IJK,NUMBER)
      Z(IJK) = (ZZ(IJK,NUMBER) + ADD(IND,NUMBER))*FACTR(IJK,NUMBER)
      THI=THETA(IJK)
      DELH(IJK)=DELHH(IND,NUMBER)
      IF(THI.GT.(5.).AND.THI.LT.(85.))Z(IJK)=0.
C      IF(THI.GT.(17.5))Z(IJK)=0.
    3 CONTINUE
      IF(NUMBER.NE.1) GO TO 100
      Z(39)=Z(40)=Z(42)=Z(100)=Z(114)=Z(120)=0.
      Z(18)=Z(26)=Z(46)=Z(50)=Z(55)=Z(56)=Z(106)=Z(107)=0.
  100 CONTINUE
      IF(NUMBER.NE.2) GO TO 101
      Z(27)=0.
  101 CONTINUE
      IF(NUMBER.NE.3) GO TO 102
      Z(43)=Z(44)=Z(50)=Z(23)=Z(17)=0.
  102 CONTINUE
C      IF(NUMBER.NE.4) GO TO 103
C  103 CONTINUE

      WRITE(6,8)Q1,Q2
      WRITE(6,9) (HN(J),J=1,N1)
C      WRITE(6,726) (Z(J),J=1,N1)
      WRITE(6,144)
  144 FORMAT(5X,*LINE NUMBER*,5X,*LINE POSITION*,7X,*ANGLE*,/)
      DO 146 IJK=1,N1
  146 WRITE(6,726) IJK,Z(IJK),THETA(IJK)
  726 FORMAT(6X,I3,9X,F10.1,11X,F8.2)
C  726 FORMAT(2X,*Z=*,10(F7.1,2X))
      DO 201 J = 1,N1
C      ERR(J)=1.
  201 FM(J)=HN(J)
```

```
      CALL CURFIT
      WRITE(6,188)
      WRITE(6,135)
      DO 220 LL=1,M
  220 GG(LL,NUMBER) = B(LL)
      WRITE(6,140)(J,B(J),B1(J),J=1,M)
      DO 300 II=1,N
  300 WRITE(6,301) II,IBB(II,1),IBB(II,2)
      SSS=0.
      SMD1=0.
      DO 555 ID=1,N
      SSS=DF(ID)**2
      SMD1=SMD1+SSS
      WRITE(6,656) ID,SSS
  555 CONTINUE
      WRITE(6,657)NUMBER,SMD1
  657 FORMAT(10X,*CASE NO.=*,I3,*SMD1=*,E13.5)
  656 FORMAT(10X,*LINE NUMBER = *,I3,5X,*SMD = *,E13.5)
  301 FORMAT(10X,*LINE NO. = *,I3,5X,*EIGENVALUE1 =*,I3,5X,
     1* EIGENVALUE 2 =*,I3)
      WRITE(6,188)
      NUMBER = NUMBER + 1
      IF ( NUMBER - NCASES) 1,1,2
    2 CONTINUE
      DO 230 LL=NUMBII,NCASES
      WRITE (6,138) LL
      WRITE (6,141) SMD(LL)
  230 WRITE (6,235) (GG(LM,LL),LM=1,M)
      STOP
      END
      SUBROUTINE CURFIT
C
C     EXAM  HANDLES ALL MATRICES OF DIMENSIONS UPTO THE DIMS.I.N. OF
C A,B,C THAT IS M IS LESS THAN OR EQUAL TO MM (SAME IS TRUE OF MATINV
C AND  JACOBI)
C
C
C     F O R T R A N  4
      DIMENSION Z(400),FM(400),FC(400),DF(400),ERR(400),B(17),B1(17),
     2 DC(4500),ABC(2),Y(4),X(400),GRAD(17),D1(17),D2(17,17),
     3 AD(10),B3(17,17),B2(17,17)
      DIMENSION AI(17,17),W(17),ZR(17,17),ZI(17,17),FV1(17),
     2FM1(2,17)
      COMMON/DATA1/ABC,Y
      COMMON/DATA2/DC
      EQUIVALENCE (Z,DC),(FM,DC(801)),(DF,DC(401)),(FC,DC(1201)),
     1(ERR,DC(1601)),(B,DC(4040)),(GRAD,DC(4057)),(B2,DC(4100)),
     2(N,DC(3675)),(L4,DC(3676)),(Q1,DC(3677)),(Q2,DC(3678)),
     3(M,DC(3679)),(I,DC(3680)),(L,DC(3681)),(D1,DC(3700)),
     4(D2,DC(3720))   ,(SMD,DC(3683)),(NUMBER,DC(3682))
      EQUIVALENCE(B1,DC(4074)),(NZ,DC(3694))
      DATA(ABC=2HNO,3HYES),(Y=1H ,1HC,1H*,1HM)
      L1 = 0
      SA = 0.0
```

```
      MM = N
      DO 1000 J =1,MM
      B1(J)=0.0
      DO 1000 K = 1,MM
 1000 B2(J,K)=0.0
      WRITE(6,901)
      NN = N
      DO 100 I8 = 1,NN
C      X(I8) = ERR(I8)**2
      L=1
      I=I8
      CALL FUNC(2)
      X(I8)=ERR(I8)**2
  901 FORMAT(5X,10H FUNC2,210  )
      DF(I8) =FM(I8) - FC(I8)
C      IF(I8.LT.5) WRITE (6,22222)(D1(J),J=1,7)
C22222 FORMAT(5X,7E14.6)
C      IF(I8.LT.5) WRITE(6,11111)DF(I8)
C11111 FORMAT (6X,7E13.5)
      DO 101 J=1,MM
      B1(J)=B1(J)-(2.0*DF(I8)*D1(J))/X(I8)
      DO 101 K=1,MM
  101 B2(J,K)=B2(J,K)-(2.0*(DF(I8)*D2(J,K)-D1(J)*D1(K)))/X(I8)
  100 SA = SA + DF(I8)**2/X(I8)
      WRITE(6,901)
      GMOD=0.0
      DO 102 J=1,MM
  102 GMOD=GMOD+B1(J)**2
      WRITE(6,243)SA,GMOD
  243 FORMAT (1X,26H*INITIAL VALUE SUM OF SQ.=E13.5,20X,17H*SQ MOD OF
     GRADIENT =E13.5)
      WRITE(6,1751)
 1751 FORMAT(14H0 DERIVATIVES-)
      WRITE(6,240)(B1(J),J=1,MM)
  240 FORMAT (15X,5(E13.5,8X)/)
      IF (SA - C1) 110, 110, 200
  110 LL = 1
      GO TO 600
  200 S = 0.0
      GMOD = 0.0
      BMOD = 0.0
      PROD = 0.0
      A2=ABC(1)
      DO 210 J =1,MM
      B1(J) = 0.0
      DO 210 K=1,MM
  210 B2(J,K) = 0.0
      WRITE(6,902)
      DO 220 I8=1,NN
      L=1
      I=I8
      CALL FUNC(2)
      X(I8)=ERR(I8)**2
  902 FORMAT(5X,10H FUNC2,210  )
```

```
      DF(I8) = FM(I8) - FC(I8)
      DO 220 J=1,MM
      B1(J) = B1(J) - (2.0*DF(I8)*D1(J))/X(I8)
      DO 220 K =1,MM
  220 B2(J,K) = B2(J,K) - (2.0*(DF(I8)*D2(J,K) -D1(J)*D1(K)))/X(I8)
      WRITE(6,902)
      DO 230 J=1,MM
  230 GRAD(J) = B1(J)
      L1 = L1 + 1
      WRITE(6,903)
      CALL EXAM (B2,B1,MM,LF)
      WRITE(6,903)
  903 FORMAT(5X,9H LXAM,230  )
      IF (LF)  250, 250, 305
  250 DO 231 II=1,MM
      DO 231 JJ=1,MM
      AI(II,JJ)=0.
  231 B3(II,JJ)=B2(II,JJ)
      WRITE(6,904)
      CALL ETRIDI(MM,MM,B3,AI,W,FV1,FV1,FM1)
      DO 1001 IR=1,MM
      DO 5000 JR=1,MM
      ZR(IR,JR)=0.
 5000 CONTINUE
      ZR(IR,IR)=1.
 1001 CONTINUE
      CALL TQL2(MM,MM,W,FV1,ZR,IERR)
      CALL HTRIBK(MM,MM,B3,AI,FM1,MM,ZR,ZI)
      DO 5005 IR=1,MM
      B3(IR,IR)=W(IR)
      DO 5005 JR=1,MM
 5005 B2(IR,JR)=ZR(JR,JR)
      WRITE(6,904)
  904 FORMAT(5X,12H JACOBI1,231  )
      DO 235 K =1,MM
  235 B1(K)=B3(K,K)
      A2=ABC(2)
      DO 260 J=1,MM
  260 D1(J) = 0.0
      DO 270 J=1,MM
      DO 270 K=1,MM
  270 D1(K) = D1(K) + B2(J,K) *GRAD(J)
      DO 275 J = 1, MM
      IF (B1(J))  280, 290, 285
  280 B1(J) = - B1(J)
  285 D1(J) = D1(J)/B1(J)
      GO TO 275
  290 D1(J) = 0.0
  275 CONTINUE
      DO 295 J=1,MM
  295 B1(J) = 0.0
      DO 300 J=1,MM
      DO 300 K=1,MM
  300 B1(J) = B1(J) + B2(J,K)*D1(K)
```

```
  305 DO 310 J=1,MM
      GMOD = GMOD + GRAD(J)**2
      BMOD = BMOD + B1(J)**2
  310 PROD = PROD + GRAD(J)*B1(J)
      IF (GMOD - Q2)  315, 315, 320
  315 LE = 2
      WRITE(6,1761) GMOD
 1761 FORMAT(5X,7H GMOD =,E13.5//)
      GO TO 600
  320 C=PROD/SQRT(BMOD*GMOD)
      IF (C) 335, 335, 400
  335 LE = 4
      GO TO 600
  400 LD = 0
      L3 = 0
      DO 410 J=1,MM
  410 GRAD(J) = B(J) - B1(J)
      WRITE(6,905)
  450 DO 420 I8=1,NN
      L=2
      I=I8
      CALL FUNC (1)
      X(I8)=ERR(I8)**2
  905 FORMAT(5X,10H FUNC1,450  )
      DF(I8) = FM(I8) - FC(I8)
  420 S = S + DF(I8)**2/X(I8)
      WRITE(6,905)
      IF (SA - S) 435, 500, 500
  435 LD = LD + 1
      WRITE(6,906)
  430 DO 440 J=1,MM
      B1(J) = B1(J)/2.0
  906 FORMAT(5X,16H BINARY CHOP,430  )
  440 GRAD(J) = B(J) - B1(J)
      WRITE(6,906)
      S = 0.0
      L3 = L3 + 1
      IF (L3-4  )450,460,460
  460 LE = 5
      GO TO 600
  500 IF (LD) 505, 505, 506
  506 LD = 0
      GO TO 430
  505 DO 510 J=1,MM
  510 B(J) = GRAD(J)
      SA = S
      IF (SA - Q1) 507, 507, 530
  507 LE = 1
      GO TO 600
  530 IF (L4) 200, 200, 900
  900 WRITE(6,920)L1,A2,L3, ,GMOD,(B(J),J=1,MM)
  920 FORMAT(//,15H ITERATION NO.=15,10X,43H    TRANSFORMATION MADE
     1TOPRINCIPAL AXES = A4,10X,   18H BINARY CHOP USED=I3,6H TIMES/1X,
     2HWEIGHTED SUM OF SQUARES = E14.7,25X,32H   SQUARE MODULUS OF GR
```

```
      1 FORMAT(8E14.7/20H  PARAMETERS B(J) -/(6E17.8)/)
        IF (L1 - L4) 200, 910, 910
  910 LE = 6
        GO TO 600
  600 DO 710 J=1,MM
        B1(J) = 0.0
        DO 710 K=1,MM
  710 B2(J,K) = 0.0
        L=1
        DO 720 I8=1,NN
        I=I8
        CALL FUNC(2)
        X(I8)=ERR(I8)**2
        DF(I8) = FT(I8) - FC(I8)
        DO 720 J=1,MM
        B1(J) = B1(J) - (2.0*DF(I8)*D1(J))/X(I8)
        DO 720 K=1,MM
  720 B2(J,K) = B2(J,K) - (2.0*(DF(I8)*D2(J,K) -D1(J)*D1(K)))/X(I8)
        CALL MATINV(B2,MM,B1,1,DETERM)
        DO 730 J=1,MM
        IF (B2(J,J)) 2001,2001,2002
 2001 B1(J) = -SQRT(-B2(J,J))
        GO TO 730
 2002 B1(J) = SQRT(B2(J,J))
  730 CONTINUE
        DO 740 J=1,MM
        DO 740 K=1,MM
  740 B2(J,K)=B2(J,K)/(B1(J)*B1(K))
        WRITE(6,551)LE,SA
  551 FORMAT(//,13H EXIT NUMBER=I3,20X,25H WEIGHTED SUM OF SQUARES=
     1E15.81//)
        SMD(NUMBER)=SA
        RETURN
        END
        SUBROUTINE FUNC(LX)
C       SUBROUTINE FUNC
        DIMENSION DC(4500),B(1[illegible],2),D1(17),FC(400),Z(400),HN(400),A(8,8),
       1R(8,8),SIGN(400),THETA(400),IBB(400,2),SP(8,12),D2(17,17),
       2ERR(400),AZ(8,8) ,SX(8,8)
        DIMENSION AR(8,8),AI(8,8),W(8),ZR(8,8),ZI(8,8),FV1(3),FM1(2,8)
        DIMENSION NR(25),NM(25),DELH(400)
        COMMON/DATA2/DC
        COMMON/DATA3/NN,MM,MM9,DELH
        EQUIVALENCE (Z,DC),(FC,DC(1201)),(THETA,DC(2001)),(B,DC(4040)),
       1(D1,DC(3700)),(D2,DC(3720)),(M,DC(3679)),(I,DC(3680)),
       2(L,DC(3681)),(HN,DC(2401)),(IBB,DC(2801)),(N,DC(3675))
       3,(NZ,DC(3694)),(NUMBER ,DC(3682)),(ERR,DC(1601))
        DATA(SP(J,1),J=1,8)/3.5,2.5,1.5,.5,-.5,-1.5,-2.5,-3.5/
        DATA(SP(J,3),J=1,8)/7.,1.,-3.,-5.,-5.,-3.,1.,7./
        DATA(SP(J,5),J=1,8)/7.,-13.,-3.,9.,9.,-3.,-13.,7./
        DATA(SP(J,8),J=1,8)/1.,-5.,9.,-5.,-5.,9.,-5.,1./
        FACTOR=92.732/66252.
        RD=3.14159264/180.
        R2=SQRT(2.0)
```

```
      R3=SQRT(3.0)
      R5=SQRT(5.0)
      R7=SQRT(7.0)
      SP(1,4)=R7/R3
      SP(2,4)=R5
      SP(3,4)=2.*R5/R3
      SP(4,4)=2.*R5/R3
      SP(5,4)=R5
      SP(6,4)=R7/R3
      SP(1,6)=R7*R3/2.
      SP(2,6)=1./(2.*R5)
      SP(3,6)=-2.*R3/R5
      SP(4,6)=-2.*R3/R5
      SP(5,6)=1./(2.*R5)
      SP(6,6)=R7*R3/2.
      SP(1,9)=2./(R7*R3)
      SP(2,9)=-2./R5
      SP(3,9)=2./(R3*R5)
      SP(4,9)=2./(R3*R5)
      SP(5,9)=-2./R5
      SP(6,9)=2./(R7*R3)
      SP(1,7)=R7/R5
      SP(2,7)=R3
      SP(3,7)=R3
      SP(4,7)=R7/R5
      SP(1,10)=R5/R7
      SP(2,10)=-1./R3
      SP(3,10)=-1./R3
      SP(4,10)=R5/R7
      SP(1,11)=2./R7
      SP(2,11)=2./R7
      SP(1,2)=R7/2.
      SP(2,2)=R3
      SP(3,2)=R3*R5/2.
      SP(4,2)=2.
      SP(5,2)=R3*R5/2.
      SP(6,2)=R3
      SP(7,2)=R7/2.
      DO 100 IX=1,8
      DO 100 JX=1,8
      AI(IX,JX)=0.
      SZ(IX,JX)=0.0
      SX(IX,JX)=0.0
      S(IX,JX) = 0.0
  100 R(IX,JX) = 0.0
      DO 505 IX=1,8
  505 SZ(IX,IX)=SP(IX,1)
      DO 506 IX=1,7
      IX1=IX+1
      SX(IX,IX1)=SP(IX,2)
      SX(IX1,IX)=SP(IX,2)
  506 CONTINUE
      IF(A(I).EQ.(0.)) GO TO 420
      IF(I.GT.NN(NUMBER)) GO TO 97
```

```
      TH=THETA(I)*3.14159264/180.
      ACOSTH=COS(TH)
      ASINTH=SIN(TH)
      PBB=B(1,L)*Z(I)*ACOSTH
      PBB = PBB*92.732/66252.
      PAA = B(2,L)*Z(I)*ASINTH
      PAA = PAA*92.732/66252.
      PAD=Z(I)*ASINTH
      PBD=Z(I)*ACOSTH
      PCC=0.
      PCD=0.
      GO TO 98
   97 CONTINUE
      TH=-THETA(I)*RD
      ACOSTH=COS(TH)
      ASINTH=SIN(TH)
      PBB=0.
      PBD=0.
      PAA=B(2,L)*Z(I)*ACOSTH*FACTOR
      PAD=Z(I)*ACOSTH
      PCC=B(2,L)*Z(I)*ASINTH*FACTOR
      PCD=Z(I)*ASINTH
   98 CONTINUE
      S(1,1)=3.5*PBB  +7.*B(3,L) +7.*B(4,L) + B(6,L)
      S(2,2)=2.5*PBB  +B(3,L) -13.*B(4,L) - 5.*B(6,L)
      S(3,3)=1.5*PBB -3.*B(3,L) -3.*B(4,L) +9.*B(6,L)
      S(4,4)=.5*PBB -5.*B(3,L) +9.*B(4,L) -5.*B(6,L)
      S(5,5)=S(4,4) -PBB
      S(6,6)=S(3,3) -3.*PBB
      S(7,7) =S(2,2)-5.*PBB
      S(8,8) =S(1,1)-7.*PBB
      S(1,5) = R7*B(5,L)/R5 +R5*B(7,L)/R7
      S(2,6) = R3*B(5,L) - B(7,L)/R3
      S(1,2)=PAA*R7/2.
      S(2,3)=PAA*R3
      S(3,4)=PAA*R3*R5/2.
      S(4,5)=PAA*2.
      S(5,6)=S(3,4)
      S(6,7)=S(2,3)
      S(7,8)=S(1,2)
      AI(1,2)=-PCC*R7/2.
      AI(2,3)=-PCC*R3
      AI(3,4)=-PCC*R3*R5/2.
      AI(4,5)=-PCC*2.
      AI(5,6)=AI(3,4)
      AI(6,7)=AI(2,3)
      AI(7,8)=AI(1,2)
      DO 901 I4=1,6
      II4 =I4+1
      II5 =8 -I4
      AI(II4,8)=AI(1,II5)
  901 S(II4,8) =S(1,II5)
      DO 902 I5 =1,4
      II6 =I5 +2
```

```
      II7 =7 -15
      AI(II6,7)=AI(2,II7)
  902 S(II6,7) = S(2,II7)
      DO 903 I6=1,2
      II8 =I6 +3
      II9 =6-I6
      AI(II8,6)=AI(3,II9)
  903 S(II8,6) = S(3,II9)
      DO 207 IY=1,8
      DO 207 JY=1,8
      IF(IY-JY) 205,205,206
  206 S(IY,JY) = S(JY,IY)
      AI(IY,JY)=-AI(JY,IY)
  205 CONTINUE
  207 CONTINUE
      DO 5006 IR=1,8
      DO 5006 JR=1,8
 5006 AR(IR,JR)=S(IR,JR)
      CALL HTRIDI(8,8,AR,AI,W,FV1,FV1,FM1)
      DO 1000 IR=1,8
      DO 5000 JR=1,8
      ZR(IR,JR)=0.
 5000 CONTINUE
      ZR(IR,IR)=1.
 1000 CONTINUE
      CALL TQL2(8,8,W,FV1,ZR,IERR)
      CALL HTRIBK(8,8,AR,AI,FM1,8,ZR,ZI)
      DO 5005 IR=1,8
      S(IR,IR) = W(IR)
      DO 5005 JR=1,8
 5005 R(IR,JR)=ZR(IR,JR)
      CBA=ABS(ABS(S(1,1)-S(2,2))-HH(I))
      IBB(I,1)=1
      IBB(1,2)=2
      I6 = 1
      I7 = 2
      DO 20 I8 = 1,7
      IZ = I8 + 1
      DO 20 I9 = IZ,8
      S1=ABS(ABS(S(I8,I8)-S(I9,I9))-HH(I))
      IF (CBA-S1)21,22,22
   22 CBA=S1
      IBB(I,1)=I3
      IBB(I,2)=I9
      I6=I8
      I7=I9
   21 CONTINUE
   20 CONTINUE
      FC(I)=ABS(S(I6,I6)-S(I7,I7))
      SIGN(I)=(S(I6,I6)-S(I7,I7))/FC(I)
      ERR(I)=0.
      DO 814 IX=1,8
      DO 814 JX=1,8
      ERR(I)=ERR(I)+FACTOR*DELH(I)*(U(1,L)*ACOSTH*SZ(IX,JX)+U(2,L)*
```

```
     1ASINTH*SX(IX,JX))*(ZR(JX,I6)*ZR(IX,I6)-ZR(JX,I7)*ZR(IX,I7))
C       ERR(I)=1.0
  814 CONTINUE
      IF(ERR(I).EQ.(0.)) WRITE (6,895) ERR(I)
  895 FORMAT(5X, 12.4)
      GO TO 421
  420 FC(I)=HN(I)  $  SIGN(I)=1. $ ERR(I)=1.
  421 CONTINUE
      IF(LX-1)110,110,121
  121 CONTINUE
      DO 235 IZ=1,7
      D1(IZ) = 0.0
      DO 235 JZ=1,7
  235 D2(IZ,JZ) =0.0
      IF(Z(I).EQ.(0.)) GO TO 110
      DO 236 IT=1,8
      RR1=(R(IT,I6)**2-R(IT,I7)**2)*SIGN(I)
     1+(ZI(IT,I6)**2 - ZI(IT,I7)**2)*SIGN(I)
      D1(1) = D1(1) + SP(IT,1)*RR1*PBD*FACTOR
      D1(3) = SP(IT,3)*RR1 +D1(3)
      D1(4) = SP(IT,5)*RR1 +D1(4)
      D1(6)=SP(IT,8)*RR1+D1(6)
  236 CONTINUE
      DO 238 IT=1,4
      IT4 = IT + 4
      RR4=2.*(R(IT,I6)*R(IT4,I6)-R(IT,I7)*R(IT4,I7))*SIGN(I)
     1+2.*(ZI(IT,I6)*ZI(IT4,I6)-ZI(IT,I7)*ZI(IT4,I7))*SIGN(I)
      RR5=-2.*(-ZR(IT,I6)*ZI(IT4,I6)+ZI(IT,I6)*ZR(IT4,I6)
     1+ZR(IT,I7)*ZI(IT4,I7)-ZI(IT,I7)*ZR(IT4,I7))*SIGN(I)
      D1(5) =SP(IT,7)*RR4 +D1(5)
      D1(7)=SP(IT,10)*RR4+D1(7)
  238 CONTINUE
      DO 401 IT=1,7
      IT1=IT+1
      RR2=2.*(R(IT,I6)*R(IT1,I6)-R(IT,I7)*R(IT1,I7))*SIGN(I)
     1+2.*(ZI(IT,I6)*ZI(IT1,I6)-ZI(IT,I7)*ZI(IT1,I7))*SIGN(I)
      RR3=-2.*(-ZR(IT,I6)*ZI(IT1,I6)+ZI(IT,I6)*ZR(IT1,I6)
     1 +ZR(IT,I7)*ZI(IT1,I7)-ZI(IT,I7)*ZR(IT1,I7))*SIGN(I)
  401 D1(2)=SP(IT,2)*(RR2*PAD+RR3*PCD)*FACTOR +D1(2)
C       IF (I.LT.5) WRITE (6,7238)(D1(JJ),JJ=1,7)
C 7238 FORMAT(5X,7E14.6)
  110 CONTINUE
      RETURN
      END
      SUBROUTINE EXAM(A,B,M,LF)
C     SUBROUTINE EXAM
C       F O R T R A N  4
      DIMENSION A(17,17),B(17),C(17)
      DO 80 J=1,M
   80 C(J)=A(J,J)
      IF(A(1,1)) 60,200,70
   60 A(1,1) =-SQRT(-A(1,1))
      GO TO 300
   70 A(1,1) =SQRT(A(1,1))
```

```
      GO TO 100
  100 IF(M-1)400,400,110
  110 DO 115 K=2,M
  115 A(1,K)=A(1,K)/(A(1,1)          )
      DO 120 J=2,M
      J1=J-1
      S=A(J,J)
      DO 125 L=1,J1
  125 S=S-A(L,J)**2
      IF (S) 50,200,40
   50 A(J,J) =SQRT(- )
      GO TO 300
   40 A(J,J) =SQRT(S)
      GO TO 130
  130 IF(J-M)135,400,400
  135 J2=J+1
      DO 120 K=J2,M
      S=A(J,K)
      DO 145 L=I,J1
  145 S=S-A(L,J)*A(L,K)
  120 A(J,K)=S/A(J,J)
  400 B(1)=B(1)/A(1,1)
      IF(M-1)420,420,405
  405 DO 410 J=2,M
      S=B(J)
      J1=J-1
      DO 415 L=1,J1
  415 S=S-A(L,J)*B(L)
  410 B(J)=S/A(J,J)
  420 B(M)=B(M)/A(M,M)
      J=M-1
  435 IF(J)450,450,425
  425 S=B(J)
      J2=J+1
      DO 430 L=J2,M
  430 S=S-A(J,L)*B(L)
      B(J)=S/A(J,J)
      J=J-1
      GO TO 435
  450 LF=1
      GO TO 460
  200 LF=0
      GO TO 460
  300 LF=-1
  460 DO 465 J=1,M
      A(J,J)=C(J)
      IF(J-M)470,475,475
  470 J2=J+1
      DO 465 K=J2,M
  465 A(J,K)=A(K,J)
  475 RETURN
      END
      SUBROUTINE MATINV(A,N,B,M,DETERM)
C     SUBROUTINE MATINV
```

```
C       F O R T R A N  4
C     MATRIX INVERSION WITH ACCOMPANYING SOLUTION OF LINEAR EQUATIONS
      DIMENSION IPIVOT(17),A(17,17),B(17,1),INDEX(17,2),PIVOT(17)
      EQUIVALENCE (IROW,JROW),(ICOLUM,JCOLUM),(AMAX,T,SWAP)
      DETERM=1.0
      DO 20 J=1,N
   20 IPIVOT(J)=0
      DO 550 I=1,N
      AMAX=0.0
      DO 105 J=1,N
      IF(IPIVOT(J)-1)60,105,60
   60 DO 100 K=1,N
      IF(IPIVOT(K)-1)80,100,740
   80 IF(ABS(AMAX)-ABS(A(J,K)))85,100,100
   85 IROW=J
      ICOLUM=K
      AMAX=A(J,K)
  100 CONTINUE
  105 CONTINUE
      IPIVOT(ICOLUM)=IPIVOT(ICOLUM)+1
      IF (IROW-ICOLUM)140,260,140
  140 DETERM=-DETERM
      DO 200 L=1,N
      SWAP=A(IROW,L)
      A(IROW,L)=A(ICOLUM,L)
  200 A(ICOLUM,L)=SWAP
      IF(M)260,260,210
  210 DO 250 L=1,M
      SWAP=B(IROW,L)
      B(IROW,L)=B(ICOLUM,L)
  250 B(ICOLUM,L)=SWAP
  260 INDEX(I,1)=IROW
      INDEX(I,2)=ICOLUM
      PIVOT(I)=A(ICOLUM,ICOLUM)
      DETERM=DETERM*PIVOT(I)
      A(ICOLUM,ICOLUM)=1.0
      DO 350 L=1,N
  350 A(ICOLUM,L)=A(ICOLUM,L)/PIVOT(I)
      IF(M)380,380,360
  360 DO 370 L=1,M
  370 B(ICOLUM,L)=B(ICOLUM,L)/PIVOT(I)
  380 DO 550 L1=1,N
      IF (L1-ICOLUM)400,550,400
  400 T=A(L1,ICOLUM)
      A(L1,ICOLUM)=0.0
      DO 450 L=1,N
  450 A(L1,L)=A(L1,L)-A(ICOLUM,L)*T
      IF(M)550,550,460
  460 DO 500 L=1,M
  500 B(L1,L)=B(L1,L)-B(ICOLUM,L)*T
  550 CONTINUE
      DO 710 I=1,N
      L=N+1-I
```

```
      IF(INDEX(L,1)-INDEX(L,2))630,710,630
  630 JROW=INDEX(L,1)
      JCOLUM=INDEX(L,2)
      DO 705 K=1,N
      SWAP=A(K,JROW)
      A(K,JROW)=A(K,JCOLUM)
      A(K,JCOLUM)=SWAP
  705 CONTINUE
  710 CONTINUE
  740 RETURN
      END
```

```
      PROGRAM RADHA(INPUT,OUTPUT,TAPE5=INPUT,TAPE6=OUTPUT)
C      PROGRAM PRITI1(TOULOUSE VERSION OF PRITI/MONTREAL)
C     NO =THE NO. OF FIRST MAG FIELD IN DATA INCLUDED IN FITTING
C     M  =NO. OF PARAMETERS
C     L4 =NO. OF ITERATIONS ALLOWED
C     LL5=PARAMETER WHICH TELLSCOMPUTATIONS OF SED OF INDIVIDUAL
C          LINES:WITH L4 ITERATIONS IF LL5=0
C               :WITHOUT ANY ITERATIONS IF LL5=1
C     Q1 =MIN. VALUE OF SUM OF SQUARES FOR FITS( CHI-SQUARE TOLERANCE)
C     Z(I)=MAGNETIC FIELD VALUES FOR FITS
C     B  =PARAMETER MATRIX
C     N  =NO. OF  DATA POINTS USED IN LEAST-SQARES FITTING
C     Q1 =N/10
C     Q2 =TOLERANCE ON GRAD(CHI**2) =APPROX .01
C     FM(I) = MEASURED VALUES
C     FC(I) = CALCULATED VALU
C     ERR(1)= STANDARD DEVIATION ON FM(I) = SQRT(FM(1))
C
C      DIMENSIONS OF A,B IN LXAM AND MATINV SUBROUTINES SHOULD BE THE
C     SAME AS THOSE OF B2,B1 RESPECTIVELY IN THE MAIN PROGRAM AND IN
C     CURFIT.
C
C     DIMENSIONS OF Q,V IN JACOBI1 SHOULD BE THE SAME AS THOSE OF
C     B3,B2 RESPECTIVELY IN CURFIT
C
C     NUMBER=INDEX THAT CHANGES WITH EACH NEW CASE
C     NCASES=NO. OF CASES CONSIDERED. ITS VALUE SHOULD BE ENTERED.
C
C     KILL=0 THE SAME CASE IS COMPUTED COMPLETELY
C          =1 THE CASE IS DROPPED AND MOVED TO NEXT ONE (NEGATIVE
C             SQUARE ROOT ENCOUNTERED)
C
C
C     THIS PROGRAM ANALYSES KRAMER'S DOUBLET. DATA
C     B(1)-B(6)=G-SQUARE COMPONENTS-(ZZ,ZX,XX,ZY,YY,XY)
C       B(7),B(8),B(9) ARE MISORIENTATION ANGLES IN
C       ZX,ZY,XY PLANE, ENTERED IN DEGREE.
C
C
C      CASE NO.1 =CD CA ACETATE/CU+2 AT LIQ. HELIUM TEMP.
C      CASE NO.2 = CA CD ACETATE/CU+2 AT LIQ. NITROGEN FOR TE"A"
C     CASE NO.3=CA-CD ACETATE/CU+2 AT LIQ.NITROGEN TEMP.FOR TYPE"B"
C
C
      DIMENSION Z(200),FM(200),FC(200),DF(200),ERR(200),B(13),B1(13),
     1B2(13,13),DC(3500),ABC(2),Y(4),THETA(200),HN(200),ZZ(200,20),
     2HHDPPH(200,20),NN(25),      GG(13,20),ML(20),IBB(200,2),
     3SSMD(200),TEETA(200,20),G(13,20),GSQRT(3),DELHH(200,20),DELH
    (200) DIMENSION AG(3,3),AAG(6),E(40),VR(3,3),VI(3,3),FREQ(20),
     1 FACTOR(20),ADD(20)
      DIMENSION FFREQ(200,20),AADD(200,20),FFACTR(200,20),BG(9)
      DIMENSION VG2(3),V3(3,3),VG(3),VG2R2(3),VGR2(3)
      COMMON/DATA1/ABC,Y
      COMMON/DATA2/DC
```

```
      COMMON/DATA3/DELH
      EQUIVALENCE(Z,DC),(FM,DC(201)),(DF,DC(401)),(FC,DC(601)),
     1(ERR,DC(801)),(THETA,DC(1001)),(RR,DC(1201)),(B,DC(2500)),
     2(B2,DC(2600)),(N,DC(1575)),(L4,DC(1576)),(Q1,DC(1577)),
     3(Q2,DC(1578)),(M,DC(1579)),(I,DC(1580)),(L,DC(1581)),
     4 (NUMBER,DC(1988)),(B1,DC(2550)),(LBB,DC(2000)),( MD,DC(1989))
       DATA(TEETA(J,1),J=1,19)/
     1 0.,5.,10.,15.,20.,25.,30.,35.,40.,
     2 45.,50.,55.,60.,65.,70.,75.,80.,85.,90./
       DATA (ZZ(J,1),J=1,19)/
     1 37.,37.625,38.375,40.,42.25,45.125,48.25,52.5,57.25,
     2 62.375,66.875,72.125,76.875,82.25,86.75,90.,91.5,92.5,94.5/
       DATA(TEETA(J,1),J=20,38)/
     1 -0.,-5.,-10.,-15.,-20.,-25.,-30.,-35.,-40.,
     2 -45.,-50.,-55.,-60.,-65.,-70.,-75.,-80.,-85.,-90./
       DATA(ZZ(J,1),J=20,38)/
     1 37.,37.625,38.375,40.,42.25,45.125,48.25,52.5,57.25,
     2 62.375,66.875,72.125,76.875,82.25,86.75,90.,91.5,92.5,94.5/
       DATA(TEETA(J,1),J=39,57)/
     1 9000.,9005.,9010.,9015.,9020.,9025.,9030.,9035.,9040.,9045.,
     2 9050.,9055.,9060.,9065.,9070.,9075.,9080.,9085.,9090./
       DATA(ZZ(J,1),J=39,57)/19*94.5/
       DATA(TEETA(J,2),J=1,19)/
     1 0.,5.,10.,15.,20.,25.,30.,35.,40.,45.,50.,55.,60.,65.,
     2 70.,75.,80.,85.,90./
       DATA(ZZ(J,2),J=1,19)/
     1 31.875,32.625,33.375,34.75,36.00,41.625,46.375,
     2 49.125,54.,59.375,64.125,69.125,73.375,78.375,
     3 81.75,86.,88.5,89.25,90.25/
       DATA(TEETA(J,2),J=20,38)/
     1 -0.,-5.,-10.,-15.,-20.,-25.,-30.,-35.,-40.,-45.,
     2 -50.,-55.,-60.,-65.,-70.,-75.,-80.,-85.,-90./
       DATA(ZZ(J,2),J=20,38)/
     1 31.875,32.625,33.375,34.75,38.,41.625,46.375,49.125,
     2 54.,59.375,64.125,69.125,73.375,78.375,81.75,
     3 86.,88.5,89.25,90.25/
       DATA(TEETA(J,2),J=39,57)/
     1 9000.,9005.,9010.,9015.,9020.,9025.,9030.,9035.,9040.,
     2 9045.,9050.,9055.,9060.,9065.,9070.,9075.,9080.,
     3 9085.,9090./
       DATA(ZZ(J,2),J=39,57)/19*90.25/
       DATA(TEETA(J,3),J=1,19)/
     1 0.,5.,10.,15.,20.,25.,30.,35.,40.,45.,50.,55.,60.,
     2 65.,70.,75.,80.,85.,90./
       DATA(ZZ(J,3),J=1,19)/
     1 93.5,95.125,96.875,100.125,104.875,113.625,124.375,
     2 135.875,148.75,159.875,171.75,183.625,196.25,203.,
     3 212.5,220.,224.,227.5,230./
       DATA(TEETA(J,3),J=20,38)/
     1 -0.,-5.,-10.,-15.,-20.,-25.,-30.,-35.,-40.,-45.,-50.,
     2 -55.,-60.,-65.,-70.,-75.,-80.,-85.,-90./
       DATA(ZZ(J,3),J=20,38)/
     1 93.5,95.125,96.875,100.125,104.875,113.625,124.375,
     2 135.875,148.75,159.875,171.75,183.625,196.25,203.,
```

```
     3 212.5,220.,224.,227.5,230./
       DATA(TEETA(J,3),J=39,57)/
     1 9000.,9005.,9010.,9015.,9020.,9025.,9030.,9035.,9040.,
     2 9045.,9050.,9055.,9060.,9065.,9070.,9075.,9080.,
     3 9085.,9090./
       DATA(ZZ(J,3),J=39,57)/19*230./
C
C      IS FIRST CONVERTED TO 355 DEG AND THEN ENTERED AS 9355.)
C
       DATA NN(1)/57/
      DATA NN(2)/57/
      DATA NN(3)/57/
       DATA(FFREQ(J,1),J=1,57)/57*9.39/
       DATA(FFREQ(J,2),J=1,57)/57*9.415/
       DATA(FFREQ(J,3),J=1,66)/57*9.427/
       DATA(AADD(J,1),J=1,57)/57*(346.720)/
       DATA(AADD(J,2),J=1,57)/57*346.54/
       DATA(AADD(J,3),J=1,66)/57*856.006/
       DATA(FFACTR(J,1),J=1,57)/57*(7.467)/
       DATA(FFACTR(J,2),J=1,57)/57*(7.4614)/
       DATA(FFACTR(J,3),J=1,57)/57*(2.978)/
       DATA(G(J,1),J=1,6)/
C     1 5.49185,.0064,4.15,.0064,4.15,-.006/
     1 5.4833,.0123,4.149,.0123,4.149,-.004/
       DATA(G(J,2),J=1,6)/
C     1 5.40622,0.,4.17332,0.,4.17332,0./
     1 5.6718,-.024,4.2646,-.024,4.2646,-.006/
       DATA(G(J,3),J=1,6)/
C     1 5.40622,0.,4.17332,0.,4.17332,0./
     1 5.6923,-.0485,4.3441,-.0485,4.3441,-.0093/
       DATA(DELHH(J,1),J=1,57)/57*6.0/
       DATA(DELHH(J,2),J=1,57)/57*6.0/
       DATA(DELHH(J,3),J=1,57)/57*6.0/
  188 FORMAT(1H1)
    8 FORMAT(1X,4HQ1 = ,E13.5,5X,4HQ2 = ,E13.5)
  137 FORMAT(3X,I2,5X,E16.6/)
  136 FORMAT(10X,* INITIAL PARAMETERS*,//3X,*J*,10X,*B(J)*//)
  135 FORMAT(1X,11H PARAMETERS,//3X,1HJ,10X,4HB(J),27X,6HERRORS//)
    9 FORMAT(2X,*HH=*,10(F9.4,4X))
  140 FORMAT(3X,I2,5X,E16.6,15X,E16.6/)
  139 FORMAT(5X,14H CASE NUMBER =,I2//)
  141 FORMAT(10X,6H SMD =,E13.5//)
  235 FORMAT (15X,5(E13.5,8X)/)

  144 FORMAT(5X,*LINE NUMBER*,5X,*LINE POSITION*,5X,*ANGLE*,/)
  145 FORMAT(6X,I3,9X,F10.1,11X,F8.2)
      RD=3.1415926/180.
      NUMBER=1
      NCASES=3
      NUMBII=NUMBER
      Q1 =1.E-8
      Q2 =1.E-20
      WRITE (6,188)
    1 CONTINUE
```

```
      M=6
      MM=M
      L4=10
      N=NN(NUMBER)
      DO 209 LL=1,9
  209 B(LL)=0.
      DO 210 LL=1,MM
  210 B(LL)=G(LL,NUMBER)
      WRITE (6,138) NUMBER
      WRITE (6,136)
      WRITE (6,137) (J,B(J),J=1,M)
      N1=N
      DO 3 IJK = 1,N1
      HN(IJK)=FFREQ(IJK,NUMBER)
      THETA(IJK)=TEETA(IJK,NUMBER)
C       Z(IJK)=ZZ(IJK,NUMBER)*FFACTR(IJK,NUMBER)+AADD(IJK,NUMBER)
      Z(IJK)=(ZZ(IJK,NUMBER)+AADD(IJK,NUMBER))*
     1FFACTR(IJK,NUMBER)
      DELH(IJK)=DELHH(IJK,NUMBER)
    3 CONTINUE
      WRITE(6,144)
      DO 146 IJK=1,N1
  146 WRITE(6,145) IJK,Z(IJK),THETA(IJK)
      WRITE(6,8)Q1,Q2
      WRITE(6,9) (HN(J),J=1,N1)
      DO 201 J = 1,N1
  201 FM(J)=HN(J)
      CALL CURFIT
      WRITE(6,188)
      WRITE(6,135)
      DO 220 LL=1,M
  220 GG(LL,NUMBER) = B(LL)
      WRITE(6,140)(J,B(J),B1(J),J=1,M)
      SSS=0.
C     SSS1 IS SMD(1),THAT IS WHEN ALL (LINES) SIGMA=1
      SSS1=0
      WRITE(6,11140) N1,N
11140 FORMAT(*N1=*,I3,*N=*,I3)
      DO 555 ID=1,N1
      SSS=DF(ID)**2
      SSS2=DF(ID)**2/(ERR(ID)**2)
      SSS1=SSS1+SSS
      WRITE(6,656) ID,SSS,Z(ID),SSS2
  555 CONTINUE
      WRITE(6,657)SSS1
  657 FORMAT(10X,*SMD(1)*,E13.5,//)
  656 FORMAT(10X,*LINE NUMBER = *,I2,5X,*SMD(1) = *,E13.5,*     MAG.
 FIELD 1VALUE = *,E13.5,*SMD=*,E13.5)
  301 FORMAT(10X,*FREQUENCY NO. = *,I3,5X,*EIGENVALUE1 =*,I3,5X,
     1* EIGENVALUE 2 =*,I3)
      WRITE(6,188)
      AG(1,1)=B(1)
      AG(1,2)=B(2)
      AG(1,3)=B(4)
```

```
      AG(2,2)=B(3)
      AG(2,3)=B(6)
      AG(3,3)=B(5)
      AG(2,1)=AG(1,2)
      AG(3,1)=AG(1,3)
      AG(3,2)=AG(2,3)
C     CALL SVLVC1(AG,50,50,E,40,VR,30,40,3,ITER)
      CALL JACOB1 (3,AG,1,NR,VR)
  995 FORMAT (5X,14)
  996 CONTINUE
      WRITE(6,998)
  998 FORMAT(5X,*EIGENVALUES OF G-SQUARE -TENSOR ARE:*,/)
                                ,II=1,3)
          -1,3
      IF(AG(J6,J6).LT.(0.)) GO TO 24
      GSQRT(J6)=SQRT(AG(J6,J6))
      WRITE(6,26) J6,GSQRT(J6)
      GO TO 23
   24 WRITE(6,25) NUMBER,J6
   23 CONTINUE
   25 FORMAT(5X,*CASE NO.=*,I3,* EIGENVALUE *,I2,* OF G-SQUARE
     1 TENSOR IS NEGATIVE*)
   26 FORMAT(5X,*EIGENVALUE *,I2,* OF G-TENSOR IS =*,E16.6)
      WRITE(6,887)
  887 FORMAT(5X,*EIGENVECTORS OF G-SQUARE -TENSOR ARE:*,/)
  888 FORMAT(5X,3(E16.6,5X),/)
      DO 885 II=1,3
  885 WRITE(6,888)(VR(JJ,II),JJ=1,3)
      VB(1,1)=B1(1)
      VB(1,2)=B1(2)
      VB(1,3)=B1(4)
      VB(2,2)=B1(3)
      VB(3,3)=B1(5)
      VB(2,3)=B1(6)
      VB(3,2)=VB(2,3)
      VB(2,1)=VB(1,2)
      VB(3,1)=VB(1,3)
C     FOLLOWING CALCULATES VARIANCES
C     VARIANCE OF G-SQUARE COMPONENTS
      WRITE(6,38)
   38 FORMAT(5X,*VARIANCES OF G-SQUARE COMPONENTSARE=*,//)
      DO 31 K=1,3
      VG2(K)=0.
      DO 31 II=1,3
      DO 31 JJ=1,3
      VG2(K)=VG2(K)+(VB(II,JJ)*VR(II,K)*VR(JJ,K))**2
      VG2R2(K)=SQRT(VG2(K))
   31 CONTINUE
      WRITE(6,32)VG2
   32 FORMAT(5X,*VG2(1)=*,E16.6,2X,*VG2(2)=*,E16.6,2X,
     1*VG2(3)=*,E16.6,//)
      WRITE(6,39)
   39 FORMAT(5X,*STANDARD DEVIATIONS OF G-SQUARE
     1TENSOR COMPONENTS ARE=*,//)
```

```
      WRITE(6,40)VG2R2
   40 FORMAT(5X,*VG2R2(1)=*,E16.6,2X,
     1*VG2R2(2)=*,E16.6,2X,
     2*VG2R2(3)=*,E16.6,//)
C     VARIANCE OF G-TENSOR COMPONENTS
      DO 33 K=1,3
      VG(K)=VG2(K)/(4.*AG(K,K))
      VGR2(K)=SQRT(VG(K))
   33 CONTINUE
      WRITE(6,35)
   35 FORMAT(5X,*VARIANCES OF G-TENSOR
     1COMPONENTS ARE=*,//)
      WRITE (6,34)VG
   34 FORMAT(5X,*VG(1)=*,E16.6,2X,*VG(2)=*,
     1E16.6,2X,*VG(3)=*,E16.6,//)
      WRITE(6,36)
   36 FORMAT(5X,*STANDARD DEVIATIONS OF
     1G-TENSOR COMPONENTS ARE=*,//)
      WRITE(6,37)VGR2
   37 FORMAT(5X,*VGR2(1)=*,E16.6,2X,*VGR2(2)=*,
     1E16.6,2X,*VGR2(3)=*,E16.6,//)
      WRITE(6,188)
      NUMBER=NUMBER+1
      IF ( NUMBER - NCASES) 1,1,2
    2 CONTINUE
      WRITE(6,188)
      DO 230 LL=NUMBI1,NCASES
      WRITE (6,138) LL
      WRITE (6,141) SMD(LL)
  230 WRITE (6,235) (GG(LM,LL),LM=1,M)
      STOP
      END

      SUBROUTINE CURFIT
C
C     EXAM  HANDLES ALL MATRICES OF DIMENSIONS UPTO THE DIMS.MM OF
C A&C THAT IS M IS LESS THAN OR EQUAL TO MM (SAME IS TRUE OF MATINV
C AND JACOBI)
C
C
C          F O R T R A N  4
      DIMENSION Z(200),FM(200),FC(200),DF(200),ERR(200),B(13),B1(13),
     2          DC(3500),ABC(2),Y(4),X(200),GRAD(13),D1(13),D2(13,13),
     3MD(10),B3(50,50) ,B2(13,13)
      DIMENSION AI(13,13),W(40),ZR(13,13),Z1(13,13),FV1(13),
     2FM1(2,13),FV2(13)
      COMMON/DATA1/ABC,Y
      COMMON/DATA2/DC
      EQUIVALENCE (Z,DC),(FM,DC(201)),(DF,DC(401)),(FC,DC(601)),
     1(ERR,DC(801)),(B,DC(2500)),(GRAD,DC(2513)),(B2,DC(2600)),
     2(M,DC(1575)),(L4,DC(1576)),(Q1,DC(1577)),(Q2,DC(1578)),
     3(M,DC(1579)),(I,DC(1580)),(L,DC(1581)),(D1,DC(2800)),
     4(D2,DC(2900))   ,(MD,DC(1989)),(NUMBER,DC(1988))
      EQUIVALENCE(B1,DC(2550)),(MZ,DC(2499))
```

```
      DATA(ABC=2HNO,3HYES),(Y=1H ,1HC,1H*,1HM)
C     DATA(ABC(I),I=1,2)/*NO*,*YES*/
C     DATA(Y(I),I=1,4)/* *,*C*,***,*M*/

      L1 = 0
      SA = 0.0
      MM = N
      DO 1000 J =1,MM
      B1(J)=0.0
      DO 1000 K = 1,MM
1000  B2(J,K)=0.0
      WRITE(6,901)
      NN = N
      DO 100 II = 1,NN
      I=II
      L=1
      CALL FUNC(2)
      X(II)=ERR(II)**2
901   FORMAT(5X,10H FUNC2,210  )
      DF(II) =FM(II) - FC(II)
      DO 101 J=1,MM
      B1(J)=B1(J)-(2.0*DF(II)*D1(J))/X(II)
      DO 101 K=1,MM
101   B2(J,K)=B2(J,K)-(2.0*(DF(II)*D2(J,K)-D1(J)*D1(K)))/X(II)
      SA = SA + DF(II)**2/X(II)
100   CONTINUE
      WRITE(6,901)
      GMOD=0.0
      DO 102 J=1,MM
102   GMOD=GMOD+B1(J)**2
      WRITE(6,243)SA,GMOD
243   FORMAT (1X,26H*INITIAL VALUE SUM OF SQ.=,E13.5,20X,
     117H*SQ MOD OF GRAD =,E13.5)
      WRITE(6,1751)
1751  FORMAT(14H0 DERIVATIVES-)
      WRITE(6,240)(B1(J),J=1,MM)
240   FORMAT (15X,5(E13.5,8X)/)
      IF (SA - Q1) 110, 110, 200
110   LL = 1
      GO TO 600
200   S = 0.0
      GMOD = 0.0
      BMOD = 0.0
      PROD = 0.0
      A2=ABC(1)
      DO 210 J =1,MM
      B1(J) = 0.0
      DO 210 K=1,MM
210   B2(J,K) = 0.0
      WRITE(6,902)
      DO 220 II=1,NN
      I=II
      L=1
      CALL FUNC(2)
```

```
      X(II)=ERR(II)**2
  902 FORMAT(5X,10H FUNC2,210  )
      DF(II) = FM(II) - FC(II)
      DO 221 J=1,MM
      B1(J) = B1(J) - (2.0*DF(II)*D1(J))/X(II)
      DO 221 K =1,MM
  221 B2(J,K) = B2(J,K) - (2.0*(DF(II)*D2(J,K) -D1(J)*D1(K)))/X(II)
  220 CONTINUE
      WRITE(6,902)
      DO 230 J=1,MM
  230 GRAD(J) = B1(J)
      L1 = L1 + 1
      WRITE(6,903)
      CALL EXAM (B2,B1,MM,LF)
      WRITE(6,903)
  903 FORMAT(5X,9H EXAM,230  )
      IF (LF)  250, 250, 305
  250 DO 231 II=1,MM
      DO 231 JJ=1,MM
      A1(II,JJ)=0.
  231 B3(II,JJ)=B2(II,JJ)
      WRITE(6,904)
C      CALL SVLVC1(B3,50,50,N,40,ZR,30,40,13,ITER)
      CALL JACOB11(13,B3,1,NR,ZR)
      DO 5005 IR=1,MM
      DO 5005 JR=1,MM
 5005 B2(IR,JR)=ZR(JR,JR)
      WRITE(6,904)
  904 FORMAT(5X,12H JACOBI1,231  )
      DO 235 K =1,MM
  235 B1(K)=B3(K,K)
      A2=ABC(2)
      DO 260 J=1,MM
  260 D1(J) = 0.0
      DO 270 J=1,MM
      DO 270 K=1,MM
  270 D1(K) = D1(K) + B2(J,K) *GRAD(J)
      DO 275 J = 1, MM
      IF (B1(J))  280, 290, 285
  280 B1(J) = - B1(J)
  285 D1(J) = D1(J)/B1(J)
      GO TO 275
  290 D1(J) = 0.0
  275 CONTINUE
      DO 295 J=1,MM
  295 B1(J) = 0.0
      DO 300 J=1,MM
      DO 300 K=1,MM
  300 B1(J) = B1(J) + B2(J,K)*D1(K)
  305 DO 310 J=1,MM
      GMOD = GMOD + GRAD(J)**2
      BMOD = BMOD + B1(J)**2
  310 PROD = PROD + GRAD(J)*B1(J)
      IF (GMOD - Q2)  315, 315, 320
```

```
  315 LE = 2
      WRITE(6,1761) GMOD
 1761 FORMAT(5X,7H GMOD =,E13.5//)
      GO TO 600
  320 C=PROD/SQRT(BMOD*GMOD)
      IF (C) 335, 335, 400
  335 LE = 4
      GO TO 600
  400 LD = 0
      L3 = 0
      DO 410 J=1,MN
  410 GRAD(J) = B(J) - B1(J)
      WRITE(6,905)
  450 DO 420 II=1,NN
      I=II
      L=2
      CALL FUNC (1)
      X(II)=ERR(II)**2
  905 FORMAT(5X,10H FUNC1,450  )
      DF(II) = FM(II) - FC(II)
      S = S + DF(II)**2/X(II)
  420 CONTINUE
      IF (SA - S) 435, 500, 500
  435 LD = LD + 1
  430 DO 440 J=1,MN
      B1(J) = B1(J)*2.0
  906 FORMAT(5X,16H BINARY CHOP,430  )
  440 GRAD(J) = B(J) - B1(J)
      S = 0.0
      L3 = L3 + 1
      IF (L3-150)450,460,460
  460 LE = 5
      GO TO 600
  500 IF (LD) 505, 505, 506
  506 LD = 0
      GO TO 430
  505 DO 510 J=1,MN
  510 B(J) = GRAD(J)
      SA = S
      IF (SA - Q1) 507, 507, 530
  507 LE = 1
      GO TO 600
  530 IF (L4) 200, 200, 900
  900 WRITE(6,920)L1,IA2,L3,S,GMOD,(B(J),J=1,MN)
  920 FORMAT(//,15H ITERATION NO.=,I5,10X,*   TRANSFORMATION MADE TO
     PRINCIPAL AXES = *,A4,10X,   18H BINARY CHOP USED=,I3,6H TIMES/1X
     ,*WEIGHTED SUM OF SQUARES = *,E14.7,25X,*   SQUARE MODULUS OF GRAD
     IENT = *,E14.7,/20H   PARAMETERS B(J) ,/(6E17.8)/)
      IF (L1 - L4) 200, 910, 910
  910 LE = 6
      GO TO 600
  600 DO 710 J=1,MN
      B1(J) = 0.0
      DO 710 K=1,MN
```

```
  710 B2(J,K) = 0.0
      L=1
      DO 721 II=1,MM
      I=II
      CALL FUNC(2)
      X(II)=ERR(II)**2
      DF(II) = FM(II) - FC(II)
      DO 720 J=1,MM
      B1(J) = B1(J) - (2.0*DF(II)*D1(J))/X(II)
      DO 720 K=1,MM
  720 B2(J,K) = B2(J,K) - ((DF(II)*D2(J,K) -D1(J)*D1(K)))/X(II)
  721 CONTINUE
      CALL MATINV(B2,MM,B1,1,DETERM)
      DO 730 J=1,MM
      IF (B2(J,J)) 2001,2001,2002
 2001 B1(J) = -SQRT(-B2(J,J))
      GO TO 730
 2002 B1(J) = SQRT(B2(J,J))
  730 CONTINUE
      DO 740 J=1,MM
      DO 740 K=1,MM
  740 B2(J,K)=B2(J,K)/(B1(J)*B1(K))
      WRITE(6,551)LL,SA
  551 FORMAT(//,* EXIT NUMBER=*,I3,20X,* WEIGHTED SUM OF SQUARES=*,
     E15.8//)
      SMD(NUMBER)=SA
      GO TO 105
  103 CONTINUE
      SMD(NUMBER)=SA
      WRITE(6,104)
  104 FORMAT(/,5X,*LL5=1, NO ITERATIONS DONE*,/)
  105 CONTINUE
      RETURN
      END
      SUBROUTINE FUNC(LX)
C     SUBROUTINE FUNC
      DIMENSION DC(3500),B(13,2),D1(13),FC(200),Z(200),HN(200),S(2,2),
     1R(2,2),SIGN(200),THETA(200),IBB(200,2),D2(13,13),ERR(200)
      DIMENSION AR(2,2),AI(2,2),W(2),ZR(2,2),ZI(2,2),FV1(2),FM1(2,2)
     1,SZ(2,2),SX(2,2),SY(2,2),SR(2,2),SI(2,2),FV2(2),BG(9)
      DIMENSION DELH(200)
      COMMON/DATA2/DC
      COMMON/DATA3/DELH
      EQUIVALENCE (Z,DC),(FC,DC(601)),(THETA,DC(1001)),(B,DC(2500)),
     1(D1,DC(2800)),(D2,DC(2900)),(M,DC(1579)),(I,DC(1580)),
     2(L,DC(1581)),(HN,DC(1201)),(IBB,DC(2000)),(N,DC(1575))
     3,(NZ,DC(2490)),(NUMBER ,DC(1988)),(ERR,DC(801))
      FACTOR=92.732/66252.
      RD=3.1415926/180.
      PI2=2.*3.1415926
      B(7,L)=0.
      B(8,L)=0.
      B(9,L)=0.
  130 CONTINUE
```

```
  131 CONTINUE
      IF(THETA(I).GT.720.) GO TO 10
      IF(THETA(I).LT.(0.)) GO TO 13
      ALZ=COS((THETA(I)+B(7,L))*RD)
      ALX=SIN((THETA(I)+B(7,L))*RD)
      ALY=0.
      GO TO 14
   13 CONTINUE
      ALZ=COS((-THETA(I)+B(8,L))*RD)
      ALX=0.
      ALY=SIN((-THETA(I)+B(8,L))*RD)
   14 CONTINUE
      GO TO 15
   10 CONTINUE
      ALZ=0.
      ALX=COS((THETA(I)+B(9,L))*RD)
      ALY=SIN((THETA(I)+B(9,L))*RD)
   15 CONTINUE
  132 CONTINUE
  139 FORMAT(5X,3(E16.6,5X),/)
      IF(Z(I).NE.(0.)) GO TO 135
      FC(I)=HN(I)
      GO TO 134
  135 CONTINUE
      FCI=(B(1,L)*ALZ*ALZ+
     1 2.*B(2,L)*ALZ*ALX+B(3,L)*ALX*ALX+2.*B(4,L)*ALZ*ALY+
     2 B(5,L)*ALY*ALY+2.*B(6,L)*ALX*ALY)
C     FOLLOWING FOR NEGATIVE FCI
      IF(FCI.GT.(0.).OR.FCI.EQ.(0.)) GO TO 192
      DO 193 JJ=1,9
  193 BG(JJ)=B(JJ,L)
      KILL=1
      WRITE(6,190) I
      WRITE(6,191) (B(JJ,L),JJ=1,9)
      LL6=I
      GO TO 110
  190 FORMAT(/,5X,*NEGATIVE FCI FOR LINE NO. =*,I3,/)
  191 FORMAT(5X,6E12.6,/)
  192 CONTINUE
      FC(I)=Z(I)*FACTOR*SQRT(FCI)
      ERR(I)=SQRT(FCI)*DELH(I)*FACTOR
  134 CONTINUE
      IF(LX-1) 110,110,121
  121 CONTINUE
      IF(Z(1).EQ.(0.)) GO TO 915
      DO 235 IZ=1,13
      D1(IZ) = 0.0
      DO 235 JZ=1,13
  235 D2(IZ,JZ) =0.0
  133 CONTINUE
      F=2.*FC(I)/((Z(I)*FACTOR)**2)
      FF=2.*RD/F
      D1(1)=ALZ**2/F
      D1(2)=2.*ALZ*ALX/F
```

```
      D1(3)=ALX**2/F
      D1(4)=2.*ALZ*ALY/F
      D1(5)=ALY**2/F
      D1(6)=2.*ALX*ALY/F
      D1(7)=0.
      D1(8)=0.
      D1(9)=0.
      IF(THETA(1).GT.(720.)) GO TO 910
      IF(THETA(I).LT.(0.)) GO TO 913
      ANG7=(THETA(I)+B(7,L))*RD
      D1(7)=FF*(B(1,L)*ALZ*(-SIN(ANG7))+B(2,L)*(ALX*
     1 (-SIN(ANG7))+ALZ*COS(ANG7))+B(3,L)*ALX*COS(ANG7))
      GO TO 914
  913 CONTINUE
      ANG8=(-THETA(I)+B(8,L))*RD
      D1(8)=FF*(B(1,L)*ALZ*(-SIN(ANG8))+B(4,L)*(ALY*
     1 (-SIN(ANG8))+ALZ*COS(ANG8))+B(5,L)*ALY*COS(ANG8))
  914 CONTINUE
      GO TO 915
  910 CONTINUE
      ANG9=(THETA(I)+B(9,L))*RD
      D1(9)=FF*(B(3,L)*ALX*(-SIN(ANG9))+B(6,L)*(ALY*
     1 (-SIN(ANG9))+ALX*COS(ANG9))+B(5,L)*ALY*COS(ANG9))
  915 CONTINUE
  110 CONTINUE
      RETURN
      END
      SUBROUTINE EXAM(A,B,M,LF)
C     SUBROUTINE EXAM
C       F O R T R A N  4
      DIMENSION A(13,13),B(13),C(13)
      DO 80 J=1,M
   80 C(J)=A(J,J)
      IF(A(1,1)) 60,200,70
   60 A(1,1) =-SQRT(-A(1,1))
      GO TO 300
   70 A(1,1) =SQRT(A(1,1))
      GO TO 100
  100 IF(M-1)400,400,110
  110 DO 115 K=2,M
  115 A(1,K)=A(1,K)/(A(1,1)          )
      DO 120 J=2,M
      J1=J-1
      S=A(J,J)
      DO 125 L=1,J1
  125 S=S-A(L,J)**2
      IF (  ) 50,200,40
   50 A(J,J) =-SQRT(-  )
      GO TO 300
   40 A(J,J) =SQRT(S)
      GO TO 130
  130 IF(J-M)135,400,400
  135 J2=J+1
      DO 120 K=J2,M
```

```
      S=A(J,K)
      DO 145 L=1,J1
  145 S=S-A(L,J)*A(L,K)
  120 A(J,K)=S/A(J,J)
  400 B(1)=B(1)/A(1,1)
      IF(N-1)420,420,405
  405 DO 410 J=2,N
      S=B(J)
      J1=J-1
      DO 415 L=1,J1
  415 S=S-A(L,J)*B(L)
  410 B(J)=S/A(J,J)
  420 B(N)=B(N)/A(N,N)
      J=N-1
  435 IF(J)450,450,425
  425 S=B(J)
      J2=J+1
      DO 430 L=J2,N
  430 S=S-A(J,L)*B(L)
      B(J)=S/A(J,J)
      J=J-1
      GO TO 435
  450 LF=1
      GO TO 460
  200 LF=0
      GO TO 460
  300 LF=-1
  460 DO 465 J=1,N
      A(J,J)=C(J)
      IF(J-N)470,475,475
  470 J2=J+1
      DO 465 K=J2,N
  465 A(J,K)=A(K,J)
  475 RETURN
      END
      SUBROUTINE MATINV(A,N,B,M,DETERM)
C     SUBROUTINE MATINV
C       F O R T R A N  4
C     MATRIX INVERSION WITH ACCOMPANYING SOLUTION OF LINEAR EQUATIONS
      DIMENSION IPIVOT(13),A(13,13),B(13,1),INDEX(13,2),PIVOT(13)
      EQUIVALENCE (IROW,JROW),(ICOLUM,JCOLUM),(AMAX,T,SWAP)
      DETERM=1.0
      DO 20 J=1,N
   20 IPIVOT(J)=0
      DO 550 I=1,N
      AMAX=0.0
      DO 105 J=1,N
      IF(IPIVOT(J)-1)60,105,60
   60 DO 100 K=1,N
      IF(IPIVOT(K)-1)80,100,740
   80 IF(ABS(AMAX)-ABS(A(J,K)))85,100,100
   85 IROW=J
      ICOLUM=K
      AMAX=A(J,K)
```

```
  100 CONTINUE
  105 CONTINUE
      IPIVOT(ICOLUM)=IPIVOT(ICOLUM)+1
      IF (IROW-ICOLUM)140,260,140
  140 DETERM=-DETERM
      DO 200 L=1,N
      SWAP=A(IROW,L)
      A(IROW,L)=A(ICOLUM,L)
  200 A(ICOLUM,L)=SWAP
      IF(M)260,260,210
  210 DO 250 L=1,M
      SWAP=B(IROW,L)
      B(IROW,L)=B(ICOLUM,L)
  250 B(ICOLUM,L)=SWAP
  260 INDEX(I,1)=IROW
      INDEX(I,2)=ICOLUM
      PIVOT(I)=A(ICOLUM,ICOLUM)
      DETERM=DETERM*PIVOT(I)
      A(ICOLUM,ICOLUM)=1.0
      DO 350 L=1,N
  350 A(ICOLUM,L)=A(ICOLUM,L)/PIVOT(I)
      IF(M)380,380,360
  360 DO 370 L=1,M
  370 B(ICOLUM,L)=B(ICOLUM,L)/PIVOT(I)
  380 DO 550 L1=1,N
      IF (L1-ICOLUM)400,550,400
  400 T=A(L1,ICOLUM)
      A(L1,ICOLUM)=0.0
      DO 450 L=1,N
  450 A(L1,L)=A(L1,L)-A(ICOLUM,L)*T
      IF(M)550,550,460
  460 DO 500 L=1,M
  500 B(L1,L)=B(L1,L)-B(ICOLUM,L)*T
  550 CONTINUE
      DO 710 I=1,N
      L=N+1-I
      IF(INDEX(L,1)-INDEX(L,2))630,710,630
  630 JROW=INDEX(L,1)
      JCOLUM=INDEX(L,2)
      DO 705 K=1,N
      SWAP=A(K,JROW)
      A(K,JROW)=A(K,JCOLUM)
      A(K,JCOLUM)=SWAP
  705 CONTINUE
  710 CONTINUE
  740 RETURN
      END
      SUBROUTINE JACOBI1(N,Q,JVEC,M,V)
C     SUBPROGRAM FOR DIAGONALIZATION OF MATRIX Q BY SUCCESSIVE ROTA
      DIMENSION Q(13,13),V(13,13),X(13),IH(13)                    TIONS
C
C     NEXT 8 STATEMENTS FOR SETTING INITIAL VALUES OF MATRIX V
C
      IF(JVEC) 10,15,10
```

```
   10 DO 14 I=1,N
      DO 14 J=1,N
      IF(I-J) 12,11,12
   11 V(I,J)=1.0
      GO TO 14
   12 V(I,J)=0.
   14 CONTINUE
C
   15 M=0
C     NEXT 8 STATEMENTS SCAN FOR LARGEST OFF DIAG. ELEM. IN EACH ROW
C     X(I) CONTAINS LARGEST ELEMENT IN ITH ROW
C     IH(I) HOLDS SECOND SUBSCRIPT DEFINING POSITION OF ELEMENT
C
      MI=N-1
      DO 30 I=1,MI
      X(I)=0.
      MJ=I+1
      DO 30 J=MJ,N
      IF (X(I)-ABS (Q(I,J))) 20,20,30
   20 X(I)=ABS (Q(I,J))
      IH(I)=J
   30 CONTINUE
C
C     NEXT 7 STATEMENTS FIND FOR MAXIMUM OF X(I)S FOR PIVOT ELEMENT
   40 DO 70 I=1,MI
      IF(I-1) 60,60,45
   45 IF (XMAX-X(I)) 60,70,70
   60 XMAX=X(I)
      IP=I
      JP=IH(I)
   70 CONTINUE
C
C     NEXT 2 STATEMENTS TEST FOR XMAX,IF LESS THAN 10**-8,GO TO 1000
C
      EPSI=1.E-12
      IF (XMAX-EPSI) 1000,1000,148
C
  148 M=M+1
C
C     NEXT 11 STATEMENTS FOR COMPUTING TANG,SINE,COSN,Q(I,I),Q(J,J)
C
      IF (Q(IP,IP)-Q(JP,JP)) 150,151,151
  150 TANG =-2.*Q(IP,JP)/(ABS(Q(IP,IP)-Q(JP,JP))+SQRT((Q(IP,IP)-Q
(JP,JP)1)**2+4.*Q(IP,JP)**2))
      GO TO 160
  151 TANG =+2.*Q(IP,JP)/(ABS(Q(IP,IP)-Q(JP,JP))+SQRT((Q(IP,IP)-Q
(JP,JP)1)**2+4.*Q(IP,JP)**2))
  160 COSN=1.0/SQRT(1.0+TANG**2)
      SINE=TANG*COSN
      QII= Q(IP,IP)
      Q(IP,IP)= COSN**2*(QII+TANG*(2.*Q(IP,JP)+TANG*Q(JP,JP)))
      Q(JP,JP)= COSN**2*(Q(JP,JP)-TANG*(2.*Q(IP,JP)-TANG*QII))
C
      Q(IP,JP)=0.
```

```
C
C     NEXT 4 STATEMENTS FOR PSEUDO RANK OF THE EIGENVALUES
C      GO TO 897
      IF (Q(IP,IP)-Q(JP,JP)) 152,153,153
  152 TEMP=Q(IP,IP)
      Q(IP,IP)=Q(JP,JP)
      Q(JP,JP)=TEMP
C
C     NEXT 6 STATEMENTS ADJUST SIN,COS FOR COMPUTATION OF Q(I,K),
C                                                        V(I,K)
      IF(SINE) 154,155,155
  154 TEMP=+COSN
      GO TO 170
  155 TEMP=-COSN
  170 COSN=ABS(SINE)
      SINE=TEMP
C
C     NEXT 10 STATEMENTS FOR INSPECTING THE I"S BETWEEN I+1 AND N-1
C  TO DETERMINE WHETHER A NEW MAXIMUM VALUE SHOULD BE COMPUTED SINCE
C     THE PRESENT MAXIMUM IS IN THE I OR J ROW
C
C  897 CONTINUE
  153 DO 350 I=1,MI
      IF (I-IP) 210,350,200
  200 IF (I-JP) 210,350,210
  210 IF (IH(I)-IP) 230,240,230
  230 IF (IH(I)-JP) 350,240,350
  240 K= IH(I)
      TEMP=Q(I,K)
      Q(I,K)=0.
      MJ=I+1
      X(I)=0.
C
C     NEXT 5 STATEMENTS SEARCH IN DEPLETED ROW FOR NEW MAXIMUM
C
      DO 320  J=MJ,N
      IF (X(I)-ABS(Q(I,J))) 300,300,320
  300 X(I)=ABS(Q(I,J))
      IH(I)=J
  320 CONTINUE
      Q(I,K)=TEMP
  350 CONTINUE
C
      X(IP)=0.
      X(JP)=0.
C
C     NEXT 30 STATEMENTS FOR CHANGING THE OTHER ELEMENTS OF Q
C
      DO 530 I=1,N
C
      IF (I-IP) 370,530,420
  370 TEMP=Q(I,IP)
      Q(I,IP)=COSN*TEMP+SINE*Q(I,JP)
      IF (X(I)-ABS(Q(I,IP))) 380,390,390
```

```
  380 X(I)=ABS(Q(I,IP))
      IH(I)=IP
  390 Q(I,JP)=-SINE*TEMP+COSN*Q(I,JP)
      IF (X(I)-ABS(Q(I,JP))) 400,530,530
  400 X(I)=ABS(Q(I,JP))
      IH(I)=JP
      GO TO 530
C
  420 IF (I-JP) 430,530,480
  430 TEMP =Q(IP,I)
      Q(IP,I)=COSN*TEMP+SINE*Q(I,JP)
      IF (X(IP)-ABS(Q(IP,I))) 440,450,450
  440 X(IP)=ABS(Q(IP,I))
      IH(IP)=I
  450 Q(I,JP)=-SINE*TEMP+COSN*Q(I,JP)
      IF (X(I)-ABS(Q(I,JP))) 400,530,530
C
  480 TEMP=Q(IP,I)
      Q(IP,I)=COSN*TEMP+SINE*Q(JP,I)
      IF(X(IP)-ABS(Q(IP,I))) 490,500,500
  490 X(IP)=ABS(Q(IP,I))
      IH(IP)=I
  500 Q(JP,I)=-SINE*TEMP+COSN*Q(JP,I)
      IF (X(JP)-ABS(Q(JP,I))) 510,530,530
  510 X(JP)=ABS(Q(JP,I))
      IH(JP)=I
  530 CONTINUE
C
C     NEXT 6 STATEMENTS TEST FOR COMPUTATION OF EIGENVECTORS
C
      IF (JVEC) 540,40,540
  540 DO 550 I=1,N
      TEMP=V(I,IP)
      V(I,IP)= COSN*TEMP+SINE*V(I,JP)
  550 V(I,JP)=-SINE*TEMP+COSN*V(I,JP)
      GO TO 40
 1000 RETURN
      END
      SUBROUTINE JACOBI(N,Q,JVEC,M,V)
C     SUBPROGRAM FOR DIAGONALIZATION OF MATRIX Q BY SUCCESSIVE ROTA
       DIMENSION Q(3,3),V(3,3),X(3),IH(3)                    TIONS
   13 FORMAT (2E15.5)
C
C     NEXT 8 STATEMENTS FOR SETTING INITIAL VALUES OF MATRIX V
C
      IF(JVEC) 10,15,10
   10 DO 14 I=1,N
      DO 14 J=1,N
      IF(I-J) 12,11,12
   11 V(I,J)=1.0
      GO TO 14
   12 V(I,J)=0.
   14 CONTINUE
C
```

```
   15 M=0
C     NEXT 8 STATEMENTS SCAN FOR LARGEST OFF DIAG. ELEM. IN EACH ROW
C     X(I) CONTAINS LARGEST ELEMENT IN ITH ROW
C     IH(I) HOLDS SECOND SUBSCRIPT DEFINING POSITION OF ELEMENT
C
      MI=N-1
      DO 30 I=1,MI
      X(I)=0.
      MJ=I+1
      DO 30 J=MJ,N
      IF (X(I)-ABS (Q(I,J))) 20,20,30
   20 X(I)=ABS (Q(I,J))
      IH(I)=J
   30 CONTINUE
C
C     NEXT 7 STATEMENTS FIND FOR MAXIMUM OF X(I) FOR PIVOT ELEMENT
   40 DO 70 I=1,MI
      IF(I-1) 60,60,45
   45 IF (XMAX-X(I)) 60,70,70
   60 XMAX=X(1)
      IP=I
      JP=IH(I)
   70 CONTINUE
C
C     NEXT 2 STATEMENTS TEST FOR XMAX,IF LESS THAN 10**-8,GO TO 1000
C
      EPSI=1.E-12
      IF (XMAX-EPSI) 1000,1000,148
C
  148 M=M+1
C
C     NEXT 11 STATEMENTS FOR COMPUTING TANG,SINE,COSN,Q(I,I),Q(J,J)
C
      IF (Q(IP,IP)-Q(JP,JP)) 150,151,151
  150 TANG =-2.*Q(IP,JP)/(ABS(Q(IP,IP)-Q(JP,JP))+SQRT((Q(IP,IP)-Q
(JP,JP))**2+4.*Q(IP,JP)**2))
      GO TO 160
  151 TANG =+2.*Q(IP,JP)/(ABS(Q(IP,IP)-Q(JP,JP))+SQRT((Q(IP,IP)-Q
(JP,JP))**2+4.*Q(IP,JP)**2))
  160 COSN=1.0/SQRT(1.0+TANG**2)
      SINE=TANG*COSN
      QII= Q(IP,IP)
      Q(IP,IP)= COSN**2*(QII+TANG*(2.*Q(IP,JP)+TANG*Q(JP,JP)))
      Q(JP,JP)= COSN**2*(Q(JP,JP)-TANG*(2.*Q(IP,JP)-TANG*QII))
C
      Q(IP,JP)=0.
C
C     NEXT 4 STATEMENTS FOR PSEUDO RANK OF THE EIGENVALUES
      IF (Q(IP,IP)-Q(JP,JP)) 152,153,153
  152 TEMP=Q(IP,IP)
      Q(IP,IP)=Q(JP,JP)
      Q(JP,JP)=TEMP
C     NEXT 6 STATEMENTS ADJUST SIN,COS FOR COMPUTATION OF Q(I,K).
C                                                        V(I,K)
```

```
      IF(SINE) 154,155,155
  154 TEMP=+COSN
      GO TO 170
  155 TEMP=-COSN
  170 COSN=ABS(SINE)
      SINE=TEMP
C
C     NEXT 10 STATEMENTS FOR INSPECTING THE IHS BETWEEN I+1 AND N-1
C TO  DETERMINE WHETHER A NEW MAXIMUM VALUE SHOULD BE COMPUTED SINCE
C     THE PRESENT MAXIMUM IS IN THE I OR J ROW
C
  153 DO 350 I=1,MI
      IF (I-IP) 210,350,200
  200 IF (I-JP) 210,350,210
  210 IF (IH(I)-IP) 230,240,230
  230 IF (IH(I)-JP) 350,240,350
  240 K= IH(I)
      TEMP=Q(I,K)
      Q(I,K)=0.
      MJ=I+1
      X(I)=0.
C
C     NEXT 5 STATEMENTS SEARCH IN DEPLETED ROW FOR NEW MAXIMUM
C
      DO 320  J=MJ,N
      IF (X(I)-ABS(Q(I,J))) 300,300,320
  300 X(I)=ABS(Q(I,J))
      IH(I)=J
  320 CONTINUE
      Q(I,K)=TEMP
  350 CONTINUE
C
      X(IP)=0.
      X(JP)=0.
C
C     NEXT 30 STATEMENTS FOR CHANGING THE OTHER ELEMENTS OF Q
C
      DO 530 I=1,N
C
      IF (I-IP) 370,530,420
  370 TEMP=Q(I,IP)
      Q(I,IP)=COSN*TEMP+SINE*Q(I,JP)
      IF (X(I)-ABS(Q(I,IP))) 380,390,390
  380 X(I)=ABS(Q(I,IP))
      IH(I)=IP
  390 Q(I,JP)=-SINE*TEMP+COSN*Q(I,JP)
      IF (X(I)-ABS(Q(I,JP))) 400,530,530
  400 X(I)=ABS(Q(I,JP))
      IH(I)=JP
      GO TO 530
C
  420 IF (I-JP) 430,530,480
  430 TEMP=Q(IP,I)
      Q(IP,I)=COSN*TEMP+SINE*Q(I,JP)
```

```
      IF (X(IP)-ABS(Q(IP,I))) 440,450,450
  440 X(IP)=ABS(Q(IP,I))
      IH(IP)=I
  450 Q(I,JP)=-SINE*TEMP+COSN*Q(I,JP)
      IF (X(I)-ABS(Q(I,JP))) 460,530,530
C
  460 TEMP=Q(IP,1)
      Q(IP,1)=COSN*TEMP+SINE*Q(JP,1)
      IF(X(IP)-ABS(Q(IP,I))) 490,500,500
  490 X(IP)=ABS(Q(IP,I))
      IH(IP)=I
  500 Q(JP,I)=-SINE*TEMP+COSN*Q(JP,I)
      IF (X(JP)-ABS(Q(JP,I))) 510,530,530
  510 X(JP)=ABS(Q(JP,1))
      IH(JP)=I
  530 CONTINUE
C
C     NEXT 6 STATEMENTS TEST FOR COMPUTATION OF EIGENVECTORS
C
      IF (JVEC) 540,40,540
  540 DO 550 I=1,N
      TEMP=V(I,IP)
      V(I,IP)= COSN*TEMP+SINE*V(I,JP)
  550 V(I,JP)=-SINE*TEMP+COSN*V(I,JP)
      GO TO 40
 1000 AAM=FLOAT(M)
      WRITE (6,13) EPSI,AAM
      RETURN
      END
```